Faculty of Mathematics and Physics
Charles University in Prague

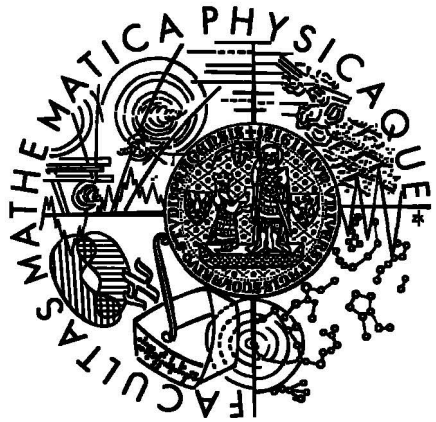

Ph.D. Thesis

THEORETICAL STUDY OF LIGAND FIELDS INFLUENCE ON PHYSICO-CHEMICAL BEHAVIOR OF COPPER CATIONS CU(I)/CU(II)

Matěj Pavelka

Supervisor: Doc. RNDr. Ing. Jaroslav Burda, CSc.
Consultant: Ing. Stanislav Záliš, CSc.

Prague 2006

Acknowledgement

I thank my wife, my family, my band Lealoo, and my friends for all-round support. I am also grateful to my high school professor Pavel Pytela for showing me the beauty of physics.
Finally, I thank Stanislav Záliš for helpful consultations and Jaroslav Burda for his self-sacrificing lead of this work.

I declare that these are results of my investigation. All resources used in this thesis are listed in the References.

Matěj Pavelka, Prague 2006

Index

1 Introduction

1.1 Copper Ions in Organisms

Importance of metal ions in organisms is illustrated by protein data bank (PDB) statistics. Nearly half of entries contain metal cofactors, which are essential for charge neutralization, structure, and function of metalloproteins. Hence, investigation of such metal sites is essential for biochemistry.

Copper, despite its toxicity in pure form, is fundamental for many in vivo processes. This toxicity is avoided by restricting the movement of Cu ions. So-called chaperone proteins, such as ATX1 (normal Cu chaperone) and CCS (Cu chaperone for superoxide dismutase), guide Cu ions to their appropriate locations in the cell. In this way, they protect the cell by keeping the concentration of free Cu ions extremely low.

1.2 Copper in Peptide Environment

Cu ions often exhibit interesting spectral properties, which originate from the unusual geometric and electronic structures that are imposed through their interactions with peptide environment. Such proteins provide many functions: electron transfer, oxidation-reduction processes, oxygen transport and insertion, and so forth. They can be organized as follows:

a) Type 1 Cu proteins also called blue copper proteins. These simplest Cu proteins have a intense blue absorption band near 600 nm in the oxidized Cu(II) state. This transition is assigned with the S(cysteine)-Cu charge transfer (CT). Structures of the active sites usually contain a four-coordinated Cu ion, although a coordination number of five was found in azurins. Structural motif consists of the arrangement Cu(I)/Cu(II):$(His)_2CysX$, where X is Met or Gln. Examples of this motif can be found in pseudoazurin, rusticyanin, plastocyanin, mavicyanin, auracyanin, stellacyanin, umecyanin, and amicyanin. Interestingly, reduction of the Cu(II) ion to Cu(I) in type 1 proteins causes minimal structural changes. It results in low activation barriers for redox processes and rapid electron-transfer rates.

b) Type 2 Cu proteins. They have an less-intense absorption band at 350-420 nm. In this group of proteins, the copper ion is usually found in a square planar or tetragonal coordination. After binding of substrate, catalytic oxidation is facilitated by vacant coordination sites around the central metal ion. Type 2 Cu proteins include superoxide dismutase (which catalyzes dismutation of superoxide radical to O_2 and H_2O_2), galactose oxidase (reduces O_2 to $H2O_2$, thus oxidizing galactose to aldehyde), and amine oxidase (which oxidatively deaminates primary amines to aldehydes).

c) Type 3 Cu proteins. This family is characterized by an antiferromagnetically coupled pair of Cu ions and a strong absorption band near 330 nm. Examples can be found in the invertebrate protein hemocyanin, which is involved in oxygen transport, and tyrosinase, which is a monooxygenase that hydroxylates monophenols and oxidizes diphenols to quinones.

d) Proteins with Cu_A site. This coupled dinuclear copper site can be found in Cytochrome C oxidase, and N_2O reductase.

e) Proteins with Cu_B site. In these peptides, there is bridging ligand between Cu_B and Fe of Heam. For example, Cytochrome C oxidase, and ubiquinone oxidase are listed.
f) Multi-copper oxidases. They combine several types of Cu sites, which can be found in Ascorbate oxidase, Ceruloplasmin, and Laccase.

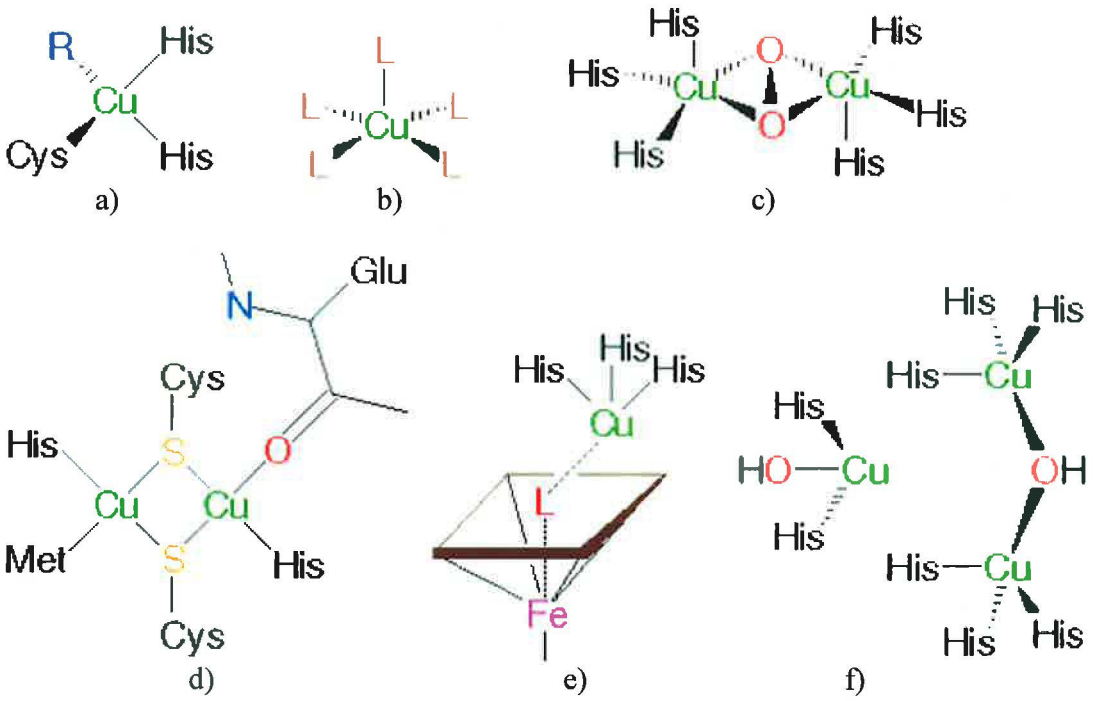

Figure 1.1. *Comparison of a) Type 1, b) Type 2, c) Type 3, d) Cu_A, e) Cu_B, and f) Multi-copper sites in proteins.*

There is a huge number of works investigating biological activity of the copper ions and their interactions using both experimental and theoretical approaches. By means of UV-VIS and EPR spectroscopy, Cu-center of Azurin was studied.[1] Spectroscopic tools in combination with DFT calculations were used to investigate the role of amino acid in axial position to the copper complex and its influence on a reduction potential.[2] Similarly, the plastocyanin model complexes were examined.[3,4] Charge transfer (CT) dynamics were carried out by pump-probe[5] and resonance Raman spectroscopy.[6] Other experimental studies should also be mentioned.[7-9] The redox process were studied on Tyrosinase.[10] A lot of computational effort was devoted to examination of copper proteins.[11-15] Theoretical studies of the copper interactions with amino acids have been reported too.[16-25] Published experimental works include fluorescence spectroscopy,[26] electron paramagnetic resonance (EPR) and electron-nucluear double resonance (ENDOR) techniques,[27] X-ray absorption near-edge structure (XANES) spectra,[28] and EPR and UV-VIS spectra.[29]
The basic aspects of a copper coordination in peptide environment are summarized in reviews.[30-33]

In such extensive area like copper proteins, my works[34,35] focus on models of active mononuclear centers.

1.3 Interaction of Copper Cations with DNA/RNA bases

Metal ions interaction with DNA/RNA bases is a key moment of many biochemical processes. Helix rollout and release of hydrogen bonds between base pairs often proceed in presence of metals or their hydrates. Hence, a great deal of work has been devoted to the investigation of copper complexes with nucleo bases. Experimental studies include crystal structures,[36] IR spectroscopy,[37] thermodynamical measurements, and so forth.[38-40] Some effort have been put into theoretical studies as well.[41-48]

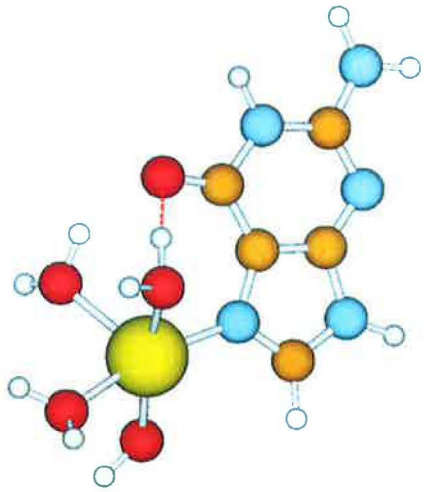

Figure 1.2. *Tetra-aqua Cu(II) complex with guanine.*

Suggested order in copper-N^7(base) bonding strength is: guanine > adenine > uracil. Such bonds have influence on Watson-Crick base pairing. Most of the studied complexes contain hydrated Cu(I) or Cu(II) cation. Therefore, interaction of hydrated Cu(II) with guanine was studied in my work.[49]

1.4 Model Copper Complexes

Many works are devoted to examination of "small inorganic complexes" in order to determine coordination geometries and electronic properties of various copper compounds. Considering such models can give deeper insight and easier interpretation of Cu(I)/Cu(II) behavior. Both Cu cations interacting with molecules like water, ammonia, or hydrogen-sulphide were intensively studied using various computational approaches.[47,50-68]
My studies[35,69] include a detailed investigation of these complexes and thus provide an important model for copper interactions with amino acids like histidine, methionine, cysteine, glutamine etc., or other bio-environment. In addition, some effort was spent to describe the hydration of copper cations.[70]

1.5 Copper Quinon Complexes

The knowledge of mechanism of valence–tautomer equilibria can help in understanding bio relevant processes (e.g. copper dependent amine oxidases).[71] Intramolecular metal-to-ligand electron transfer equilibrium (according to formula 1.1) was observed in a narrow temperature range for copper complexes.[72]

(eq 1.1) $[(L)Cu^{II}(Q^{2-})] \rightleftharpoons [(L)Cu^{I}(Q^{\cdot-})]$

The temperature-dependent electron transfer equilibrium has been quantitatively explored by EPR as a function of the non-innocent o-quinonoid ligand Q and of the co-ligand L.[73] The following investigation[74] of temperature dependent EPR spectra found the variation of g-tensor. Anisotropic g-tensor corresponding to Cu^{II}/catecholate varies to isotropic g-factor, which indicates the electron density localization at semiquinone ligand in Cu^{I}/semiquinone form. This phenomena has also been discussed with respect to potential applications in molecular electronics.[75-78] The electron density redistribution within the molecule should be accompanied by the geometry change from closely planar to closely tetrahedral. Such process should depend on the oxidation state of the central copper atom.[71] However, individual valence isomers were not experimentally isolated and thus the structures are unknown. Hence, geometry optimizations using quantum chemical methods can be necessary to identify the corresponding valence-tautomers.[79]

1.6 Cisplatin

In the family of antitumor metallodrugs, platinum compounds represent the time-proven class of drugs. Cisplatin is one of the earliest drug used and together with carboplatin they are most common Pt derivates.[80] However, second and third generation drugs (like carboplatin, oxaliplatin, Pt(IV) complex JM216 or trinuclear BBR 3464) were serched in order to eliminate some of the side-effects of cisplatin like high toxicity and a partial resistance of tumor cells. Many of these Pt(II)/Pt(IV) complexes were examined in oncological in vivo research as well as in vitro experiments.[81-89] Physico-chemical description of these complexes is important for further progress in the area and computational chemistry can give this more detailed insight into their structural and bonding relations.

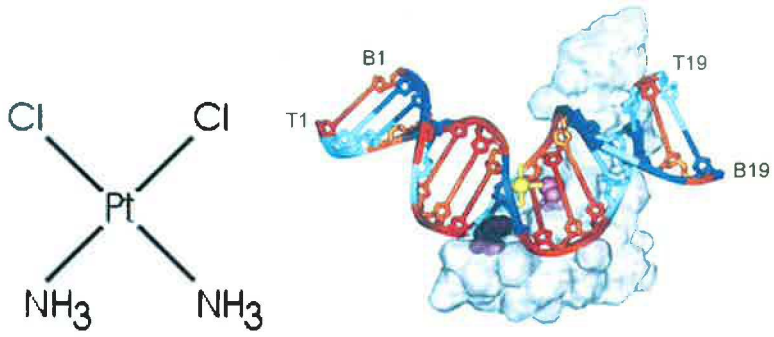

Figure 1.3. *Cisplatin formula and X-ray structure of DNA/cisplatin adduct with attached HMG protein.*

The final DNA adduct of cisplatin (and some other platinum drugs, too) includes the cis-$[Pt(NH_3)_2$-1,2-d(GpG)$]^{2+}$ fragment. These adducts cause a roll of 25-50 degrees between the guanine bases involved in the cross-link and a global bend of the helix axis towards major groove about 20-40 degrees.[90-92] Such a bend is recognized by high mobility group (HMG) protein and subsequent process of apoptosis can be started. The crystal structure of DNA oligomer with cisplatin and HMG-protein was reported.[93,94] There is also evidence of interstrand cisplatin bridge[95] and some other platinum complexes.[96-102] Reviews of current state in Pt antitumor drugs can be found in works of Wong[103] and Reedijk.[104] Computational studies from this field usually concern Pt-nucleobases interactions.[105-117] My work[118] investigates cis- and trans-platin interaction with two bases (AG, GG, and CG) in both "head to head" and "head to tail" orientations.

2 Methods

2.1 Computational Chemistry Methodology

For a couple of decades, utilization of computers in chemistry advanced insomuch that computational chemistry does stand as equal partner for experimental methods. There are several ways how theoretical studies can support experiments:

- reproducing experiments and at the same time adding information, which can not be obtained from experiment
- enhancing resolution of X-ray and NMR structural studies
- providing interpretation of experimental outcomes
- predicting results for systems with no available experimental data.

Theoretical methods can be divided into two extensive groups: Quantum chemistry and Molecular mechanics.

2.1.1 Quantum Chemistry

Methods based on quantum mechanics (QM) arise from solving Schrödinger equation (eq 2.1) for electrons and nuclei. QM results provide not only structural information but also complete electronic description of studied complex. These methods are usually called ab initio, since they use as little empirical parameters as possible. Such calculations are computationally expensive; hence they are limited to small systems.

2.1.2 Molecular Mechanics

Molecular mechanics (MM) provide powerful tool for structural studies. Moreover, molecular dynamics (MD) computations are quite common in MM approximation. Its main advantage lies in omitting electronic problem and approximating forces between particular atoms by empirical force field (FF). Therefore MM studies must be confronted with experiment.

2.1.3 Combined methods

Very promising methodology combines Molecular mechanics and Quantum mechanics together (QM/MM). MM methods can simulate very large systems quickly and QM is able to compute many important properties at more reliable level. It is possible to combine these two approaches into one calculation in order to describe very large compound or set of compounds using molecular mechanics and the key part of the system is treated at the QM level of theory. This is also used for description of a molecules surrounded by solvent.

2.2 Ab Initio

2.2.1 Schrödinger Equation and Wave Function

By solving time-independent Schrödinger equation (eq 2.1) energy E and wave function Ψ are obtained and in this way, all information about system is obtained too.

(eq 2.1) $\quad E\Psi = \hat{H}\Psi$

$\hat{H}$ is Hamilton operator, which includes specific terms when formulated for a molecule.

(eq 2.2) $$\left(\sum_{i=1}^{N}\hat{T}_i+\sum_{A=1}^{M}\hat{T}_A-\sum_{i=1}^{N}\sum_{A=1}^{M}\frac{Z_A}{r_{iA}}+\sum_{i=1}^{N}\sum_{j=1}^{N}\frac{1}{2}\frac{1}{r_{ij}}+\sum_{A=1}^{M}\sum_{B=1}^{M}\frac{1}{2}\frac{Z_A Z_B}{r_{AB}}\right)\Psi=E\Psi,$$

$\hat{T}$ represents operator of kinetic energy, Z_A is atomic number and r is position vector, i,j are electronic indexes, and A, B are indexes for nuclei.

Born-Oppenheimer approximation comes with separation of the problems for nuclei and electron subsystems $\Psi(r_i,r_A)=\Phi_{r_A}(r_i)v(r_A)$ and solves them independently;

(eq 2.3) $$\left(\sum_{i=1}^{N}T_i+V_{r_A}\right)\Phi_{r_A}(r_i)=U_{r_A}\Phi_{r_A}(r_i)$$

(eq 2.4) $$\left(\sum_{A=1}^{M}T_A+U(r_A)\right)v(r_A)=Ev(r_A)$$

where $\Phi_{r_A}(r_i)$ and $v(r_A)$ (V and U) represents wave function (interaction potentials) for electrons and nuclei, respectively. The role of r_A is considered in $\Phi_{r_A}(r_i)$ parametrically.

In molecular orbital (MO) approach, many-electron wave function Φ is treated as an appropriate combination of one-electron wave functions ψ_k called molecular orbitals. Since antisymmetric character of the wave function is required, the simplest form is Slater determinant:

(eq 2.5) $$\Phi(r_{1..N})=\frac{1}{\sqrt{N!}}\begin{vmatrix}\psi_1(r_1) & \cdots & \psi_1(r_N)\\ \vdots & \ddots & \vdots\\ \psi_N(r_1) & \cdots & \psi_N(r_N)\end{vmatrix}.$$

2.2.2 Basis sets

Within all QM approaches, it is necessary to choose a basis set for a construction of wave function. This is usually a set of exponential functions (Slater or gaussian type of orbital) centered on the different atoms in a molecule. These functions are used to expand the molecular orbitals into linear combination of atomic orbitals (LCAO).

(eq 2.6) $$\psi_i=\sum C_{\mu i}\phi_{\mu}$$

Within gaussian basis sets, it is easier to calculate overlap and other integrals resulting in substantial computational savings.

Today, there are hundreds of optimized basis sets. The smallest ones are called minimal basis sets, within which there is only one AO function per electron. The valence electrons are responsible for the bonding. Due to this fact, it is common to represent valence AO by more than one basis function (split-valence). It is also common to include polarization functions. These auxiliary functions with higher angular momentum bring additional flexibility within the basis set. Hence it allows proper description of polarization effects. It is important condition when considering accurate representations of a bonding in molecules. It is also possible to add diffuse functions, which are represented by very shallow gaussian functions (with small exponents), and describing more accurately the limiting behavior of the atomic orbitals. These additional basis functions can be important when considering anions, other soft molecular systems and excitations.

2.2.3 Hartree-Fock and Configuration Interaction

Single-determinant approximation and variation principle lead to Hartree-Fock (HF) equation:

$$\left[-\frac{1}{2}\Delta_1 - \sum_{A=1}\frac{Z_A}{r_{1A}} + \sum_{k=1}^{N}\int\frac{|\psi_k(r_2)|^2}{r_{12}}d^3r_2\right]\psi_i(r_1) - \sum_{k=1}^{N}\int\frac{\psi_k^*(r_2)\psi_i(r_2)}{r_{12}}d^3r_2\,\psi_k(r_1) = \varepsilon_i\psi_i(r_1).$$

Although the method produces one-electron molecular orbitals, which have straightforward chemical interpretation, Hartree-Fock method has its deficiencies. In particular cases (e.g. bond breaking, high-spin states) HF scheme is inadequate and more determinants are needed for the correct description of wave function.

This simplest type of ab initio electronic calculation also suffers from the poorly accounted electron-electron interaction. Many types of calculations, known as post-Hartree-Fock methods (e.g. Perturbation Theory, Coupled Clusters), begin with a HF scheme and subsequently correct for electron-electron repulsion, also referred as dynamic electronic correlation. An example of such method is Möller-Plesset[119] (MP) scheme that uses the Rayleigh-Schrödinger perturbation theory to estimate the electronic correlation energy. Unperturbed HF wave function is corrected by the perturbation expansion. Especially MP2 calculations are quite popular, because they can be performed in relatively short time by modern programs (within Resolution Identity (RI) approximation). Another popular method Coupled Clusters[120] (CC) provides a very reliable description of electron correlation at the expense of longer computational time. One of the reasons why coupled cluster calculations are so computationally expensive is the iterative nature of the CC solution.

In order to obtain better description of heavy atoms, it is necessary to include spin orbital interaction and other relativistic terms. Such effects are approximately covered by pseudopotential methods, where inner electrons are omitted from wave function and their interaction with outer (valence) electrons is provided by pseudopotentials.

2.2.4 Density Functional Theory

Density functional theory (DFT) is an alternative and modern approach, which has become popular in solid-phase physics first. Nowadays, it is commonly used in chemistry. Advantage of DFT is that it does not use the wave function to describe the system. Instead, the electron density is used as the prime source of information. This approach has other advantage: computation of electron correlation is less expensive than for all other post-HF methods.

According to Hohenberg-Kohn theorem[121], ground state of a system is completely described by electron density. Energy functional can be split in three terms (eq. 2.7) in analogy to methods based on wave function.

(eq. 2.7) $$E = T + E_{ne} + E_{ee}$$

T is functional of the kinetic energy, E_{ne} is functional of the nuclei-electron-interaction, and E_{ee} represents functional of the electron-electron interaction, which can be split into Coulomb and exchange part E_x. The problem is that the exact form of kinetic and exchange term is unknown. Kinetic energy can be written as a sum of an exactly computable term T_s and a small correction term attached to exchange term E_x. Using molecular orbitals

(eq. 2.8) $$\rho(r)=\prod_{j=1}^{N}|\psi_j(r)|^2,$$

Kohn and Sham[122] introduced the calculation of T_s under the assumption of non-interacting particles. This way equation (eq. 2.9) is valid;

(eq. 2.9) $$\left[-\frac{1}{2}\Delta+v_r(r)\right]\psi_j(r)=\varepsilon_j\psi_j(r)$$

where $v_r(r)$ stands as external potential. Now, the DFT energy can be expressed as follows,

(eq. 2.10) $$E[\rho(r)]=T_s[\rho(r)]+\int v_r(r)\rho(r)\,dr+\int\frac{\rho(r,r')}{|(r-r')|}\,dr+E_{xc}[\rho(r)]$$

where E_{xc} represents the exchange-correlation functional. For last decades, the great effort was put in finding the most suitable form of E_{xc} functional.

- Local Density Approximation (LDA) regards the density as a local and homogeneous electron gas. In open shell systems, it is called LSDA (Local Spin Density Approximation).
- Gradient Corrected methods (GGA) assume an inhomogeneous electron gas. Therefore, E_{xc} is not only dependent on the density but also on the derivatives of the density (nonlocal methods).
- Hybrid Methods are based on a relation between E_{xc} of a non-interacting system and an interacting system. Then E_{xc} is fitted combination of DFT exchange-correlation term and Hartree-Fock exchange term.

In the present DFT studies, I used B3PW91[123] and B3LYP[124] hybrid functionals composed of B3 exchange-correlation part and PW91 and LYP correlation functionals, respectively.

2.3 Solvation

Most of biochemical processes take place in liquid phase. Hence, it is essential to somehow include interaction with environment.

2.3.1 Explicit Solvation

The straightforward and reliable approximation of environment effects is to explicitly include solvent molecules into the system. On the other hand, number of involved molecules should be considered, since the quantum calculations are very expensive for large systems. A reasonable approach includes only few important solvent molecules with the rest of environment effect covered up alternatively.

2.3.2 Polarized Continuum Models

Alternative approach to explicit solvation is Polarized Continuum Model (PCM). There are several PCM methods. The most common is the Conductor-like Screening Model (COSMO, also CPCM). The basic idea of PCM methods is to represent solvent by a continuum, which describes the electrostatic behavior of the solvent. The polarization of dielectric continuum, induced by the solute, is described by the screened charge density appearing at the boundary between the continuum and the solute. The dielectric boundary condition can be used to calculate the screening charge density. The advantage of

COSMO is in replacing this condition by the simpler boundary condition of vanishing potential on the surface of conducting medium.

2.3.3 Point Charge Interaction

For the last decade, simple point-charge (SPC) interaction with solute starts to be more popular thanks to pronounced development in combined QM/MM approach. The solute molecule is treated ab initio in the external field created by point-charges of solvent.

2.4 Properties

2.4.1 Time-Dependent DFT

Time-Dependent Density Functional Theory (TDDFT) was developed[125] in order to allow calculations of electronic excitations and oscillator strengths at DFT level. It can be regarded as an extension of DFT theory to time-dependent problems. In analogy, TDDFT describes system by one-body electron density $\rho(r,t)$. The advantage is clear: a wave-function with 3N-dimensions (N is number of electrons) is replaced by a real function that depends solely on the coordinates. The $\rho(r,t)$ is usually obtained using auxiliary system of non-interacting electrons that feel an effective time-dependent potential, the time-dependent Kohn-Sham potential. However, its exact form is unknown and needs to be approximated.

2.4.2 Electron Distribution Analyses

The properties such as charge and spin distribution are important for understanding the electronic structure. The simplest way how to obtain partial atomic charges is Mulliken scheme. It assumes the total charge density on the atom is a sum (eq 2.11) over those atomic orbitals, which are attached to the designated atom.

(eq 2.11) $$\rho(r) = \sum_{\mu\upsilon}\left[\sum_{i} C_{\mu i} C_{\upsilon i}^{*}\right]\phi_{\mu}(r)\phi_{\upsilon}(r)^{*}$$

Mulliken method has several deficiencies. They are related with the simple way, how electron density $\rho(r)$ is partitioned to individual atoms. The problems are:

- $\rho(r)$ has sometimes negative value.
- Mulliken population exhibits strong basis set dependency.
- The population incorrectly describes charge distribution of bonds with considerable ionic character.

Using HF or DFT procedure, orthogonal molecular orbitals are obtained. Some methods of computing electron population work within non-orthogonalized MOs. It can partially improve the problem of negative density $\rho(r)$. However, the charge is not always correctly assigned.

Alternative way of analyzing electron distribution is called Natural Population Analysis (NPA) [126], which overcomes some of the problems of Mulliken scheme. Present method is based on the rearrangement of the electron density into natural atomic orbitals basis (NAO). Construction of NAO is usually done in two steps: (i) diagonalization of blocks of one-center angularly symmetric density matrix, and (ii) removing the redundant interatomic overlap. In the first step, orbitals are divided in two sets: minimal set and Rydberg set. Note, minimal set is occupied in the ground state of individual atoms.

Population of the Rydberg set is non-zero when the atom is part of a molecule, but it is still very small. There is other way of improving charge distribution analysis. It involves empirical atomic radii, which help to assign density to particular atoms.

2.4.3 EPR

Electron paramagnetic resonance (EPR) is experimental method based on magnetic behavior of unpaired electron(s) in a molecule. The key tensor property called g-factor describes how the local magnetic field is induced by the external magnetic field. It approaches the value of 2.0023 for single free electron. Similar values should be obtained for systems with delocalized unpaired electrons. Otherwise, it can markedly rise. Linear response theory makes possible calculation of molecule's EPR information among others.

2.4.3 Vibration Analysis

Vibration analysis is commonly based on harmonic oscillator approximation. It requires computation of second derivation of Hamiltonian, which can be very time-consuming procedure. It results in vibration frequencies for a molecule and can also be used for calculation of thermodynamic data (zero-point vibration energy, enthalpy, Gibbs free energy at given temperature).

2.4.5 Energy Analyses

In the accurate energy investigation, it is essential to include Basis Set Superposition Error (BSSE) corrections, when dealing with localized basis sets. It improves the dependence between the computed energy and the size of the used atomic basis set. In the calculation of stabilization energy (eq 2.12),

(eq 2.12) $$\Delta E^{Stab} = -(E_{complex} - \sum E_{monomer})$$

it is not recommended to use only AOs localized on atoms of concerning monomer. For each monomer, AOs localized on all other centers have to be included too. Moreover, the deformation energies of individual monomers should be considered in the ΔE^{Stab} estimation. The final expression of the energy formula is

(eq 2.13) $$\Delta E^{Stab} = -(E_{complex} - \sum E_{monomer} - \sum E^{deform}).$$

Besides ΔE^{Stab} energies, coordination (ΔE^{Coord}) and sterically corrected stabilization (ΔE^{Stex}) energies can also be computed, when dealing with metal complexes. Coordination energies are evaluated considering only directly bonded (first shell) ligands in the equation (eq 2.13) using the optimized geometry of the whole complex. ΔE^{Stex} is obtained when all interacting ligand molecules are treated as one subsystem and the central metal atom as another one. The difference between ΔE^{Stab} and ΔE^{Stex} then basically reflects the energy investment that would be necessary to form the ligand shell arrangement in the absence of the ion. In addition, bond dissociation energies (ΔE^{BDE}) can be estimated using the same BSSE scheme but without monomer deformation corrections. In this energy determination, partition of the complex in two parts (usually ligand and the rest of the complex) is done. It cleaves the examined metal-ligand bond giving bonding energy of the desired ligand. Problems in ΔE^{BDE} interpretation can appear, when more bonds or additional hydrogen-bonds are broken, simultaneously.

2.4.6 Electron Affinity and Ionization Potential

Electron affinity (EA) and ionization potential (IP) are important properties. They are essential for characterization of redox reactions. Vertical and adiabatic ionization potentials can be calculated according to formula (eq 2.14),

(eq 2.14) $$IP = E_{(\text{charged})} - E_{(\text{neutral})}$$

where $E_{(neutral)}$ stands as energy of neutral structure. In the case of vertical IP, the $E_{(charged)}$ term represents the energy of a charged system. It is calculated within the neutral structure. Hence, vertical IP represents instant ionization without any change of the molecular geometry. For adiabatic IP, the $E_{(charged)}$ energy is computed after structure relaxation of charged complex. The electron affinity is calculated by analogy. Vertical IP's and EA's can also be estimated by Koopmans' theorem or more accurately by method based on outer valence Green functions[127] propagators.

3 Results

3.1 Hydration of Copper Cations

In order to investigate hydration of copper cations, optimizations of $[Cu(H_2O)_n]^{2+/+}$ complexes (where *n* varies from 1 to 6) were performed at the DFT level. Following analyses revealed several trends.

The most stable Cu(I) structures have only two coordinated H_2O molecules. Remaining water molecules are arranged in the second solvation shell (see ***Figure 3.1***).

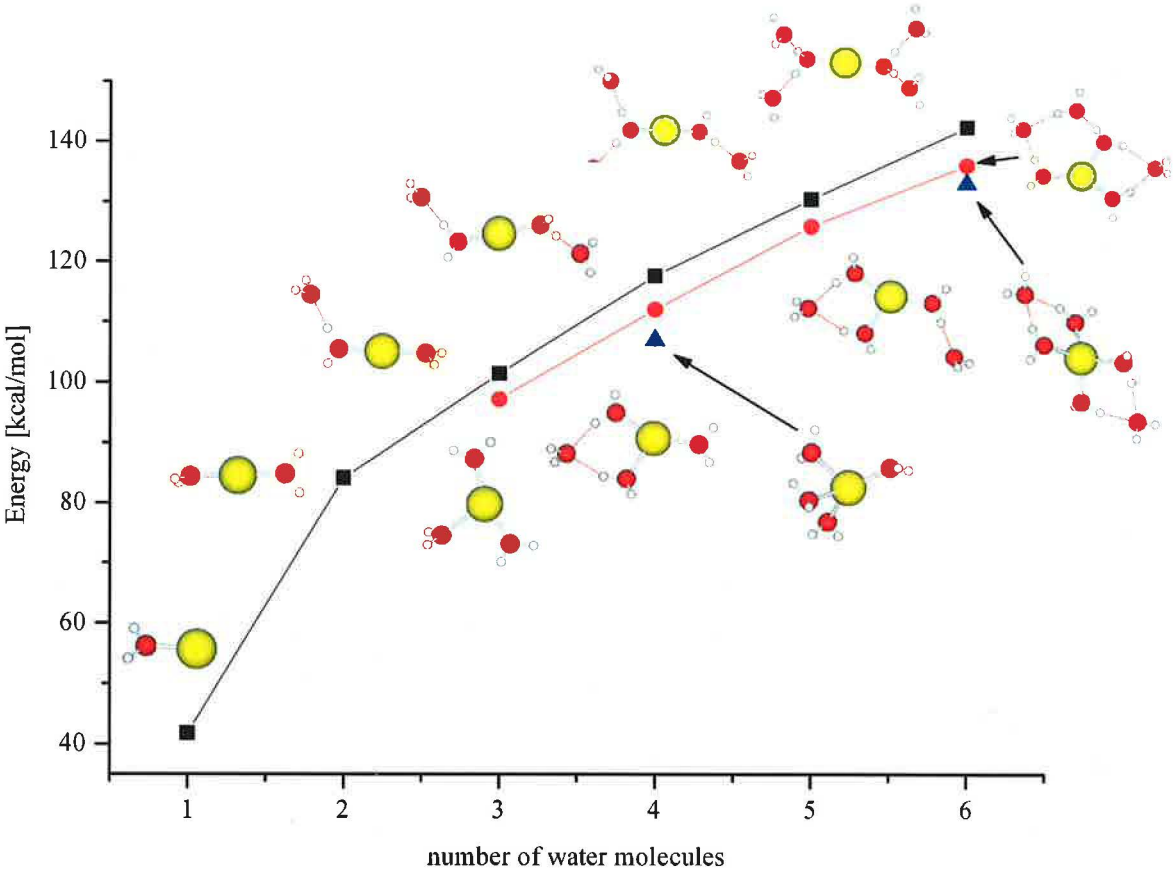

Figure 3.1. *Stabilization energies of the Cu(I) systems.*

A different trend was obtained at the Hartree-Fock level, where the most prefered coordination number is three. It can be explained by overestimated polarization and Coulomb interaction in metal-ligand binding. These individual contributions were obtained by Morokuma's energy decomposition.

For Cu(II) systems, the most preferred coordination is four or five (see ***Fig. 3.2***). All observations considering coordination preferences are in good agreement with experiments.

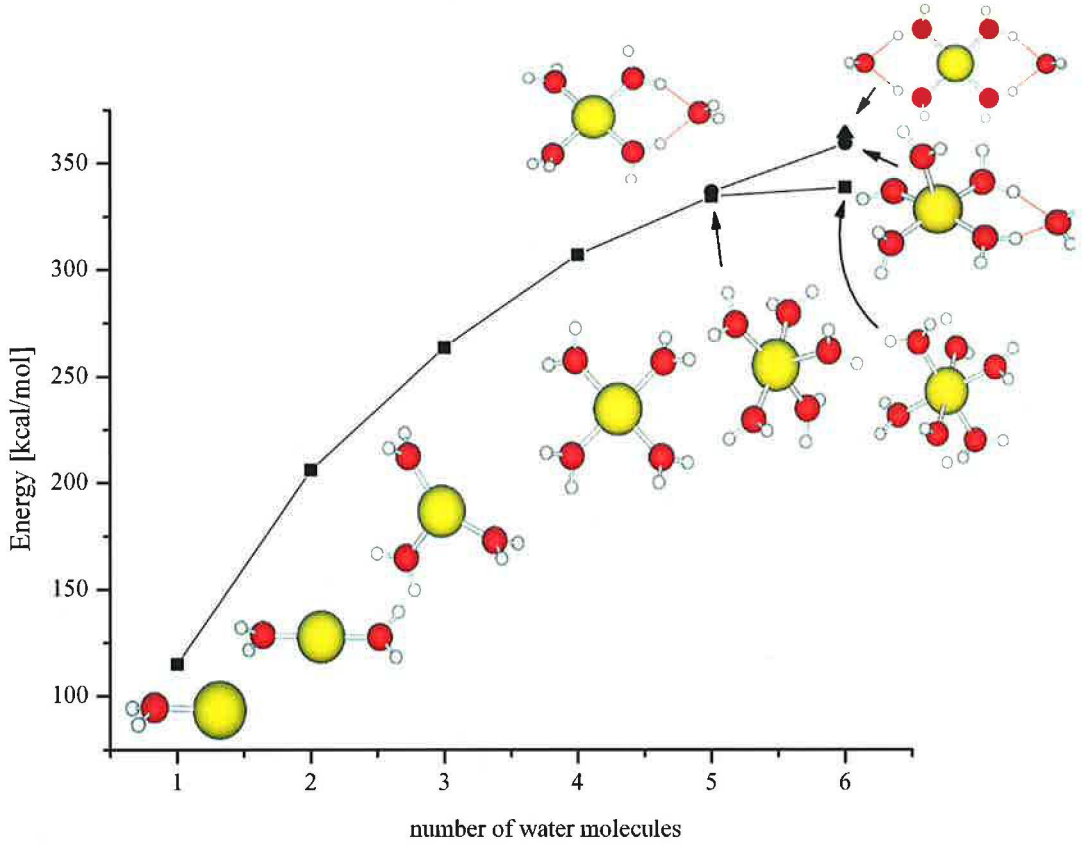

Figure 3.2. *Stabilization energies of the Cu(II) systems.*

Charge distribution analysis was performed, which includes atomic partial charges (based on NPA) and occupation of valence AOs. For Cu(I) systems, the occupation of Cu 4s orbital points to the extent of water ligands donation. In the case of Cu(II) complexes, only partial charges could be used for investigation of donation effects since it has unsaturated d^9 configuration. Calculations revealed that the highest donation occurs for the most stable complexes (2-coordinated Cu(I) and 4-/5-coordinated Cu(II)).

3.2 Model of Cu(I)/Cu(II) Interactions in Aqua-Amine Ligand Field

Subject of the second study was various-coordinated $[Cu(NH_3)_m(H_2O)_n]^{2+/+}$ complexes, where *n* progresses from *0* to *4* or *6* and $m + n = 4$ or *6*. Such model represents variable aqua-amine ligand field. This work is continuation of the previous study of copper cations in pure aqua environment. Extension to NH_3 ligands allowed the more general conclusions. There is also a large amount of theoretical and experimental studies to compare with. The most stable Cu(I) structures are two-coordinated, regardless the ligand type. Similarly to previous study, four-coordination is preferred in the case of Cu(II) complexes (see ***Fig. 3.3***). Actually, some five-coordinated structures of Cu^{2+} are fairly stable, too.

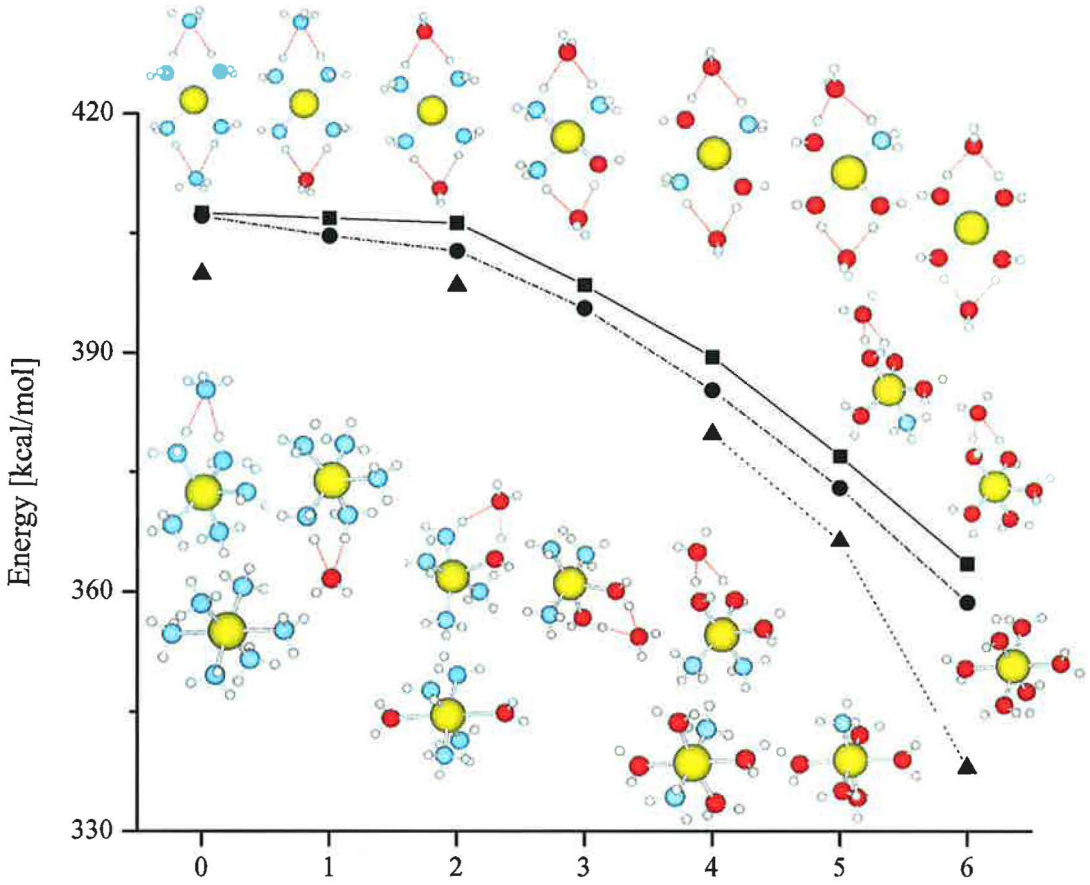

Figure 3.3. *Stabilization energies of the various-coordinated* $[Cu(NH_3)_m(H_2O)_n]^{2+}$ *complexes, where n progresses from 0 to 6 and* $m + n = 6$.

It was found that mixed water-ammonium complexes always prefer coordination with NH_3 molecules in the first solvation shell. In accord with HSAB (hard-soft acid-base) theory, Cu-N bonds were shown to be stronger than Cu-O bonds. Strength of copper-ligand bond is also affected by geometry. On the ***Figure 3.4***, different angles between dative lone pairs of ligand and Cu-ligand bond can be observed.

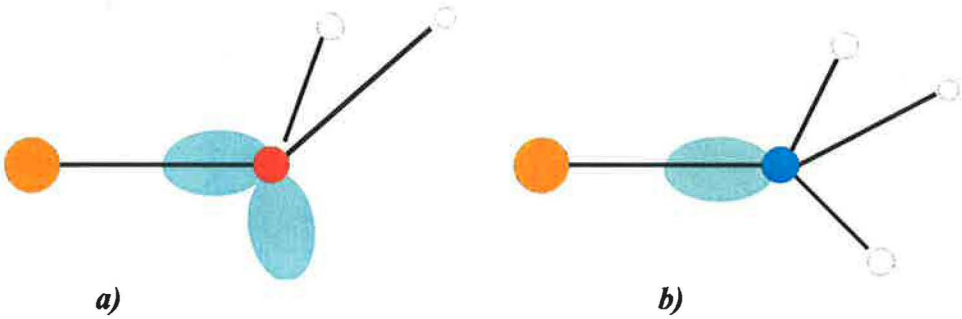

Figure 3.4. *Metal-ligand arrangements for* ***a)*** *water and* ***b)*** *ammonium molecules. Green ellipses represent dative lone pairs of ligands.*

Donation effect was investigated in terms of copper partial charge and occupations of Cu 4s and 3d AOs using NPA method. The analysis explains the strongest copper coordination-covalent interaction with two ligands in Cu(I), and four ligands in Cu(II) complexes by the most pronounced electron density redistribution. It also confirms copper-amine bonding to be preferred over copper-aqua one.

3.3 Copper Cations Interactions with Biologically Essential Types of Ligands

This work concerns small complexes of Cu(I)/Cu(II) cations with variable hydrogen sulphide-ammine-aqua ligand field. Investigation of such complexes is necessary in order to obtain deeper insight into behavior of copper cations in the presence of S-, N-, and O-types of ligands. These ligands represent biologically most common environment for copper.

The optimizations of the $[Cu(H_2S)_m(H_2O)_n(NH_3)_k]^{2+}$ complexes were performed at the DFT level (where *n*, *m* and k are equal to 0, 2, 4 and 6, along with the restriction $m + n + k = 4$ or 6). In the case of Cu(I) complexes, only the 4-ligated systems ($m + n + k = 4$) were examined since maximum coordination number four was reported in our previous studies. The optimizations resulted in various stable coordinations and following energy analyses revealed several trends:

a) The Cu(I) systems prefer coordination number two (followed by three and four) in the presence of the ammine and aqua ligand field. The 3- and 4-coordinated structures are favored when the H_2S molecules occupy the first solvation shell.
b) For the divalent copper compounds, the 4- and 5-coordinated structures represent the most stable forms, regardless of the ligand types.
c) The highest stabilization energies were found for ammine ligands followed by hydrogen-sulphide and aqua ligands in the case of the Cu(I) complexes. The order of the last two ligands is inverted in the Cu(II) systems due to a higher electrostatic contribution to the stabilization energy of aqua ligands.

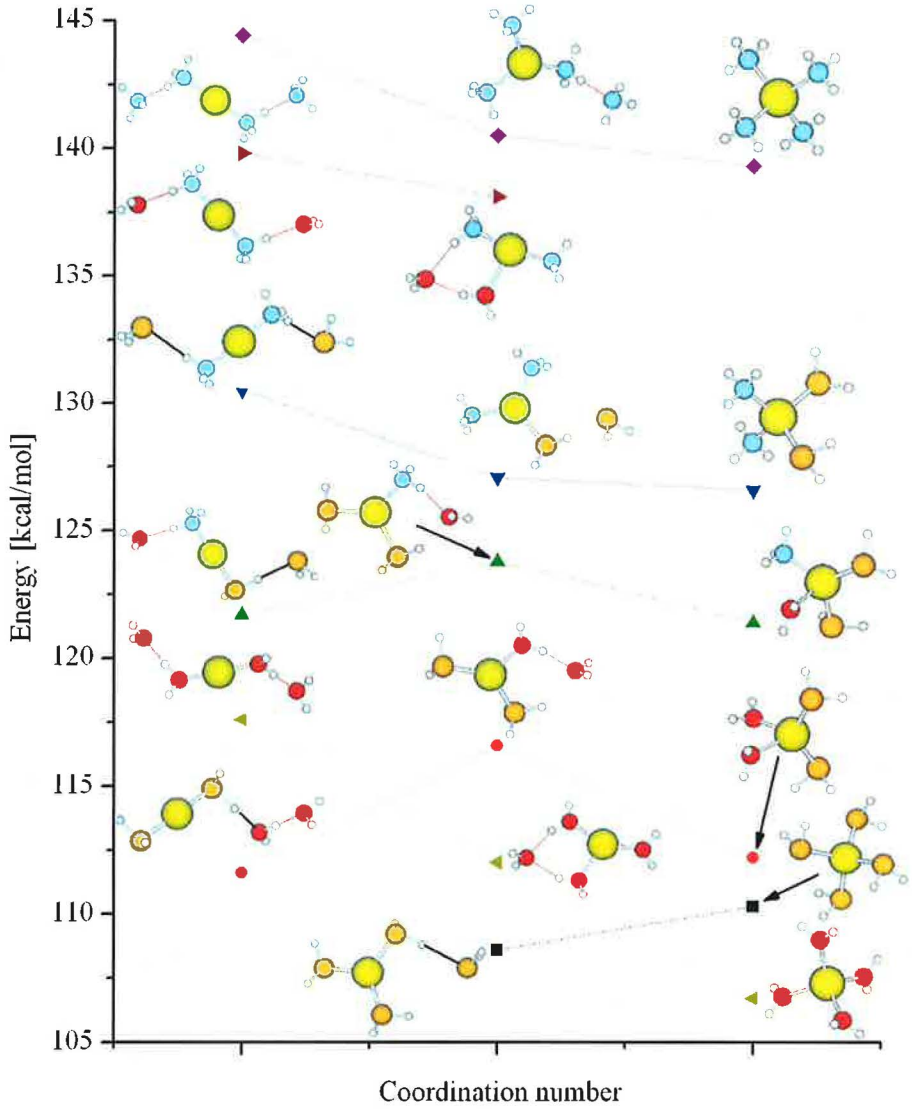

Figure 3.5. *Stabilization energies for the mixed* $[Cu(H_2S)_m(H_2O)_n(NH_3)_k]^+$ *compounds (*$n + m + k = 4$*).*

In order to explain our findings, molecular orbitals (***Figure 3.6***) and the NPA charge distribution were analyzed. The largest dative contribution to the Cu-X bond was obtained in the sulphur case followed by nitrogen. Oxygen exhibited the weakest donor ability. It is in agreement with the order of the softness parameter from the HSAB principle. It also solves why the higher coordination is stable for complexes of Cu^+ cation with hydrogen sulphide. The fact that water molecules often escape to the second solvation shell is linked with the strong hydrogen bonds formed by polar ligands. Such H-bonds can stabilize the system as well as dative bonds. Hence lower coordination occurs for polar NH_3 or H_2O ligands and higher coordination prevails in case of H_2S compounds, where weak H-bonds can be formed.

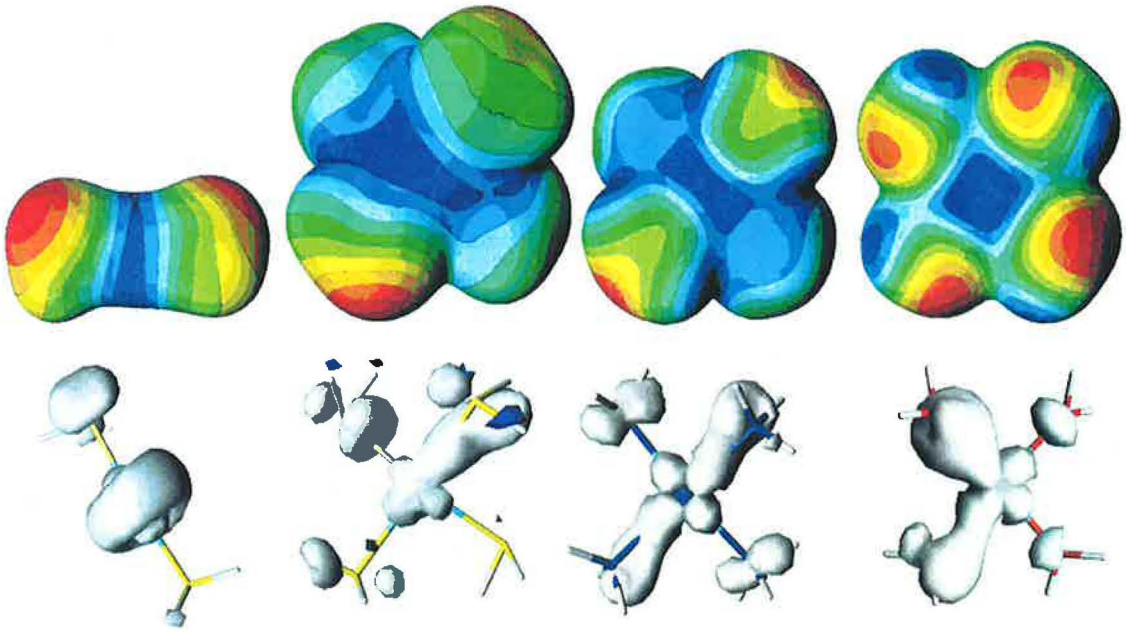

Figure 3.6. *The plots of spin-densities and maps of electrostatic potentials for the disulphide, square-planar tetraaqua, tetraamine, and tetrasulphide Cu(II) complexes.*

Revealed preferences can be generalized for peptide environment. Nitrogen containing ligands (like histidine) form stronger bonds with copper cations than the sulphur-ligands (methionine) or oxygen-coordinated glutamine. However, this preference must be taken with care since the remaining part of the ligated molecule can change electron density characteristics. Moreover, back-donation effect has to be considered, when ligand has LUMO (lowest unoccupied MO) of anti-bonding π-character.
In order to describe possible transitions between the Cu(I) and Cu(II) oxidation states (***Figure 3.7***), both vertical and adiabatic ionization potentials (IP) as well as electron affinities EA were calculated. The highest *IP* values were obtained for the complexes containing H_2S molecules.

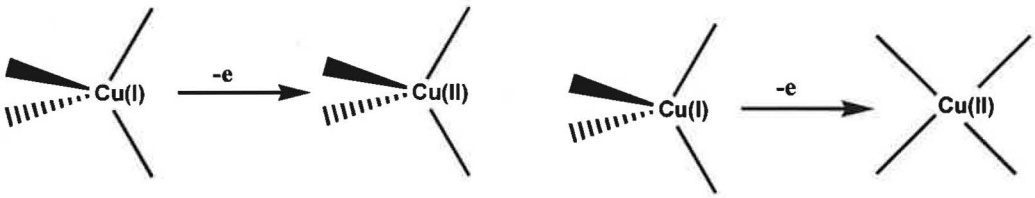

Figure 3.7. *Schema of vertical and adiabatic ionization for the 4-coordinated Cu(I) system.*

The data presented in this work provide an extended and systematic set of structures and energies for Cu(I)/Cu(II) compounds of biological relevance. Such data can be used for calibration of other computational methods such as Cu-containing force fields. It can also be used to rationalize selected aspects of the physical chemistry of Cu interactions in bio-environment.

3.4 Redox Centers of Blue Copper Proteins

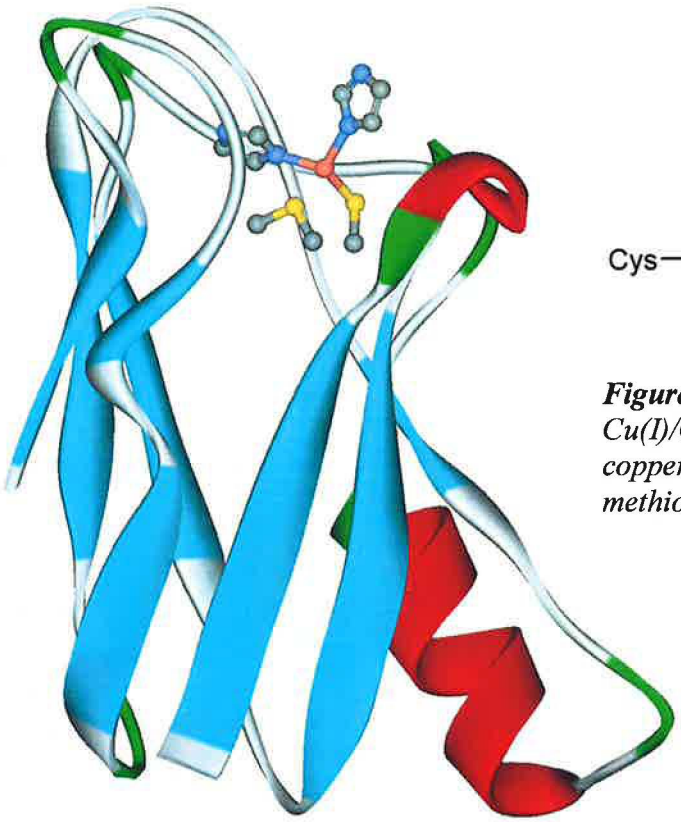

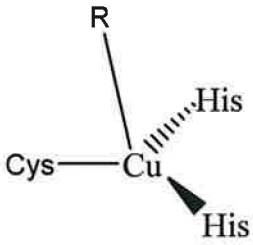

Figure 3.9. *4-coordinated Cu(I)/Cu(II) redox center of blue copper proteins. Residue R can be methionine or glutamine.*

Figure 3.8. *PDB structure of plastocyanin (1KDI).*

The work is focused on models of active mononuclear centers, which are present in blue copper proteins (***Figure 3.8***). Although this work utilizes experiences obtained from our previous papers concerning small inorganic models,[35,69,70] it is based on extensive quantum chemical investigation of these unusual redox centers. The study provides deeper insight into interactions in these Cu(I)/Cu(II) complexes than other papers and reviews.
In examined active sites, the Cu(I)/Cu(II) cation is coordinated by four ligands (***Figure 3.9***): cysteine, two histidines, and methionine (or glutamine). In the family of Type A blue proteins (with Met residue), the following protein structures from PDB database were considered: amicyanin, auracyanin, plastocyanin, and rustycyanin. In the case of Type B centers (with Gln residue), the following peptides were analyzed: mavicyanin, stellacyanin, and umecyanin. The studied systems were optimized at the DFT level in both oxidation states in vacuo and using conductor-like polarized continuum model (COSMO) in order to reflect the interaction with protein and water environment.

There is a number of works devoted to investigation of protein constraints on active centers in blue copper proteins. Earlier paper[128] suggested that there were no constraints on copper site geometry. However, such proposals had to be revised.[12,13,129] The role of axial ligand has also been widely studied.[2-4,12,130,131] This work provides answers to some

of the questions regarding structures, which are imposed by peptide backbone. For example, neither oxidized nor reduced protein structures exhibit their optimal geometries, which were obtained by full optimizations. When no constraints are applied, axial copper-ligand bond elongates/shortens in dependence of reduced/oxidized state of metal, regardless the type of 4th residue (Gln or Met). In reduced centers, relaxation of coordination bonds correspond to fact that Cu(I) complexes prefer geometry with lower-coordination (***Figure 3.10a***). Analogously, models of fully relaxed oxidized Cu(II) centers tend to four "equivalent" bonds (***Figure 3.10b***).

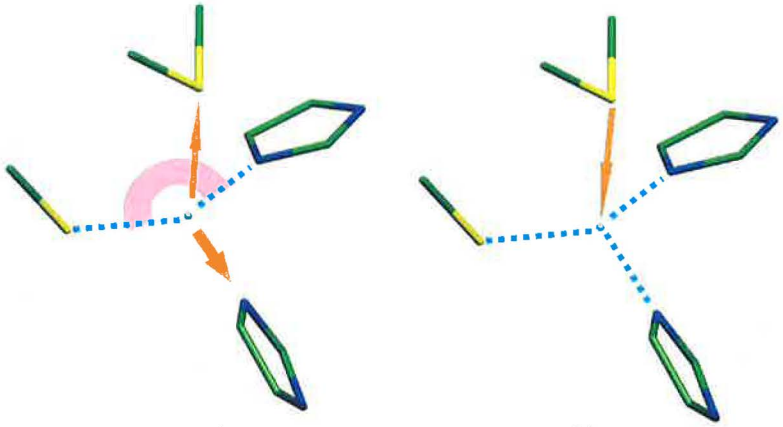

a) ***b)***

Figure 3.10. *Illustration of results of full optimization in vacuo for* ***a)*** *reduced Cu(I) and* ***b)*** *oxidized Cu(II) centers.*

Fully optimized oxidized Type B center exhibits several interesting features, which derive from its distinct geometry halfway between square-planar and tetrahedral. Atypical electronic structure is illustrated by its single occupied MO in ***Figure 3.11***. This complex also possesses very similar $g_{=}$ and $g_{\perp}$ values (in calculated EPR spectrum) in comparison with the rest of the models, where $g_{=}$ are larger than $g_{\perp}$.

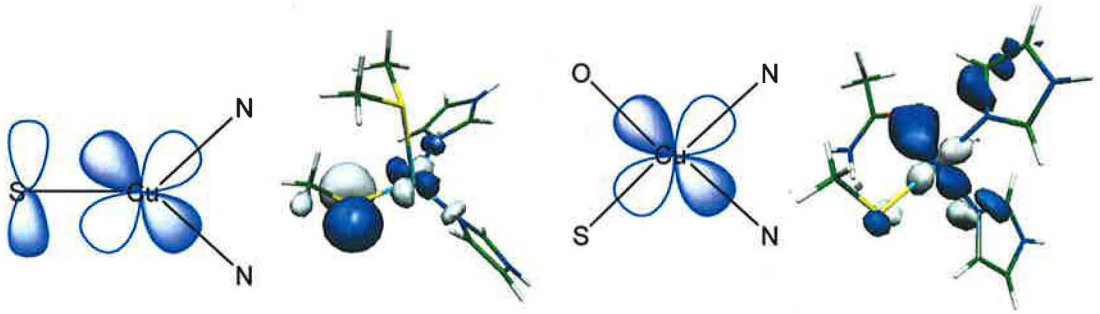

a) ***b)***

Figure 3.11. *The different schemes of SOMO (with examples) for* ***a)*** *Type A centers (protein constrained structure), and for* ***b)*** *fully optimized Type B center.*

Charge and spin distribution was obtained by NPA method. They revealed that most of the spin density (80-90%) is located on Cu-S(Cys) bond, which corresponds to strong dative interaction between copper cation and cystein model. Type B centers exhibit larger portion of spin density on Cu and greater copper partial charge in comparison with Type A centers. Such behavior reflects stronger ability of Gln residue to donate electron density.

Interaction with protein-like and water environment was provided by COSMO. Surrounding continuum with non-zero permittivity influenced the studied systems by screening of electrostatic interaction between Cu(I)/Cu(II) cation and ligands (especially negatively charged cysteine model). Estimated stabilization and bonding energies showed several trends. Under protein constraints, reduced Cu(I) complexes are less stable than oxidized complexes in the both Types of centers. From ***Figure 3.12***, larger energy relaxation after full optimization can be observed for Type B centers. These relaxation energies are the least pronounced in peptide-like environment.

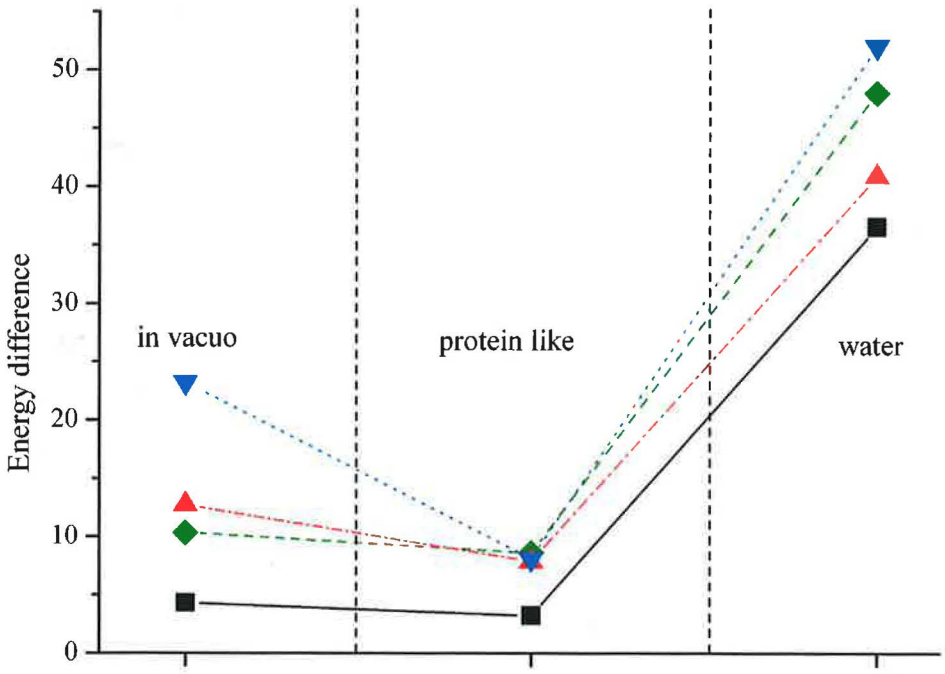

Figure 3.12. *The relaxation energies (in kcal/mol), which were estimated as relative differences of stabilization energies of constrained and fully optimized structures for:*
—■— *oxidized Type A centers,* --◆-- *oxidized Type B centers,*
-.-▲-.- *reduced Type A centers, and* ...▼... *reduced Type B centers.*

In order to describe transition between Cu(II) and Cu(I) oxidation states, ionization potentials were computed. For protein constrained structures, ***IP***(type A) > ***IP***(type B) trend was obtained for all types of environment. Interestingly, the order is altered for fully optimized complexes in vacuo and in water. It reflexes the ability of surrounding to

influence the redox properties of studied proteins. These redox processes are illustrated in ***Figures 3.13***. Although our calculations are not able to reveal redox potential E_0 values for individual proteins, it is possible to compare relative difference between type A and type B proteins. The relative difference $\Delta E_0 = 0.14$ eV obtained from experiment is in good agreement with the difference ***IP***(type A) - ***IP***(type B) from present work, 0.20 eV.

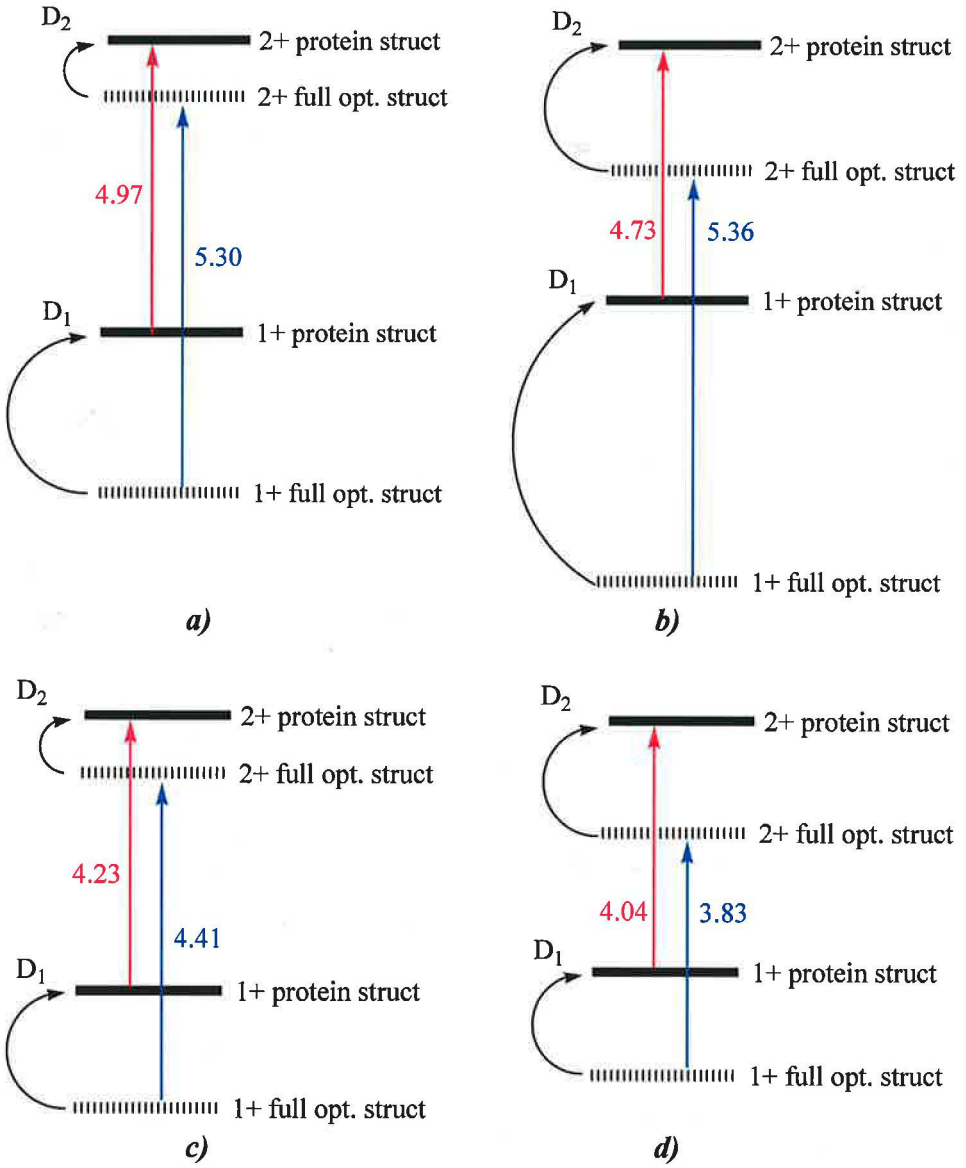

Figure 3.13*. The studied redox processes for* ***a)*** *Type A and* ***b)*** *Type B centers in vacuo. Scheme is also illustrated for centers* ***c)*** *and* ***d)*** *optimized in protein-like environment. Solid and dashed lines stand for energies of crystal structures and fully optimized structures, respectively. Red and blue arrows represent adiabatic ionization potentials.*

3.5 Hydrated Cu(II) in Interaction with Guanine

Present study[49] explores the hydrated Cu(II)(N7-Guanine) structures. Detailed optimization revealed large number of minima structures on potential energy surface. For selected conformers, several types of energy decompositions were performed together with determination of electronic properties (partial charges, electron spin densities, electrostatic potentials, MO analysis).

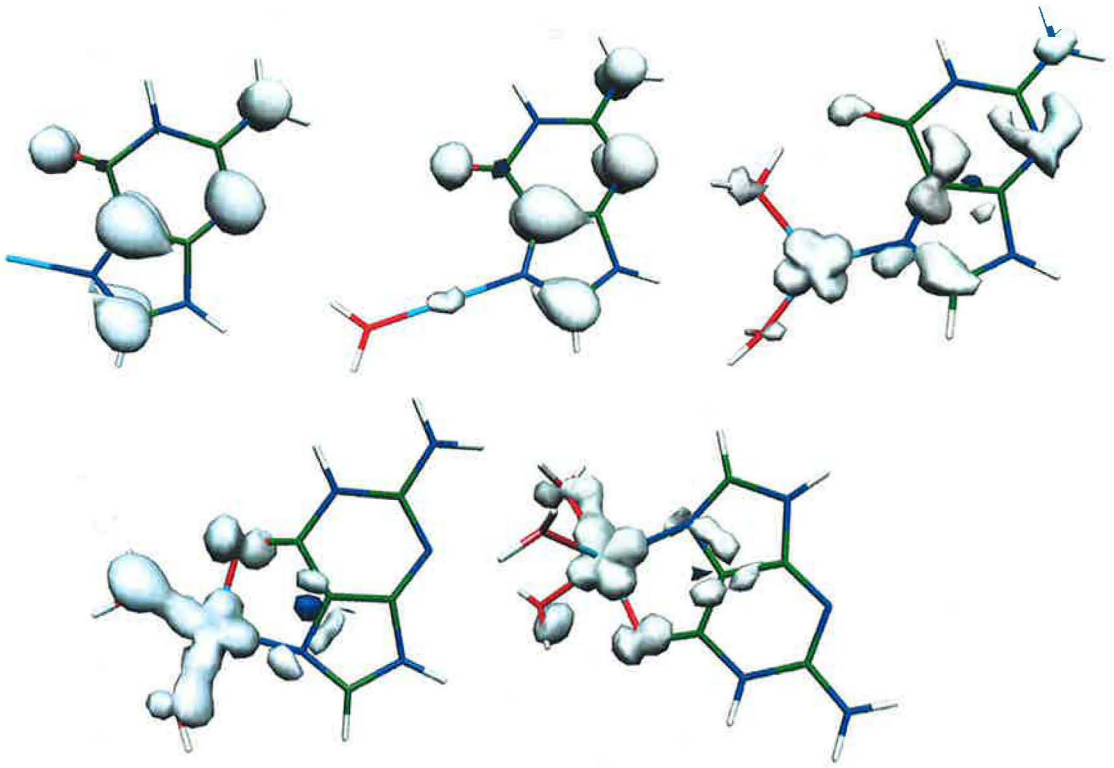

Figure 3.14. *Plots of spin density for the selected* $[Cu(II)G(H_2O)_n]^{2+}$ *complexes, where n varies from 0 to 4.*

For system without water molecules or with one water, charge transfer from guanine to Cu(II) occurs, which results in reduced Cu(I) cation. A complex with two aqua ligands is a borderline system with charge +0.7e on guanine with similar amount of spin density (0.62) localized there. Only when four-coordination on copper was achieved, the prevailing electron spin density (more than 0.7) is localized on copper cation. Described electron transfer is illustrated in ***Figure 3.14***.

Energy analyses revealed several trends:

a) In case of lower numbers of coordinated aqua ligands, the three-aqua Cu-(N7-guanine) structure is preffered over diaqua Cu-(N7,O6-guanine) chelate by more than 15 kcal/mol.
b) Similar situation occurs for tetraaqua complexes where the largest stability was obtained for three coordinated aqua ligands with one water molecule in second solvation shell of Cu(II) cation.

c) Moreover neither pentacoordinated triaqua chelate is more stable than tetracoordinated complex (***Figure 3.15***).

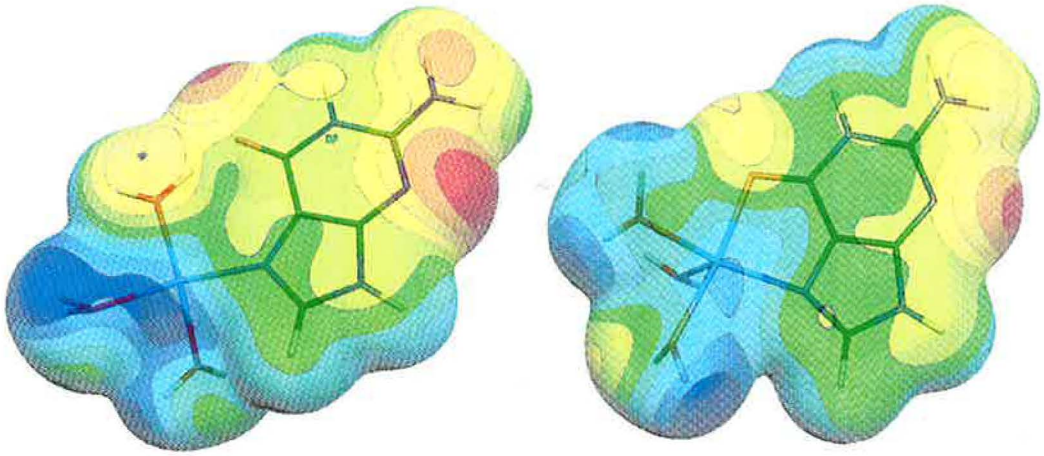

Figure 3.15. *The structures of the 4-coordinated and 5-coordinated (chelate) triaqua complexes with the maps of electrostatic potentials.*

It was found that more bulky guanine ligand causes less convenient pentacoordination in these complexes than in case of small inorganic complexes above.[69,70]

3.7 Interstrand cisplatin and transplatin bridges

This work investigates theoretical models of various platinum cross-links (***Figure 3.16***) with two DNA bases, namely: adenine, cytosine, and guanine. Such structures occur in many cis/trans-platinated double-helixes or single-stranded adducts. In these models, no sterical hindrance from sugar-phosphate backbone or other surroundings are considered. Such restrictions can change bonding picture partially but hopefully the basic energy characteristics will not be changed substantially.

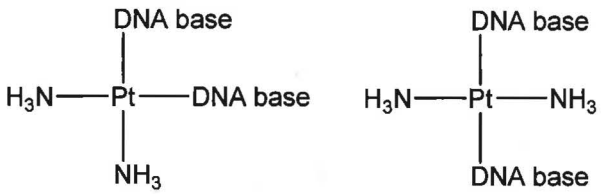

Figure 3.16. *Cis and trans-platin cross-links with two DNA bases.*

The optimizations of the explored structures were performed at the DFT level. For the single-point energy and electron-property analyses, the perturbation theory at the MP2 level was employed. It was found that the most stable structures are the diguanine complexes (***Figure 3.17***) followed by guanine-cytosine Pt-cross-links. Even less stable complexes contain adenine.
The bond-dissociation energies (BDE) were calculated to elucidate the coordination competition of different DNA bases. The strength of Pt-N bonds follows the order:

guanine > cytosine > adenine. It is in accord with the stabilization energies. Moreover, these values allow to further estimate energy contributions of hydrogen-bonding.

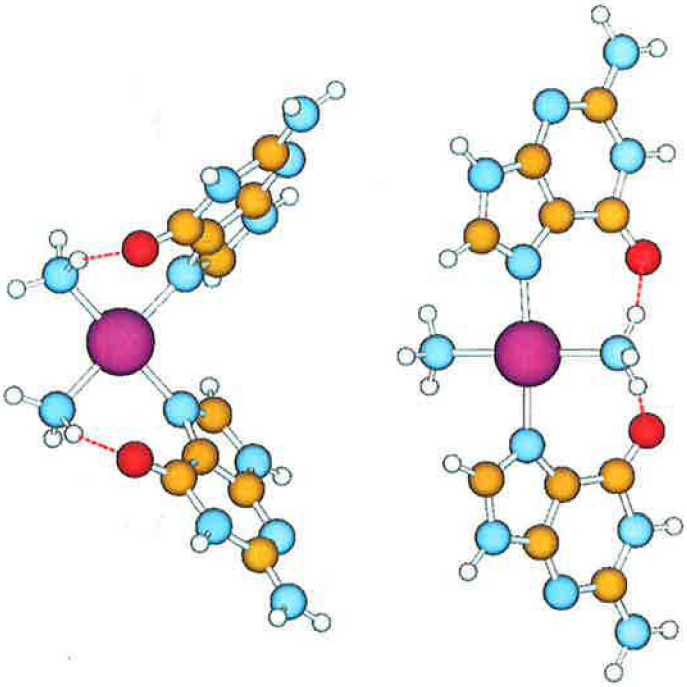

Figure 3.17. *Cis- and trans-platin adducts with two guanine bases in the head-to-head conformation.*

For better understanding dative and electrostatic contributions to Pt-N bonds, Natural Population Analysis (NPA), determination of electrostatic potentials, and canonical Molecular Orbital description of the examined systems were done. The most positive partial atomic charge on Pt was found in diguanine systems. It points to relatively smaller donation of electron density from the guanine bases in comparison with other explored nucleobases, which can be ordered as follows: guanine-adenine and guanine-cytosine adducts. Especially, structures formed with cytosine and guanine bound in N^1 position display significantly lowest charges. The strength of Pt-N bonds can be explained as a sum of dative interaction and electrostatic forces, which are larger in guanine case. Polarization effects can be deduced from the changes of partial charges on the selected atoms. The calculated tensor axes of base polarizability decrease as follows: N1-guanine > N7-guanine > adenine > cytosine. Dipole moments and main axes of polarizability tensor can be seen from ***Figure 3.18***.

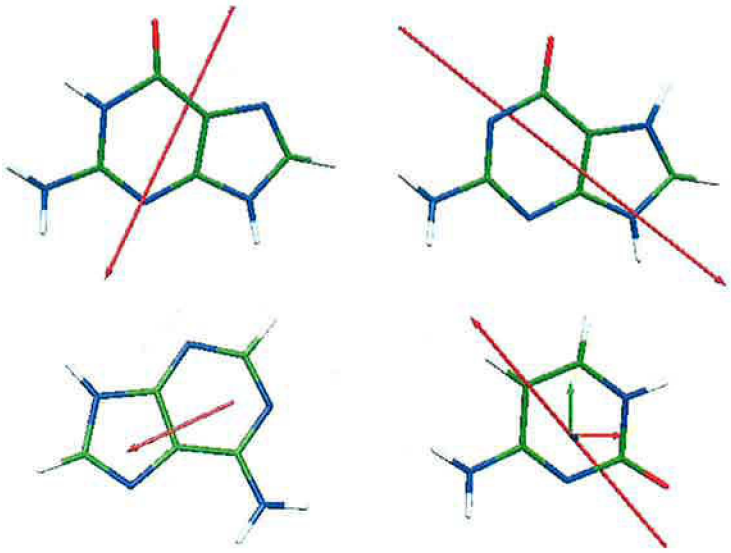

Figure 3.18. *Optimized conformers of DNA bases and their dipole moments*

The thermodynamics (Gibbs heat of reaction) of aqua-ligand replacement by the second DNA bases were evaluated and discussed. It confirms founding from other energy analyses.

3.6 EPR Spectrum of Cu-Quinone Complexes

The $[(L)Cu^{n+}(Q)^{n-}]$, where L = (mtq - 8-methylthioquinoline (***Figure 3.19a***) or mmb - 1-methyl-2- (methylthiomethyl)-1 benzimidazole (***Figure 3.19b***)) and Q=2-methyl-o-quinone, complexes were examined at the DFT level in vacuo and in solvent modeled by conductor-like polarizable continuum model.[79] In such neutral open shell systems, the central Cu^{+} or Cu^{2+} cation with $3d^{10}$ or $3d^{9}$ valence electron configuration is coordinated by neutral ligand and charged quinon (Q^{1-} or Q^{2-}):

$[(L)Cu^{II}(Q^{2-})] \longleftrightarrow [(L)Cu^{I}(Q^{-})]$.

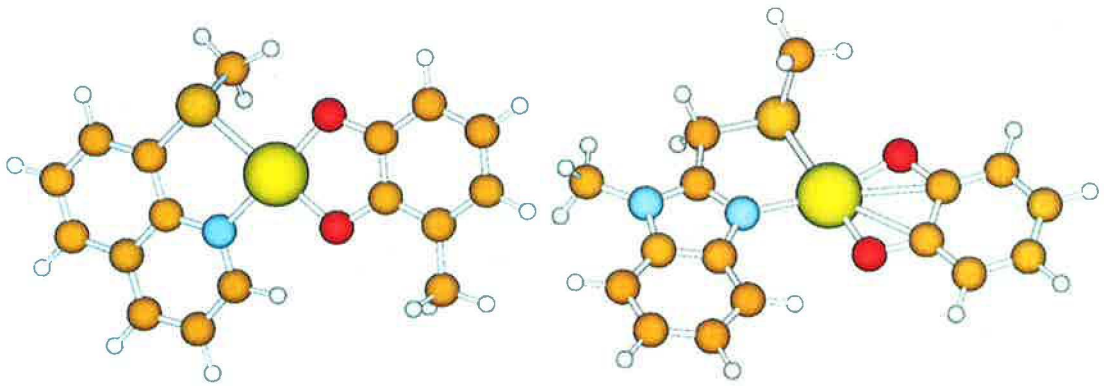

a) ***b)***

Figure 3.19. *Structures of pseudo square-planar* ***a)*** *Cu-quinon-mtq and* ***b)*** *Cu-quinon-mmb tautomers obtained at the DFT/CPCM level.*

The complexes were also studied by EPR laboratory at Stuttgart University, where two distinct g-tensors were obtained for each valence tautomer. Present work provides interpretation of experimental values as well as deeper analyses of charge and spin distribution.

The pseudo square-planar $Cu^{2+}Q^{2-}$ complexes exhibit spin density localized on copper resulting in higher g-factors. As indicated the transition energy search, potential energy surfaces were rather flat. The slightly more stable pseudo tetrahedral $Cu^{+}Q^{\cdot}$ tautomers (4.8 kcal/mol and 3.9 kcal/mol for mmb and mtq ligand) posses unpaired electron delocalized on quinon ring giving isotropic g-factors close to those of free electron (2.0023). The calculated EPR anisotropic g-values reflect the differences in electron density redistribution in agreement with experiment.

4 Conclusion

Primary objective of my thesis is to explore the aspects of copper cations interaction in organism. This goal was accomplished by using quantum chemical methods.
The work begins with investigation of Cu(I)/Cu(II) cations hydration at the DFT and ab initio level of theory.[70] Following studies extend subjects of copper interaction by biologically essential types of ligands.[35,69] The detailed study of copper cations in variable hydrogen sulphide-aqua-ammine ligand fields revealed several trends. The most important findings are:

a) The Cu(I) systems prefer two-coordinated structures, when aqua and ammine ligands are considered. In case of H_2S molecules, the most stable complexes are four-coordinated.
b) The complexes of Cu^{2+} cation (with d^9 electron configuration) exhibit preference of four- and five-coordinated geometries, regardless the types of interacting ligands.
c) The strongest metal-ligand interaction occurred with NH_3 molecules followed by almost equivalent H_2S and H_2O ligands.

The study of such small inorganic complexes gives an advantage for later exploration of larger biological systems.
Interaction of hydrated Cu(II) with guanine was examined.[49] Moreover, Pt-bridges in various single-strand and double-helix DNA/RNA sequences were studied.[118]
Crucial portion[34] of my work presents theoretical model of redox centers of blue copper proteins, which are involved in electron-transfer. It is based on sequential structure optimizations followed by further energy and electron structure analyses of these active centers in both reduced and oxidized states. Other published works did not provide that thorough investigation. Questions regarding the structure constraints imposed by protein backbone as well as the role of axial ligand are answered.
In cooperation with the EPR laboratory at Stuttgart University, several copper-quinone valence tautomers were examined in order to interpret experimental results.[79]
The thesis led to seven published or submitted articles in recognized international journals and demonstrates successful application of modern quantum chemical methods in study of transition metals activity in a living cell.

References

(1) Wang, X.; Berry, S. M.; Xia, Y.; Lu, Y. *J. Am. Chem. Soc.* **1999**, *121*, 7449.
(2) Palmer, A. E.; Randall, D. W.; Xu, F.; Solomon, E. I. *J Am. Chem. Soc.* **1999**, *121*, 7138.
(3) Randall, D. W.; Gamelin, D. R.; LaCroix, L. B.; Solomon, E. I. *J. Biol. Inorg. Chem.* **2000**, *5*, 15.
(4) Randall, D. W.; George, S. D.; Hedman, B.; Hodgson, K. O.; Fujisawa, K.; Solomon, E. I. *J. Am. Chem. Soc.* **2000**, *122*, 11620.
(5) Book, L. D.; Arnett, D. C.; Hu, H.; Scherer, N. F. *J. Phys. Chem. A* **1998**, *102*, 4350.
(6) Fraga, E.; Webb, M. A.; Loppnow, G. R. *J. Phys. Chem.* **1996**, *100*, 3278.
(7) Holland, A. W.; Bergman, R. G. *J. Am. Chem. Soc.* **2002**, *124*, 9010.
(8) Holland, P. L.; Tolman, W. B. *J Am Chem. Soc.* **1999**, *121*, 7270.
(9) Taylor, M. K.; Stevenson, D. E.; Berlouis, L. E. A.; Kennedy, A. R.; Reglinski, J. *J. Innorg. Biochem.* **2005**, *100*, 250.
(10) Siegbahn. Electronic Structure Calculations for Molecules Containing Transition Metals. In *Advances in Chemical Physics, Volume XCIII*; Prigogine, I., Rice, S. A., Eds.; John Wilet & Sons, Ltd., 1996; Vol. XCIII; pp 333.
(11) Olsson, M. H. M.; Hong, G. Y.; Warshel, A. *J. Am. Chem. Soc.* **2003**, *125*, 5025.
(12) Olsson, M. H. M.; Ryde, U. *J. Biol. Inorg. Chem.* **1999**, *4*, 654.
(13) Olsson, M. H. M.; Ryde, U.; Roos, B. O.; Pierloot, K. *J. Biol. Inorg. Chem.* **1998**, *3*, 109.
(14) Warshel, A. *Computer Modeling of Chemical Reactions in Enzymes and Solutions*; John Wiley & Sons, Ltd.: New York, 1991.
(15) Prabhakar, R.; Siegbahn, P. E. M. *J. Phys. Chem. B* **2003**, *107*, 3944.
(16) Sabolovic, J.; Liedl, K. R. *J. Am. Chem. Soc.* **1999**.
(17) Sabolovic, J.; Tautermann, C. S.; Loerting, T.; Liedl, K. R. *Inorg. Chem.* **2003**, *42*, 2268.
(18) Katz, A.; Shimoni-Livny, L.; Navon, O.; Navon, N.; Bock, C.; Glusker, J. *Helv. Chim. Acta* **2003**, *86*, 1320
(19) Rulíšek, L. *Chemicke Listy* **2002**, *96*, 132.
(20) Rulíšek, L.; Havlas, Z. *J. Am. Chem. Soc.* **2000**, *122*, 10428.
(21) Rulíšek, L.; Havlas, Z. *J. Phys. Chem. A* **2002**, *106*, 3855.
(22) Rulíšek, L.; Havlas, Z. *J. Phys. Chem. B* **2003**, *107*, 2376.
(23) Bertran, J.; Rodrigues-Santiago, L.; Sodupe, M. *J. Phys. Chem. B* **1999**, *103*, 2310.
(24) Shoeib, T.; Rodriquez, C. F.; Siu, K. W. M.; Hopkinson, A. C. *Phys. Chem. Chem. Phys.* **2001**, *3*, 853.
(25) Caraiman, D.; Shoeib, T.; Siu, K.; Hopkinson, A.; Bohme, D. *Int. J. Mass Spectrom.* **2003**, *228*, 629.
(26) Santra, S.; Zhang, P.; Tan, W. *J. Phys. Chem. A* **2000**, *104*, 12021.
(27) Manikandan, P.; Epel, B.; Goldfarb, D. *Inorg. Chem.* **2001**, *40*, 781.
(28) Shimizu, K.; Maeshima, H.; Yoshida, H.; Satsuma, A.; Hattori, T. *Phys. Chem. Chem. Phys.* **2001**, *3*, 862.
(29) Sigman, J. A.; Kwok, B. C.; Gengenbach, A.; Lu, Y. *J Am. Chem. Soc.* **1999**, *121*, 8949.
(30) Gray, H. B.; Malmstroem, B. G.; Williams, R. J. P. *J. Biol. Inorg. Chem.* **2000**, *5*, 551.
(31) Solomon, E. I.; Baldwin, M. J.; Lowery, M. D. *Chem. Rev.* **1992**, *92*, 521.
(32) Solomon, E. I.; Szilagyi, R. K.; George, S. D.; Basumallick, L. *Chem. Rev.* **2004**, *104*, 419.
(33) Mirica, L. M.; Ottenwaelder, X.; Stack, T. D. P. *Chem. Rev.* **2004**, *104*, 1013.
(34) Pavelka, M.; Burda, J. V. *J. Phys. Chem B* **2006**, submitted.
(35) Pavelka, M.; Šimánek, M.; Šponer, J.; Burda, J. V. *J. Phys. Chem. A* **2006**, *110*, 4795.
(36) Hemmert, C.; Pitie, M.; Renz, M.; Gornitzka, H.; Soulet, S.; Meunier, B. *J. Biol. Inorg. Chem.* **2001**, *6*, 14.
(37) Hackl, E. V.; Kornilova, S. V.; Kapinos, L. E.; Andruschenko, V. V.; Galkin, V. L.; Grigoriev, D. N.; Blagoi, Y. P. *J. Molec. Struct.* **1997**, *408*, 229.
(38) Atwell, S.; Meggers, E.; Spraggon, G.; Schultz, P. G. *J. Am. Chem. Soc.* **2001**, *123*, 12364.
(39) Meggers, E.; Holland, P. L.; Tolman, W. B.; Romesberg, F. E.; Schultz, P. G. *J. Am. Chem. Soc.* **2000**, *122*, 10714.
(40) Schoentjes, B.; Lehn, J.-M. *Helv. Chim. Acta* **1995**, *78*, 1.

(41) Lamsabhi, A.; Alcami, M.; Mo, O.; Yanez, M.; Tortajada, J. *ChemPhysChem* **2004**, *5*, 1871.
(42) Gasowska, A.; Lomozik, L. *Monatshefte fur Chemie* **1995**, *126*, 13.
(43) Burda, J. V.; Šponer, J.; Hobza, P. *J. Phys. Chem.* **1996**, *100*, 7250.
(44) Burda, J. V.; Šponer, J.; Leszczynski, J.; Hobza, P. *J. Phys. Chem. B* **1997**, *101*, 9670.
(45) Šponer, J.; Sabat, M.; Burda, J.; Leszczynski, J.; Hobza, P.; Lippert, B. *J. Biol. Inorg. Chem.* **1999**, *4*, 537.
(46) Rulíšek, L.; Šponer, J. *Journal of Physical Chemistry B* **2003**, *106*, 1913.
(47) Tachikawa, H. *Chem. Phys.Lett.* **1996**, *260*, 582.
(48) Burda, J. V.; Shukla, M. K.; Leszczynski, J. *J. Mol. Model.* **2005**, *11*, 362.
(49) Pavelka, M.; Shukla, M. K.; Leszczynski, J.; Burda, J. V. *J. Phys. Chem A* **2006**, *in preparation.*
(50) Hamilton, I. P. *Chem. Phys. Lett.* **2004**, *390*, 517.
(51) Feller, D.; Glendening, E. D.; de Jong, W. A. *J. Chem. Phys.* **1999**, *110*, 1475.
(52) Schroeder, D.; Schwartz, H.; Wu, J.; Wesdemiotis, C. *Chem. Phys. Lett.* **2001**, *343*, 258.
(53) Marini, G. W.; Liedl, K. R.; Rode, B. M. *J. Phys. Chem. A* **1999**, *103*, 11387.
(54) Schwenk, C.; Rode, B. *ChemPhysChem* **2004**, *5*, 342.
(55) Schwenk, C. F.; Rode, B. M. *Phys. Chem. Chem. Phys.* **2003**, *5*, 3418.
(56) Pranowo, H. *Chem. Phys.* **2003**, *291*, 153.
(57) Berces, A.; Nukada, T.; Margl, P.; Ziegler, T. *J. Phys. Chem. A* **1999**, *103*, 9693.
(58) Pranowo, H. D.; Rode, B. M. *J. Phys. Chem. A* **1999**, *103*, 4298.
(59) Pranowo, H. D.; Setiajin, A. H. B.; Rode, B. M. *J. Phys. Chem. A* **1999**, *103*, 11115.
(60) Pranowo, H. D.; Rode, B. M. *Chem. Phys* **2001**, *263*, 1.
(61) Haeffner, F.; Brinck, T.; Haeberlein, M.; Moberg, C. *Chem. Phys. Lett.* **1997**, *397*, 39.
(62) Cordeiro, N. M. D. S.; Gomes, J. A. N. F. *J. Comput. Chem.* **1993**, *14*, 629.
(63) Subramanian, V.; Shankaranarayanan, C.; Nair, B. U.; Kanthimathi, M.; Manickkavachagam, R.; Ramasami, T. *Chem. Phys. Lett.* **1997**, *274*, 275.
(64) Gresh, N.; Policar, C.; Giessner-Prettre, C. *J. Phys. Chem.* **2002**, *106*, 5660.
(65) Ledecq, M.; Lebon, F.; Durant, F.; Giessner-Prettre, C.; Marquez, A.; Gresh, N. *J. Phys. Chem. B* **2003**, *107*, 10640.
(66) Schwerdtfeger, P.; Krawczyk, R. P.; Hammerl, A.; Brown, R. *Inorg. Chem.* **2004**, *43*, 6707.
(67) Neese, F. *Magn. Res. Chem.* **2004**, *42*, S187.
(68) Konopka, M.; Rousseau, R.; Stich, I.; Marx, D. *J. Am. Chem. Soc.* **2004**, *126*, 12103.
(69) Pavelka, M.; Burda, J. V. *Chem. Phys.* **2005**, *312*, 193.
(70) Burda, J. V.; Pavelka, M.; Šimánek, M. *J. Molec. Struct.* **2004**, *683*, 183.
(71) Mure, M. *Acc. Chem. Res.* **2004**, *37*, 131.
(72) Rall, J.; Wanner, M.; Albrecht, M.; Hornung, F. M.; Kaim, W. *Chem. Eur. J.* **1999**, *5*, 2802.
(73) Kaim, W.; Wanner, M.; Knodler, A.; Zalis, S. *Inorg. Chim. Acta* **2002**, *337*, 163.
(74) Ye, S.; Sarkar, B.; Niemeyer, M.; Kaim, W. *Eur. J. Inorg. Chem.* **2005**, 4735.
(75) Kahn, O.; Launay, J. P. *Chemtronics* **1998**, *3*, 140.
(76) Speier, G.; Tyeklár, Z.; Töth, P.; Speier, E.; Tisza, S.; Rockenbauer, A.; Whalen, A. M.; Alkire, N.; Pierpont, C. G. *Inorg. Chem.* **2001**, *40*, 5653.
(77) Dei, A.; Gatteschi, D.; Sangregorio, C.; Sorace, L. *Acc. Chem. Res.* **2004**, *37*, 827.
(78) Ohtsu, H.; Tanaka, K. *Angew. Chem. Int. Ed.* **2004**, *43*, 6301.
(79) Pavelka, M.; Sarkar, B.; Kaim, W.; Záliš, S. *Inorg. Chem.* **2006**, submitted.
(80) Kaim, W.; Schwederski, B. *Bioinorganic Chemistry: Inorganic Elements in the Chemistry of Life.*; John Wiley & Sons Ltd: Chichester, England, 1994.
(81) Beljanski, V.; Villanueva, J. M.; Doetsch, P. W.; al., e. *J. Am. Chem. Soc.* **2005**, *127*, 15833.
(82) Najajreh, Y.; Kasparkova, J.; Marini, V.; al., e. *J. Biol. Innorg. Chem.* **2005**, *10*, 722.
(83) Marini, V.; Christofis, P.; Novakova, O.; al., e. *Nucleic Acids Res.* **2005**, *33*, 5819.
(84) Bhattacharyya, D.; Marzilli, P. A.; Marzilli, L. G. *Inor. Chem.* **2005**, *44*, 7644.
(85) Brabec, V.; Kasparkova, J. *Drug Res. Upd.* **2005**, *8*, 131.
(86) Malina, J.; Voitiskova, M.; Brabec, V.; al., e. *Biochem. Biophys. Res. Comm.* **2005**, *332*, 1034.
(87) Bivian-Castro, E. Y.; Roitzsch, M.; Gupta, D.; al., e. *Innorg. Chim. Act.* **2005**, *358*, 2395.
(88) Barnes, K. R.; Lippard, S. J. *Met. Ion. Biol. Sys.* **2004**, *42*, 143.
(89) Carlone, M.; Marzilli, L. G.; Natile, G. *Eur. J. Innorg. Chem.* **2005**, *7*, 1264.
(90) Wing, R. M.; Pjura, P.; Drew, H. R.; Dickerson, R. E. *EMBO J.* **1984**, *3*, 1201.
(91) Takahara, P. M.; Rosenzweig, A. C.; Frederick, C. A.; Lippard, S. J. *Nature* **1995**, *377*, 649.

(92) Lilley, D. M. J. *J. Biol. Inorg. Chem.* **1996**, *1*, 189.
(93) Ohndorf, U.-M.; Rould, M. A.; He, Q.; Pabo, C. O.; Lippard, S. J. *Nature* **1999**, *399*, 708.
(94) Jamieson, E. R.; Lippard, S. J. *Chem. Rev.* **1999**, *99*, 2467.
(95) Coste, F.; Malinge, J. M.; Serre, L.; Shepard, W.; Roth, M.; Leng, M.; Zelwer, C. *Nucleic Acids Res.* **1999**, *27*, 1837.
(96) Silverman, A. P.; Bu, W.; Cohen, S. M.; Lippard, S. J. *J. Biol. Chem.* **2002**, *277*, 49743.
(97) Parkinson, G. N.; Arvantis, G. M.; Lessinger, L.; Ginell, S. L.; Jones, R.; Gaffney, B.; Berman, H. M. *Biochemistry* **1995**, *34*, 15487.
(98) Kašparková, J.; Mackay, F. S.; Brabec, V.; Sadler, P. J. *J. Biol. Inorg. Chem.* **2003**, *8*, 741.
(99) Choi, S.; Delaney, S.; Orbai, L.; Padgett, E. J.; Hakemian, A. S. *Inorg. Chem.* **2001**, *40*, 5481.
(100) Junicke, H.; Bruhn, C.; Kluge, R.; Serianni, A. S.; Steinborn, D. *J. Am. Chem. Soc.* **1999**, *121*, 6232.
(101) Song, R.; Kim, K. M.; Lee, S. S.; Sohn, Y. S. *Inorg. Chem.* **2000**, *39*, 3567.
(102) Watanabe, M.; Kai, M.; Asanuma, S.; Yoshikane, M.; Horiuchi, A.; Ogasawara, A.; Watanabe, T.; Mikami, T.; Matsumoto, T. *Inor. Chem.* **2001**, *40*, 1496.
(103) Wong, E.; Giandomenico, C. M. *Chem. Rev.* **1999**, *99*, 2451.
(104) Reedijk, J. *Chem. Comm.* **1996**, *7*, 801.
(105) Carloni, P.; Sprik, M.; Andreoni, W. *J. Phys. Chem. B* **2000**, *104*, 823.
(106) Baik, M.-H.; Friesner, R. A.; Lippard, S. J. *J. Am. Chem. Soc.* **2002**, *124*, 4495.
(107) Baik, M. H.; Friesner, R. A.; Lippard, S. J. *Inorganic Chemistry* **2003**, *42*, 8615.
(108) Eriksson, L. A.; Raber, J.; Zhu, C. *J. Phys. Chem.* **2005**, 000.
(109) Chval, Z.; Šíp, M. *Collection of Czechoslovak Chemical Communications* **2003**, *68*, 1105.
(110) Burda, J. V.; Leszczynski, J. *Inorg. Chem.* **2003**, *42.*, 7162.
(111) Burda, J. V.; Šponer, J.; Hrabáková, J.; Zeizinger, M.; Leszczynski, J. *J. Phys. Chem. B* **2003**, *107*, 5349.
(112) Zeizinger, M.; Burda, J. V.; Leszczynski, J. *PCCP* **2004**, *6*, 3585.
(113) Deubel, D. V. *J. Am. Chem. Soc.* **2002**, *124*, 12312.
(114) Zeizinger, M.; Burda, J. V.; Šponer, J.; Kapsa, V.; Leszczynski, J. *J. Phys. Chem. A*, **2001**, *105*, 8086.
(115) Burda, J. V.; Zeizinger, M.; Leszczynski, J. *J. Chem. Phys.* **2004**, *120*, 1253.
(116) Burda, J. V.; Zeizinger, M.; Leszczynski, J. *J. Comput. Chem.* **2005**, *29*, 907.
(117) Zimmermann, T.; Zeizinger, M.; Burda, J. V. *J. Phys. Chem. B* **2005**, *99*, 2184.
(118) Pavelka, M.; Burda, J. V. *J. Mol. Model.* **2005**, in print.
(119) Møller, C.; Plesset, M. S. *Phys. Rev.* **1934**, *46*, 618–622.
(120) Cízek, J.; Paldus, J. *Int. J. Quantum Chem.* **1971**, *5*, 359.
(121) Hohenberg, P. C.; Kohn, W. *Phys. Rev.* **1964**, *136*, B864.
(122) Hohenberg, P. C.; Kohn, W.; Sham, L. J. *Advances in quantum Chemistry* **1990**, *21*.
(123) Perdew, J. P.; Chevary, J. A.; Vosko, S. H.; Jackson, K. A.; Pederson, M. R.; Singh, D. J.; Fiolhais, C. *Phys. Rev.* **1992**, *??*, 6671.
(124) Lee, C.; Yang, W.; Parr, R. G. *Phys. Rev.* **1988**, *37*, 785.
(125) Casida, M. E.; Jamorski, C.; Casida, K. C.; Salahub, D. R. *J. Chem. Phys.* **1998**, *108*, 4439.
(126) Reed, A. E.; Weinstock, R. B.; Weinhold, F. *J. Chem. Phys.* **1985**, *83*, 735.
(127) Ortiz, J. V. *J. Chem. Phys.* **1988**, *89*, 6348.
(128) Ryde, U.; Olsson, M. H. M.; Pierloot, K.; Roos, B. O. *J. Mol. Biol.* **1996**, *261*, 586.
(129) Pierloot, K.; De Kerpel, J. O. A.; Ryde, U.; Roos, B. O. *J. Am. Chem. Soc.* **1997**, *119*, 218.
(130) Guckert, J. A.; Lowery, M. D.; Solomon, E. I. *J. Am. Chem. Soc.* **1995**, *117*, 2817.
(131) Solomon, E. I.; Penfield, K. W.; Gewirth, A. A.; al, e. *Innorg. Chim. Acta* **1996**, *243*, 67.

List of Publications

Present work is based on seven papers listed bellow:

Burda J. V., Pavelka M., Šimánek M.,
Theoretical Model of Copper Cu(I)/Cu(II) Hydration. DFT and Ab initio Quantum Chemical Study., J. Molec. Struct., 683 (2004), 183-193

Pavelka M., Burda J. V.,
Theoretical description of copper Cu(I)/Cu(II) complexes in mixed ammine-aqua environment. DFT and ab initio quantum chemical study., Chem. Phys., 312 (2005), 193-204

Pavelka M., Šimánek M., Šponer J., Burda J. V.,
Copper cation interactions with biologically essential types of ligands: A computational DFT study., J. Phys. Chem. A, 110 (2006), 4795-4809

Pavelka M., Burda J. V.,
Computational DFT Study of Redox Centers of Blue Copper Proteins., J. Phys. Chem. B, (2006), submitted

Pavelka M., Shukla M. K., Burda J. V.,
Theoretical model of hydrated Cu(II) with guanine . DFT and ab initio quantum chemical study., J. Phys. Chem. A, (2006), submitted

Pavelka M., Sarkar B., Kaim W., Záliš S.
The DFT calculations of valence tautomer equilibrium of $[(L)Cu^{n+}(Q)^{n-}]$ (L=mtq or mmb, n=1 or 2, Q=quinone) complexes., Innorg. Chem., (2006), submitted

Pavelka M., Burda J. V.,
Pt-bridges in various single-strand and double-helix DNA sequences. DFT and MP2 study of the cisplatin coordination with guanine, adenine, and cytosine., J. Mol. Model., (2006), in print, published online *10.1007/s00894-006-0151-x*

The complete versions can be found in annex.

Annex

ELSEVIER

Journal of Molecular Structure (Theochem) 683 (2004) 183–193

THEO CHEM

www.elsevier.com/locate/theochem

Theoretical model of copper Cu(I)/Cu(II) hydration. DFT and ab initio quantum chemical study

Jaroslav V. Burda*, Matěj Pavelka, Milan Šimánek

Department of Chemical Physics and Optics, Faculty of Mathematics and Physics, Charles University, Ke Karlovu 3, 12116 Prague 2, Czech Republic

Received 13 March 2004; revised 24 May 2004; accepted 18 June 2004
Available online 11 August 2004

Abstract

Hydration study of both Cu^+ and Cu^{2+} cations in variable water environment was performed using the DFT method. After optimization using B3PW91 functional, stabilization energies with and without ligand repulsion were calculated using B3LYP functional. It was found that optimal Cu^+ coordination involves two directly bonded solvent molecules while Cu^{2+} cation prefers 4 (or 5) coordinated waters in the first solvation shell. Higher coordination corresponds to lower stabilization energies. Morokuma's energy decomposition (for Cu^+ complexes only) was used to elucidate bonding characteristics in detail. NBO partial charges and MO's analyses support the explanation for these energy results.

Keywords: Hydration; Stabilization energies; Solvent molecules; Transition metal complexes

1. Introduction

There can be found large abundance of theoretical papers in biodisciplines, which concern to interaction of copper cations with DNA/RNA bases [1–4]. Some experimental structures are available for comparison [5–9]. Interactions with amino acids are computed in works [10–16]. Also for these calculations, one can find many experimental evidences, e.g. in works [17,18]. Great attention is directed to solve structures and clarify properties of so-called blue proteins. Basic role of the copper Cu(I)/Cu(II) redox possibility can be demonstrated on their models. Blue copper proteins are a group of electron transfer proteins characterized by several unusual properties—bright blue color, narrow hyperfine splitting in the electronic spin resonance spectra and high reduction potentials. The Cu ion is bound to the protein in an approximate trigonal plane formed by a cystine (Cys) thiolate group and two histidine (His) nitrogen atoms. In most of these blue copper proteins, the coordination sphere is completed with one or two S-ligands, typically a methionine (Met) thioether group, but sometimes also of a carbonyl oxygen atom from the side chain of glutamine. Such geometry is similar to what can be expected for Cu(I) complexes. Copper coordination geometries of reduced blue copper proteins are very close to those of the oxidized proteins [19–26]. Some interesting experimental works on charge transfer on blue peptides were recently published [27,28], which enable comparison with theoretical studies.

Copper is a part of some oxidation enzymes—indophenoloxidases, and is also present in fourth cycle of respiration chain in the so-called terminal oxidation operating as redox center of metalloprotein. It is included in many other biomolecules, for example: cytochrom *c* oxidase, superoxidase dismutase, tyrosinase [29], and many other. All of them require copper in the active sites in order to be biochemically active [30].

Water is the most usual environment for solvation. Consequently, contribution of this work is a closer insight in mechanisms of copper Cu(I)/Cu(II) cations interactions with water molecules. There could be seen some basic differences between the coordination of both copper cations which are important in many vivo processes, as mentioned above. Importance of this very simple model is reflected in number of papers studying copper hydration using either

* Corresponding author. Tel.: +420-221911246; fax: +420-221911249.
E-mail address: burda@karlov.mff.cuni.cz (J.V. Burda).

0166-1280/$ - see front matter © 2004 Elsevier B.V. All rights reserved.
doi:10.1016/j.theochem.2004.06.013

static [31,32] or dynamic [33,34] approach or both [35–38]. Also Cu(I) hydration was thoroughly explored by Feller et al. [39]. Experimental work in gas phase confirms high stability of some low-coordinated Cu(II) complexes [40].

Some effort was also devoted to design parameters for empirical force field [41–43] to enable faster classical MD approach to such problems.

In work of Luna, difficulties at G2 level of Gaussian theory were noticed dealing with copper complexes [44] on the contrary to DFT calculations and similar problems were also noticed for calculations with QCISD method [45].

The aim of the present study is to describe stable-coordinated structures of Cu(I) and Cu(II) interacting with one to six water molecules. For the examination of these systems, geometric, energetic and population analyses have been done.

Next objectives to study are stability and energetic relations between structures with various coordination numbers, deformation of molecules interacting with Cu^+ and Cu^{2+} atoms, verification of Jahn–Teller first and second order effect on the copper complexes and a comparison of our results with calculations presented in works of other authors [33,46,47].

2. Computational details

All the $[Cu(H_2O)_n]^+$ structures (where $n=1$–6) are closed shell systems with singlet electron configuration. Geometry optimization was performed at DFT level with B3PW91 functional, which compared to B3LYP functional gives slightly better structure results and vibrational properties [48–51]. Although geometries obtained by B3LYP are not qualitatively different. The standard 6-31+G(d) basis set was chosen with added polarization and diffuse functions due to the fact that enhanced variation of copper wide 4s AO provides the satisfaction of the donation effects. Hence, it strongly affects stabilization of some Cu(I) complexes. The Cu atom was described by averaged relativistic effective pseudopotentials (AREP) [52], extended by a set of diffuse ($\alpha_s=0.025$, $\alpha_p=0.35$, and $\alpha_d=0.07$) and polarization ($\alpha_f=3.75$) functions. Several structures, which differ usually by rotation of water molecules around the Cu–O axe or by different H-bonding pattern, were found in a few kilocalorie per mole range. This made the optimization and the following single-point analyses slightly more demanding. In the discussion part, only global minima are mentioned. Some local minima were presented in study [39]. Energy characteristics and charge distribution analysis were performed on the optimized structures using B3LYP functional and 6-311++G(2df,2pd) basis set on oxygen and hydrogen atoms. Set of AOs on the Cu atom was enlarged by s, p, d diffuse functions and by 2f, 1g polarization functions ($\alpha_f=$ 4.97, 1.30, and $\alpha_g=3.28$) in a consistent way. The exponents were optimized using CCSD method on the ground state electronic configuration ^{2}X(Cu). The stabilization energies with their appropriate counterpoise corrections [53] (including BSSE and deformation corrections) were calculated according to formula:

$$\Delta E^{\text{Stab}} = -\left(E_{\text{complex}} - \sum E_{\text{monomer}} - \sum E^{\text{deform}}\right), \quad (1)$$

where E_{monomer} denotes the energy of the given monomer including the AOs of ghost atoms. Besides the ΔE^{Stab} energies, sterically corrected stabilization ΔE^{Stex} was determined, too. In this case, all the ligands were considered as one 'monomer' and central Cu cation as another. The third characteristics—coordination energy ΔE^{coord} was considered in the case of Cu(I) interactions where some water molecules stay in second hydration shell. The coordination energy is evaluated like ΔE^{Stab} when only directly bonded water ligands are considered using the geometry optimized for the whole complex.

Since the Cu^{2+} ion is an open shell system with 3d [9] valence electron configuration, the Cu(II) complexes were considered as doublets. Therefore, determination of the correct wave function had to be done with care. The correct wave function was constructed in reduced basis set with Restricted Open Shell Hartree-Fock (ROHF) procedure first. When correct occupation was obtained, bigger basis 6-31+G* was used and UHF geometry optimization performed. Finally, DFT re-optimization was done. In analogy to Cu(I) complexes, several local minima, which are not presented here (some of them can be found, e.g. in Ref. [35]), are close in energy. Determination of energy characteristics and charge distribution analyses were solved using B3LYP functional in 6-311++G(2df,2pd) basis in analogy to Cu(I) systems. For Natural Population Analysis (NPA) [54], 1g function had to be removed because used program GAUSSIAN 98 [55] did not support NPA with g functions. These methodology was applied to coordinated structures including divalent copper in water ligand fields $[Cu(H_2O)_n]^{2+}$ ($n=1,\ldots,6$). Morokuma decomposition analysis was performed using GAMESS-US program [56] for hydrated Cu(I) systems.

Visualization of geometries, MOs, and vibrational modes was done with programs MOLDEN 4.0 [57] and MOLEKEL 4.3 [58,59].

3. Results and discussion

The goal of the optimization process for Cu(I) complexes was to find stable-coordinated structures. A problem dwells in very similar values of copper-ligand bond energy at one side and H-bonding of water molecules in second solvation shell on the other side. Therefore, it was difficult to find more than 3-coordinated structures and no stable 5- and 6-coordinated Cu(I) structures were found.

Table 1
The Cu–O distances and average Cu–O distances (in Å)

System	c.n.	Cu–O1	Cu–O2	Cu–O3	Cu–O4	Cu–O5	Cu–O6	Average Cu–O
$[Cu(H_2O)]^+$	1	1.929						1.929
$[Cu(H_2O)_2]^+$	2	1.899	1.899					1.899
$[Cu(H_2O)_3]^+$	2	1.903	1.873					1.888
	3	1.944	1.959	2.249				2.051
$[Cu(H_2O)_4]^+$	2	1.878	1.878					1.878
	3	1.970	1.976	2.143				2.030
	4	1.998	2.085	2.207	2.257			2.137
$[Cu(H_2O)_5]^+$	2	1.883	1.863					1.873
	3	1.932	1.974	2.180				2.029
$[Cu(H_2O)_6]^+$	2	1.866	1.866					1.866
	3	1.969	2.019	2.058				2.015
	4	2.126	2.126	2.126	2.126			2.126
$[Cu(H_2O)]^{2+}$	1	1.864						1.864
$[Cu(H_2O)_2]^{2+}$	2	1.852	1.852					1.852
$[Cu(H_2O)_3]^{2+}$	3	1.901	1.901	1.911				1.904
$[Cu(H_2O)_4]^{2+}$	4	1.960	1.960	1.959	1.963			1.961
$[Cu(H_2O)_5]^{2+}$	4	1.939	1.941	1.972	1.977			1.957
	5	2.170	2.013	1.974	2.013	1.974		2.029
$[Cu(H_2O)_6]^{2+}$	4	1.956	1.956	1.956	1.956			1.956
	5	1.974	1.975	1.998	2.008	2.212		2.033
	6	2.026	2.026	2.003	2.003	2.281	2.281	2.103

c.n., the coordination number.

3.1. Structures of Cu(I)/Cu(II) hydrates

Described methodology was applied on systems of monovalent copper cation (Cu^+) and variable number of water molecules. It was found for $[Cu(H_2O)_n]^+$ structures, that only 1, 2, 3 and 4-coordinated structures form stable minima. The Cu–O distances for ligated waters are compiled in the first part of Table 1.

Short distances for 2-coordinated Cu(I), remarkable from the Table 1, are an interesting feature of these systems. They are even shorter than in case of $[Cu(H_2O)]^+$ where only one Cu–O bond exists (1.929 Å). Possible explanation of this fact insists in surprisingly small donation of single water. This is supported by the facts that partial charge on Cu cation in single-water system is much higher (+0.96—practically unchanged by interaction with water) than in the rest of investigated complexes, and polarization and charge transfer terms are very small in comparison with other systems, when Morokoma's energy decomposition is performed (cf. below). From all the explored systems, where n waters ($n>1$) interact with Cu(I), the 2-coordinated complexes represent the most stable ones. Distinct shortening of Cu–O bond with higher numbers of water molecules in second shell is visible from Table 1. The shortest average distance is 1.866 Å in 2-coordinated $[Cu(H_2O)_6]^+$ complex.[1] The 3-coordinated complexes always have smaller stabilization energy and their structures exhibit marked deformation: one of the bonds is usually longer than the other two and large deviations from 120 degrees occur for O–Cu–O valence angles. The largest deformation occurs for 'isolated' $[Cu(H_2O)_3]^+$ without any water in second shell. Outer waters stabilize the dative coordination interactions in the same way like in 2-coordinated complexes. Analogous effect is also noticeable in 4-coorditated complexes where two additional outer water molecules make the four coordination bonds equivalent, on the contrary to $[Cu(H_2O)_4]^+$ complex. However, this quasi-equivalence is connected with substantial change of geometry. While $[Cu(H_2O)_4]^+$ system has a shape of deformed trigonal pyramide, 4-coordinated $[Cu(H_2O)_6]^+$ system is a flattered tetraeder. Interestingly, in the case of five water molecules no stable 4-coordinated structure was found, probably due to highly asymmetrical destabilization of single outer water.

In case of $[Cu(H_2O)_6]^{2+}$ structure, some other results are available, e.g. in Ref. [33] Cu–O distances are 2.07 Å for equatorial and 2.24 Å for axial bonds, which is in very good accord with our data in Table 1. Also the Ziegler group [35] published extensive work with structures of Cu(II) hydrates, which match with our data closely, e.g. d(Cu–O) = 1.965 and 1.923 Å for 3-coordinated triaqua complex or d = 1.983, 1.997, 1.997, 2.011 in $[Cu(H_2O)_4]^{2+}$ complex.

As to H-bond lengths, 3 different types can be found. First, in 2-coordinated complexes, 1–4 molecules were attached to one of the four hydrogens of coordinated ligands. These H-bonds are the shortest (< 1.70 Å). In 3- or 4-coordinated complexes, usually 6-member rings appear

[1] HF results differ in this point preferring usually 3-coordinated complexes as the global minima. This is due to larger accent on electrostatic and polarization interactions in uncorrelated HF method. Also, 6-coordinated complex was found as a stable local minimum at the HF level.

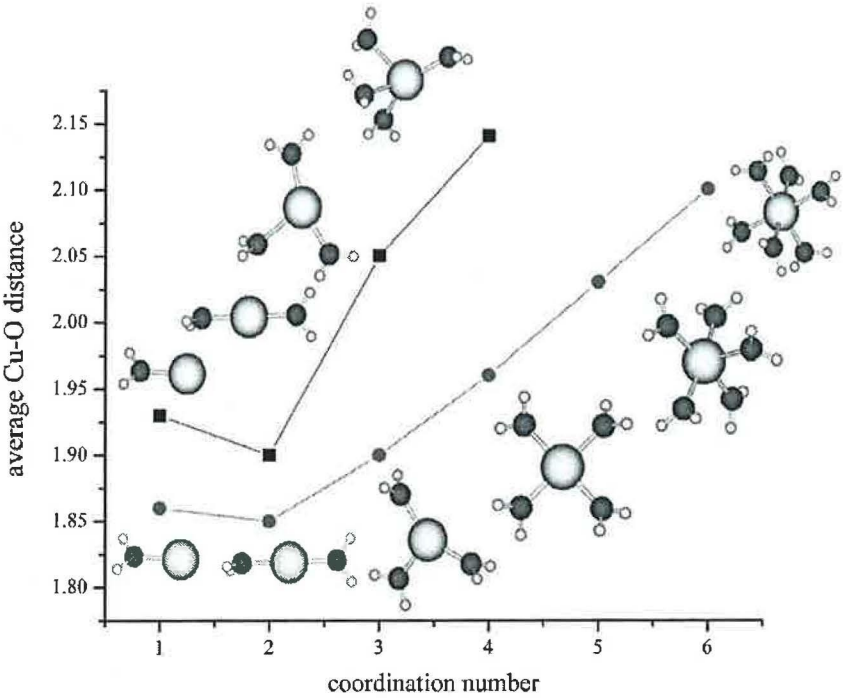

Fig. 1. The average Cu–O distances of the Cu(I)/Cu(II) aqua-systems in Å units.

with two H-bonds, which have protons from ligated waters oriented towards oxygen in outer solvent molecule. Such H-bonds exhibit usually distances in the range 1.70–1.85 Å. At last, H-bonds between waters in second solvation shells of higher-member rings have distances slightly above 1.85 Å. In such rings, first and third types of H-bonds are mixed. From many papers, which deal with pure water clusters, e.g. Refs. [60–64] it can be seen that the usual H-bond length is about 1.81–1.88. This is in good accord with our findings since water molecules from the first (and partially also from the second) solvation shells are polarized by Cu^+ cation, which causes slightly shorter H-bonds.

In the case of Cu(II) complexes, different relations were found. The higher coordination is substantially more stable. Global minima are usually 4-coordinated complexes but 5-coordinated complexes are in very close proximity (within 2–5 kcal/mol, cf. below). This is in very good accord with recent experimental discovery: 5-coordinated water complexes were measured with extended X-ray absorption fine structure (EXAFS) and X-ray absorption near-edge structure (XANES) [65]. In this work, theoretical approach (CPMD) was also used and a very good accordance for the pair correlation functions $g_{CuO}(r)$ and XANES spectra was obtained.

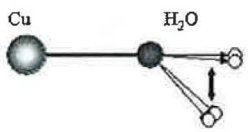

Scheme 1.

Shorter distances basically indicate stronger Cu–O bonds. Thus an estimation of the complex stability can be obtained from Table 1 or/and Fig. 1. In analogy with $[Cu(H_2O)]^+$, the Cu–O bond distance for monoaqua complex is slightly longer than for diaqua-structure. The explanation is similar—smaller donation of water lone pair (cf. below). The difference is much smaller here, however. A minimum can be observed in Fig. 1 where Cu–O bond length dependences on water coordination number are drawn.

Interesting situation concerns the deviation angle of the Cu–O bond from the water-molecule plain (cf. Scheme 1). While in $[Cu(H_2O)]^+$ this bond lies nearly in the plain (8°), approximately 26° deviation occurs in Cu(II) case. The situation is changed for diaqua-complexes—19° in Cu(I) complex vs. 14° in Cu(II) one. In case of 3- and 4-coordinated Cu(I) structures,

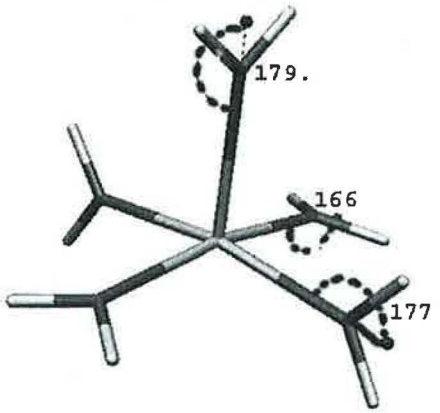

Fig. 2. The angle between the Cu–O line and H–O–H plane.

these angles are above 20°, while analogous Cu(II) complexes have Cu–O bond practically in the water plain (deviation <6°). The only exception is a deformed octahedral pentaaqua-complex (cf. Fig. 2). Nonplanarity appears in order to minimize repulsion among Cu and hydrogens. In Cu^+ complexes, a weaker repulsion between partial charges on hydrogens and copper cation cannot push out Cu–O from 'optimal' position, corresponding to dative character, which follows a higher electron density of one of the lone pairs in sp^3 configuration on the oxygen. Since $[Cu(H_2O)]^+$ exhibits very small donation, the angle is governd by the electrostatic repulsion only.

3.2. Hydration energies

3.2.1. Cu(I) complexes

After geometry optimization using the B3PW91 functional, stabilization energies (with and without sterical repulsion) were calculated. In Table 2, stabilization energies ΔE^{Stab} and sterically corrected stabilizations ΔE^{Stex} are collected. Since several water molecules stay in second hydration shell when Cu^+ cation interacts with higher number of water molecules, coordination energies were calculated in such cases, too.

From the first two rows, it can be seen that longer Cu–O bond distance in monoaqua than in diaqua Cu(I) complexes reflects in the stabilization energies. However, stabilization of these two complexes per bond is nearly the same (cf. Fig. 3a). In complexes with higher coordination, the stabilization energy per Cu–O bond rapidly decreases. While optimized 3-coordinated complexes represent local minima on potential energy surface for systems with any larger number of water ($n \geq 3$), 4-coordinated complex was found as a stable local minimum only in 4 and 6 watered systems. On the contrary, Hartree-Fock optimizations predict 3-coordinated Cu^+ complexes as global minima, as mentioned above.

Higher number of water molecules exhibits rapid saturation in stabilization energy. Passing from 5 to 6 interacting waters, the total stabilization energy is increased only by 12 kcal/mol. This is just an energy of one additional H-bond in linear 2-coordinated structure (global minimum). Values of coordination energies demonstrate small influence of water molecules from the second shell on the dative bonds, i.e. coordination energies ΔE^{coord} vary less than 1 kcal/mol with number of outer waters. The stabilization energy increase for the first water in second hydration shell is about 18 kcal/mol (difference between ΔE^{Stab} and ΔE^{coord}) and it goes to 15 kcal/mol per one H-bond in the 2-coordinated system with six interacting solvent molecules, cf. Fig. 3a. This cannot be regarded as a pure H-bond strength since interaction with remote Cu cation is also involved. Nevertheless, it can be seen that the dominant part is of H-bonding origin (between polarized (ligated) water...water (outer)). Complete occupation of the second shell will probably decrease this energy to ca. 10–12 kcal/mol that is already close to situation in pure water clusters (about 9.0 kcal/mol of H-bonds at similar level of calculations [60]). Clearly, diaqua complexes of the Cu(I) cation represent the most stable form in water solutions. One particular detail deals with reduction of stabilization energy ($\Delta E^{Stab} - \Delta E^{Stex}$ is ca. +3 kcal/mol) when sterical repulsions are corrected in 3-coordinated $[Cu(H_2O)_6]^+$. This is caused by the fact, that not only sterical repulsions are subtracted in the used formula, but also attractive

Table 2
The stabilization energies of the Cu(I) and Cu(II) hydrates

System	c.n.	ΔE^{Stab}	ΔE^{Stab}/n.w.	ΔE^{Stex}	ΔE^{coord}
$[Cu(H_2O)]^+$	1	41.8	41.8	42.1	41.8
$[Cu(H_2O)_2]^+$	2	84.1	42.1	86.2	42.1
$[Cu(H_2O)_3]^+$	2	101.4		102.8	41.6
	3	97.1	32.4	101.8	32.4
$[Cu(H_2O)_4]^+$	2	117.6		118.3	41.2
	3	112.0		114.5	31.1
	4	106.9	26.7	112.8	26.7
$[Cu(H_2O)_5]^+$	2	130.3		130.7	41.1
	3	125.8		128.0	30.9
$[Cu(H_2O)_6]^+$	2	142.2		142.0	41.1
	3	135.9		132.9	30.9
	4	132.9		135.8	25.3
$[Cu(H_2O)]^{2+}$	1	114.7	114.7	116.3	114.7
$[Cu(H_2O)_2]^{2+}$	2	205.8	102.9	209.0	102.9
$[Cu(H_2O)_3]^{2+}$	3	263.5	87.8	271.4	87.8
$[Cu(H_2O)_4]^{2+}$	4	306.7	76.7	322.8	76.7
$[Cu(H_2O)_5]^{2+}$	4	336.2		353.4	75.4
	5	334.0	66.8	354.3	66.8
$[Cu(H_2O)_6]^{2+}$	4	363.4		381.1	74.4
	5	358.6		380.2	65.7
	6	338.0	56.3	363.9	56.3

n.w., number of water molecules.

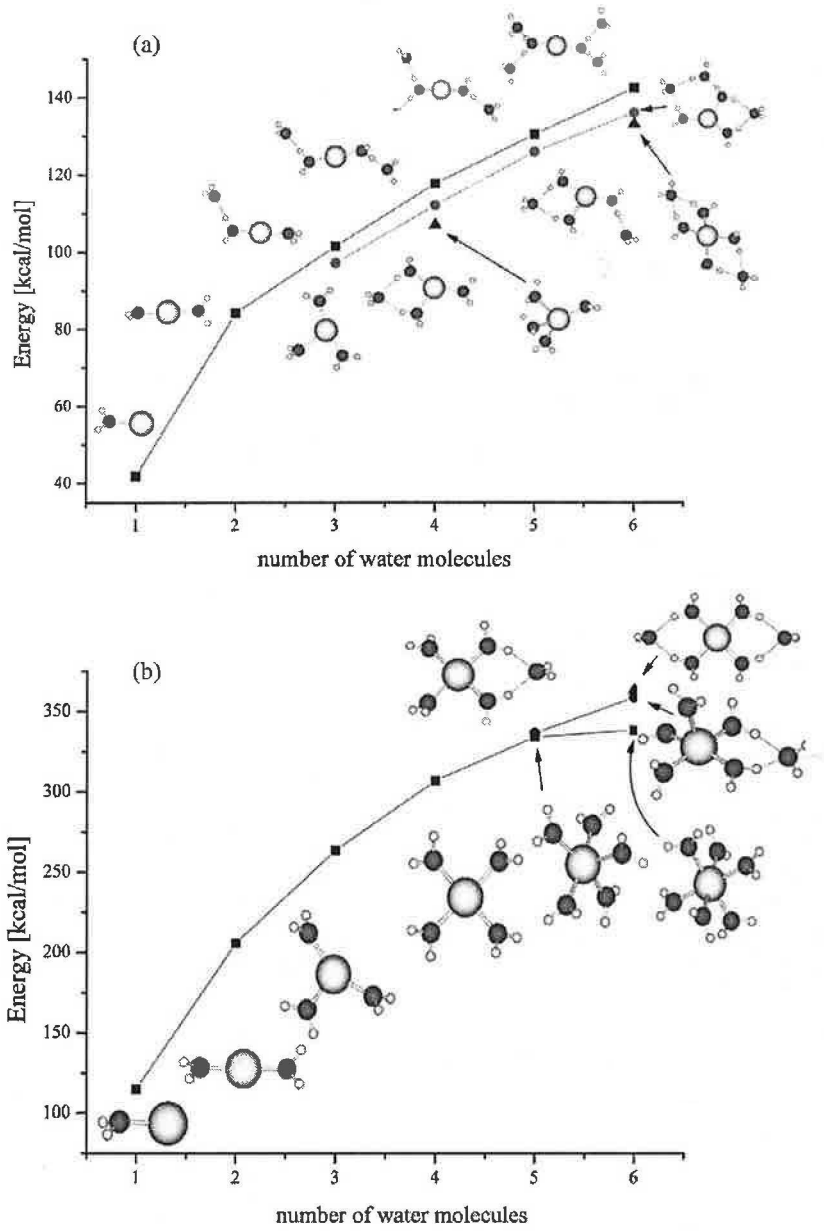

Fig. 3. (a) The stabilization energies of the Cu(I) systems. (b) The stabilization energies of the Cu(II) systems.

H-bonding interactions, which can prevail for weaker and lower coordinations when sufficient number of water molecules is present.

In the case of closed shell Cu(I) complexes, Morokuma's energy decomposition was performed to bring light in the bonding characteristics of the complexes. In Table 3a, one can clearly see that besides Coulomb interaction, polarization effects play very important role. Especially in case of 2-coordinated systems, polarization contributions are even larger than Coulomb energies. In $[Cu(H_2O)]^+$ case, small polarization leads to lower stabilization energy (see above). From the last column of Table 3a, it can be shown that the role of correlation contributions is also very important. For instance, for systems with 6 waters, 4-coordinated structure has the largest interaction energy but the energy order is completely inverted when correlation effects are included. The same was found for stabilization energies ΔE^{Stab} at HF/6-311++G(2df,2pd)//HF/6-31+G(d) level where the 3-coordinated complexes were the most stable minima for 3, 4, and 5 watered systems and 4-coordinated complex in the case of 6 watered systems. The explanation insists mainly in exaggerated electrostatic and polarization contributions (not presented here). Only after inclusion of correlation contributions either at MP2 or B3LYP level, the correct energy order was obtained. In Table 3b, the extent of polarization on individual water molecules is demonstrated.

Table 3a
Morokuma's energy decomposition analysis for Cu(I) complexes

System	c.n.	E^{Elst}	E^{Ex}	E^{Pol}	$E^{CT+PL+X}$	ΔE^{HF}	ΔE^{MP2}
$[Cu(H_2O)]^+$	1	−59.08	45.70	−27.40	−22.93	−32.39	−9.03
$[Cu(H_2O)_2]^+$	2	−123.59	105.57	−201.46	−61.12	−62.93	−24.15
$[Cu(H_2O)_3]^+$	2	−153.16	132.10	−224.97	−78.71	−79.37	−28.47
	3	−142.19	102.01	−148.66	−52.44	−78.87	−22.27
$[Cu(H_2O)_4]^+$	2	−180.21	154.83	−244.17	−93.85	−95.09	−32.10
	3	−169.31	118.89	−128.20	−58.87	−94.93	−21.02
	4	−157.05	98.11	−84.21	−41.74	−92.27	−21.28
$[Cu(H_2O)_5]^+$	2	−200.93	168.02	−257.84	−101.47	−107.87	−34.71
	3	−193.07	138.33	−152.78	−71.48	−108.54	−28.07
$[Cu(H_2O)_6]^+$	2	−220.66	182.95	−271.62	−111.27	−119.56	−37.72
	3	−215.05	152.11	−118.23	−74.08	−119.95	−30.42
	4	−203.44	124.32	−56.55	−50.45	−120.70	−24.64

It is clearly seen that while directly coordinated waters exhibit relatively high polarization energy (more than 10 kcal/mol in 3-coordinated and even up to 30 kcal/mol in 2-coordinted complexes), polarization energy for the water molecules in second hydration shell is substantially reduced (below 5 kcal/mol). This also supports the conclusion from previous paragraph that additional water molecules will feel the influence of Cu(I) cation only marginally.

3.2.2. *Cu(II) complexes*

Despite a similar trend for Cu–O distances (the shortest bonds in diaqua followed by monoaqua complex) for both Cu(I) and Cu(II) cations, the stabilization energy related to number of Cu–O bonds ΔE^{Stab}/n.w. is larger in $[Cu(H_2O)]^{2+}$ than in corresponding diaqua system. On the contrary to structures containing hydrated Cu^+ cation, 4- (or maybe 5-) coordinated complexes are the most stable ones between all of the investigated hydrates of the Cu^{2+} ion. The stabilization energy behavior exhibits clear saturation for Cu(II) complexes (cf. Fig. 3b). In case of 5 and 6 watered complexes, one or two waters try to escape to second solvation shell. The stabilization energies for Cu^{2+} with 5 water molecules exhibit practical degeneracy for 4- and 5-coordinated complexes (difference 2 kcal/mol and about 3 kcal/mol if total energies are compared). The inclusion of sterical repulsion corrections reverts the order, preferring 5-coordinated complex by about 1 kcal/mol. Thus, one can expect that the stability of both complexes will be very similar. When ZPVE corrections are calculated and entropy contributions evaluated, it can be found that the relative occurrence of 5-coordinated species according to Boltzmann law for Gibbs energy is about 9% at 298 K (in comparison with 0.2% for total energies). The same picture is also remarkable for Cu^{2+} systems with 6 water molecules. The differences in total and stabilization energies are slightly more pronounced—about 4 kcal/mol (ΔE^{Stab}(4-coord) − ΔE^{Stab}(5-coord)) and about 25 kcal/mol (ΔE^{Stab}(4–6)). The sterical-repulsion corrections decrease the differences to 1 and 16 kcal/mol. A smaller difference in ΔE^{Stex} energies can be explained by the fact that the higher is the coordination the larger sterical corrections occur.

Stabilization energy for $[Cu(H_2O)_6]^{2+}$ can be compared with formation energy published by Marini et al. [33] giving an excellent agreement (ca. 320 kcal/mol). Also Berces et al. [35] demonstrate very close stabilization of 4- and 5-coordinated structures for both penta- and hexa-aqua complexes. Their bonding energies: 90.8 (for triaqua), 78.6 (tetraaqua), 69.8, and 67.9 (4- and 5-coordinated pentaaqua), and 62.9, 61.9, 60.0 kcal/mol for hexaaqua complexes match very well with our results.

Table 3b
The decomposition of charge transfer+polarization energy for particular monomers

System	c.n.	Cu	*w1*	*w2*	*w3*	*w4*	*w5*	*w6*
$[Cu(H_2O)]^+$	1	−10.61	−12.32					
$[Cu(H_2O)_2]^+$	2	−29.77	−15.68	−15.68				
$[Cu(H_2O)_3]^+$	2	−33.10	−15.86	−24.53	*−5.21*			
	3	−22.71	−12.54	−11.52	*−5.67*			
$[Cu(H_2O)_4]^+$	2	−35.91	−24.10	−24.10	*−4.87*	*−4.87*		
	3	−21.61	−11.25	−8.55	−13.76	*−3.70*		
	4	−16.18	−6.80	−9.72	−4.12	−4.92		
$[Cu(H_2O)_5]^+$	2	−37.90	−27.84	−23.67	*−3.74*	*−3.74*	*−4.57*	
	3	−24.09	−14.08	−18.30	−7.89	*−3.48*	*−3.64*	
$[Cu(H_2O)_6]^+$	2	−40.37	−28.23	−28.23	*−3.67*	*−3.55*	*−3.67*	*−3.55*
	3	−22.42	−14.64	−14.06	−12.30	*−4.33*	*−3.18*	*−3.15*
	4	−14.10	−7.56	−7.56	−7.56	−7.56	*−3.05*	*−3.05*

All energies (in kcal/mol) are computed at RHF level for DFT structures; italics denotes water molecules in 2nd solvation shell.

Comparing stabilization energies of both cations, values for Cu(I) are markedly lower (more than twice) in comparison with Cu(II) complexes. This clearly shows that not only electrostatic interaction (twice higher charge) is stronger but also polarization energy and covalent bonding with higher donation (cf. below in discussion of partial charges) have to play important role. This is in accord with Morokuma energy decomposition performed for Cu(I) complexes where the role of polarization energy was also clearly demonstrated.

Complexes with the same coordination can be compared when the total number of water molecules increases. Coordination energy ΔE^{coord} is reduced as a reaction on a geometry deviation from the optimal structure (without any water in second shell). Thus this energy mirrors the deformation effects of the inner part of complexes. The energy differences are relatively very small and converge quickly as can be noticed for 2-coordinated Cu(I) systems.

3.2.3. Charge distribution

In order to obtain a deeper insight to studied systems, Weinhold NPA [66] partial charges were calculated and analyses of MOs were performed. There is one MO of the non-bonding orbitals of water, which can take part in σ-dative coordination to metal cation. Based on symmetry condition, such an orbital will contain admixture of vacant atomic orbitals of Cu, predominately 4s. An interesting detail deals with longer Cu–O distances in both Cu(I)/Cu(II) in monoaqua than in diaqua complexes. While in $[Cu(H_2O)]^{n+}$ complexes, admixture of Cu 4s AO exists in 8th MO in Cu^+ (see the MO in Fig. 4a) and 8th(alpha)/7th(beta) in Cu^{2+} case, two analogous MOs exist in $[Cu(H_2O)_2]^{n+}$ structure. The latter MOs exhibit substantially larger expansion coefficients of 4s (higher donation) which corresponds to ca. 0.3e from both oxygens (cf. 7th and 11th MOs for $[Cu(H_2O)_2]^+$ in Fig. 4b and c; analogous orbital in Cu^{2+} are the 7th and 12th(alpha)/13th(beta) MOs). These orbitals demonstrate existence of substantially stronger dative bonds in diaqua complexes. This also corresponds to higher polarization energies found in Morokuma's decomposition for Cu^+ complexes.

Besides MO characteristics, occupation of individual valence atomic orbitals of Cu cation can be used for the quantification of donation effects, especially the occupation of 4s AO. In Table 4 occupations of 4s and 3d valence orbitals of copper cations are collected.

In case of Cu(I) complexes, it can be noticed that the highest donation occurs in cases of 2-coordinated structures. This is in accord with stabilization energies of these complexes. Also, the increasing donation passing from two interacting waters to six molecules gives another explanation why the 2-coordinated complex is the strongest between systems with six waters. In the higher part of Table 5, NBO partial charges of heavy elements of Cu(I) are present. As mentioned above, Cu charge deviates only slightly from 1+ in monoaqua complex pointing on small electron density changes upon single water interaction as discussed above. Charge densities on O–H bonds of the coordinated waters are decreased due to H-bonding with second hydration shell, which leads to higher (more negative) partial charges on the donating oxygens. Higher charges on directly coordinated oxygens are visible in Table 5. Waters from second shell exhibit much smaller deviation from electron distribution in isolated water.

In Cu(II) systems, the situation is slightly more complicated since some donation can cause increased occupation of SOMO, cf. lower part of Table 4. Since some additional density appears in SOMO, only the partial

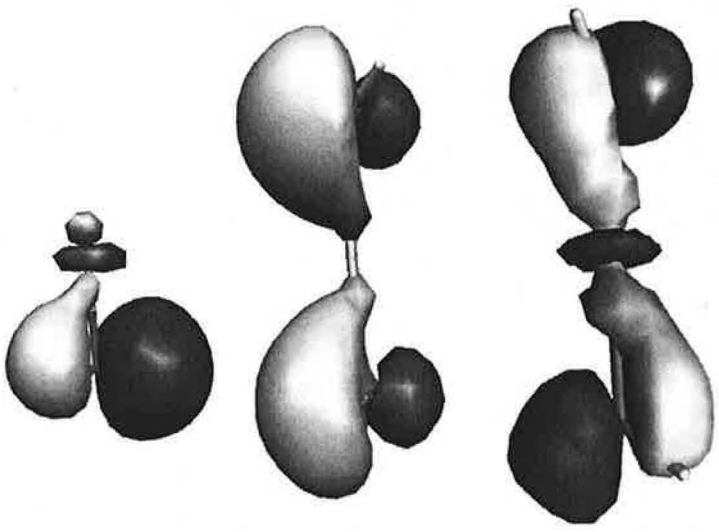

(a) (b) (c)

Fig. 4. MO involved in water donation: (a) 8^{th}MO of $[Cu(H_2O)]^+$ (b) 7^{th} MO of $[Cu(H_2O)_2]^+$ (c) 11^{th} MO of $[Cu(H_2O)_2]\supset +$.

Table 4
The occupation of some valence Cu AO

System		4s	3dx2y2	3dz2
$[Cu(H_2O)]^+$	1	0.102	2.000	1.941
$[Cu(H_2O)_2]^+$	2	0.338	1.872	1.957
$[Cu(H_2O)_3]^+$	2	0.385	1.931	1.950
	3	0.261	1.941	1.954
$[Cu(H_2O)_4]^+$	2	0.411	1.898	1.988
	3	0.242	1.967	1.948
	4	0.190	1.961	1.981
$[Cu(H_2O)_5]^+$	2	0.431	1.876	1.973
	3	0.271	1.928	1.951
$[Cu(H_2O)_6]^+$	2	0.453	1.843	1.952
	3	0.234	1.965	1.947
	4	0.144	1.988	1.995
$[Cu(H_2O)]^{2+}$	1	0.069	1.999	1.201
$[Cu(H_2O)_2]^{2+}$	2	0.164	1.776	1.379
$[Cu(H_2O)_3]^{2+}$	3	0.223	1.202	1.976
$[Cu(H_2O)_4]^{2+}$	4	0.241	1.241	1.978
$[Cu(H_2O)_5]^{2+}$	4	0.250	1.228	1.975
	5	0.233	1.184	1.982
$[Cu(H_2O)_6]^{2+}$	4	0.261	1.244	1.974
	5	0.241	1.216	1.985
	6	0.236	1.434	1.790

charges represent the unique criterion for donation extent. From the lower part of Table 5, it is evident that the smallest positive Cu partial charge is in the four-coordinated structure tightly followed by 5-coordinated (especially in the case of system with six water molecules). This means the largest electron donation occurs in these complexes. The strong donation correlates with the largest stabilization energies of these 4-(5-)coordinated complexes.

4. Conclusions

Optimizations of the complexes containing Cu^+/Cu^{2+} cations with varying number of water molecules (from one to six) were done using DFT method with B3PW91 functional.

It was found that the most stable structures with Cu^+ cation have only two coordinated water molecules.

Table 5
The NPA partial charges of the Cu and O atoms

System	Coord.	Cu	O1	O2	O3	O4	O5	O6
$[Cu(H_2O)]^+$	1	0.96	−1.03					
$[Cu(H_2O)_2]^+$	2	0.83	−0.98	−0.98				
$[Cu(H_2O)_3]^+$	2	0.81	−0.97	−1.01	*−0.95*			
	3	0.86	−0.98	−0.99	−0.99			
$[Cu(H_2O)_4]^+$	2	0.80	−1.01	−1.01	*−0.96*	*−0.96*		
	3	0.87	−0.98	−1.01	−1.01	*−0.97*		
	4	0.88	−0.99	−0.98	−0.99	−0.99		
$[Cu(H_2O)_5]^+$	2	0.78	−1.00	−1.03	*−0.96*	*−0.96*	*−0.96*	
	3	0.86	−1.01	−1.00	−1.01	*−0.96*	*−0.97*	
$[Cu(H_2O)_6]^+$	2	0.77	−1.02	−1.02	*−0.96*	*−0.95*	*−0.95*	*−0.96*
	3	0.87	−1.00	−1.01	−1.04	*−0.97*	*−0.97*	*−0.97*
	4	0.89	−1.00	−1.00	−1.00	−1.00	*−0.97*	*−0.97*
$[Cu(H_2O)]^{2+}$	1	1.72	−0.91					
$[Cu(H_2O)_2]^{2+}$	2	1.69	−1.01	−1.01				
$[Cu(H_2O)_3]^{2+}$	3	1.59	−0.99	−0.99	−1.00			
$[Cu(H_2O)_4]^{2+}$	4	1.56	−0.99	−0.99	−0.99	−0.99		
$[Cu(H_2O)_5]^{2+}$	4	1.54	−1.00	−0.99	−0.99	−0.99	*−0.98*	
	5	1.58	−1.02	−0.99	−0.98	−0.99	−0.98	
$[Cu(H_2O)_6]^{2+}$	4	1.56	−1.01	−1.00	−0.99	−0.99	*−0.98*	*−0.98*
	5	1.56	−1.00	−0.99	−0.99	−1.01	−0.98	*−0.98*
	6	1.64	−1.00	−0.98	−1.00	−1.01	−0.98	−1.01

δ(O), −0.93 for isolated water. Italics denotes oxygen from water molecules in 2nd solvation shell.

The other molecules prefer to stay in the second hydration shell. This is not the case of Hartree-Fock calculations where 3-coordinated (or 4-coordinated in $[Cu(H_2O)_6]^{+}$ case) complexes represent the most stable structures. An explanation of this fact can be seen in overestimated role of electrostatic and polarization contributions to total energies. More sophisticated methods, which include correlation effects (MP2, DFT) correct this artifact.

The most stable coordination for Cu^{2+} complex is four or maybe five. Both these coordinations exhibit similar stabilization energies especially when mutual repulsion of ligands is excluded. This is in very good accordance with experimental observations published in Ref. [65].

Stabilization energies with and without sterical corrections were determined for all complexes. With increasing number of coordinated molecules, the repulsion is increasing up to 30 kcal/mol in case of the 6-coordinated Cu^{2+} complex. The difference is substantially smaller for Cu^{+} systems (e.g. 6 kcal/mol in case of the 4-coordinated complex). Morokuma's energy decomposition enlightens the importance of individual contributions. It is shown that at the Hartree-Fock level Coulomb and polarization terms predominate as one could expect for charged systems with metal cation.

Occupation of valence AOs (especially to 4s orbital) on Cu^{+} cation points to the extent of water ligands donation. In case of Cu^{2+} complexes, partial charges (based on NBO analysis) could be used for illustration of donation effects. Analysis of MOs was used to explain differences in donation of monoaqua and diaqua complexes.

Acknowledgements

This study was supported by Charles University grant 181/2002/B_FYZ/MFF, and grant NSF -MŠMT CR ME-517. Special thank should be given to the computational resources from Meta-Centres in Prague, Brno, and Pilsen for excellent access to their supercomputer facilities and their kind understanding. We would also like to acknowledge the Mississippi Supercomputing Research Center that supported many of the calculations.

References

[1] J.V. Burda, J. Šponer, P. Hobza, J. Phys. Chem. 100 (1996) 7250–7255.
[2] J.V. Burda, J. Šponer, J. Leszczynski, P. Hobza, J. Phys. Chem. B 101 (1997) 9670–9677.
[3] A. Gasowska, L. Lomozik, Monatshefte fur Chemie 126 (1995) 13–22.
[4] J. Šponer, M. Sabat, J. Burda, J. Leszczynski, P. Hobza, B. Lippert, J. Biol. Inorg. Chem. 4 (1999) 537–545.
[5] E.V. Hackl, S.V. Kornilova, L.E. Kapinos, V.V. Andruschenko, V.L. Galkin, D.N. Grigoriev, Y.P. Blagoi, J. Mol. Struct. 408/409 (1997) 229–232.
[6] L.A. Herrero, A. Terron, J. Biol. Inorg. Chem. 5 (2000) 269–275.
[7] E. Meggers, P.L. Holland, W.B. Tolman, F.E. Romesberg, P.G. Schultz, J. Am. Chem. Soc. 122 (2000) 10714–10715.
[8] B. Schoentjes, J.-M. Lehn, Helvetica Chim. Acta 78 (1995) 1–12.
[9] S. Atwell, E. Meggers, G. Spraggon, P.G. Schultz, J. Am. Chem. Soc. 123 (2001) 12364–12367.
[10] J. Sabolovic, C.S. Tautermann, T. Loerting, K.R. Liedl, Inorg. Chem. 42 (2003) 2268–2279.
[11] J. Sabolovic, K.R. Liedl, Inorg. Chem. 38 (1999) 2764–2774.
[12] J. Bertran, L. Rodrigues-Santiago, M. Sodupe, J. Phys. Chem. B 103 (1999) 2310–2317.
[13] L. Rulíšek, Z. Havlas, J. Am. Chem. Soc. 122 (2000) 10428–10439.
[14] S. Santra, P. Zhang, W. Tan, J. Phys. Chem. A 104 (2000) 12021–12028.
[15] T. Shoeib, C.F. Rodriquez, K.W.M. Siu, A.C. Hopkinson, Phys. Chem. Chem. Phys. 3 (2001) 853–861.
[16] R. Prabhakar, P.E.M. Siegbahn, J. Phys. Chem. B 107 (2003) 3944–3953.
[17] P. Manikandan, B. Epel, D. Goldfarb, Inorg. Chem. 40 (2001) 781–787.
[18] K. Shimizu, H. Maeshima, H. Yoshida, A. Satsuma, T. Hattori, Phys. Chem. Chem. Phys. 3 (2001) 862–866.
[19] M.H.M. Olsson, U. Ryde, J. Biol. Inorg. Chem. 4 (1999) 654–663.
[20] M.H.M. Olsson, U. Ryde, B.O. Roos, K. Pierloot, J. Biol. Inorg. Chem. 3 (1998) 109–125.
[21] D.W. Randall, S.D. George, B. Hedman, K.O. Hodgson, K. Fujisawa, E.I. Solomon, J. Am. Chem. Soc. 122 (2000) 11620–11631.
[22] D.W. Randall, S.D. George, P.L. Holland, B. Hedman, K.O. Hodgson, W.B. Tolman, E.I. Solomon, J. Am. Chem. Soc. 122 (2000) 11632–11648.
[23] U. Ryde, M.H.M. Olsson, B.O. Roos, J.O.A. De Kerpel, K. Pierloot, J. Biol. Inorg. Chem. 5 (2000) 565–574.
[24] P.L. Holland, W.B. Tolman, J. Am. Chem. Soc. 121 (1999) 7270–7271.
[25] P.L. Holland, W.B. Tolman, J. Am. Chem. Soc. 122 (2000) 6331–6332.
[26] H.B. Gray, B.G. Malmstroem, R.J.P. Williams, J. Biol. Inorg. Chem. 5 (2000) 551–559.
[27] E. Fraga, M.A. Webb, G.R. Loppnow, J. Phys. Chem. 100 (1996) 3278–3287.
[28] L.D. Book, D.C. Arnett, H. Hu, N.F. Scherer, J. Phys. Chem. A 102 (1998) 4350–4359.
[29] P.E.M. Siegbahn, M. Wirstam, J. Am. Chem. Soc. 123 (2001) 11819–11820.
[30] P.E.M. Siegbahn, J. Comp. Chem. 22 (2001) 1634–1645.
[31] H. Tachikawa, Chem. Phys. Lett. 260 (1996) 582–588.
[32] D. Schroeder, H. Schwartz, J. Wu, C. Wesdemiotis, Chem. Phys. Lett. 343 (2001) 258–264.
[33] G.W. Marini, K.R. Liedl, B.M. Rode, J. Phys. Chem. A 103 (1999) 11387–11393.
[34] C.F. Schwenk, B.M. Rode, Phys. Chem. Chem. Phys. 5 (2003) 3418–3427.
[35] A. Berces, T. Nukada, P. Margl, T. Ziegler, J. Phys. Chem. A 103 (1999) 9693–9701.
[36] H.D. Pranowo, A.H.B. Setiajin, B.M. Rode, J. Phys. Chem. A 103 (1999) 11115–11120.
[37] H.D. Pranowo, B.M. Rode, J. Phys. Chem. A 103 (1999) 4298–4302.
[38] H.D. Pranowo, B.M. Rode, Chem. Phys. 263 (2001) 1–6.
[39] D. Feller, E.D. Glendening, W.A. de Jong, J. Chem. Phys. 110 (1999) 1475–1491.
[40] J.A. Stone, D. Vukomanovic, Chem. Phys. Lett. 346 (2001) 419–422.
[41] F. Haeffner, T. Brinck, M. Haeberlein, C. Moberg, Chem. Phys. Lett. 397 (1997) 39–50.
[42] N.M.D.S. Cordeiro, J.A.N.F. Gomes, J. Comput. Chem. 14 (1993) 629–638.

[43] V. Subramanian, C. Shankaranarayanan, B.U. Nair, M. Kanthimathi, R. Manickkavachagam, T. Ramasami, Chem. Phys. Lett. 274 (1997) 275–280.
[44] A. Luna, M. Alcami, O. Mo, M. Yanez, Chem. Phys. Lett. 320 (2000) 129–138.
[45] M. Böhme, G. Frenklin, Chem. Phys. Lett. 224 (1994) 195–199.
[46] I. Persson, P. Persson, M. Sandstrom, A.S. Ullstrom, J. Chem. Soc. Dalton Trans. 2002; 1256–1265.
[47] S.K. Hoffmann, J. Goslar, W. Hilczer, M.A. Augustyniak, M. Marciniak, J. Phys. Chem. A 102 (1998) 1697–1707.
[48] M. Baranska, K. Chruszcz, B. Boduszek, L.M. Proniewicz, Vib. Spectrosc. 31 (2003) 295–311.
[49] F.S. Legge, G.L. Nyberg, J.B. Peel, J. Phys. Chem. 105 (2001) 7905–7916.
[50] A. Luna, B. Amekraz, J. Tortajada, Chem. Phys. Lett. 266 (1997) 31–37.
[51] X. Xu, W.A. Goddard, J. Phys. Chem. 108 (2004) 2305–2313.
[52] M.M. Hurley, L.F. Pacios, P.A. Christiansen, R.B. Ross, W.C. Ermler, J. Chem. Phys. 84 (1986) 6840–6853.
[53] S.F. Boys, F. Bernardi, Mol. Phys. 19 (1970) 553–566.
[54] A.E. Reed, R.B. Weinstock, F. Weinhold, J. Chem. Phys. 78 (1987) 4066.
[55] M.J. Frisch, G.W.T., H.B. Schlegel, G.E. Scuseria, M.A. Robb, J.R.C., V.G. Zakrzewski, J.A. Montgomery Jr., R.E. Stratmann, J.C. Burant, S.D., J.M. Millam, A.D. Daniels, K.N. Kudin, M.C. Strain, O. Farkas, J. Tomasi, V.B., M. Cossi, R. Cammi, B. Mennucci, C. Pomelli, C. Adamo, S. Clifford, J. Ochterski, G.A.P., P.Y. Ayala, Q. Cui, K. Morokuma, P. Salvador, J.J. Dannenberg, D.K. Malick, A.D.R., K. Raghavachari, J.B. Foresman, J. Cioslowski, J.V. Ortiz, A.G. Baboul, B.B.S., G. Liu, A. Liashenko, P. Piskorz, I. Komaromi, R. Gomperts, R.L. Martin, D.J.F., T. Keith, M.A. Al-Laham, C.Y. Peng, A. Nanayakkara, M. Challacombe, P.M.W. Gill, B.J., W. Chen, M.W. Wong, J.L. Andres, C. Gonzalez, M. Head-Gordon, E.S.R., J.A. Pople, Gaussian 98 (Revision A.1x), Gaussian, Inc., Pittsburgh PA, 2001.
[56] M.W. Schmidt, K.K. Baldridge, J.A. Boatz, S.T. Elbert, M.S. Gordon, J.J. Jensen, S. Koseki, N. Matsunaga, K.A. Nguyen, S. Su, T.L. Windus, M. Dupuis, J.A. Montgomery, J. Comput. Chem. 14 (1993) 1347–1363.
[57] G. Schaftenaar, In: http://www.cmbi.kun.nl/~schaft/molden/molden.html; 3.9 ed.
[58] P.F. Flükiger, http://www.cscs.ch/molekel/.
[59] S. Portmann, H.P. Lüthi, Chimia 54 (2000) 766–770.
[60] S. Maheshwary, N. Patel, N. Sathyamurthy, A.D. Kulkarni, S.R. Gadre, J. Phys. Chem. A 105 (2001) 10525–10537.
[61] T. Miyake, M. Aida, Chem. Phys. Lett. 363 (2002) 106–110.
[62] D.J. Anick, J. Phys. Chem. A 107 (2003) 1348–1358.
[63] B. Hartke, Z. Phys. Chem. 214 (2000) 1251–1264.
[64] H. Kabrede, R. Hentschke, J. Phys. Chem. B 107 (2003) 3914–3920.
[65] A. Pasquarello, I. Petri, P.S. Salmon, O. Parisel, R. Car, E. Toth, D.H. Powell, H.E. Fischer, L. Heim, A.E. Merbach, Science 291 (2001) 856–859.
[66] A.E. Reed, R.B. Weinstock, F. Weinhold, J. Chem. Phys. 83 (1985) 735–746.

Available online at www.sciencedirect.com
SCIENCE DIRECT®
Chemical Physics 312 (2005) 193–204
Chemical Physics
www.elsevier.com/locate/chemphys

Theoretical description of copper Cu(I)/Cu(II) complexes in mixed ammine-aqua environment. DFT and ab initio quantum chemical study

Matěj Pavelka, Jaroslav V. Burda *

Department of Chemical Physics and Optics, Faculty of Mathematics and Physics, Charles University, Ke Karlovu 3, 121 16 Prague 2, Czech Republic

Received 17 August 2004; accepted 27 November 2004
Available online 19 December 2004

Abstract

This work is devoted to investigate the interactions of the Cu(I)/Cu(II) cation with variable ammonia–water ligand field by the quantum chemical approach. For that purpose, the optimization of the $[Cu(NH_3)_m(H_2O)_n]^{2+/+}$ complexes (where n varies from 0 to 4 or 6 and $m+n=4$ or 6) has been performed at the DFT/6-31+G(d) level of theory in conjunction with the B3PW91 hybrid functional. Based on the results of the single-point B3LYP/6-311++G(2df,2pd) calculations, the stabilization energies were determined. The two-coordinated copper(I) complexes appeared to be the most stable compounds with the remaining water or ammonia molecules in the second solvation shell. In the case of the Cu(II) systems, four-coordinated complexes were found to be the most stable. In order to examine and explain bonding characteristics, Morokuma interaction energy decomposition (for selected Cu^+ complexes) and Natural Population Analysis for all systems were performed. It was found that the most stable structures correlate with the highest donation effects. Therefore, more polarizable ammonia molecules exhibit higher donation than water and thus make stronger bonds to copper. This can be demonstrated by the fact that the NH_3 molecule always tries to occupy the first solvation shell in mixed ammine-aqua complexes.

Keywords: DFT calculations; Copper complexes

1. Introduction

Copper is essential for an "au naturel" occurrence of many processes in bioorganisms. Hence, there is a huge number of works investigating biological activity of the copper ions and their interactions using both experimental and theoretical approaches. Copper cation interactions with amino acids were investigated in studies [1–9] using various computational approaches. Experimental measurements, which were published, e.g., in [10–12] initiated some of these studies and were basically confirmed or some of their conclusions were explained by above-mentioned theoretical works. Very prosperous is the exploration of the so-called blue proteins, a group of electron transfer systems characterized by a bright blue color, a narrow hyperfine splitting in the electronic spin resonance spectra and especially high reduction potential. Their active centers are formed by a redox copper Cu(I)/Cu(II) cation coordinated usually with cysteine and histidine side chains. The coordination sphere is typically completed by the methionine side chain. A comparison of the geometry arrangements in reduced and oxidized protein centers were studied by Olsson's group [13–16]. The authors have pointed to large similarity of both forms. This structural feature is also discussed by Randall et al. [17,18] and in some other works [19–21]. These results can be compared with, e.g., pump and probe spectroscopy [22] or

* Corresponding author. Tel.: +420221911246; fax: +420221911249.
E-mail address: burda@karlov.mff.cni.cz (J.V. Burda).

0301-0104/$ - see front matter © 2004 Elsevier B.V. All rights reserved.
doi:10.1016/j.chemphys.2004.11.034

measurements of resonance Raman intensities [23]. Finally, copper plays an important role in many other enzymatic processes [24] – e.g. cytochrome *c* oxidase, lactase [25], Cu,Zn-superoxidase dismutase, ceruloplasmin, diammineoxidase, azurin [26] and indophenol-oxidase or tyrosinase [27].

Other interesting topics deal with adducts of copper and DNA/RNA bases studied with ab initio techniques [28–31], for which one can find many experimental evidences [32–37].

Many studies are devoted to examination of simple models in order to determine electronic properties of various copper complexes. The Cu cations in water or ammonium solution are subjects investigated via static [38–40] and dynamic [41–44] approaches or methods combining both tools [45–48]. Stable two-coordinated Cu(II) complexes were observed experimentally in gas phase [49]. On the contrary, the high-coordination was treated as preferred in solution or in solid state [50]. Copper force-field parameters were subject of several studies [51–53] since the requirement of large-scale MM/MD molecular simulations is very urgent in biodisciplines. The SIBFA method presented in paper of Gresh [54] is one of the interesting and promising approaches in this field. Some of Cu(I) and Cu(II) complexes were successfully solved using this technique [55,56].

The aim of this study is to find energetic and electronic relations between the structures of Cu(I)/Cu(II) cations interacting with variable ammonia–water environment. In the present paper, a thorough comparison with similar results found in the literature [2,3,41–43,45–47,50,57] was also done. Finally, it should be mentioned that this work complements our previous study of copper hydration [64].

2. Computational details

Since the investigated $[Cu(NH_3)_m(H_2O)_n]^+$ complexes, where n varies from 0 to 4 or 6 and $m+n=4$ or 6 are the closed shell systems, singlet electronic configuration represents the ground state of these compounds. Detailed geometry search was performed. Several local minima were obtained. Similar situation was already described, e.g., in studies [39,45]. In this work, only the most stable various-coordinated structures are presented. The optimized geometries were obtained at the DFT level of theory using the B3PW91 functional. In comparison with B3LYP, structures and frequency properties obtained using the B3PW91 functional are slightly better [58–61]. All the low-lying minima were confirmed by the frequency analysis. Standard 6-31+G(d) basis set with diffusion functions was used for the ligand description. Electrons on the copper atom were described by Christiansen averaged relativistic effective pseudopotential (AREP) [62]. Basis set of pseudoorbitals was extended by diffuse and polarization functions ($\alpha_s = 0.025$, $\alpha_p = 0.35$, $\alpha_d = 0.07$ and $\alpha_f = 3.75$) in correspondence with 6-31+G(d) set [63].

The open shell Cu^{2+} cation has the $3d^9$ electron configuration. Consequently, the ground states of $[Cu(NH_3)_m(H_2O)_n]^{2+}$ complexes were considered as doublets. Besides a few systems, computational procedure in 6-31+G(d) basis came to wrong orbital occupation or failed completely when general guess was applied. Therefore at first, an appropriate wavefunction was constructed in minimal basis set using Restricted Open Shell Hartree-Fock (ROHF) procedure, and used as a guess for calculation with augmented basis set ROHF/6-31+G(d). Then geometry optimization at the unrestricted Hartree-Fock (UHF) level was performed. Finally, the UHF structure was re-optimized with the B3PW91 functional.

Analysis of the energy characteristics and the charge distribution was performed on the most stable structures using B3LYP functional. Extended basis set 6-311++G(2df,2pd) was utilized for the oxygen, nitrogen and hydrogen atoms. Basis set on the Cu atom was enlarged accordingly by s, p, d diffuse functions and by 2f, 1g polarization functions ($\alpha_f = 4.97$, 1.30 and $\alpha_g = 3.28$) in a consistent way [64]. The stabilization energies with the basis set superposition error corrections (BSSE) and deformation energies [65] were determined according to equation:

$$\Delta E^{\text{Stab}} = -\left(E_{\text{complex}} - \sum E_{\text{monomer}} - \sum E^{\text{deform}}\right), \quad (1)$$

where E_{complex} represents the total energy of a whole complex and E_{monomer} labels the energy of the individual parts computed with basis functions on the ghost atoms from the rest of the system. Besides the ΔE^{stab} energies, coordination (ΔE^{coord}) and sterically corrected stabilization (ΔE^{stex}) energies were computed in selected cases, as well. The coordination energy was established especially for the Cu(I) systems where ligand molecules often escaped to second hydration shell. For calculation of coordination energy, only directly bonded ligands were considered in Eq. (1) using the optimized geometry of a whole complex. Calculating ΔE^{stex}, all the interacting molecules were treated as one part simultaneously (only without the central Cu ion) in Eq. (1). These energies were determined for the Cu(II) complexes where a higher coordination is linked with increased repulsion among ligands.

For the structures with a monovalent copper, Morokuma decomposition analysis was performed using GAMESS-US program [66]. *Gaussian 98* program package [67] was used for the rest of quantum chemical calculations. For visualization of geometries, MOs, and vibrational modes, programs Molden 3.7 [68] and Molekel 4.3 [69,70] were applied.

3. Results and discussion

3.1. Cu(I) and Cu(II) structures

The objective of optimization process was to find stable Cu(I) and Cu(II) complexes with various coordination numbers, compare their stability and other properties.

For complexes with a monovalent copper, metal–ligand interaction (dative bonds together with their monopole–dipole electrostatic term) competes with a hydrogen bonding among first and second shell molecules that have very similar energy. The structures of the Cu(I) optimized complexes with 4 or 6 ammonia–water molecules are illustrated in Fig. 1.

In the two-coordinated $[Cu(NH_3)_4]^+$ complex (structure **0a**) copper makes relatively strong coordination bonds with ammine ligands in the first solvation shell (their lengths are 1.91 Å). This is also demonstrated by the increased coordination energy, Morokuma decomposition analysis, and NPA charge distribution that will be discussed below. The other two ammonia are H-bonded to the first shell where the N···H distance is about 1.9 Å.

For a less stable three-coordinated system (structure **0b**), the first coordination shell is nearly planar (bond lengths: 2.07, 2.07 and 2.00 Å) with the remaining NH_3 molecule attached to one of the ligands by the hydrogen bond (1.96 Å). The complex with 4 coordinated ammine ligands (**0c**) creates the longest Cu–N bonds (2.14 Å) with a small deviation from T_d symmetry. For all the Cu(I) complexes, copper–ligand distances are presented in Table 1. The averaged Cu–N bond dependences on the ligand type and coordination number are for a more illustrative view presented in Figs. 3(a) and (b). The shortest distances were obtained for the most stable two-coordinated structures and the longest distances for four-coordinated complexes. Both the Cu–N and Cu–O bonds are shortened with increasing number of water molecules in the first solvation shell. It is caused by stronger copper interaction with NH_3 ligands in competition with aqua ligands. The

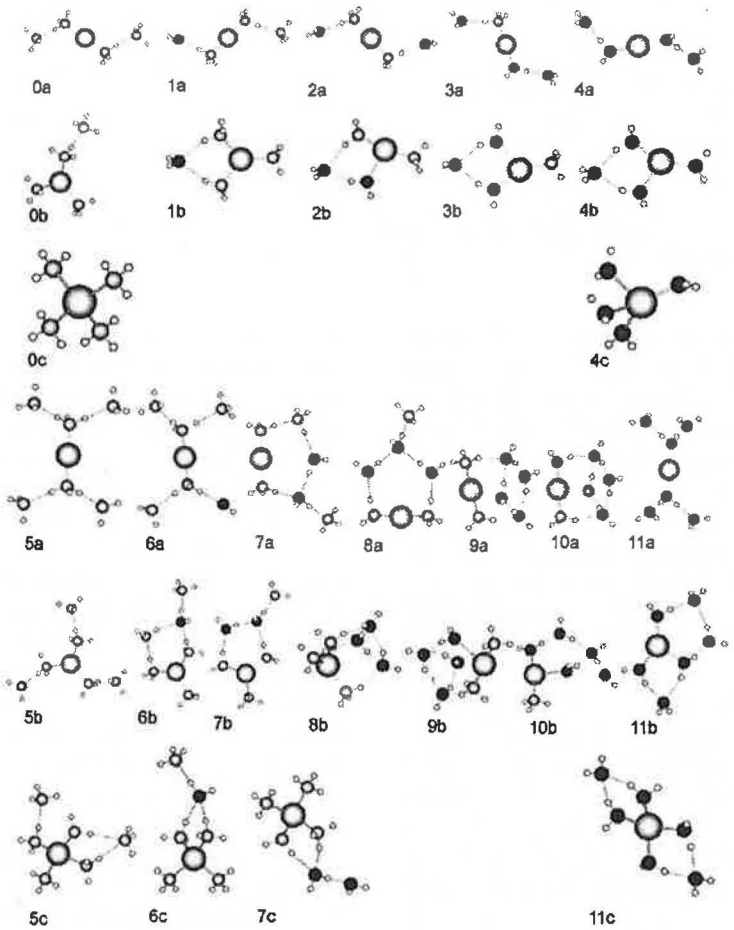

Fig. 1. (structures **0a–11c**) The optimized Cu(I) complexes. Systems **0–4** and **5–11** represent the $[Cu(NH_3)_m(H_2O)_n]^+$ structures, with 4 ($m+n=4$; $n=0$ to 4) and 6 ($m+n=6$; $n=0$ to 6) ammonia–water molecules, respectively. Letters a, b and c correspond to two-, three- and four-coordination.

Table 1
Copper–ligand distances (in Å) for all presented Cu(I) complexes

System	c.n.	Cu–Lig1 (Å)	Cu–Lig2 (Å)	Cu–Lig3 (Å)	Cu–Lig4 (Å)
[Cu(lig)$_4$]$^+$					
[Cu(NH$_3$)$_4$]$^+$	2	1.91*	1.91*		
	3	2.07*	2.00*	2.08*	
	4	2.14*	2.14*	2.14*	2.14*
[Cu(NH$_3$)$_3$(H$_2$O)]$^+$	2	1.91*	1.90*		
	3	2.06*	2.06*	2.01*	
[Cu(NH$_3$)$_2$(H$_2$O)$_2$]$^+$	2	1.91*	1.91*		
	3	2.35	1.94*	1.94*	
[Cu(NH$_3$)(H$_2$O)$_3$]$^+$	2	1.89	1.90*		
	3	1.98	2.20	1.94*	
[Cu(H$_2$O)$_4$]$^+$	2	1.88	1.88		
	3	1.97	1.98	2.14	
	4	2.00	2.09	2.21	2.26
[Cu(lig)$_6$]$^+$					
[Cu(NH$_3$)$_6$]$^+$	2	1.90*	1.90*		
	3	2.04*	2.04*	2.04*	
	4	2.07*	2.14*	2.16*	2.16*
[Cu(NH$_3$)$_5$(H$_2$O)]$^+$	2	1.90*	1.90*		
	3	2.01*	2.03*	2.10*	
	4	2.09*	2.14*	2.15*	2.16*
[Cu(NH$_3$)$_4$(H$_2$O)$_2$]$^+$	2	1.90*	1.91*		
	3	2.02*	2.04*	2.07*	
	4	2.13*	2.13*	2.14*	2.14*
[Cu(NH$_3$)$_3$(H$_2$O)$_3$]$^+$	2	1.90*	1.90*		
	3	2.04*	2.04*	2.04*	
[Cu(NH$_3$)$_2$(H$_2$O)$_4$]$^+$	2	1.91*	1.91*		
	3	2.51	1.92*	1.92*	
[Cu(NH$_3$)(H$_2$O)$_5$]$^+$	2	1.90	1.90*		
	3	1.93	2.37	1.91*	
[Cu(H$_2$O)$_6$]$^+$	2	1.87	1.87		
	3	1.97	2.02	2.06	
	4	2.13	2.13	2.13	2.13

Values with and without * indicate Cu–N and Cu–O bonds, respectively.
Shortcut c.n. means coordination number.

Cu–N/Cu–O distances are also shortened by the presence of other molecules in the second shell. The reason can be seen in a fact that the electron density of N–H or O–H bonds in the ligand is decreased by the interactions of this positively charged hydrogen with a lone pair of electronegative atom from the second shell molecule. This induces a strengthening of the Cu–N/Cu–O dative bond in the complex. In the case of three-coordinated complexes, one of the bonds is usually longer than the remaining two. Interestingly, no five- or higher-coordinated complexes were found. Feller et al. [39] have studied the interactions of the Cu^+ cation with water using various ab initio approaches. Their Cu–O distances at the MP2/6-31+G(f)(RECP) level for all the (two- and three-coordinated) complexes match very well with our geometrical parameters. For the four-coordinated tetra-aqua system, we have obtained similar bond lengths but with the geometry in C_1 symmetry on the contrary to their structures in C_2 and S_4 point group of symmetry.

The optimized $[Cu(ligand)_K]^{2+}$ structures (where $K=4$ or 6) are displayed in Fig. 2. The Cu(II) complexes prefer higher coordination, especially four- and in some cases also five-coordination. Actually, theoretical calculations performed by Schwenk and Rode [43] predict predominately six-coordinated structures of Cu(II) in liquid ammonia in case of HF QM/MM simulation, whereas the five- and six-coordinated complexes were obtained in a ratio of 2:1 in the B3LYP simulation case. This finding is in good agreement with our experience that the HF method exaggerates coordination number, e.g., in the Cu(I) case, the three-coordination is preferred over two-coordination as a global minimum in all the examined systems. The same authors have obtained the six-coordinated monoammine [1 + 5] and diammine [2 + 4] Cu^{2+} complexes in water [43]. There are also works devoted in four-coordinated copper structures, usually because of copper interaction with amino acids. For example, the extensive study of Katz et al. [2] has explored the tetraammine Cu(I)/Cu(II) structures. The pure ammine–copper(II) and aqua–copper(II) structures were subject of study performed by Berces et al. [45]. The authors have found that more than four-ligated complexes do not enhance the stabil-

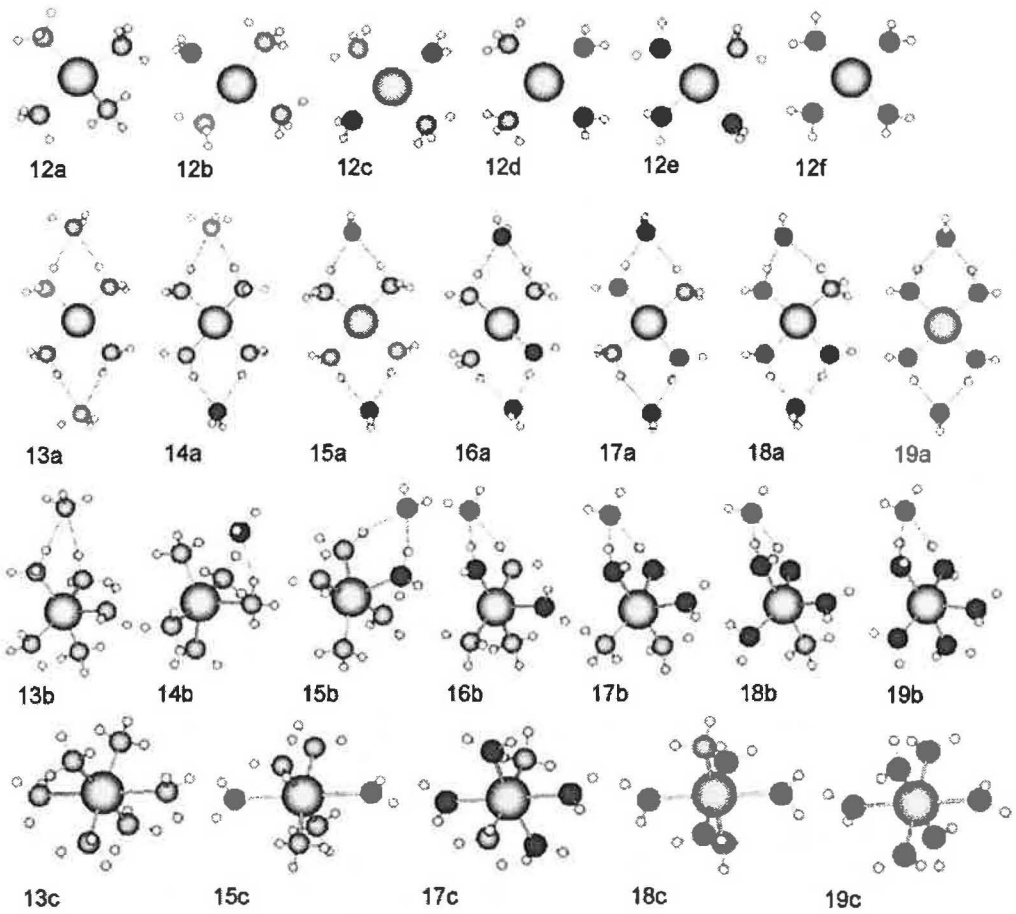

Fig. 2. (structures **12a–19c**) The optimized Cu(II) complexes. Systems **12a–f** represent four-coordinated $[Cu(NH_3)_m(H_2O)_n]^+$ structures ($m+n=4$; $n=0$ to 4). Systems **13–19** represent the $[Cu(NH_3)_m(H_2O)_n]^+$ structures ($m+n=6$; $n=0$ to 6). Letters a, b and c correspond to four-, five- and six-coordination.

ization energy of the molecule. However, there are also both experimental [50] and computational [47] studies which predict a coordination number six or even higher. Nevertheless, the calculations in the last mentioned paper were performed at the HF level, which reliability was discussed above.

Obtained copper–ligand distances are collected in Table 2. Shorter distances for Cu(II) complexes in comparison with the distances found in the Cu(I) systems indicate stronger Cu–L bonds. In analogy with the Cu^+ cation complexes, both Cu–N and Cu–O bond lengths shorten with number of aqua ligands. This fact is illustrated by the averaged coordination distances in Fig. 4. The only exception represents Cu–N bonds in the *trans*-$[Cu(NH_3)_2(H_2O)_2]^{2+}$ complex (structure **12d** in Fig. 2) due to a pronounced *trans*-effect. This conformer is not the lowest minimum of diammine-diaqua system. The *cis*-$[Cu(NH_3)_2(H_2O)_2]^{2+}$ complex (**12c**) possesses a lower energy and larger stabilization (see below).

The five-coordinated structures (**13–19b**) form the octahedral complexes, which are deformed by a missing axial vertex. Cu–L distances were found to be in very good agreement with other theoretical papers [2,42,43,45].

3.2. Energy

In order to analyze the optimized structures, the stabilization, coordination and sterically corrected energies were calculated at the DFT level of theory with the B3LYP functional and an extended triple-zeta basis set.

Table 3 contains the ΔE^{stab} stabilization energies for all the Cu(I) systems. Due to the fact that several molecules stay in second shell in the most of the explored structures (0–4a–b and 5–11a–c in Fig. 1), coordination energies ΔE^{coord} were calculated in order to estimate bonding energies per ligand.

From Table 3, it can be seen that two-coordinated complexes represent the global minima of the explored structures. This result is contradictive to the results obtained using the Hartree–Fock method that predict the three-coordinated Cu^+ systems as the global minima.

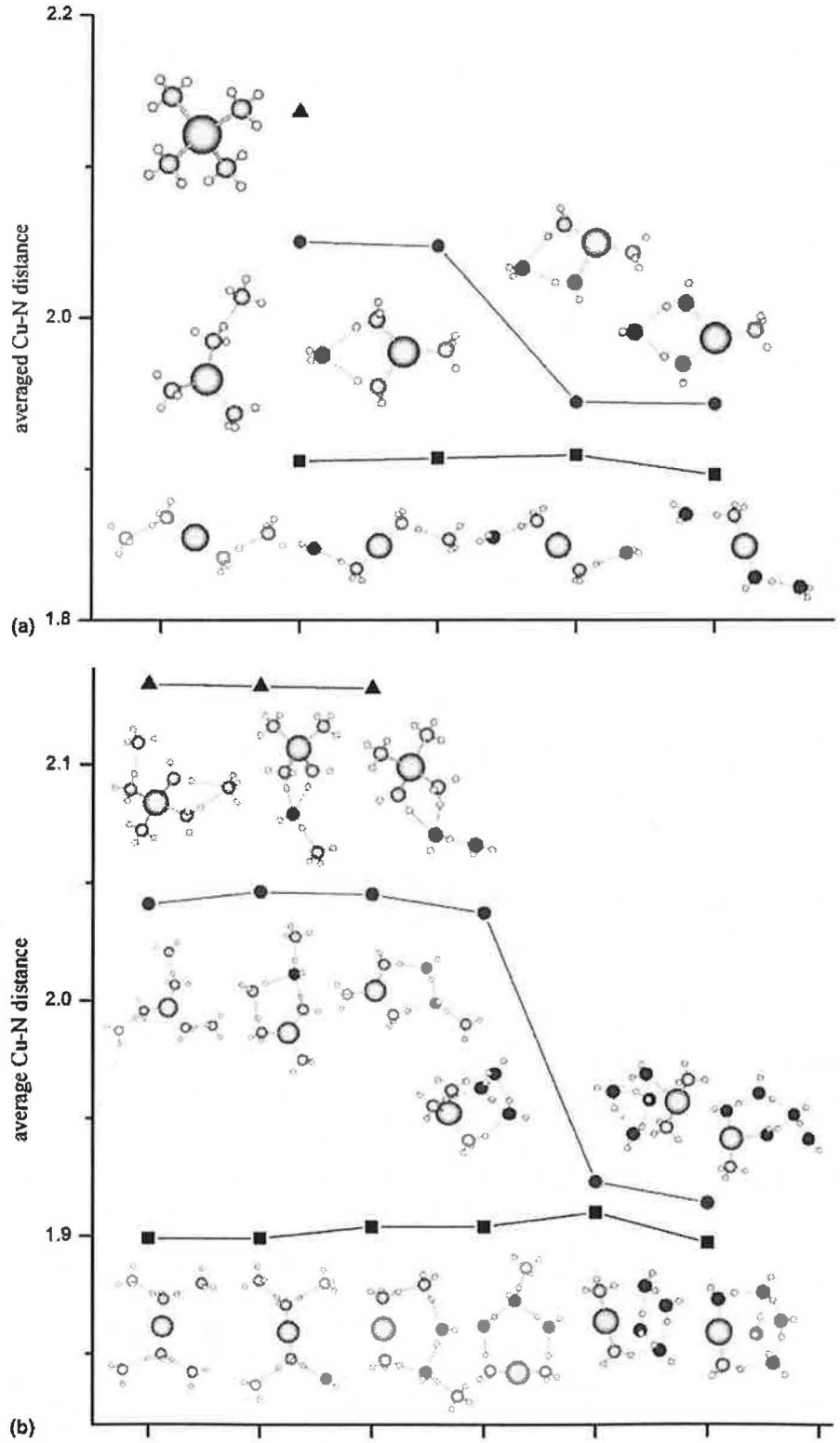

Fig. 3. (a) Dependence of the averaged Cu–N coordination bond lengths (in Å) for the $[Cu(NH_3)_m(H_2O)_n]^+$ structures ($m+n=4$; $n=0$ to 4) on increasing number of water molecules in system. ▲, for four-coordinated systems; ●, for three-coordinated systems and ■, for two-coordinated systems. (b) Dependence of the averaged Cu–N coordination bond lengths (in Å) for the $[Cu(NH_3)_m(H_2O)_n]^+$ structures ($m+n=6$; $n=0$ to 6) on increasing number of water molecules in system. ▲, for four-coordinated systems; ●, for three-coordinated systems and ■, for two-coordinated systems.

Table 2
Copper–ligand distances (in Å) for all presented Cu(II) complexes

System	c.n.	Cu–Lig1 (Å)	Cu–Lig2 (Å)	Cu–Lig3 (Å)	Cu–Lig4 (Å)	Cu–Lig5 (Å)	Cu–Lig6 (Å)
$[Cu(lig)_4]^{2+}$							
$[Cu(NH_3)_4]^{2+}$	4	2.05*	2.05*	2.05*	2.05*		
$[Cu(NH_3)_3(H_2O)]^{2+}$	4	2.01*	2.01*	2.04*	2.11		
cis-$[Cu(NH_3)_2(H_2O)_2]^{2+}$	4	2.00*	2.00*	2.02	2.02		
trans-$[Cu(NH_3)_2(H_2O)_2]^{2+}$	4	2.06*	2.06*	1.99	1.99		
$[Cu(NH_3)(H_2O)_3]^{2+}$	4	1.98*	1.98	1.99	2.01		
$[Cu(H_2O)_4]^{2+}$	4	1.96	1.96	1.96	1.96		
$[Cu(lig)_6]^{2+}$							
$[Cu(NH_3)_6]^{2+}$	4	2.04*	2.04*	2.04*	2.04*		
	5	2.07*	2.10*	2.10*	2.07*	2.28*	
	6	2.17*	2.17*	2.17*	2.17*	2.51*	2.51*
$[Cu(NH_3)_5(H_2O)]^{2+}$	4	2.04*	2.04*	2.04*	2.04*		
	5	2.08*	2.06*	2.07*	2.06*	2.30*	
$[Cu(NH_3)_4(H_2O)_2]^{2+}$	4	2.05*	2.05*	2.05*	2.05*		
	5	2.08*	2.10*	2.08*	2.12*	2.24	
	6	2.06*	2.06*	2.06*	2.06*	2.60	2.58
$[Cu(NH_3)_3(H_2O)_3]^{2+}$	4	2.05*	2.05*	2.05*	2.05		
	5	2.04*	2.06*	2.03*	2.04	2.33	
$[Cu(NH_3)_2(H_2O)_4]^{2+}$	4	2.01*	2.01*	1.98	1.98		
	5	2.04*	2.06*	2.03	2.04	2.33	
	6	1.99*	1.99*	2.18	2.18	2.35	2.33
$[Cu(NH_3)(H_2O)_5]^{2+}$	4	1.99*	1.98	1.97	1.96		
	5	1.99*	2.02	1.98	2.07	2.23	
	6	1.99*	2.10	2.10	2.00	2.30	2.29
$[Cu(H_2O)_6]^{2+}$	4	2.03	2.03	2.03	2.03		
	5	1.97	1.96	2.06	2.08	2.09	
	6	1.98	1.98	2.01	2.01	2.24	2.24

Values with and without * indicate Cu-N and Cu-O bonds, respectively.
Shortcut c.n. means coordination number.

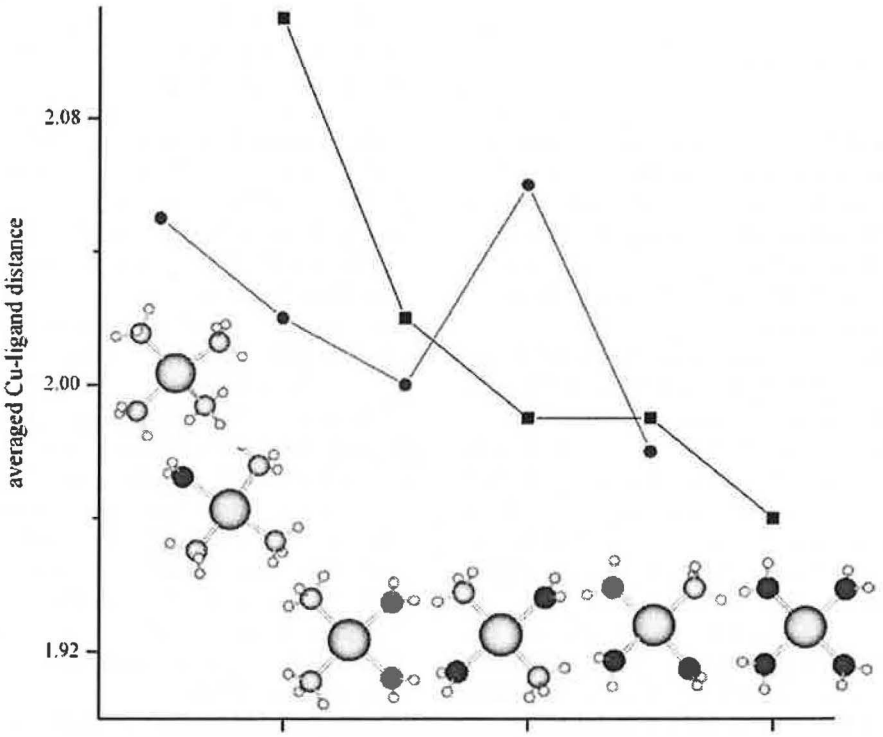

Fig. 4. The variation of averaged Cu(II)–N and Cu(II)–O distances (in Å) for the $[Cu(NH_3)_m(H_2O)_n]^{2+}$ ($m+n=4$; $n=0$ to 4) structures with number of water molecules. ●, for Cu–N bonds and ■, for Cu–O bonds.

Table 3
Stabilization ΔE^{stab} (total) and coordination ΔE^{coord} (related to a ligand bond) energies for all Cu(I) systems (in kcal/mol)

System	c.n.	E^{stab} (kcal/mol)	E^{coord} (kcal/mol)
[Cu(lig)$_4$]$^+$			
$[Cu(NH_3)_4]^+$	2	144.4	58.8
	3	140.5	43.3
	4	139.3	34.8
$[Cu(NH_3)_3(H_2O)]^+$	2	142.1	59.0
	3	140.6	43.2
$[Cu(NH_3)_2(H_2O)_2]^+$	2	139.8	59.2
	3	138.1	41.3
$[Cu(NH_3)(H_2O)_3]^+$	2	129.1	50.5
	3	126.9	36.3
$[Cu(H_2O)_4]^+$	2	117.6	41.8
	3	112.0	31.1
	4	106.7	26.7
[Cu(lig)$_6$]$^+$			
$[Cu(NH_3)_6]^+$	2	163.0	58.8
	3	158.5	43.1
	4	155.5	34.5
$[Cu(NH_3)_5(H_2O)]^+$	2	161.5	58.8
	3	161.1	43.2
	4	160.2	34.6
$[Cu(NH_3)_4(H_2O)_2]^+$	2	162.6	58.5
	3	162.6	42.9
	4	157.5	34.6
$[Cu(NH_3)_3(H_2O)_3]^+$	2	164.9	58.9
	3	159.3	43.0
$[Cu(NH_3)_2(H_2O)_4]^+$	2	162.7	59.0
	3	158.1	41.7
$[Cu(NH_3)(H_2O)_5]^+$	2	151.0	50.0
	3	149.6	36.5
$[Cu(H_2O)_6]^+$	4	142.2	41.1
	5	135.9	30.5
	6	132.9	25.1

Shortcut c.n. means coordination number.

In the complexes with higher coordination, the stabilization energy per bond rapidly decreases. The systems containing higher number of molecules quickly reach the saturation of the stabilization energy. Passing from 4 to 6 interacting molecules this energy is changed only due to the formation of H-bonds and Cu-remote molecule non-bonding interactions.

From water–ammonia arrangement in optimized systems, one can see that the ammine–Cu bond is stronger than aqua–Cu bond because ammine ligands are preferred in the first solvation shell. Actually, the Cu–N bonds are shorter in a presence of the directly ligated water molecules. As mentioned above, the stabilization energies correspond with stronger Cu–N than Cu–O interactions. This result is in agreement with the HSAB (hard-soft acid base) theory [71].

For some chosen Cu(I) complexes, Morokuma energy decomposition was computed (using RHF/6-31+G*) to acquire closer insight into the cation–ligand bonding. In Table 4, the basic contributions to the interaction are collected. On the contrary to relatively conserved electrostatic interaction, absolute values of

Table 4
Selected terms from Morokuma energy decomposition analysis for some Cu(I) structures: electrostatic interaction E^{elec}, exchange energy E^{exch} and polarization energy E^{polar}

System	c.n.	E^{elec} (kcal/mol)	E^{exch} (kcal/mol)	E^{polar} (kcal/mol)
$[Cu(NH_3)_4]^+$	2	−226.1	196.7	−355.9
	4	−219.6	148.8	−89.7
$[Cu(NH_3)_3(H_2O)]^+$	2	−219.4	187.2	−351.1
$[Cu(NH_3)_2(H_2O)_2]^+$	2	−212.8	177.5	−346.2
$[Cu(NH_3)(H_2O)_3]^+$	2	−197.	167.6	−295.5
	3	−195.0	143.6	−197.8
$[Cu(H_2O)_4]^+$	2	−180.2	154.8	−244.2
	3	−169.3	118.9	−128.2
	4	−157.1	98.1	−84.2

Shortcut c.n. means coordination number.

polarization and exchange repulsion terms decrease with increasing of a coordination number. Nonetheless, the polarization energy decreases faster. Thus the lack of polarization energy causes the destabilization of the higher-coordinated complexes. The lower stabilization of Cu-complexes with the two aqua–ligands (two-coordinated system) can be explained by reduced polarization energy by ca. 50 kcal/mol per coordinated water molecule. For higher Cu-coordinations, the polarization contributions rapidly decrease so that relatively constant electrostatic term prevails. This is also demonstrated by the higher donation of the nitrogen electron density to copper atom (cf. discussion of partial charges bellow). From the polarization energies of pure tetraammine (−89.7 kcal/mol) and tetraaqua complexes (−84.2), it can be seen that it is practically constant for all tetra-coordinated species.

For the Cu(II) systems, stabilization (ΔE^{stab}) and sterically corrected stabilization (ΔE^{stex}) energies are presented in Table 5. The dependence of ΔE^{stab} in the $[Cu(NH_3)_m(H_2O)_n]^{2+}$ structures (**13a–19c**) is also shown in Fig. 5 for better insight. In analogy to Cu(I) complexes, Cu–N bonds were found stronger than Cu–O one. Therefore stabilization of the whole system depends basically on the number of ammine ligands in the first coordination shell. But unlike Cu^+ structures, higher coordination is preferred, namely four-coordination.

In case of the $[Cu(NH_3)_6]^{2+}$ systems (**13a–c**), five-coordinated Cu(II) cation is practically degenerated to four-coordinated complex. The stabilization energy of the five-coordinated complex is about 0.4 kcal/mol smaller. It is within the error of the energy determination. When the corrections on sterical repulsion are taken into account, the pure Cu–N bonding energy is larger in the five-coordinated systems (by 7 kcal/mol). Also six-coordinated system has its ΔE^{stex} larger than four-coordinated one.

Similar situation occurs for the $[Cu(NH_3)_5H_2O]^{2+}$ system, where one water molecule remains in outer shell, leaving the directly bonded $[Cu(NH_3)_n]^{2+}$ complex prac-

Table 5
Stabilization ΔE^{stab} and sterically corrected stabilization ΔE^{stex} energies for all Cu(II) systems (in kcal/mol)

System	c.n.	E^{stab} (kcal/mol)	E^{stex} (kcal/mol)
[Cu(lig)$_4$]$^{2+}$			
$[Cu(NH_3)_4]^{2+}$	4	366.8	391.8
$[Cu(NH_3)_3(H_2O)]^{2+}$	4	353.6	376.6
cis-$[Cu(NH_3)_2(H_2O)_2]^{2+}$	4	340.2	359.5
trans-$[Cu(NH_3)_2(H_2O)_2]^{2+}$	4	339.7	359.9
$[Cu(NH_3)(H_2O)_3]^{2+}$	4	323.5	340.0
$[Cu(H_2O)_4]^{2+}$	4	306.9	321.1
[Cu(lig)$_6$]$^{2+}$			
$[Cu(NH_3)_6]^{2+}$	4	407.5	437.7
	5	407.1	444.6
	6	399.9	443.7
$[Cu(NH_3)_5(H_2O)]^{2+}$	4	406.8	437.8
	5	404.6	441.6
$[Cu(NH_3)_4(H_2O)_2]^{2+}$	4	406.2	438.0
	5	402.7	435.1
	6	398.4	435.8
$[Cu(NH_3)_3(H_2O)_3]^{2+}$	4	398.4	425.2
	5	395.5	425.1
$[Cu(NH_3)_2(H_2O)_4]^{2+}$	4	389.4	411.1
	5	385.2	409.6
	6	379.7	411.6
$[Cu(NH_3)(H_2O)_5]^{2+}$	4	376.9	393.6
	5	372.9	393.4
	6	366.3	394.5
$[Cu(H_2O)_6]^{2+}$	4	363.4	376.4
	5	358.6	377.1
	6	338.0	362.2

Shortcut c.n. means coordination number.

tically unchanged in comparison with the hexaammine system ($n = 4$ or 5). In remaining mixed ammonia–water compounds, the differences in the sterical repulsion correction between ligands are not so large going from four- to six-coordinated complexes to be able to change the order of the ΔE^{stex} values in comparison with ΔE^{stab} (like it was seen in the $[Cu(NH_3)_6]^{2+}$ or $[Cu(NH_3)_5(H_2O)]^{2+}$ cases). Thus, similar order of ΔE^{stab} and ΔE^{stex} values for the coordination number varying from 4 to 6 is visible from Table 5 preferring the coordination number of 4 (or 5).

In case of the hexaaqua complexes (**19a–c**), the six-coordination arrangement displays the largest energy $\Delta E^{stab}(4) - \Delta E^{stab}(6)$ difference (25.4 kcal/mol) among all ammonia–water systems.

Similar results were published by Berces et al. [45] for the pure ammine–Cu(II) and aqua–Cu(II) complexes. A good agreement in differences of stabilization energies between four-, five- and six-coordinated species was obtained. They found an energy preference for four- over five-coordination by about 4 and 1 kcal/mol for the $[Cu(H_2O)_6]^{2+}$ and $[Cu(NH_3)_6]^{2+}$ systems, respectively. In the present study, the corresponding differences are 5 and 0.5 kcal/mol. They also predict a lower stabilization of six-coordination (compared to four-coordination) by about 14 and 25 kcal/mol for the $[Cu(H_2O)_6]^{2+}$ and $[Cu(NH_3)_6]^{2+}$ systems, respectively. This matches with our results where these differences were determined to be 25 and 8 kcal/mol.

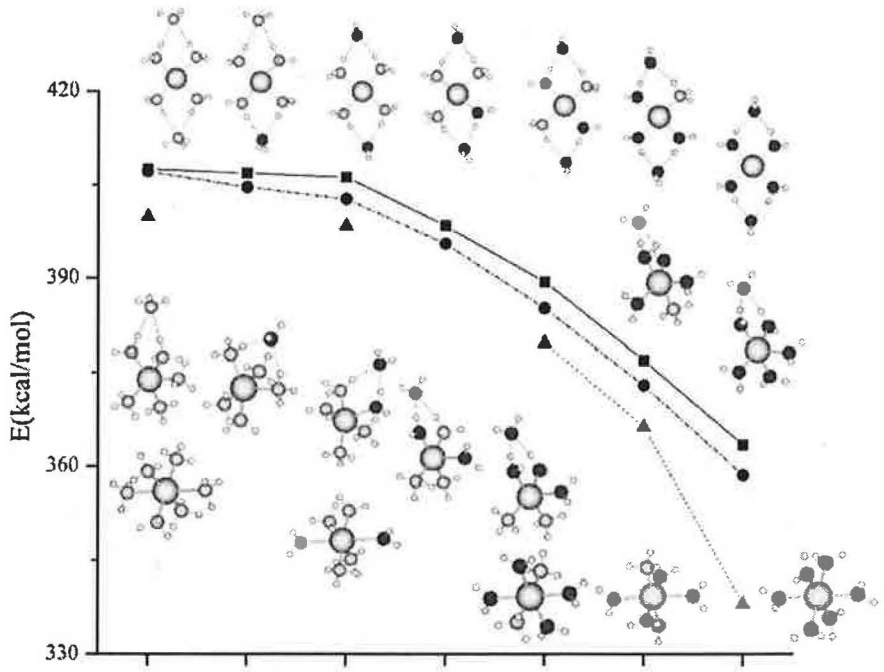

Fig. 5. The trend of stabilization energies (in kcal/mol) for the $[Cu(NH_3)_m(H_2O)_n]^{2+}$ complexes ($m + n = 6$; $n = 0$ to 6) in dependence on the number of water molecules. ▲, for six-coordinated systems; ●, for six-coordinated systems and ■, for four-coordinated systems.

As to four-molecular systems, it is worth to point to a very small difference between the *cis*-$[Cu(NH_3)_2(H_2O)_2]^{2+}$ and *trans*-conformer that is less than 1 kcal/mol. Similar preference was also published in paper [43].

3.3. Charge analyses

In order to get deeper insight into the dependences of the energy and geometry parameters, the partial charges based on natural population analysis (NPA) were determined. In addition, occupations of some important Cu atomic orbitals were explored, too. Both quantities are presented in Tables 6 and 7 for the Cu(I) and Cu(II) systems, respectively.

For the donation of the electron lone pairs from ligands, the vacant Cu orbitals play the fundamental role, especially 4s AO. Hence, its occupation was used for quantification of the strength of dative bonds in the case of Cu(I) complexes. In the two-coordinated Cu^+ systems, the donation is remarkably higher (0.56e) than for the three- (0.34e) and four-coordination (0.24e in case of the $[Cu(NH_3)_4]^+$ system). Similar trend is also evident in the $[Cu(NH_3)_6]^+$ complex and generally in all the examined Cu(I) systems. Higher occupation of 4s orbital correlates with stronger coordination-covalent character of such bonds and matches with the pronounced polarization energies in two-coordinated complexes as mentioned above when the Morokuma's energy decomposition was discussed. Decreased occupation of 4s Cu AO with increasing number of aqua ligands is in correspondence with the lower water polarizability and lower donation ability since the water lone pairs are not usually oriented in Cu–O bond direction as it was stressed in our previous paper [64]. Partial charge on the Cu^+ cation varies from 0.63e (for the two-coordinated hexaammine complexes) to 0.80e (for the two-coordinated tetra-aqua complexes). The influence of additional molecules in outer solvation shell on the occupation of copper 4s AO and on the partial charge of Cu atom is only marginal.

Investigation of the divalent copper structures is a little more complicated since the donation also partially increases the occupation of SOMO [72]. Therefore, only the net charge distribution represents the unique criterion for the donation extent. From data presented in Table 7, one can see that the smallest positive Cu partial charge appears for the four-coordinated complexes. This reflects the largest electron

Table 6
Occupations of Cu 4s AO and the partial charges on copper for all presented Cu(I) systems (in e)

System	c.n.	4s	δ (Cu)
[Cu(lig)$_4$]$^+$			
$[Cu(NH_3)_4]^+$	2	0.56	0.65
	3	0.34	0.76
	4	0.24	0.80
$[Cu(NH_3)_3(H_2O)]^+$	2	0.55	0.66
	3	0.34	0.76
$[Cu(NH_3)_2(H_2O)_2]^+$	2	0.55	0.66
	3	0.44	0.73
$[Cu(NH_3)(H_2O)_3]^+$	2	0.48	0.73
	3	0.33	0.81
$[Cu(H_2O)_4]^+$	2	0.41	0.80
	3	0.24	0.87
	4	0.19	0.88
[Cu(lig)$_6$]$^+$			
$[Cu(NH_3)_6]^+$	2	0.59	0.63
	3	0.34	0.75
	4	0.26	0.80
$[Cu(NH_3)_5(H_2O)]^+$	2	0.58	0.63
	3	0.35	0.75
	4	0.25	0.80
$[Cu(NH_3)_4(H_2O)_2]^+$	2	0.55	0.66
	3	0.34	0.76
	4	0.25	0.80
$[Cu(NH_3)_3(H_2O)_3]^+$	2	0.55	0.66
	3	0.32	0.77
$[Cu(NH_3)_2(H_2O)_4]^+$	2	0.53	0.67
	3	0.48	0.71
$[Cu(NH_3)(H_2O)_5]^+$	2	0.47	0.73
	3	0.41	0.77
$[Cu(H_2O)_6]^+$	2	0.45	0.77
	3	0.23	0.87
	4	0.14	0.89

Shortcut c.n. means coordination number.

Table 7
Occupations of Cu 4s and $3d_{x2-y2}$ AOs and the partial charges on copper for all presented Cu(II) systems (in e)

System	c.n.	4s	$3d(x^2-y^2)$	δ (Cu)
[Cu(lig)$_4$]$^{2+}$				
$[Cu(NH_3)_4]^{2+}$	4	0.36	1.39	1.30
$[Cu(NH_3)_3(H_2O)]^{2+}$	4	0.33	1.40	1.36
cis-$[Cu(NH_3)_2(H_2O)_2]^{2+}$	4	0.31	1.31	1.40
trans-$[Cu(NH_3)_2(H_2O)_2]^{2+}$	4	0.32	1.29	1.41
$[Cu(NH_3)(H_2O)_3]^{2+}$	4	0.28	1.38	1.48
$[Cu(H_2O)_4]^{2+}$	4	0.24	1.24	1.56
[Cu(lig)$_6$]$^{2+}$				
$[Cu(NH_3)_6]^{2+}$	4	0.37	1.38	1.27
	5	0.34	1.32	1.33
	6	0.34	1.30	1.35
$[Cu(NH_3)_5(H_2O)]^{2+}$	4	0.37	1.38	1.27
	5	0.34	1.34	1.34
$[Cu(NH_3)_4(H_2O)_2]^{2+}$	4	0.37	1.38	1.27
	5	0.33	1.34	1.34
	6	0.33	1.36	1.34
$[Cu(NH_3)_3(H_2O)_3]^{2+}$	4	0.34	1.36	1.33
	5	0.32	1.31	1.38
$[Cu(NH_3)_2(H_2O)_4]^{2+}$	4	0.31	1.29	1.41
	5	0.30	1.30	1.42
	6	0.28	1.36	1.46
$[Cu(NH_3)(H_2O)_5]^{2+}$	4	0.29	1.27	1.46
	5	0.26	1.32	1.50
	6	0.25	1.29	1.52
$[Cu(H_2O)_6]^{2+}$	4	0.26	1.24	1.56
	5	0.24	1.22	1.56
	6	0.24	1.43	1.64

Shortcut c.n. means coordination number.

donation and the largest polarization energy contribution in analogy with the Cu(I) systems. The interesting situation was found for the Cu(II) systems with 6 water molecules (structures **19a–c**). Here, nearly the same partial charges for four- and five-coordination can be observed. Since the water polarizability and donation ability is low as already mentioned above, the electrostatic part prevails and the changes in polarization are minimal. Generally, the deviations from the hypothetical 2+ charge of the Cu cation are quite large. Partial charges vary from 1.27e for tetraammine coordinated complexes (**13a**) to value 1.64e for the complexes with six coordinated water molecules (**19c**). The results can also be compared with work of Katz et al. [2] for tetraammine systems. They obtained at the MP2/LANL2DZ(d) level partial charges of 0.87e and 1.65e for their Cu(I) and Cu(II) complexes, respectively. Corresponding values from Tables 6 and 7 are 0.80 and 1.30e. This discrepancy in the Cu(II) case can be explained by the different geometry, since their Cu(II) complex have not the square planar symmetry.

4. Conclusion

In the present study, the various-coordinated $[Cu(NH_3)_m(H_2O)_n]^{2+/+}$ complexes were examined where n ranges from 0 to 4 or and $m+n=4$ or 6. After the B3PW91/6-31+G(d) optimizations, single-point calculations of the stabilization energies including the BSSE and deformation corrections were performed at the B3LYP/6-311++G(2df,2pd) level of theory. It was found that the most stable Cu(I) and Cu(II) complexes are the two-coordinated and four-coordinated structures, respectively. Actually, some five-coordinated complexes of Cu^{2+} are fairly stable, too. The most preferable coordination numbers were discussed and compared with other works [3,42,43,45,46,50,57].

The most stable structures exhibit the shortest Cu–N (1.9/2.05 Å for Cu(I)/Cu(II) species) and Cu–O bonds (1.87/1.96 Å). Obtained distances of all the explored compounds are also in very good agreement with the results of other studies [2,42,43,45,57].

In addition, the donation effect was investigated in terms of the copper partial charge and occupation numbers of Cu 4s and 3d AOs using the NPA method. The analysis explains the strongest copper coordination-covalent interactions with 2 ligands in monovalent, and 4 ligands in divalent systems by the most pronounced electron density redistribution. The both energetic and wave function analyses also confirm copper–ammine bonding to be preferred over copper-aqua one. Thus, mixed water/ammonia complexes always prefer to form structures with the NH_3 molecules in the first hydration shell. Moreover, the Morokuma energy decomposition analysis enlightens the role of Coulomb, exchange repulsion and polarization terms at the Hartree-Fock level of theory.

Acknowledgments

This study was supported by Charles University Grant 438/2004/B_CH/MFF, and Grant NSF-MŠMT ČR ME-517. The computational resources from MetaCenters in Prague, Brno, and Pilsen are acknowledged for excellent access to their supercomputer facilities. Special thank should be given to Mgr. M. Šimánek for administration of our computer cluster and help with numerous obstacles.

References

[1] J. Sabolovic, C.S. Tautermann, T. Loerting, K.R. Liedl, Inorg. Chem. 42 (2003) 2268.
[2] A. Katz, L. Shimoni-Livny, O. Navon, N. Navon, C. Bock, J. Glusker, Helv. Chim. Atca 123 (2003) 782.
[3] J. Sabolovic, K.R. Liedl, J. Am. Chem. Soc. 38 (1999) 2764.
[4] J. Bertran, L. Rodrigues-Santiago, M. Sodupe, J. Phys. Chem. B 103 (1999) 2310.
[5] L. Rulíšek, Z. Havlas, J. Am. Chem. Soc. 122 (2000) 10428.
[6] S. Santra, P. Zhang, W. Tan, J. Phys. Chem. A 104 (2000) 12021.
[7] T. Shoeib, C.F. Rodriquez, K.W.M. Siu, A.C. Hopkinson, Phys. Chem. Chem. Phys. 3 (2001) 853.
[8] R. Prabhakar, P.E.M. Siegbahn, J. Phys. Chem. B 107 (2003) 3944.
[9] D. Caraiman, T. Shoeib, K. Siu, A. Hopkinson, D. Bohme, Int. J. Mass Spectr. 228 (2–3) (2003).
[10] P. Manikandan, B. Epel, D. Goldfarb, Inorg. Chem. 40 (2001) 781.
[11] K. Shimizu, H. Maeshima, H. Yoshida, A. Satsuma, T. Hattori, Phys. Chem. Chem. Phys. 3 (2001) 862.
[12] J.A. Sigman, B.C. Kwok, A. Gengenbach, Y. Lu, J Am. Chem. Soc. 121 (1999) 8949.
[13] M.H.M. Olsson, U. Ryde, J. Biol. Inorg. Chem. 4 (1999) 654.
[14] M.H.M. Olsson, G.Y. Hong, A. Warshel, J. Am. Chem. Soc. 125 (2003) 5025.
[15] M.H.M. Olsson, U. Ryde, B.O. Roos, K. Pierloot, J. Biol. Inorg. Chem. 3 (1998) 109.
[16] U. Ryde, M.H.M. Olsson, B.O. Roos, J.O.A. De Kerpel, K. Pierloot, J. Biol. Inorg. Chem. 5 (2000) 565.
[17] D.W. Randall, S.D. George, B. Hedman, K.O. Hodgson, K. Fujisawa, E.I. Solomon, J. Am. Chem. Soc. 122 (2000) 11620.
[18] D.W. Randall, S.D. George, P.L. Holland, B. Hedman, K.O. Hodgson, W.B. Tolman, E.I. Solomon, J. Am. Chem. Soc. 122 (2000) 11632.
[19] P.L. Holland, W.B. Tolman, J. Am. Chem. Soc. 121 (1999) 7270.
[20] P.L. Holland, W.B. Tolman, J. Am. Chem. Soc. 122 (2000) 6331.
[21] H.B. Gray, B.G. Malmstroem, R.J.P. Williams, J. Biol. Inorg. Chem. 5 (2000) 551.
[22] L.D. Book, D.C. Arnett, H. Hu, N.F. Scherer, J. Phys. Chem. A 102 (1998) 4350.
[23] E. Fraga, M.A. Webb, G.R. Loppnow, J. Phys. Chem. 100 (1996) 3278.
[24] P.E.M. Siegbahn, J. Comp. Chem. 22 (2001) 1634.
[25] A.E. Palmer, D.W. Randall, F. Xu, E.I. Solomon, J. Am. Chem. Soc. 121 (1999) 7138.

[26] X. Wang, S.M. Berry, Y. Xia, Y. Lu, J. Am. Chem. Soc. 121 (1999) 7449.
[27] P.E.M. Siegbahn, M. Wirstam, J. Am. Chem. Soc. 123 (2001) 11819.
[28] J.V. Burda, J. Šponer, P. Hobza, J. Phys. Chem. 100 (1996) 7250.
[29] J.V. Burda, J. Šponer, J. Leszczynski, P. Hobza, J. Phys. Chem. B 101 (1997) 9670.
[30] A. Gasowska, L. Lomozik, Monatshefte fur Chemie 126 (1995) 13.
[31] J. Šponer, M. Sabat, J. Burda, J. Leszczynski, P. Hobza, B. Lippert, J. Biol. Inorg. Chem. 4 (1999) 537.
[32] E.V. Hackl, S.V. Kornilova, L.E. Kapinos, V.V. Andruschenko, V.L. Galkin, D.N. Grigoriev, Y.P. Blagoi, J. Mol. Struct. 408/409 (1997) 229.
[33] C. Hemmert, M. Pitie, M. Renz, H. Gornitzka, S. Soulet, B. Meunier, J. Biol. Inorg. Chem. 6 (2001) 14.
[34] L.A. Herrero, A. Terron, J. Biol. Inorg. Chem. 5 (2000) 269.
[35] E. Meggers, P.L. Holland, W.B. Tolman, F.E. Romesberg, P.G. Schultz, J. Am. Chem. Soc. 122 (2000) 10714.
[36] B. Schoentjes, J.-M. Lehn, Helv. Chim. Acta 78 (1995) 1.
[37] S. Atwell, E. Meggers, G. Spraggon, P.G. Schultz, J. Am. Chem. Soc. 123 (2001) 12364.
[38] H. Tachikawa, Chem. Phys.Lett. 260 (1996) 582.
[39] D. Feller, E.D. Glendening, W.A. de Jong, J. Chem. Phys. 110 (1999) 1475.
[40] D. Schroeder, H. Schwartz, J. Wu, C. Wesdemiotis, Chem. Phys. Lett. 343 (2001) 258.
[41] G.W. Marini, K.R. Liedl, B.M. Rode, J. Phys. Chem. A 103 (1999) 11387.
[42] C. Schwenk, B. Rode, Chem. Phys. Chem. 5 (3) (2004).
[43] C.F. Schwenk, B.M. Rode, Phys. Chem. Chem. Phys. 5 (2003) 3418.
[44] H. Pranowo, Chem. Phys. 291 (2) (2003).
[45] A. Berces, T. Nukada, P. Margl, T. Ziegler, J. Phys. Chem. A 103 (1999) 9693.
[46] H.D. Pranowo, A.H.B. Setiajin, B.M. Rode, J. Phys. Chem. A 103 (1999) 11115.
[47] H.D. Pranowo, B.M. Rode, J. Phys. Chem. A 103 (1999) 4298.
[48] H.D. Pranowo, B.M. Rode, Chem. Phys 263 (2001) 1.
[49] J.A. Stone, D. Vukomanovic, Chem. Phys. Lett. 346 (2001) 419.
[50] N.R. Walker, S. Firth, A.J. Stace, Chem. Phys. Lett. 292 (1998) 125.
[51] F. Haeffner, T. Brinck, M. Haeberlein, C. Moberg, Chem. Phys. Lett. 397 (1997) 39.
[52] N.M.D.S. Cordeiro, J.A.N.F. Gomes, J. Comput. Chem. 14 (1993) 629.
[53] V. Subramanian, C. Shankaranarayanan, B.U. Nair, M. Kanthimathi, R. Manickkavachagam, T. Ramasami, Chem. Phys. Lett. 274 (1997) 275.
[54] J. Piquemal, B. Williams-Hubbard, N. Fey, R. Deeth, N. Gresh, C. Giessner-Prettre, J. Comput. Chem. 24 (16) (2003).
[55] N. Gresh, C. Policar, C. Giessner-Prettre, J. Phys. Chem. 106 (2002) 5660.
[56] M. Ledecq, F. Lebon, F. Durant, C. Giessner-Prettre, A. Marquez, N. Gresh, J. Phys. Chem. B 107 (38) (2003).
[57] D. Feller, E. Glendening, W. de Jong, J Chem. Phys. 110 (3) (1999).
[58] X. Xu, W.A. Goddard, J. Phys. Chem. 108 (2004) 2305.
[59] A. Luna, B. Amekraz, J. Tortajada, Chem. Phys. Lett. 266 (1997) 31.
[60] F.S. Legge, G.L. Nyberg, J.B. Peel, J. Phys. Chem. 105 (2001) 7905.
[61] M. Baranska, K. Chruszcz, B. Boduszek, L.M. Proniewicz, Vibr. Spectrosc. 31 (2003) 295.
[62] M.M. Hurley, L.F. Pacios, P.A. Christiansen, R.B. Ross, W.C. Ermler, J. Chem. Phys. 84 (1986) 6840.
[63] Note, The usage of originally suggested pseudoorbitals leads to wrong description of basic physical properties like IP or EA of copper atom. Here, at least qualitative agreement can be obtained when original orbitals are augmented with diffuse and polarization functions..
[64] J.V. Burda, M. Pavelka, M. Šimánek, J. Molec. Struct. THEOCHEM 683 (2004) 183.
[65] S.F. Boys, F. Bernardi, Mol. Phys. 19 (1970) 553.
[66] M.W. Schmidt, K.K. Baldridge, J.A. Boatz, S.T. Elbert, M.S. Gordon, J.J. Jensen, S. Koseki, N. Matsunaga, K.A. Nguyen, S. Su, T.L. Windus, M. Dupuis, J.A. Montgomery, J. Comput. Chem. 14 (1993) 1347.
[67] G.W.T.M.J. Frisch, H.B. Schlegel, G.E. Scuseria, M.J.R.C.A. Robb, V.G. Zakrzewski, J.A. Montgomery Jr., R.E. Stratmann, J.C.S.D. Burant, J.M. Millam, A.D. Daniels, K.N. Kudin, M.C. Strain, O. Farkas, J.V.B. Tomasi, M. Cossi, R. Cammi, B. Mennucci, C. Pomelli, C. Adamo, S. Clifford, J.G.A.P. Ochterski, P.Y. Ayala, Q. Cui, K. Morokuma, P. Salvador, J.J. Dannenberg,, A.D.R.D.K. Malick, K. Raghavachari, J.B. Foresman, J. Cioslowski, J.V. Ortiz, A.B.B.S.G. Baboul, G. Liu, A. Liashenko, P. Piskorz, I. Komaromi, R. Gomperts, R.L.D.J.F. Martin, T. Keith, M.A. Al-Laham, C.Y. Peng, A. Nanayakkara, M. Challacombe,, B.J.P.M.W. Gill, W. Chen, M.W. Wong, J.L. Andres, C. Gonzalez, M.E.S.R. Head-Gordon, J.A. Pople, Gaussian 98 (Revision A.1x), Gaussian, Inc., Pittsburgh PA, 2001.
[68] G. Schaftenaar, Molden, Available from: <http://www.cmbi.kun.nl/~schaft/molden/molden.html>.
[69] P.F. Flükiger, Available from: <http://www.cscs.ch/molekel/>.
[70] S. Portmann, H.P. Lüthi, Chimia 54 (2000) 766.
[71] R.G. Parr, R.G. Pearson, J. Am. Chem. Soc. 105 (1983) 7512.
[72] Note, SOMO character is generally dependent on the coordination number. However, square planar complexes can be considered as a subset of octahedral symmetry where σxy lies in equatorial plane (for 5- and 6-coordination) or simply in ligand plane (for 4-coordination) and thus SOMO has always $3d_{x2-y2}$ character.

Copper Cation Interactions with Biologically Essential Types of Ligands: A Computational DFT Study

Matěj Pavelka,† Milan Šimánek,† Jiří Šponer,‡ and Jaroslav V. Burda*,†

Department of Chemical Physics and Optics, Faculty of Mathematics and Physics, Charles University, Ke Karlovu 3, 121 16 Prague 2, Czech Republic, and Institute of Biophysics, Academy of Sciences of the Czech Republic, Královopolská 135, 612 65 Brno, Czech Republic

Received: November 27, 2005; In Final Form: February 1, 2006

This work presents a systematic theoretical study on Cu(I) and Cu(II) cations in variable hydrogen sulfide−aqua−ammine ligand fields. These ligands model the biologically most common environment for Cu ions. Molecular structures of the complexes were optimized at the density functional theory (DFT) level. Subsequent thorough energy analyses revealed the following trends: (i) The ammine complexes are the most stable, followed by those containing the aqua and hydrogen sulfide ligands, which are characterized by similar stabilization energies. (ii) The most preferred Cu(I) coordination number is 2 in ammine or aqua ligand fields. A qualitatively different binding picture was obtained for complexes with H_2S ligands where the 4-coordination is favored. (iii) The 4- and 5-coordinated structures belong to the most stable complexes for Cu(II), regardless of the ligand types. Vertical and adiabatic ionization potentials of Cu(I) complexes were calculated. Charge distribution (using the natural population analysis (NPA) method) and molecular orbital analyses were performed to elucidate the nature of bonding in the examined systems. The results provide in-depth insight into the Cu-binding properties and can be, among others, used for the calibration of bioinorganic force fields.

1. Introduction

The improved quantum-chemical approaches and high performance computers led in the past decades to intensified study of transition-metal complexes in many theoretical laboratories. Copper, despite its toxicity in pure form, is fundamental for the activity of many enzymes, which are important in oxygen transport and insertion, electron transfer, oxidation−reduction processes, and so forth. In some cases, the activity is connected with a relatively high electron affinity and the Cu(II) oxidation state can be easily reduced to Cu(I). There are many theoretical and experimental studies exploring copper proteins. For instance, Siegbahn et al.[1] studied the redox process on tyrosinase. In another work, the authors studied the molecular mechanism of the oxidation reaction on a center of copper amine oxidase using the B3LYP technique.[2] Wang et al. studied the importance of histidine ligands in a Cu center of azurin using ultraviolet−visible (UV−vis) and electron paramagnetic resonance (EPR) spectra.[3] In Solomon's group,[4] spectroscopic tools in combination with density functional theory (DFT) calculations were used to investigate the role of an amino acid in the axial position to the copper complex and its influence on the reduction potential. Similarly, the plastocyanin model complexes were examined in studies,[5,6] where also several spectroscopic techniques in combination with DFT calculations were applied. The calculations have confirmed the role of ligand−metal charge transfer (LMCT) S $p\pi \rightarrow$ Cu on various spectra intensities. The related experimental works from Tolman's group should also be mentioned.[7,8] The basic aspects of a copper coordination in blue proteins are summarized in a short review.[9] A lot of computational effort was devoted to studies of blue proteins by Olsson et al.[10−13] An interesting study of plastocyanin and rusticyanin was performed by Olsson and Warshel,[10] where an approach to computing the reduction potential is presented. A pump−probe study of CT dynamics in the excited state was carried out by Book et al.[14] The wave-resolved signal of vibration on 500 cm^{-1} was assigned to the excited-state lifetime in a copper complex of plastocyanin and ceruloplasmin in spinach. Also, Fraga et al.[15] studied the CT dynamics of plastocyanin using resonance Raman spectroscopy.

Some other theoretical studies of the copper interactions with amino acids have been reported recently, including an attempt to explain the nonplanar arrangement of the copper(II) complexes with amino acids in crystal structures using the ab initio method and molecular mechanics.[16] The same authors have published a new force field parametrization of Cu(II)[17] based on gas phase B3LYP calculations. Plenty of inspiration can be found in a study of Glusker's group on copper-binding motifs.[18] A similar combination of database structures and quantum-chemical calculations can be found in very extensive studies performed by Rulíšek et al.[19−22] The Cu(I)−Cu(II) bonding in relation to glycine was scrutinized by Bertran et al.[23] Shoeib et al.[24] studied the Cu^+/Ag^+ cation interactions with glycine molecules using the B3LYP/PVDZ method. They showed that while the Ag^+ cation prefers 3- and 4-coordinated complexes, a lower coordination (2) occurs in the Cu^+ cases. The same group also examined some other aspects of Cu interactions.[25]

Many experimental works were published on the coordination of copper cations with various amino acids. Among others, a recent study of Santra et al.[26] should be mentioned. The authors dealt with the interactions of the Cu^{2+}(glutamate) complex with cyclodextrine and benzonitrile using the fluorescence spectroscopy. EPR and electron−nuclear double resonance (ENDOR) techniques were used[27] to determine Cu(II)−histidine complexes. Six-membered chelating rings are formed when histidine

* Corresponding author. E-mail: burda@karlov.mff.cuni.cz.
† Charles University.
‡ Academy of Sciences of the Czech Republic.

10.1021/jp056868z CCC: $33.50
Published on Web 03/22/2006

molecules bind the Cu^{2+} cation. X-ray absorption near-edge structure (XANES) spectra for a series of Cu(II) compounds[28] were utilized to interpret a ligand field theory in the explored Cu(II) compounds. Sigman et al.[29] have examined the Cu(II) coordination site in cytochrome c peroxidase with EPR and UV−vis spectra.

A great deal of work is devoted to the examination of copper complexes with DNA/RNA bases. IR spectra were measured and interpreted for interactions of DNA with several divalent cations in a solution.[30] The crystal structures of several metal complexes and DNA cleaving activity were characterized in study.[31] Thermodynamical measurements[32] on nucleosides coordinated with Ca and Cu divalent cations suggest the following order in bonding strength: $Cu^{2+} > Ca^{2+}$ and GMP > IMP > AMP > CMP = UMP for the nucleotides. Formation of macrochelates was found to be energetically favorable but entropically unfavorable. Melting curves of copper(II) linked in a duplex DNA oligomer were measured in a study of Meggers et al.[33] The same authors have also explored the structural aspects of a copper(II) coordination influence on Watson−Crick (WC) base pairing.[34] The interactions of the polynuclear copper-(I) complexes with double-stranded DNA oligomers were explored by Lehn's group.[35]

A theoretical study of Cu^{2+} association with uracil and its thio derivatives has been published recently.[36] Coordination and stability of Cu(II) and Zn(II) complexes with adenosine and cytidine were investigated by Gasowska.[37] Binding of Cu^{+} cations to guanine and adenine,[38] WC AT and GC base pairs,[39] and in a noncomplementary DNA C−A base pair[40] was explored in our previous studies. Recently, Noguera[41] examined WC GC base pair interacting with Ca^{2+}, Cu^{+}, and Cu^{2+} cations where both naked and hydrated cations were considered. The outer-shell and inner-shell coordination of a phosphate group to hydrated metal ions (Mg^{2+}, Cu^{2+}, Zn^{2+}, Cd^{2+}) in the presence and absence of nucleobase was explored in the work of Rulíšek.[42] Hydrated Cu(I) association to guanine has been published recently.[43]

Small inorganic complexes of Cu cations are also intensively studied. Many works (already mentioned in our previous studies) are devoted to the study of the coordination geometries and/or electronic properties of Cu cations interacting with molecules such as water or ammonia[44−64] using various computational approaches. In our previous papers,[65,66] hydration of both Cu(I) and Cu(II) cations and their interactions with variable ammonia−water surroundings were systematically examined.

The present study provides a new detailed investigation of Cu(I)/Cu(II) interactions with an extended sulfide−aqua−ammine ligand field. Structural, thermodynamic, and electronic properties are determined and used to characterize such copper complexes. A comparison with previous results underlines new qualitative features which appear in the presence of coordinated sulfur-containing ligands. This work thus provides an important approximate model for copper interactions with amino acids such as histidine, methionine, cysteine, and glutamine or other bioenvironments.

2. Computational Details

The $[Cu(H_2S)_n(H_2O)_m(NH_3)_k]^{2+}$ complexes were studied, where n, m, and k were equal to 0, 2, 4, or 6 with the $m + n + k$ sum being 4 or 6. In the case of Cu(I) complexes, these systems were reduced to four molecules in a metal proximity, since stable Cu(I) compounds with higher coordination numbers are very rare. Some additional calculations were carried out with uneven numbers of ligands. Note also that in some calculations a ligand was drifted to the second hydration shell, which leads to an uneven number of ligands in the first ligand shell.

In many cases, we attempted multiple gradient optimizations utilizing different starting geometries. This often resulted in distinct local minima. However, only the lowest energy conformer for every coordination number was considered in the further analyses.

Quantum-chemical calculations were performed at the density functional theory (DFT) level using the B3PW91 functional. For the H, O, and N atoms, the 6-31+G(d) basis set was applied. The copper and sulfur core electrons were described by Christiansen averaged relativistic effective pseudopotentials (AREP).[67] A consistent basis set was adopted for the valence electrons. Double-ζ pseudoorbitals of Cu were augmented by diffuse and polarization functions ($\alpha_s = 0.025$, $\alpha_p = 0.35$, $\alpha_d = 0.07$, and $\alpha_f = 3.75$).[68] Similarly, pseudoorbitals of the sulfur atom were extended by analogous functions with exponents: $\alpha_s = 0.077$, $\alpha_p = 0.015$, and $\alpha_d = 0.50$.

Compounds with the Cu^{+} cation are represented by a closed-shell singlet electronic ground state. Cu(II) complexes contain copper in the $3d^9$ electron configuration resulting in doublet ground states. A lot of attention was devoted to the construction of an appropriate initial guess for the self-consistent field (SCF) procedure. First, the correct wave function was constructed in a minimal basis set using the restricted open-shell Hartree−Fock (ROHF) method, going subsequently to the final unrestricted B3PW91/6-31+G(d) level.

Energy and charge distribution analyses were calculated with the B3LYP functional and extended 6-311++G(2df,2pd) basis set for the H, N, and O atoms. Consistently, the basis sets on the copper/sulfur atoms were enlarged by spd/sp diffuse functions and 2fg,2df polarization functions ($\alpha_f = 4.97$, 1.30, $\alpha_g = 3.28/\alpha_d = 0.92$, 0.29, $\alpha_f = 0.57$).[65] Recently, new studies have appeared where BHLYP is recommended over B3LYP;[69] however, no substantial difference was found in our case for selected test systems.

The energetics of interactions was evaluated on the basis of several quantities. First, the conventional stabilization energies with the basis set superposition error (BSSE) corrections and corrections on the deformation energies[70] were determined according to the equation

$$\Delta E^{stab} = -(E_{complex} - \sum E_{monomer} - \sum E^{deform}) \quad (1)$$

where $E_{complex}$ represents total energy of the whole complex and $E_{monomer}$ represents the energy of a given subsystem computed with basis functions on the ghost atoms from the complementary part of the system. Besides the ΔE^{stab} energies, we also computed coordination energies (ΔE^{coord}) and *st*abilization energies with *ex*clusion of sterical repulsion and weak associative interactions (ΔE^{stex}). The coordination energies were evaluated for the Cu(I) systems, where ligand molecules often escape to the second solvation shell. In such calculations, only directly bonded (first-shell) ligands were considered in eq 1 using the optimized geometry of the whole complex. The ΔE^{stab} and ΔE^{coord} terms are identical when all ligands remain in the first shell. ΔE^{stex} is obtained when all of the interacting ligand molecules are treated in eq 1 as one subsystem and the central Cu ion as another one. That is, this energy is equal to the binding energy of the cation with a given ligand shell. The ΔE^{stex} energy was evaluated only for the Cu(II) complexes where a higher coordination causes an increased electrostatic repulsion of the ligands. The difference between ΔE^{stab} and ΔE^{stex} then basically reflects the energy investment that would be necessary to form the ligand-shell arrangement in the absence of the ion.

Note, however, that the actual interligand repulsion in the presence of the Cu cation is even larger, due to interligand electrostatic repulsion caused by the polarization/charge transfer effects of the metal cation. For further discussion on the estimation of polarization and CT energies, the studies of Tiraboschi[71,72] or Šponer[73] can be used. In addition, the bonding energies (ΔE^{BE}) were estimated using the same (BSSE) scheme of eq 1 but without the monomer deformation corrections. In this energy determination, partition of the complex to two parts (ligand and the rest of the complex) splits the examined Cu−X bond, giving the binding energy of the desired ligand. Only 4-coordinated Cu(I) and Cu(II) complexes were considered for comparison. Various energy evaluation schemes, as specified above, allow a more thorough insight into the balance of forces in the calculated systems.

Further vertical and adiabatic ionization potentials (IPs) were calculated for the monovalent copper compounds according to formula 2:

$$\mathrm{IP} = E_{\mathrm{Cu(II)}} - E_{\mathrm{Cu(I)}} \qquad (2)$$

In the case of the vertical IP, the $E_{\mathrm{Cu(II)}}$ term represents the energy of a (2+) charged system calculated in the Cu(I) optimized structure. For the adiabatic IP, the $E_{\mathrm{Cu(II)}}$ energy was computed using the Cu(II) optimized structure. For the sake of consistency, selected electron affinities were also calculated. Determined IPs and electron affinities (EAs) were compared with energies based on Koopmans' theorem and values calculated based on outer valence Green function propagators in the 6-31+G(d) basis set. The method is based on the eigenvalue of the canonical molecular orbital (MO) (highest occupied molecular orbital (HOMO) for IP or lowest unoccupied molecular orbital (LUMO) for EA) from Koopmans' theorem corrected by algebraic expressions similar to perturbation theory.[74,75]

For deeper insight into the electronic properties of the examined systems, molecular orbitals and electrostatic potentials were analyzed. Further, partial charges and spin densities on atoms were determined using the natural population analysis (NPA) method.[76] The program package Gaussian 98[77] was used for all quantum-chemical calculations, and the program NBO v. 5.0 from Wisconsin University[78] was used for evaluation of the natural bond orbital (NBO) characteristics. Visualization of geometries, MOs, vibrational modes, and maps of electrostatic potentials was performed using the Molden 4.4[79] and Molekel 4.3[80,81] programs.

3. Results and Discussion

3.1. Structural Parameters. All geometries reported in this paper are available in the Supporting Information. The present calculations thus can be easily used for the verification/calibration of lower quality methods, and they can be easily extended, for example, for a subset of structures, by higher level calculations.

First, structures of the Cu(I) and Cu(II) complexes coordinated exclusively with H_2S molecules were studied. These systems contain copper with $(H_2S)_n$ molecules considering the coordination number (n) varying from 1 to 4 in the Cu(I) complexes and from 1 to 6 in the Cu(II) complexes. The structures of these compounds are displayed in Figure 1 for Cu(I) and in Figure 2 for Cu(II). For the $[Cu(H_2S)]^+$ complex (**1a**), the coordination distance (2.21 Å) can be compared with the results of Hamilton's[45] study, where a shorter Cu−S bond (2.13 Å) is reported using the DFT(B3P86/DZP) method. For the $[Cu(H_2S)]^{2+}$ (**2a**) and $[Cu(H_2S)_2]^{2+}$ (**2b**) structures, Cu−S distances of 2.32 and 2.29 Å were obtained. The explanation of the shorter Cu−S bonds in a 2-coordinated Cu(II) system compared to a single-ligated complex is in section 3.5 below and was also discussed in previous studies.[65,66] For higher coordination numbers, the bond lengths elongate monotonically with the increasing number of ligands from 2.2 to 2.4 Å in the Cu(I) complexes and from 2.3 to 2.5 Å in the Cu(II) complexes. All optimized Cu−S distances are presented in Table 1.

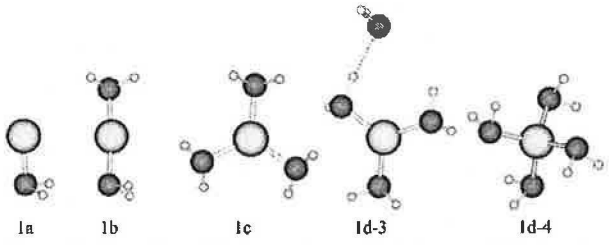

Figure 1. Homoligated Cu(I) complexes with hydrogen sulfide ligands.

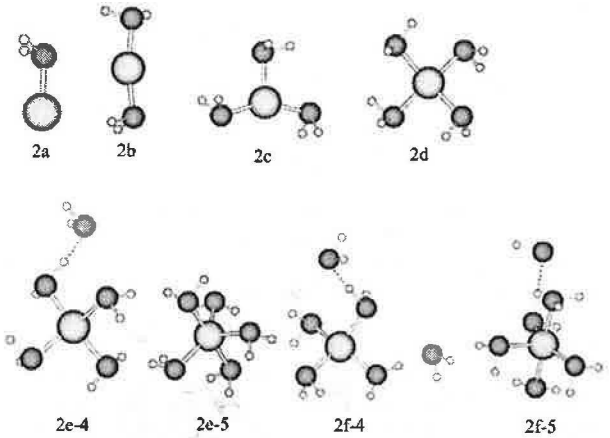

Figure 2. Homoligated Cu(II) complexes with hydrogen sulfide ligands.

It is interesting to mention that monovalent copper forms shorter Cu−S bonds than its divalent cation. On the other hand, in copper−water−ammonium complexes, the bonds of Cu^+ cation are longer (cf. refs 65 and 66). An explanation of the shorter Cu−S distances in monovalent complexes can be seen in the fact that the sulfur atom (still) keeps a negative partial charge in the Cu^+ complexes. On the contrary, in the $[Cu(H_2S)]^{2+}$ complex, a positive partial charge is located on the sulfur atom. This means that partial electrostatic repulsion is responsible for the elongation of the Cu−S bond in this complex. With the increasing number of ligands in the $[Cu(H_2S)_n]^{2+}$ complexes, the partial charge on sulfur atoms decreases up to $-0.2e$. Nevertheless, a less negative partial charge can always be found in the Cu(II) complexes as compared with the corresponding Cu(I) ones. Moreover, for donor−acceptor bonding, the polarizability or softness/hardness characterization must also be considered. The hardness of H_2S is about 6.2. It matches the Cu^+ value of 6.3. On the other hand, the Cu^{2+} cation keeps the electrons more tightly and the hardness increases to 8.3 (the data are taken from the work of Pearson[82]). Therefore, the higher covalent contribution of the Cu−S bond results in shorter bond lengths in the Cu(I) complexes. Water and ammonia are more polar molecules (μ = 1.92 and 1.53, respectively) in comparison with the H_2S molecule (μ = 1.08 D at the B3LYP/6-311++G-(2df,2pd) level of theory). Therefore, a strong electrostatic contribution to the Cu−O/Cu−N bonds leads to a shorter distance in the case of Cu^{2+}.

TABLE 1: Selected Parameters of $[Cu(H_2S)_k]^{2+/+}$ Complexes: Cu−S Distances (in Å), ΔE^{stab}, ΔE^{stex}, and ΔE^{coord} Energies (in kcal/mol, See Method for Definition), Occupation of 4s (and 3d) Copper AO, Partial Charges δ(Cu), and Spin Densities ρ_S(Cu) (in e)[a]

system	c.n.	struct	Cu−S	ΔE^{stab}	ΔE^{coord}	4s	δ(Cu)
$[Cu(H_2S)]^+$	1	1a	2.208	49.1	49.1	0.27	0.79
$[Cu(H_2S)_2]^+$	2	1b	2.221, 2.221	90.5	90.6	0.53	0.57
$[Cu(H_2S)_3]^+$	3	1c	2.300, 2.301, 2.304	103.3	103.2	0.44	0.62
$[Cu(H_2S)_4]^+$	3	1d-3	2.291, 2.302, 2.305	108.6	102.9	0.45	0.61
	4	1d-4	2.386, 2.388, 2.388, 2.388	110.3	110.4	0.43	0.60

system	c.n.	struct	Cu−S	ΔE^{stab}	ΔE^{stex}	4s	3d	δ(Cu)	ρ_S(Cu)
$[Cu(H_2S)]^{2+}$	1	2a	2.323	146.4	146.4	0.12	9.58	1.29	0.44
$[Cu(H_2S)_2]^{2+}$	2	2b	2.291, 2.291	223.5	224.2	0.39	9.39	1.19	0.73
$[Cu(H_2S)_3]^{2+}$	3	2c	2.360, 2.314, 2.309	276.0	280.5	0.53	9.53	0.91	0.44
$[Cu(H_2S)_4]^{2+}$	4	2d	2.391, 2.403, 2.406, 2.425	303.6	313.9	0.53	9.56	0.87	0.40
$[Cu(H_2S)_5]^{2+}$	4	2e-4	2.333, 2.397, 2.415, 2.439	317.2	331.5	0.53	9.56	0.87	0.40
	5	2e-5	2.425, 2.442, 2.488, 2.492, 2.548	318.3	333.3	0.53	9.55	0.86	0.41
$[Cu(H_2S)_6]^{2+}$	4	2f-4	2.337, 2.382, 2.406, 2.414	329.4	346.3	0.52	9.58	0.86	0.38
	5	2f-5	2.411, 2.434, 2.446, 2.488, 2.592	329.4	347.2	0.53	9.56	0.86	0.40

[a] The abbreviation c.n. is used for coordination number, and struct corresponds to the identification number used in Figures 1−5.

The 2-coordinated structures deviate from the assumed linearity by approximately 10°. The 3-coordinated Cu(I) complex (1c) has practically C_s symmetry in the heavy-atom backbone with the same Cu−S distance (2.30 Å). The Cu(II) structure (2c) resembles a deformed planar T shape with one of the Cu−S distances elongated to 2.36 Å. The global minimum for the 4-coordinated Cu(I) complex (1d-4) was obtained in a near tetrahedral conformation with equal Cu−S bond lengths. In the $[Cu(H_2S)_4]^+$ system, other (less) stable structures with a coordination number of 3 were found. The geometry of the most stable one is illustrated in Figure 1 (1d-3). The H···S distance between the first- and second-shell ligands is relatively long in the Cu(I) (1d-3) structure, about 2.44 Å. The global minimum of the $[Cu(H_2S)_4]^{2+}$ cation (2d) has distorted square-planar configurations with a dihedral angle of ~20°. Interestingly, no stable 6-coordinated Cu(II) complex was found. The 5-coordinated structures favor a distorted tetragonal-pyramid arrangement with one of the equatorial Cu−S bonds elongated (2e-5 and 2f-5). Unlike in hexaaqua−copper complexes, the outer H_2S molecule does not prefer the formation of H-bonded cross-links and remains coordinated to only one first-shell ligand. For the Cu(II) complexes, H-bond lengths vary from 1.98 to 2.10 Å.

The angle between the H_2S plane and Cu−S bond increases with the increasing number of ligand molecules (from 104 to 111°) in the Cu(I) structures. In the $[Cu(H_2S)n]^{2+}$ systems (n = 2−6), the angles are generally slightly larger and vary from 106 to 112°. However, the largest angle (118°) was found in the monosulfide Cu(II) compound (2a). A different situation occurred in our previous study,[65] where purely aqua ligands were explored. Angles of 172 and 154° were observed in the $[Cu(H_2O)]^+$ and $[Cu(H_2O)]^{2+}$ complexes, while angles of 104 and 118° occur in $[Cu(H_2S)]^+$ and $[Cu(H_2S)]^{2+}$, respectively. In the remaining Cu(II) aqua complexes, the angles were larger—up to about 176°. Such an angle is the result of two competing factors: (a) the angle corresponding to a dative bond tends to be ~109° (according to the tetrahedral sp^3 hybridization of water or hydrogen sulfide), and (b) the electrostatic term, based on a metal−ligand/monopole−dipole moment interaction, favors an angle of 180°. Larger angles of aqua ligands can be explained by a prevailing role of electrostatic factors, while in the H_2S complexes the dative character clearly dominates. The similar structures were described in the case of Zn^{2+} by Pullman et al.[83] or later by Gresh[84,85]

In the next part, systems with a variable sulfide−aqua−ammine ligand field were explored. For the $[Cu(H_2S)_m(H_2O)_n(NH_3)_k]^+$ systems, stable 2-, 3-, and 4-coordinated geometries were localized. However, in the $[Cu(H_2S)_4]^+$ system (1d = 3a), no stable 2-coordinated structure exists. On the contrary, for the $[Cu(H_2O)_2(NH_3)_2]^+$ complex (3g), no 4-coordinated structure was found. The obtained Cu−X (X = S, O, and N) bond lengths of the most stable structures are compiled in the upper part of Table 2, and the optimized structures are depicted in Figure 3.

Generally, bond lengths increase with increasing coordination number. For the 2-, 3-, and 4-coordinated structures, the Cu−S distances vary from 2.2 to 2.4 Å, respectively. The same behavior was found for Cu−NH_3, where bonds elongate from 1.9 to 2.1 Å. The Cu−O distances display the largest variability changing from 1.9 to 2.4 Å. On the basis of the optimized structures, it can be concluded that the most preferred ligand (most frequently occurring in the first solvation shell) is ammonia followed by H_2S (for both Cu(I) and Cu(II) cations), leaving water as the least favored ligand.

Optimized structures of the divalent $[Cu(H_2S)_m(H_2O)_n(NH_3)_k]^{2+}$ complexes (where $m + n + k = 4$ or 6) are presented in the lower part of Table 2 and in Figures 4 and 5. The 4-coordinated Cu(II) complexes favor partially deformed square-planar geometry in contrast to the tetrahedral structures of Cu(I). Such a conclusion can also be found in some other works, for example, in ref 86.

To determine the ligand arrangement of the 5-coordinated structures, the Cu−X metal−ligand distances and X−Cu−X angles have been measured. Trigonal bipyramid reveals an angle distribution close to 180 and 120°. This arrangement was found only in the $[Cu(H_2S)_4(NH_3)_2]^{2+}$ (5h-5) complex. In all other cases, a distorted octahedral configuration was found with an angle distribution close to 90 and 180°. More quantitative expression can be based on evaluation of the so-called τ-parameter, which is defined as $\tau = (\theta - \varphi)/60°$. Here, the θ and φ angles are the two largest valence angles in the complex. From Table 3, it can be seen that the only τ value larger than 0.6 is for the 5h-5 structure. Two borderline structures with τ values around 0.4−0.6 are the $[Cu(H_2S)_6]^{2+}$ and $[Cu(H_2S)_2(H_2O)_2(NH_3)_2]^{2+}$ complexes which "optically" can be considered closer to the tetragonal-pyramid shape.

The structures with six directly bonded molecules (5b-6, 5c-6, 5d-6, 5e-6, and 5f-6) exhibit distorted O_h symmetry with the axial bonds elongated due to the Jahn−Teller effect known from classical textbooks. However, in three cases—$[Cu(H_2S)_6]^{2+}$,

TABLE 2: Copper–Ligand Distances (in Å) for the Cu(I) and Cu(II) Complexes[a]

system	c.n.	struct	Cu–lig1	Cu–lig2	Cu–lig3	Cu–lig4	Cu–lig5	Cu–lig6
$[Cu(H_2S)_4]^+$	3	3a-3	2.291*	2.302*	2.305*			
	4	3a-4	2.386*	2.388*	2.388*	2.388*		
$[Cu(H_2S)_2(H_2O)_2]^+$	2	3b-2	2.200*	2.219*				
	3	*3b-3*	*2.247**	*2.284**	*2.050***			
	4	3b-4	2.282*	2.286*	2.172**	2.282**		
$[Cu(H_2S)_2(H_2O)(NH_3)]^+$	2	3c-2	1.922	2.193*				
	3	*3c-3*	*2.022*	*2.271**	*2.327**			
	4	3c-4	2.043	2.310*	2.312*	2.435**		
$[Cu(H_2S)_2(NH_3)_2]^+$	2	*3d-2*	*1.912*	*1.912*				
	3	3d-3	2.041	2.044	2.287*			
	4	3d-4	2.105	2.119	2.383*	2.385*		
$[Cu(H_2O)_4]^+$	2	*3e-2*	*1.878***	*1.878***				
	3	3e-3	1.970**	1.976**	2.143**			
	4	3e-4	1.998**	2.085**	2.207**	2.257**		
$[Cu(H_2O)_2(NH_3)_2]^+$	2	*3f-2*	*1.909*	*1.909*				
	3	3f-3	1.944	1.944	2.349**			
$[Cu(NH_3)_4]^+$	2	*3g-2*	*1.905*	*1.905*				
	3	3g-3	1.998	2.073	2.078			
	4	3g-4	2.136	2.136	2.136	2.136		
$[Cu(H_2S)_4]^{2+}$	4	4a	2.391*	2.403*	2.406*	2.425*		
$[Cu(H_2S)_2(H_2O)_2]^{2+}$	4	4b	2.354*	2.360*	1.996**	2.052**		
$[Cu(H_2S)_2(H_2O)(NH_3)]^{2+}$	4	4c	2.008	2.429*	2.351*	2.090**		
$[Cu(H_2S)_2(NH_3)_2]^{2+}$	4	4d	2.007	2.019	2.455*	2.467*		
$[Cu(H_2O)_4]^{2+}$	4	4e	1.957**	1.959**	1.960**	1.963**		
$[Cu(H_2O)_2(NH_3)_2]^{2+}$	4	4f	2.003	2.003	2.023**	2.023**		
$[Cu(NH_3)_4]^{2+}$	4	4 g	2.051	2.051	2.051	2.051		
$[Cu(H_2S)_6]^{2+}$	4	5a-4	2.382*	2.337*	2.406*	2.414*		
	5	*5a-5*	*2.411**	*2.434**	*2.446**	*2.488**	*2.592**	
$[Cu(H_2O)_6]^{2+}$	*4*	*5b-4*	*2.033***	*2.033***	*2.033***	*2.033***		
	5	5b-5	1.957**	1.963**	2.074**	2.081**	2.086**	
	6	5b-6	1.984**	1.984**	2.010**	2.010**	2.242**	2.242**
$[Cu(NH_3)_6]^{2+}$	*4*	*5c-4*	*2.042*	*2.043*	*2.043*	*2.044*		
	5	5c-5	2.071	2.071	2.098	2.099	2.285	
	6	5c-6	2.171	2.171	2.174	2.174	2.512	2.512
$[Cu(H_2S)_2(H_2O)_4]^{2+}$	*4*	*5d-4*	*2.356**	*2.389**	*1.955***	*1.997***		
	5	5d-5	2.380*	2.411*	2.024**	2.037**	2.219**	
	6	5d-6	2.408*	2.408*	2.054**	2.054**	2.353**	2.353**
$[Cu(H_2S)_4(H_2O)_2]^{2+}$	*4*	*5e-4*	*2.398**	*2.390**	*2.410**	*2.379**		
	5	5e-5	2.434*	2.435*	2.439*	2.440*	2.191**	
	6	5e-6	2.426*	2.437*	2.438*	2.477*	2.376**	2.477**
$[Cu(H_2S)_2(H_2O)_2(NH_3)_2]^{2+}$	*4*	*5f-4*	*2.011*	*2.018*	*2.431**	*1.981***		
	5	5f-5	2.009	2.014	2.527*	2.611*	2.118**	
	6	5f-6	2.011	2.011	2.532*	2.533*	2.429**	2.596**
$[Cu(H_2S)_2(NH_3)_4]^{2+}$	*4*	*5g-4*	*2.046*	*2.047*	*2.053*	*2.053*		
	5	5g-5	2.059	2.062	2.077	2.080	2.840*	
$[Cu(H_2S)_4(NH_3)_2]^{2+}$	*4*	*5h-4*	*2.014*	*2.015*	*2.430**	*2.440**		
	5	5h-5	2.018	2.025	2.489*	2.608*	2.608*	

[a] The abbreviation c.n. represents the coordination number, and struct specifies the optimized structure. Italic font indicates the global minimum. One asterisk denotes Cu–S bond lengths, and two asterisks denote Cu–O bond lengths, while all remaining values are those for Cu–N bonds.

$[Cu(H_2S)_4(NH_3)_2]^{2+}$, and $[Cu(H_2S)_2(NH_3)_4]^{2+}$—no stable 6-coordinated geometries have been found.

The Cu(II)–ligand distances are presented in the second part of Table 2. Generally, Cu–S bond lengths in mixed 4-coordinated complexes are approximately 2.4 Å long. Cu–N distances are about 2.0–2.1 Å, and Cu–O bonds are in the range 2.0–2.4 Å. They again display the largest variability. If the number of ligated molecules is higher than four, the analogous trends remain valid. However, individual distances exhibits higher variability; the bonds elongate typically to 2.84, 2.51, and 2.35 Å for the Cu–S, Cu–N, and Cu–O bonds, respectively.

Katz's work[18] presents the optimized 4-coordinated $[Cu(H_2S)_m(NH_3)_n]^{2+/+}$ complexes (where $m + n = 4$) at the MP2/LANL2DZ+d level, which can be confronted with our structures. They have found values of 2.36 and 2.45 Å for the Cu–S bonds in the $[Cu(H_2S)_4]^{2+}$ and $[Cu(H_2S)_2(NH_3)_2]^{2+}$ systems, respectively. The values are in good agreement with the present distances (2.41 and 2.46 Å). However, they report the tetrahedral geometries in comparison with the distorted square-planar structures found in our study. In the case of Cu(I) compounds, the Cu–S bonds differ only slightly: 2.42 and 2.44 Å versus 2.39 and 2.38 Å (this work) for $[Cu(H_2S)_4]^+$ and $[Cu(H_2S)_2(NH_3)_2]^+$, respectively.

The extensive study of Katz et al.[18] also examines approximately 6000 entries in the Cambridge Structural Database (CSD). More than 50% of the mentioned Cu(I) structures are of the 4-coordinated type. The rest is divided between 2- and 3-coordinated complexes. The ligands with coordinated nitrogen (60%) and sulfur (35%) elements are preferred. For the Cu(II) entries, the most usual are 4- and 5-ligated complexes and only about 25% belongs to octahedral (6-coordinated) structures. In these octahedral complexes, copper is preferably coordinated with a ligand by the oxygen (50%) and nitrogen (50%) atoms. The database also indicates the copper–ligand bond lengths. Table 4 compares our averaged Cu–X (S, O, N) distances with the corresponding CSD values for both Cu^+ and Cu^{2+} cations with various coordination numbers. The

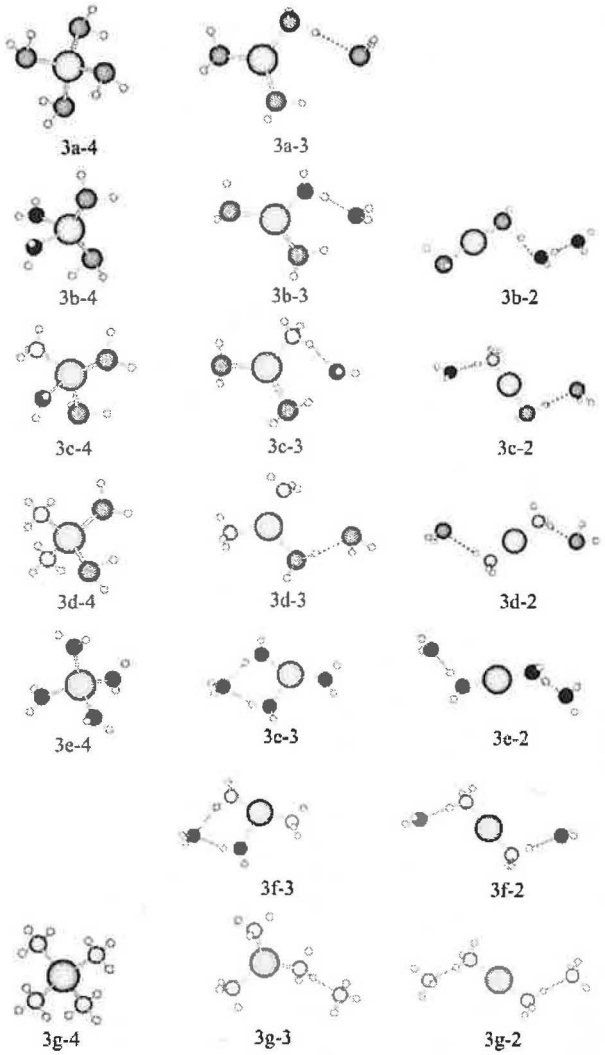

Figure 3. Cu(I) complexes containing mixed ligand molecules.

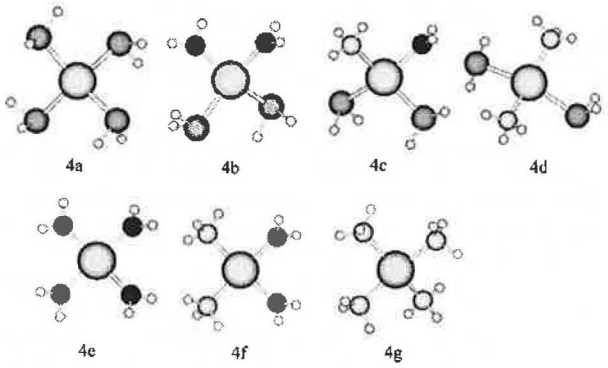

Figure 4. Cu(II) complexes with four mixed ligand molecules.

calculated bond lengths match well with the data presented in the database.

3.2. Stabilization Energies. Energy parameters of purely hydrogen sulfide systems $[Cu(H_2S)_n]^{2+/+}$ are listed in Table 1. Figure 6 shows the dependence of the ΔE^{stab} stabilization energies on the number of coordinated ligands for the Cu(I) complexes. An analogous plot in the case of the Cu(II) compounds is displayed in Figure 7. In the case of both monovalent and

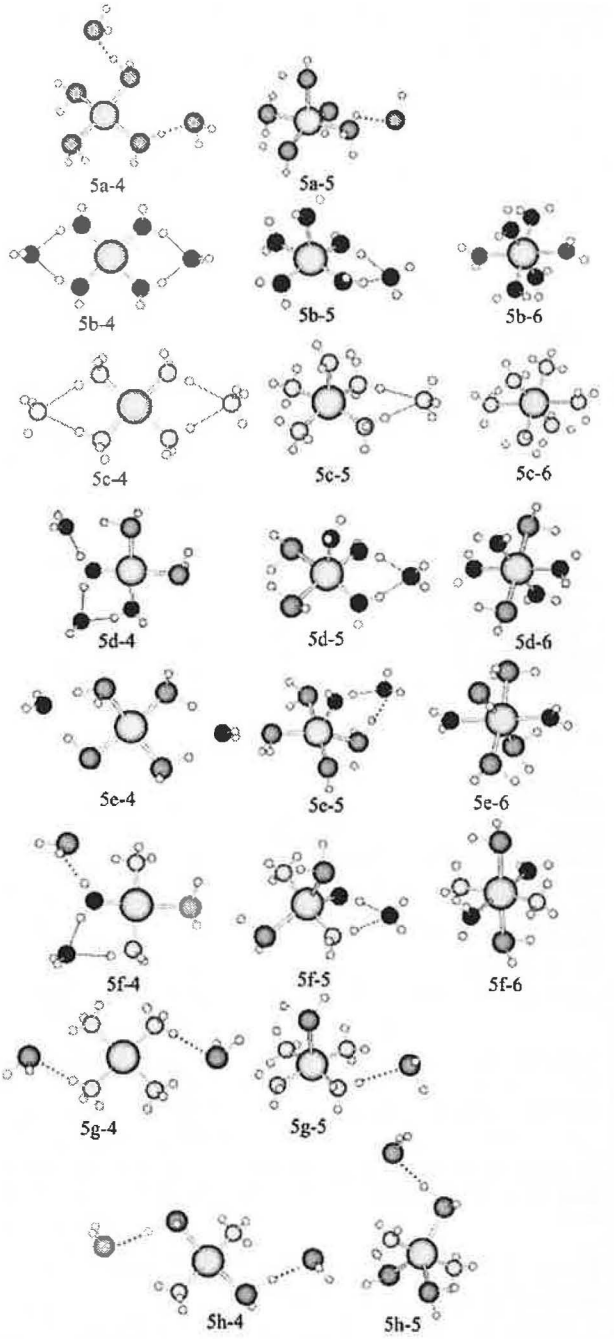

Figure 5. Cu(II) complexes with six mixed ligand molecules.

divalent complexes, stabilization energy increases with an increasing number of directly bonded molecules.

Hamilton[45] found the stabilization of the $[Cu(H_2S)]^+$ complex to be about 50 kcal/mol using B3P86 and the polarized double-ξ basis set. The value is in very good agreement with the presented result (49 kcal/mol) despite the fact that the Cu−S bond length was found to be different by almost 0.1 Å (see above).

When compared to previous calculations, where only water and ammonia molecules were included, an important difference can be noticed. The $[Cu(H_2S)_4]^+$ systems prefer the 4-coordinated structures (**1d-4**). The reason is the larger polarizability of the sulfur atom in the H_2S molecule and the higher donation affinity. Simultaneously, the very weak H-bonding cannot compete with the Cu−S dative interactions. Since mutual

TABLE 3: τ-Parameter for the 5-Coordinated Cu(II) Complexes[a]

system	struct	θ	φ	τ
$[Cu(H_2S)_6]^{2+}$	5a-5	177.3	152.2	0.42
$[Cu(H_2O)_6]^{2+}$	5b-5	170.9	165.5	0.09
$[Cu(NH_3)_6]^{2+}$	5c-5	163.0	163.0	0.00
$[Cu(H_2S)_2(H_2O)_4]^{2+}$	5d-5	172.5	160.9	0.19
$[Cu(H_2S)_4(H_2O)_2]^{2+}$	5e-5	178.8	158.7	0.33
$[Cu(H_2S)_2(H_2O)_2(NH_3)_2]^{2+}$	5f-5	174.6	143.6	0.52
$[Cu(H_2S)_2(NH_3)_4]^{2+}$	5g-5	172.5	166.7	0.10
$[Cu(H_2S)_4(NH_3)_2]^{2+}$	5h-5	179.4	129.8	0.83

[a] θ is the largest valence ligand−metal−ligand angle, and φ is the second largest angle. The abbreviation struct is used for identification of the optimized structures.

TABLE 4: Average Cu−X (S, O, N) Bond Lengths (in Å) and Corresponding Values Obtained from the CSD Database by Katz et al.[18a]

	present			CSD		
Cu(I)	2-coord	3-coord	4-coord	2-coord	3-coord	4-coord
Cu−N	1.91	2.02	2.12	1.90	1.98	2.04
Cu−O	1.88	2.04	2.21	1.84	2.14	2.05
Cu−S	2.19	2.29	2.35	2.17	2.26	2.33
	present			CSD		
Cu(II)	4-coord.	5-coord.	6-coord.	4-coord.	5-coord.	6-coord.
Cu−N	2.03	2.09	2.28	1.98	2.03	2.34
Cu−O	2.01	2.06[a]	2.13	1.93	2.07	2.36
Cu−S	2.40	2.49	2.41	2.28	2.43	2.72

[a] A value of 2.16 is obtained when the (5d-5) structure is considered as a regular 5-coordinated complex.

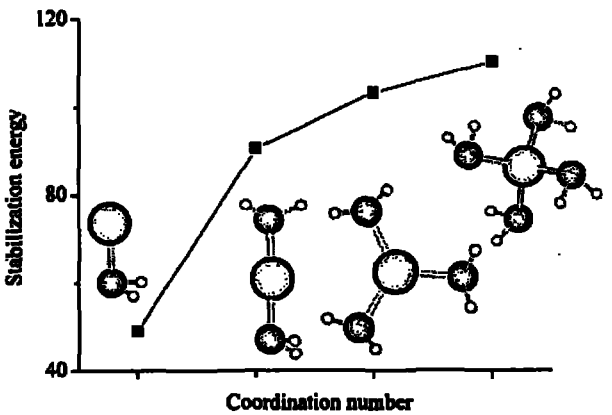

Figure 6. Dependence of stabilization energy (ΔE^{stab}) on the number of coordinated sulfide molecules in the Cu(I) compounds.

electrostatic repulsion of the H_2S molecules is relatively small due to a small dipole moment, a lower coordination leads to less stable systems. Also, electrostatic repulsion in the case of a larger number of ligands is reduced as a consequence of longer metal−ligand distances. This situation can be demonstrated on the structure (**1d-3**) where the three first-shell H_2S ligands contribute to the total stabilization by 34.3 kcal/mol each (from a ΔE^{coord} value of 102.9 kcal/mol), while the remaining H_2S molecule outside the first shell is attracted to the complex (H-bonding to the first-shell H_2S + electrostatic interaction with Cu^+) by only 5.7 kcal/mol, resulting in a final ΔE^{stab} value of 108.6 kcal/mol.

In the case of $[Cu(H_2S)_6]^{2+}$, a slightly larger donation from 5-coordinated ligands (**2f-5**) than from 4-coordinated ligands (**2f-4**) was found. The difference in the ΔE^{inter} values is about 1 kcal/mol. Larger ΔE^{inter} energy values are compensated by

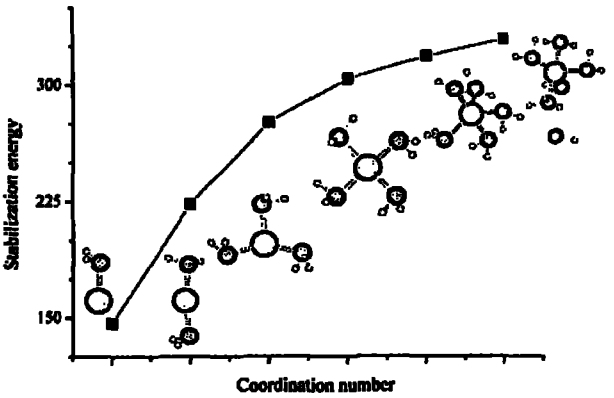

Figure 7. Dependence of stabilization energies (ΔE^{stab}) on the coordination number of the H_2S molecules in the $[Cu(H_2S)_n]^{2+}$ complexes ($n = 1-6$).

TABLE 5: ΔE^{stab} Stabilization Energies (in kcal/mol), the 4s AO Occupations, and the Partial Charges (in e) on the Cu Atom for Mixed Cu(I) Systems[a]

system	struct	ΔE^{stab}	δ(Cu)	4s
$[Cu(H_2S)_4]^+$	3a-3	108.6	0.61	0.45
	3a-4	*110.3*	*0.60*	*0.43*
$[Cu(H_2S)_2(H_2O)_2]^+$	3b-2	112.1	0.67	0.54
	3b-3	*116.6*	*0.70*	*0.37*
	3b-4	112.2	0.73	0.34
$[Cu(H_2S)_2(H_2O)(NH_3)]^+$	3c-2	121.7	0.62	0.53
	3c-3	*123.8*	*0.67*	*0.41*
	3c-4	121.4	0.71	0.36
$[Cu(H_2S)_2(NH_3)_2]^+$	*3d-2*	*130.5*	*0.67*	*0.54*
	3d-3	127.1	0.73	0.36
	3d-4	126.6	0.73	0.33
$[Cu(H_2O)_4]^+$	*3e-2*	*117.6*	*0.80*	*0.41*
	3e-3	112.0	0.87	0.24
	3e-4	106.7	0.88	0.19
$[Cu(H_2O)_2(NH_3)_2]^+$	*3f-2*	*139.8*	*0.66*	*0.55*
	3f-3	138.1	0.73	0.44
$[Cu(NH_3)_4]^+$	*3g-2*	*144.4*	*0.65*	*0.56*
	3g-3	140.5	0.76	0.34
	3g-4	139.3	0.80	0.24

[a] Italic font indicates the global minima. The abbreviation struct is used for exact identification of the optimized structure.

larger ligand repulsion, giving the same ΔE^{stab} stabilization energy. A similar situation occurs also in the $[Cu(H_2S)_5]^{2+}$ complexes, where the final preference for the 5-coordinated structure is slightly more distinct. A ligand repulsion can be evaluated from differences between corresponding ΔE^{stab} and ΔE^{inter} values (see method). These differences are up to 18 kcal/mol for 5-coordinated complexes.

Table 5 collects the ΔE^{stab} stabilization energies for the monovalent copper cation in a mixed ligand environment. It was found that 2-coordination is preferred in complexes with at least two ammine ligands or more than two aqua ligands. Other mixed systems prefer the 3-coordinated structures as the most stable and only the tetrasulfide complex has the highest stabilization in a 4-coordinated arrangement. Comparing 4-coordinated complexes, $[Cu(NH_3)_4]^+$ is the most stable complex with ΔE^{stab} values equal to 139 kcal/mol. $[Cu(H_2S)_4]^+$ displays about 30 kcal/mol lower of a stabilization energy. The 4-coordinated $[Cu(H_2O)_4]^+$ is the least stable complex. However, the 4-coordinated $[Cu(H_2O)_4]^+$ structure does not represent the most stable structure analogously to the tetraamine compounds. For example, the 3-coordinated $[Cu(H_2O)_4]^+$ complex has larger stabilization than any $[Cu(H_2S)_4]^+$ system. The higher stability is connected with a relatively strong H-bond of the water

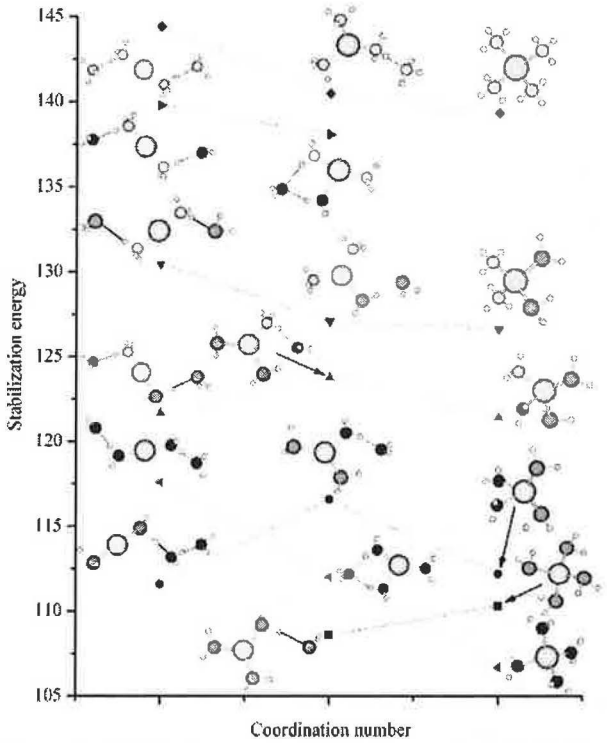

Figure 8. Stabilization energies (ΔE^{stab}) for the mixed $[Cu(H_2S)_m(H_2O)_n(NH_3)_k]^+$ compounds ($n + m + k = 4$): (▼) $[Cu(H_2S)_2(NH_3)2]^{2+}$; (▲) $[Cu(H_2S)_2(H_2O)(NH_3)]^{2+}$; (●) $[Cu(H_2S)_2(H_2O)_2]^{2+}$; (■) $[Cu(H_2S)_4]^{2+}$; (right-pointing triangle) $[Cu(H_2O)_4]^{2+}$; (left-pointing triangle) $[Cu(H_2O)_2(NH_3)_2]^{2+}$; (◆) $[Cu(NH_3)_4]^{2+}$.

molecule in the second solvation shell which masks the correct binding trend. This trend can be recovered from the coordination energies. The ΔE^{coord} value of the Cu−S bond is about 31.3 kcal/mol (from Table 1). It is practically identical to the corresponding value for the Cu−O bond (31.1 kcal/mol), published earlier.[65]

The preference order of the ΔE^{stab} energies, $Cu^+-N > Cu^+-S \geq Cu^+-O$, can be observed also for other systems in Table 5. Figure 8 helps to highlight the obtained trends. For instance, the most stable conformer of the $[Cu(H_2S)_2(H_2O)_2]^+$ system forms two Cu−S bonds while expelling the water molecules to the second solvation shell. The inverted conformer with two aqua ligands and two sulfide molecules in the second shell possesses about 6.6 kcal/mol lower stabilization energy.

Comparing the ΔE^{stab} values in a series of 4-coordinated $[Cu(H_2S)_2(X)_2]^+$ complexes (X = NH_3, H_2O, H_2S), the higher stabilization of the diaqua complex seemingly violates the overall trend. However, less bulky ligands (NH_3 or H_2O) allow shorter Cu−S distances, that is, larger overlap and stronger dative bonds, which leads to better stabilization of the mixed 4-coordinated $[Cu(H_2S)_2(H_2O)_2]^+$ complex. This is also supported by the bonding energies (see the upper part of Table 7). The disulfide−diaqua system possesses the largest ΔE^{BE} values for the Cu−S bonds in all Cu(I) complexes. Moreover, a small O−Cu−O angle (80°) and a HO−H···OH_2 distance of 2.6 Å clearly point to an additional interligand H-bond stabilization.

Stabilization energies for Cu(II) complexes are collected in Table 6. In the upper part of Table 6, the ΔE^{stab} and ΔE^{stex} energies of 4-coordinated Cu(II) complexes exhibit one important difference in comparison with the Cu(I) systems. The order of binding preference changes to Cu−N > Cu−O ≥ Cu−S. This is due to a larger electrostatic contribution to the metal−ligand bond. The stabilization energy of $[Cu(H_2O)_4]^{2+}$ is comparable to the ΔE^{stab} value of $[Cu(H_2S)_2(H_2O)_2]^{2+}$ and is about 3 kcal/mol higher than that of $[Cu(H_2S)_4]^{2+}$. The differences become more distinct when sterical corrections and H-bonding interactions are omitted, as was found for the ΔE^{stex} values.

In the lowest part of Table 6, the complexes with six interacting molecules are collected. Three different coordinations were examined. In all cases, 4-coordinated structures represent the most stable complexes. Nevertheless, sometimes (e.g., $[Cu(H_2S)_6]^{2+}$ or $[Cu(NH_3)_6]^{2+}$), the stabilization of 5-coordinated complexes is quite comparable (structures **5a-5** and **5c-5**). Moreover, the ΔE^{stex} energies, which evaluate the pure Cu/ligands interaction, are larger for 5-coordinated structures in all three homoligated systems. The largest interligand repulsion occurs in the case of 5-coordinated $[Cu(H_2S)_2(NH_3)_4]^{2+}$, where four ammine ligands occupy the first solvation shell. Figure 9 illustrates the dependence of the stabilization energy on the composition of these Cu(II) complexes. The strongest Cu−N bonding energies and larger stabilization energies in ammine-containing complexes are clearly demonstrated.

3.3. Ligand Bonding Energy (BE). The ΔE^{BE} energies of all Cu−X bonds (X = NH_3, H_2O, and H_2S) are presented in the upper part of Table 7 for the 4-coordinated Cu(I) complexes. Partition of the complex into two parts (ligand and the remaining part of the complex) in eq 1 enables a deeper insight into the strength of the individual Cu−X bonds. The ΔE^{BE} energies reflect closely the copper−ligand distances. In agreement with previous observations, the largest values in homoligated complexes (**3a-4**, **3e-4**, and **3g-4**) were found for the Cu−N bonds (about 21.1 kcal/mol). They are followed by an average ΔE^{BE} value of 17.7 kcal/mol for Cu−O and 15.6 kcal/mol for Cu−S. The strongest Cu−N bond occurs in the mixed $[Cu(H_2S)_2(H_2O)(NH_3)]^+$ complex characterized by about 29.9 kcal/mol. In this complex, the donation competition from the other ligands is relatively weak. The inconsistency in ($\Delta E^{BE}([Cu(H_2O)_4]^+) - \Delta E^{BE}([Cu(H_2S)_4]^+)$) versus ($\Delta E^{stab}([Cu(H_2O)_4]^+) - \Delta E^{stab}([Cu(H_2S)_4]^+)$) energies can be explained by stronger (repulsive) dipole/dipole interaction of water molecules, which lowers the stabilization energy of the tetraaqua complexes.

The ΔE^{BE} energies for the $[Cu(ligand)_4]^{2+}$ complexes are listed in the second part of Table 7. Similar to the Cu(I) systems, the relation between the BE values and the Cu−X distances (X = NH_3, H_2O, and H_2S) was found. Surprisingly, for the pure tetraamine, tetraaqua, and tetrasulfide complexes, very similar BEs for Cu−N and Cu−O were obtained (49.9 and 49.6 kcal/mol, respectively). The BE value of Cu−S is substantially smaller (34.8 kcal/mol). In accordance with the suggested stabilization order, an analogous preference of BE can be noticed. In the mixed Cu(II) systems, dependence of the ΔE^{BE} energies on various Cu−X bonds is more complex. An interesting situation occurs in the $[Cu(H_2S)_2(NH_3)_2]^{2+}$ system, where the ΔE^{BE}'s of Cu−N are not as high as those in the $[Cu(H_2O)_2(NH_3)_2]^{2+}$ complex. Similarly, the smallest value of Cu−S can also be seen in the $[Cu(H_2S)_2(NH_3)_2]^{2+}$ complex. This can be explained by different conformations. While the global minimum is the trans conformer in $[Cu(H_2S)_2(NH_3)_2]^{2+}$, all remaining 4-coordinated complexes prefer cis conformers as the most stable arrangements. The trans effect leads to the largest BE values for the Cu−N bond in the *cis*-$[Cu(H_2O)_2(NH_3)_2]^{2+}$ complex. This effect also results in lower BE values of the Cu−O bond in comparison with the tetraaqua complex (by about 10 kcal/mol). Simultaneously, the BE of Cu−N is

TABLE 6: Stabilization ΔE^{stab} and Sterically Corrected Stabilization ΔE^{ster} Energies (in kcal/mol), Partial Charges δ(Cu), Spin Densities ρ_S(Cu), and 4s and 3d Occupations of the Copper AO (in e) for the Cu(II) Systems[a]

system	struct	ΔE^{stab}	ΔE^{ster}	δ(Cu)	ρ_S(Cu)	4s	3d
$[Cu(H_2S)_4]^{2+}$	4a	303.6	313.9	0.87	0.40	0.53	9.56
$[Cu(H_2S)_2(H_2O)_2]^{2+}$	4b	306.4	316.7	1.12	0.54	0.44	9.41
$[Cu(H_2S)_2(H_2O)(NH_3)]^{2+}$	4c	321.1	334.4	1.13	0.54	0.42	9.42
$[Cu(H_2S)_2(NH_3)_2]^{2+}$	4d	335.3	349.6	1.16	0.53	0.39	9.41
$[Cu(H_2O)_4]^{2+}$	4e	306.9	321.1	1.56	0.77	0.24	9.18
$[Cu(H_2O)_2(NH_3)_2]^{2+}$	4f	340.2	359.5	1.40	0.68	0.31	9.27
$[Cu(NH_3)_4]^{2+}$	4g	366.8	391.8	1.30	0.63	0.36	9.32
$[Cu(H_2S)_6]^{2+}$	5a-4	329.4	346.3	0.86	0.38	0.52	9.58
	5a-5	*329.4*	*347.2*	*0.86*	*0.40*	*0.53*	*9.56*
$[Cu(H_2O)_6]^{2+}$	*5b-4*	*363.4*	*376.4*	*1.24*	*0.74*	*0.26*	*9.21*
	5b-5	358.6	377.1	1.22	0.79	0.24	9.18
	5b-6	338.0	362.2	1.43	0.88	0.24	9.10
$[Cu(NH_3)_6]^{2+}$	*5c-4*	*407.5*	*437.7*	*1.38*	*0.60*	*0.37*	*9.34*
	5c-5	407.1	444.6	1.32	0.66	0.34	9.30
	5c-6	399.9	443.7	1.30	0.68	0.34	9.28
$[Cu(H_2S)_2(H_2O)_4]^{2+}$	*5d-4*	*356.7*	*370.4*	*1.19*	*0.56*	*0.39*	*9.39*
	5d-5	351.7	368.1	1.24	0.60	0.36	9.36
	5d-6	343.7	364.2	1.28	0.65	0.35	9.33
$[Cu(H_2S)_4(H_2O)_2]^{2+}$	*5e-4*	*342.9*	*359.2*	*0.86*	*0.56*	*0.53*	*9.56*
	5e-5	342.5	356.7	0.95	0.60	0.48	9.53
	5e-6	336.0	355.0	0.98	0.46	0.46	9.51
$[Cu(H_2S)_2(H_2O)_2(NH_3)_2]^{2+}$	*5f-4*	*376.0*	*397.1*	*1.26*	*0.60*	*0.38*	*9.34*
	5f-5	375.0	396.5	1.23	0.61	0.39	9.34
	5f-6	368.9	394.4	1.20	0.58	0.39	9.37
$[Cu(H_2S)_2(NH_3)_4]^{2+}$	*5g-4*	*389.0*	*421.4*	*1.28*	*0.60*	*0.37*	*9.34*
	5g-5	387.6	420.5	1.29	0.63	0.37	9.32
$[Cu(H_2S)_4(NH_3)_2]^{2+}$	5h-4	359.6	*385.5*	1.09	0.50	0.44	9.43
	5h-5	*360.3*	384.7	*1.10*	*0.54*	*0.45*	*9.41*

[a] The abbreviation struct is used for exact identification of the optimized structure. Italic font indicates the global minima.

TABLE 7: Bonding Energies ΔE^{BE} (in kcal/mol) for the 4-Coordinated Cu(I) and Cu(II) Complexes[a]

system	struct	Cu−X1	Cu−X2	Cu−X3	Cu−X4
$[Cu(H_2S)_4]^{+}$	3a-4	15.6*	15.6*	15.6*	15.6*
$[Cu(H_2S)_2(H_2O)_2]^{+}$	3b-4	22.9*	22.1*	14.0**	12.5**
$[Cu(H_2S)_2(H_2O)(NH_3)]^{+}$	3c-4	29.9	18.8*	18.6*	9.5**
$[Cu(H_2S)_2(NH_3)_2]^{+}$	3d-4	23.3	22.5	13.0*	12.6*
$[Cu(H_2O)_4]^{+}$	3e-4	24.8**	18.1**	14.6**	13.4**
$[Cu(NH_3)_4]^{+}$	3g-4	21.1	21.1	21.1	21.1
$[Cu(H_2S)_4]^{2+}$	4a	35.3*	34.8*	34.5*	34.4*
$[Cu(H_2S)_2(H_2O)_2]^{2+}$	4b	46.8*	46.1*	38.0**	37.0**
$[Cu(H_2S)_2(H_2O)(NH_3)]^{2+}$	4c	55.5	40.9*	40.2*	32.7**
$[Cu(H_2S)_2(NH_3)_2]^{2+}$	4d	54.9	54.7	31.2*	30.9*
$[Cu(H_2O)_4]^{2+}$	4e	49.6**	49.6**	49.6**	49.6**
$[Cu(H_2O)_2(NH_3)_2]^{2+}$	4f	62.9	62.9	39.2**	39.2**
$[Cu(NH_3)_4]^{2+}$	4g	49.9	49.9	49.9	49.9

[a] The abbreviation struct is used for exact identification of the optimized structure. One asterisk denotes Cu−S bond lengths, and two asterisks denote Cu−O bond lengths, while all remaining values are those for Cu−N bonds.

increased by a similar amount of energy as compared to the tetraammine complex. Also, in the $[Cu(H_2S)_2(H_2O)_2]^{2+}$ complex, similar BE shifts can be observed. The ΔE^{BE} values of the Cu−S and Cu−O bonds respectively are larger by about 10 kcal/mol and smaller by about the same amount than the ΔE^{BE} energies in the corresponding homoligated complexes. Moreover, in the $[Cu(H_2S)_2(H_2O)_2]^{2+}$ and $[Cu(H_2S)_2(H_2O)(NH_3)]^{2+}$ complexes, the Cu−S bonds are characterized by larger ΔE^{BE} values than the Cu−O bonds. This is caused by a larger donation contribution in the Cu−S bonds, which can be demonstrated in the framework of the natural bond orbital (NBO) analysis. The donation of a lone pair of the sulfur atom to the first virtual orbital of Cu can be evaluated in terms of the $E(2)$ energies (the second-order perturbation theory of the Fock matrix in the basis of NBO) to be about 40 kcal/mol. The same $E(2)$ energies from the lone pairs of oxygen atoms are lower by about 20 kcal/mol. In the case of the $[Cu(H_2S)_2(H_2O)(NH_3)]^{2+}$ complexes, a similar situation was obtained. The $E(2)$ energies are the following: $E(2)$(O→Cu) ≈ 15 kcal/mol, $E(2)$(N→Cu) ≈ 30 kcal/mol, and $E(2)$(S→Cu) ≈ 40 kcal/mol.

3.4. IPs and EAs. To describe transitions between Cu(I) and Cu(II) oxidation states, the vertical and adiabatic ionization potentials were calculated. In the case of IP_{vert}, both HF and DFT levels were considered. In the case of IP_{adiab}, only the DFT method was used. The IP values are compiled in Table 8.

At the DFT level, the IP_{vert} values decrease with increasing coordination number. In 4-coordinated systems, the highest values (12.0−12.7 eV) were obtained for the sulfide-containing complexes. Slightly lower IPs were obtained for the tetraaqua and tetraamine complexes (11.9 and 11.3 eV, respectively). The IP_{adiab} values are lower by approximately 0.5 eV. Interestingly, for the $[Cu(H_2O)_4]^{2+/+}$ system, practically the same vertical and adiabatic IPs were obtained. From the difference between IP values, one can estimate the relaxation strain, which pushes the instantly oxidized Cu(I) structure toward the optimal Cu(II) geometry. In the case of the tetraaqua complex, this points to a very flat potential energy surface in relation to the deformation of torsion angles. In blue copper proteins, the ligand arrangement of the active center usually has a distorted tetrahedral structure, which is probably also enforced for the Cu(II) structure. This fact partially explains their large reduction potential. The $[Cu(H_2S)_2(NH_3)_2]^{+}$ complex can be of particular interest, since its IPs might give insight into the redox center of proteins such as plastocyanin or azurin. They contain two histidines, one methionine, and cysteine amino acid side chains coordinated to the copper cation. In the $[Cu(H_2S)_2(NH_3)_2]^{+}$ complex, the IP_{vert} value is equal to 12.0 eV and IP_{adiab} = 11.5 eV. Unfortunately, we are not aware of any experimental data for these small complexes that could be compared with the presented results. Nevertheless, theoretical papers presenting the ionization potentials for similar compounds exist. In the study of Taylor,[87] vertical IP = 6.27 eV was calculated for the neutral $Cu(H_2O)$ molecule at the CCSD(T) level. The values of the

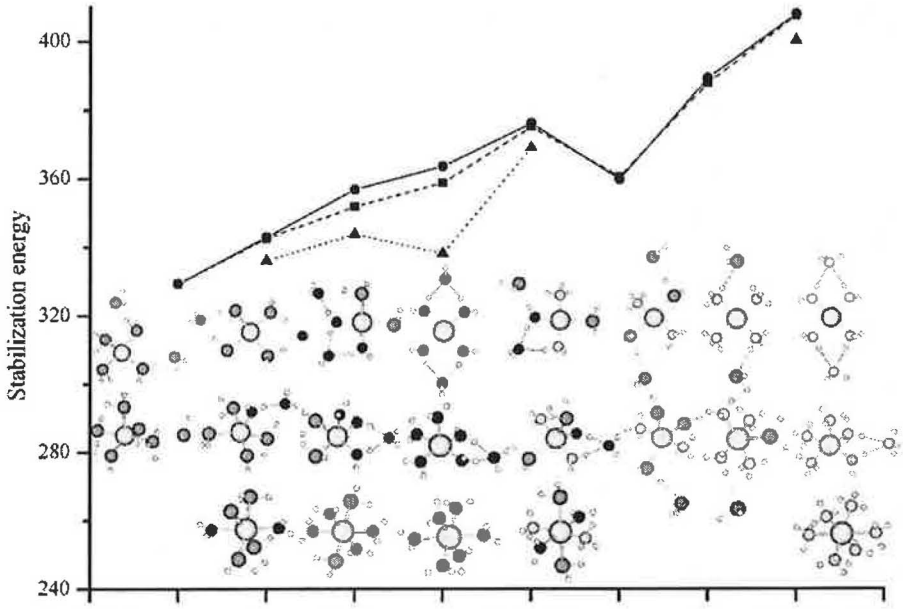

Figure 9. Dependence of stabilization energy on the coordination number of the Cu(II) complexes: (●) 4-coordinated, (■) 5-coordinated, and (▲) 6-coordinated structures.

TABLE 8: Ionization Potentials (in eV) IP_{vert}, IP_{adiab}, IP_{Koop}, and IP_{OVGF} and Electron Affinities EA_{vert} and EA_{OVGF} for the Cu(I) Complexes[a]

system	struct	IP_{vert} DFT	IP_{adiab} DFT	IP_{Koop} DFT	IP_{vert} HF	IP_{Koop} HF	IP_{OVGF} HF	EA_{vert} DFT	EA_{OVGF} HF
$[Cu(H_2S)_4]^+$	**3a-3**	12.6		10.8	13.6	13.8	13.2	3.5	2.9
	3a-4	*12.6*	*12.2*	*10.7*	*13.2*	*14.5*	*14.9*	*3.5*[b]	*2.9*
$[Cu(H_2S)_2(H_2O)_2]^+$	**3b-2**	13.6		11.4	14.5	15.1	16.3	3.3	2.7
	3b-3	13.0		10.8	13.7	14.8	15.5	3.5	2.7
	3b-4	*12.7*	*12.1*	*10.6*	*13.6*	*14.6*	*15.4*	*3.5*	*2.9*
$[Cu(H_2S)_2(H_2O)(NH_3)]^+$	**3c-2**	12.9		10.8	14.6	13.8	13.1	3.3	2.6
	3c-3	12.5		10.5	13.4	14.3	15.2	3.4	2.7
	3c-4	*12.4*	*11.9*	*10.4*	*13.3*	*14.3*	*15.2*	*3.4*	*2.8*
$[Cu(H_2S)_2(NH_3)_2]^+$	**3d-2**	12.4		10.7	12.4	13.8	13.1	3.3	2.5
	3d-3	12.1		10.2	12.2	13.6	13.0	3.4	2.8
	3d-4	*12.0*	*11.5*	*10.0*	*12.9*	*13.9*	*14.8*	*3.4*	*2.8*
$[Cu(H_2O)_4]^+$	**3e-2**	13.7		10.9	15.2	15.5	79.8	3.5	2.4
	3e-3	13.0		10.1	15.1	15.5	36.9	3.7	2.8
	3e-4	*11.9*	*11.9*	*10.0*	*15.2*	*14.0*	*27.9*	*2.9*	*2.8*
$[Cu(H_2O)_2(NH_3)_2]^+$	**3f-2**	13.2		10.6	14.5	14.8		3.2	2.9
	3f-3	*12.5*	*11.8*	*9.9*	*15.6*	*14.4*	*34.4*	*3.3*	*2.4*
$[Cu(NH_3)_4]^+$	**3g-2**	12.8		10.5	10.0	14.6	36.0	3.0	2.7
	3g-3	11.9		9.4	12.9	14.5	26.7	3.2	2.6
	3g-4	*11.3*	*10.7*	*8.8*	*13.8*	*14.0*	*47.4*	*3.3*	*2.6*

[a] Italic font indicates transitions between the 4-coordinated structures. The abbreviation struct is used for the optimized structure. [b] The adiabatic EA of the $[Cu(H_2S)_4]^+$ complex is 3.5 eV. The neutral structure of 4-coordinated $[Cu(H_2S)_4]$ has a tetrahedral geometry with Cu−S distances of ~2.38 Å.

vertical and adiabatic IPs of phthalocyanine were determined to be 6.48 and 6.47 eV, respectively, by Lee[88] using the BPW91 method. Olsson[10] calculated the vertical QM/MM energy difference of the two states in the presence of protein point charges and obtained 4.22 and 6.78 eV for plastocyanin and rusticyanin, respectively. Our results can be compared with the vertical IPs of Satta et al.[89] who investigate neutral $Cu(NH_3)_n$ systems at the B3LYP level. They found vertical IP = 3.70, 3.65, and 2.90 eV for n = 2, 3, and 4, respectively. Our estimation of the EA value for $[Cu(NH_3)_4]^+$ is 3.3 eV, which is in good accord with the energy computed by Satta.

For the Cu(I) systems, the IP_{Koop} ionization potentials based on Koopmans' theorem are presented as well. These values are systematically about 2 eV lower at the DFT level and about 1 eV higher at the HF level than the corresponding IP_{vert} energies. Comparing the IP_{vert} energies obtained at the HF and DFT levels, one can see that the DFT values are generally lower.

An estimation of the adiabatic electron affinity was performed. However, the only stable neutral structure was found for the 4-coordinated $[Cu(H_2S)_4]$ system. The calculated adiabatic electron affinity is about 3.5 eV. The additional electron is located in the LUMO of the Cu(I) structures that is composed by the copper 4s atomic orbital (AO) with an antibonding admixture of sulfide MOs. The vertical EA_{vert}(DFT) electron affinity values were evaluated for all studied Cu(I) complexes. They range from 2.9 to 3.7 eV.

Results from outer valence Green function propagators systematically overestimate IPs (even more than 2.0 eV) and underestimate EAs (on average by 0.5 eV). Also, the trend in IP^{OVGF} is not correct, since the IP increases with increasing coordination.

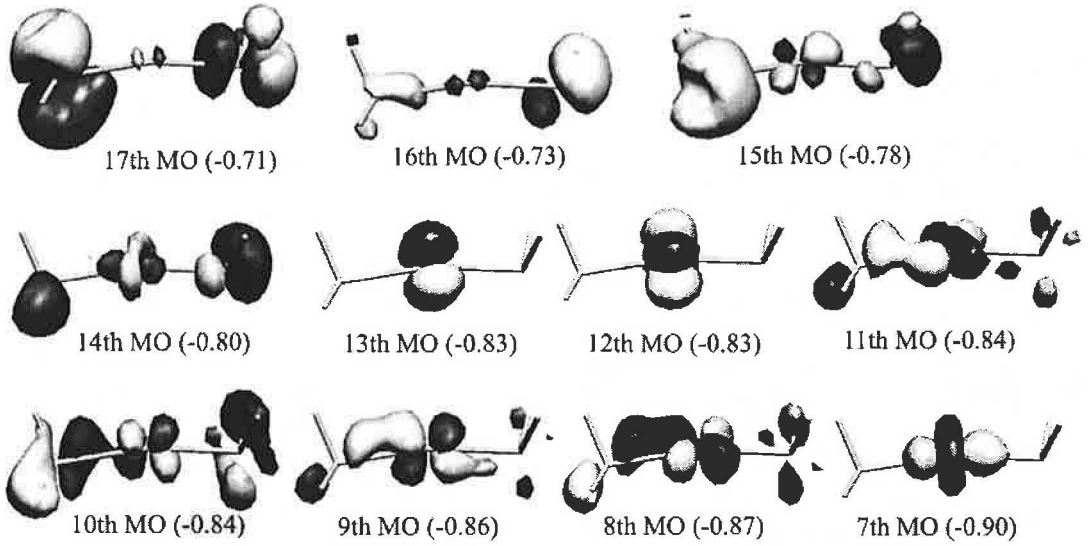

Figure 10. Valence α-MOs of the $[Cu(H_2S)_2]^{2+}$ system. The orbital energies of the corresponding MOs are in parentheses (in au). The 11th α-MO (SOMO) has no corresponding MO in the β-set.

For an accuracy estimation, the experimentally measured first and second ionization potentials and the EA of the isolated Cu atom (IP^{first} = 7.7 eV, IP^{second} = 20.3 eV, EA = 1.2 eV[90]) were compared with the calculated values (IP^{first} = 8.2 eV, IP^{second} = 20.5 eV, EA = 1.3 eV). Relatively similar values at least partially justify the methods and basis set used in this section.

3.5. Charge and Wave Function Analyses. The partial charges were determined by the NPA method,[76] and an analysis of molecular orbitals (MOs) was performed in order to get a deeper insight into the interactions in the examined structures. The Cu(II) complexes contain copper in the $3d^9$ configuration, giving an open-shell wave function with the doublet electronic ground state. According to the arrangement of ligand molecules in the first solvation shell, the single occupied molecular orbital (SOMO) is formed by different Cu 3d atomic orbitals (AOs). In the $[Cu(H_2S)]^{2+}$ and $[Cu(H_2S)_2]^{2+}$ structures, the SOMO is composed of the $3d_{z^2}$ AO (11th MO in Figure 10) with the z-axis collinear to the copper−ligand bond. In the most stable square-planar 4-coordinated complexes, the $3d_{x^2-y^2}$ AO of the Cu atom forms the SOMO. This can be observed in Figure 11 and Supporting Information Figures 1 and 2. For the 5- and 6-coordinated structures, the SOMOs are also based on the $3d_{x^2-y^2}$ AO with partial admixture of Cu $3d_{z^2}$.

Table 1 contains the copper partial charges for all studied copper sulfide compounds. In both monovalent and divalent cations, the Cu 4s AO plays a key role in donation effects. Occupations of this orbital (and 3d AOs in the case of the Cu(II) systems) are also presented in Table 1. Increasing coordination number leads to the saturation of the acceptor ability of the Cu ions. In the case of three or more ligands, no substantial change of the Cu partial charge occurs (about 0.6 and 0.9e in the monovalent and divalent complexes, respectively). The value of the metal partial charge results from the extent of the ligand electron-density donation, which is a consequence of the chemical potential minimization of the whole system. Also, the spin density localized on the Cu atom closely follows the size of partial charge, as can be seen from Table 1 for homoligated structures and Table 6 for mixed ligand complexes. An interesting exception from this correspondence between partial charges and spin densities is the system $[Cu(H_2S)_2]^{2+}$ where a relatively high spin density on the Cu atom can be noticed. A possible explanation comes from the different donation in the case of the monosulfide $[Cu(H_2S)]^{2+}$ complex where the main dative contribution to 3d can be noticed (9.58e). In the disulfide complex, practically the same donation to the 4s Cu AO is visible (0.39) comparing to 9.39e in 3d AOs. It means that the smaller portion of the α-spin electron density from $3d_{x^2-y^2}$ is compensated in this complex. When more than two ligands are present, the accepting capability of the Cu^{2+} cation is already saturated as follows from the nearly constant occupation of both the 3d (≈9.56e) and 4s (≈0.53e) AOs of the Cu atom. The donation to different types of Cu AOs for mono- and di-ligated complexes is general, and it also was observed in the previous studies with water[65] and ammonia[66] ligands. Here, a different target (different AO of Cu) caused stronger and shorter Cu−O and Cu−N bonds (or higher stabilization) in diaqua or diammine complexes than it would correspond to monotonic trends when number of ligands was increased.

The NPA partial charges of the monovalent Cu complexes in a mixed sulfide−water−ammonium environment are compiled in Table 5. In the Cu(I) water−ammonium compounds, the highest donation and thus the lowest Cu partial charge occurs in 2-coordinated structures. In the presence of hydrogen sulfide molecules, lower partial charges on the Cu cations point to a higher donation. This observation is in agreement with the coordination preferences found in the energy section above. The same dependence of the partial charges on the ligand type can also be found in the mixed Cu(II) systems in Table 6. These trends correspond to increasing values of hardness, $\mu(H_2S)$ = 6.2, $\mu(NH_3)$ = 8.2, $\mu(H_2O)$ = 9.5,[91] and reflect the principle of the HSAB theory.[82]

Detailed insight into the donor−acceptor bonding character can be achieved by molecular orbital (MO) analysis. For the demonstration, 2-coordinated $[Cu(H_2S)_2]^{2+}$ (in Figure 10) and 4-coordinated homoligated complexes were chosen. Several highest valence MOs are depicted for the tetrasulfide complex in Figure 11. Supporting Information Figure 1 shows valence MOs for the tetraammine Cu(II) structure, and MOs of the tetraaqua Cu(II) complexes are depicted in Supporting Information Figure 2. In 4-coordinated complexes, the proper $d_{x^2-y^2}$ character of the SOMO (13th MO in Figure 11, 21st MO in Supporting Information Figure 1, and 17th MO in Supporting Information Figure 2) can be seen. The lower occupation of

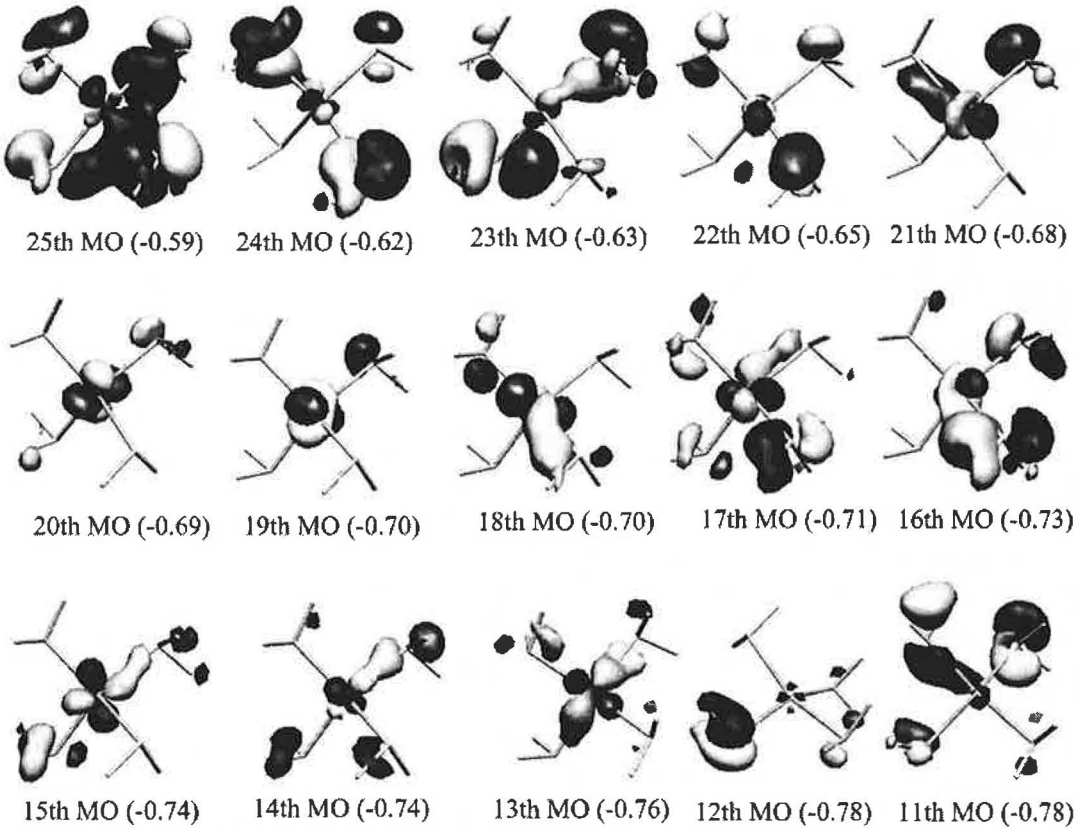

Figure 11. Valence α-MOs of the $[Cu(H_2S)_4]^{2+}$ system. The SOMO is represented by the 13th MO.

the $3d_{x^2-y^2}$ AO minimizes the repulsion between the Cu electron density and the donating ligand lone pairs. The varying "position" of the SOMO orbital is connected with the different eigenvalues of the MOs in isolated ligand molecules and with the usage of an unrestricted method. In Figure 11, the first three MOs (23rd to 25th) display the nonbonding combinations of lone pairs of the H_2S ligands (with small admixture of Cu AOs $3d_{x^2-y^2}$, $3d_{xz}$, and $3d_{yz}$ according to the symmetry of the ligands). In the four following orbitals, the Cu 3d AOs dominate (19th to 22nd): d_{z^2}, d_{xy}, d_{xz}, d_{yz}. Then, another set of five MOs appears where only a small contribution of the Cu d AO is admixtured to ligand MOs. Finally, the 13th α-orbital with $d_{x^2-y^2}$ character appears, which has no similar counterpart among the occupied β-orbitals. An analogous discussion applies also to the remaining two cases. No back-donation strengthening of the Cu−X bonds can occur in the examined complexes, since none of the examined ligands possess proper π^*-antibonding orbitals.

In the first column of Figure 12, the spin densities (on the isodensity surface of $\rho = 0.005$ e/bohr^3) for linear disulfide, square-planar tetraaqua, tetraamine, and tetrasulfide Cu(II) complexes are depicted. Except for the first linear one, all of the other densities show the same shape in which the character of the copper $3d_{x^2-y^2}$ AO can be easily recognized. The second column of Figure 12 presents maps of electrostatic potentials projected on the isodensity surface ($\rho = 0.001$). A higher maximum of the electrostatic potential (V_{max}) in the case of the tetraaqua complex corresponds to a relatively smaller donation in accord with the NPA partial charges.

Using the MP2/6-31+G(d) method, Katz et al.[18] determined partial charges of 0.71 and 1.38*e* on the Cu atom in the $[Cu(H_2S)_4]^+$ and $[Cu(H_2S)_4]^{2+}$ systems, respectively. However, the present values for the Cu(I) and Cu(II) structures are substantially lower (0.4 and 0.8*e*, respectively) using a larger basis set (B3LYP/6-311++G(2df,2pd)). For the $[Cu(NH_3)_4]^{2+/+}$ complexes, similar (but not so significant) differences between the MP2/6-31+G(d) and B3LYP/6-311++G(2df,2pd) results can be noticed (1.3 and 1.6*e* compared with 0.8 and 0.87*e* for Cu(I) and Cu(II), respectively). An explanation of the remarkably higher Cu partial charges can be seen in inaccurate description of sulfur-containing systems using the MP2 method (cf. ref 92) and a slightly less flexible (smaller) basis set in the case of Katz's calculation.

4. Conclusion

A systematic investigation of the Cu(I)/Cu(II) cation interactions with biologically important types of ligands (water, ammonium, and hydrogen sulfide) at the DFT level was performed. The $[Cu(H_2S)_m(H_2O)_n(NH_3)_k]^{2+}$ complexes (where n, m, and k are equal to 0, 2, 4, and 6, along with the restriction $m + n + k = 4$ or 6) were optimized using the B3PW91/6-31G(d) method, often using distinct geometries as starting points. In the case of the Cu(I) complexes, only the 4-ligated systems ($m + n + k = 4$) were examined, since a maximum coordination number of 4 was reported in previous studies. The optimizations reveal various stable coordinations.

The lowest conformers of all coordinations were analyzed in terms of the ΔE^{stab} and ΔE^{stex} stabilization energies, ΔE^{coord} coordination energies and ΔE^{BE} bonding energies at the B3LYP/6-311++G(2df,2pd) level. The different schemes to describe the energetics help one to better understand the balance of forces

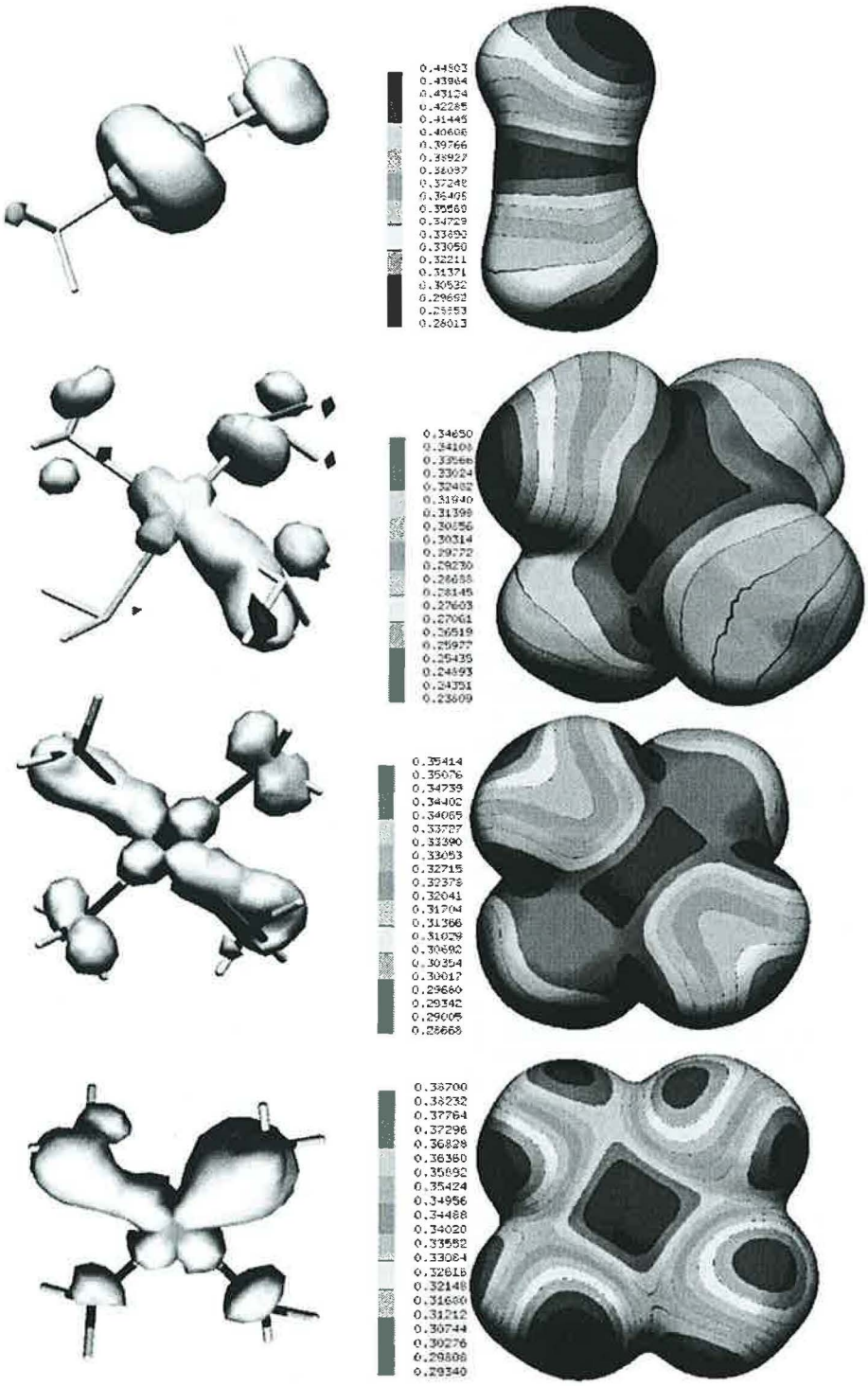

Figure 12. Plots of spin densities and maps of electrostatic potentials for the disulfide, square-planar tetraaqua, tetraamine, and tetrasulfide Cu(II) complexes. The extrema of the maps (in electronvolts) are as follows: $[Cu(H_2S)_2]^{2+}$ $V_{min} = 0.28$, $V_{max} = 0.45$; $[Cu(NH_3)_4]^{2+}$ $V_{min} = 0.27$, $V_{max} = 0.35$; $[Cu(H_2O)_4]^{2+}$ $V_{min} = 0.29$, $V_{max} = 0.39$; $[Cu(H_2S)_4]^{2+}$ $V_{min} = 0.24$, $V_{max} = 0.35$.

in the studied systems. Furthermore, the different energy evaluations may be useful when the presented results are to be compared with other methods, namely, the force fields.

The Cu(I) systems prefer a coordination number of 2 (followed by 3 and 4) in the presence of the ammine and aqua ligand field. The 3- and 4-coordinated structures are favored when the H_2S molecules occupy the first solvation shell. For the divalent copper compounds, the 4- and 5-coordinated structures represent the most stable forms.

The highest stabilization energies were found for ammine ligands followed by hydrogen sulfide and aqua ligands in the case of the Cu(I) complexes. The order of the last two ligands is inverted in the Cu(II) systems due to a higher electrostatic contribution to the stabilization energy.

On the basis of the MO and NBO analysis, the largest dative contribution to the Cu−X bond occurs in the sulfur case followed by nitrogen. The weakest donor ability is exhibited by oxygen. It is in agreement with the order of the softness parameter from the HSAB principle. This can explain the higher coordination of the Cu^+ cations in sulfide-containing complexes. Another reason the water molecules often escape to the second solvation shell is linked to a non-negligible energy release by the formation of strong H-bonds with other polarized ligands (either NH_3 or H_2O). Therefore, the final arrangement of the ligand molecules in solvation shells is a consequence of several factors. In the case of more polar molecules (NH_3 and H_2O in the present study), the system can be stabilized by the formation of both dative bonds and H-bonds. Lower coordination prevails when the H-bonding is accompanied by a sufficient energy release. The dative bonding is preferable in the presence of less polar H_2S molecules where only very weak H-bonds can be formed.

The revealed preference can be generalized as follows: nitrogen-containing ligands (like histidine) form stronger bonds with the copper cations than the Cu−S bonds in, for example, cysteine or methionine and the Cu−O coordination with, for example, serine or tyrosine. However, this preference must be taken with care, since the remaining part of the ligated molecule can mask electron-density characteristics substantially.

Both vertical IP_{vert} and adiabatic IP_{adiab} ionization potentials (as well as electron affinities, EA) were calculated to describe possible transitions between the Cu(I) and Cu(II) oxidation states. The highest IP values were obtained for the complexes containing the H_2S molecules.

The partial charges were computed by the NPA method. The partial charge located on the Cu atom corresponds to the extent of the total donation. The copper 4s AO is the main target of the donation effects. Therefore, its occupation was observed. In the Cu(II) complexes, the occupation numbers of the Cu 3d AOs also need to be considered.

The presented data provide a systematic and wide set of structures and energies of Cu-containing clusters of biological relevance. The data can be used to rationalize selected aspects of the physical chemistry of Cu interactions in biopolymers and can also be used for calibration of other computational methods such as Cu-containing force fields. To simplify this task, all studied structures are available as Supporting Information.

Acknowledgment. This study was supported by Charles University grant 438/2004/B_CH/MFF, grant NSF-MŠMT ČR 1P05 ME-784, and grant MSM 0021620835. J.Š. acknowledges support by grant 203/05/0388, Grant Agency of the Czech Republic. The Institute of Biophysics is supported by grant AVOZ50040507, Ministry of Education of the Czech Republic. The computational resources from Meta-Centers in Prague, Brno, and Pilsen are acknowledged for access to their excellent supercomputer facilities.

Supporting Information Available: Tables showing the coordinates of the examined structures and figures showing MOs. This material is available free of charge via the Internet at http://pubs.acs.org.

References and Notes

(1) Siegbahn, P. E. M.; Wirstam, M. *J. Am. Chem. Soc.* **2001**, *123*, 11819.
(2) Prabhakar, R.; Siegbahn, P. E. M. *J. Phys. Chem. B* **2003**, *107*, 3944.
(3) Wang, X.; Berry, S. M.; Xia, Y.; Lu, Y. *J. Am. Chem. Soc.* **1999**, *121*, 7449.
(4) Palmer, A. E.; Randall, D. W.; Xu, F.; Solomon, E. I. *J Am. Chem. Soc.* **1999**, *121*, 7138.
(5) Randall, D. W.; George, S. D.; Hedman, B.; Hodgson, K. O.; Fujisawa, K.; Solomon, E. I. *J. Am. Chem. Soc.* **2000**, *122*, 11620.
(6) Randall, D. W.; George, S. D.; Holland, P. L.; Hedman, B.; Hodgson, K. O.; Tolman, W. B.; Solomon, E. I. *J. Am. Chem. Soc.* **2000**, *122*, 11632.
(7) Holland, P. L.; Tolman, W. B. *J. Am. Chem. Soc.* **2000**, *122*, 6331.
(8) Holland, P. L.; Tolman, W. B. *J. Am. Chem. Soc.* **1999**, *121*, 7270.
(9) Gray, H. B.; Malmstroem, B. G.; Williams, R. J. P. *J. Biol. Inorg. Chem.* **2000**, *5*, 551.
(10) Olsson, M. H. M.; Hong, G. Y.; Warshel, A. *J. Am. Chem. Soc.* **2003**, *125*, 5025.
(11) Olsson, M. H. M.; Ryde, U. *J. Biol. Inorg. Chem.* **1999**, *4*, 654.
(12) Olsson, M. H. M.; Ryde, U.; Roos, B. O.; Pierloot, K. *J. Biol. Inorg. Chem.* **1998**, *3*, 109.
(13) Ryde, U.; Olsson, M. H. M.; Roos, B. O.; De Kerpel, J. O. A.; Pierloot, K. *J. Biol. Inorg. Chem.* **2000**, *5*, 565.
(14) Book, L. D.; Arnett, D. C.; Hu, H.; Scherer, N. F. *J. Phys. Chem. A* **1998**, *102*, 4350.
(15) Fraga, E.; Webb, M. A.; Loppnow, G. R. *J. Phys. Chem.* **1996**, *100*, 3278.
(16) Sabolovic, J.; Liedl, K. R. *J. Am. Chem. Soc.* **1999**.
(17) Sabolovic, J.; Tautermann, C. S.; Loerting, T.; Liedl, K. R. *Inorg. Chem.* **2003**, *42*, 2268.
(18) Katz, A.; Shimoni-Livny, L.; Navon, O.; Navon, N.; Bock, C.; Glusker, J. *Helv. Chim. Acta* **2003**, *86*, 1320.
(19) Rulíšek, L.; Havlas, Z. *J. Am. Chem. Soc.* **2000**, *122*, 10428.
(20) Rulíšek, L.; Havlas, Z. *J. Phys. Chem. A* **2002**, *106*, 3855.
(21) Rulíšek, L. *Chem. Listy* **2002**, *96*, 132.
(22) Rulíšek, L.; Havlas, Z. *J. Phys. Chem. B* **2003**, *107*, 2376.
(23) Bertran, J.; Rodrigues-Santiago, L.; Sodupe, M. *J. Phys. Chem. B* **1999**, *103*, 2310.
(24) Shoeib, T.; Rodriquez, C. F.; Siu, K. W. M.; Hopkinson, A. C. *Phys. Chem. Chem. Phys.* **2001**, *3*, 853.
(25) Caraiman, D.; Shoeib, T.; Siu, K.; Hopkinson, A.; Bohme, D. *Int. J. Mass Spectrom.* **2003**, *228*, 629.
(26) Santra, S.; Zhang, P.; Tan, W. *J. Phys. Chem. A* **2000**, *104*, 12021.
(27) Manikandan, P.; Epel, B.; Goldfarb, D. *Inorg. Chem.* **2001**, *40*, 781.
(28) Shimizu, K.; Maeshima, H.; Yoshida, H.; Satsuma, A.; Hattori, T. *Phys. Chem. Chem. Phys.* **2001**, *3*, 862.
(29) Sigman, J. A.; Kwok, B. C.; Gengenbach, A.; Lu, Y. *J Am. Chem. Soc.* **1999**, *121*, 8949.
(30) Hackl, E. V.; Kornilova, S. V.; Kapinos, L. E.; Andruschenko, V. V.; Galkin, V. L.; Grigoriev, D. N.; Blagoi, Y. P. *J. Mol. Struct.* **1997**, *408*, 229.
(31) Hemmert, C.; Pitie, M.; Renz, M.; Gornitzka, H.; Soulet, S.; Meunier, B. *J. Biol. Inorg. Chem.* **2001**, *6*, 14.
(32) Herrero, L. A.; Terron, A. *J. Biol. Inorg. Chem.* **2000**, *5*, 269.
(33) Meggers, E.; Holland, P. L.; Tolman, W. B.; Romesberg, F. E.; Schultz, P. G. *J. Am. Chem. Soc.* **2000**, *122*, 10714.
(34) Atwell, S.; Meggers, E.; Spraggon, G.; Schultz, P. G. *J. Am. Chem. Soc.* **2001**, *123*, 12364.
(35) Schoentjes, B.; Lehn, J.-M. *Helv. Chim. Acta* **1995**, *78*, 1.
(36) Lamsabhi, A.; Alcami, M.; Mo, O.; Yanez, M.; Tortajada, J. *ChemPhysChem* **2004**, *5*, 1871.
(37) Gasowska, A.; Lomozik, L. *Monatsh. Chem.* **1995**, *126*, 13.
(38) Burda, J. V.; Šponer, J.; Hobza, P. *J. Phys. Chem.* **1996**, *100*, 7250.
(39) Burda, J. V.; Šponer, J.; Leszczynski, J.; Hobza, P. *J. Phys. Chem. B* **1997**, *101*, 9670.
(40) Šponer, J.; Sabat, M.; Burda, J.; Leszczynski, J.; Hobza, P.; Lippert, B. *J. Biol. Inorg. Chem.* **1999**, *4*, 537.
(41) Noguera, M.; Bertran, J.; Sodupe, M. *J. Phys. Chem. A* **2004**, *108*, 333.
(42) Rulíšek, L.; Šponer, J. *J. Phys. Chem. B* **2003**, *106*, 1913.
(43) Burda, J. V.; Shukla, M. K.; Leszczynski, J. *J. Mol. Model.* **2005**, *11*, 362.
(44) Tachikawa, H. *Chem. Phys. Lett.* **1996**, *260*, 582.
(45) Hamilton, I. P. *Chem. Phys. Lett.* **2004**, *390*, 517.
(46) Feller, D.; Glendening, E. D.; de Jong, W. A. *J. Chem. Phys.* **1999**, *110*, 1475.
(47) Schroeder, D.; Schwartz, H.; Wu, J.; Wesdemiotis, C. *Chem. Phys. Lett.* **2001**, *343*, 258.
(48) Marini, G. W.; Liedl, K. R.; Rode, B. M. *J. Phys. Chem. A* **1999**, *103*, 11387.
(49) Schwenk, C.; Rode, B. *ChemPhysChem* **2004**, *5*, 342.
(50) Schwenk, C. F.; Rode, B. M. *Phys. Chem. Chem. Phys.* **2003**, *5*, 3418.
(51) Pranowo, H. *Chem. Phys.* **2003**, *291*, 153.

(52) Berces, A.; Nukada, T.; Margl, P.; Ziegler, T. *J. Phys. Chem. A* 1999, *103*, 9693.
(53) Pranowo, H. D.; Rode, B. M. *J. Phys. Chem. A* 1999, *103*, 4298.
(54) Pranowo, H. D.; Setiajin, A. H. B.; Rode, B. M. *J. Phys. Chem. A* 1999, *103*, 11115.
(55) Pranowo, H. D.; Rode, B. M. *Chem. Phys.* 2001, *263*, 1.
(56) Haeffner, F.; Brinck, T.; Haeberlein, M.; Moberg, C. *Chem. Phys. Lett.* 1997, *397*, 39.
(57) Cordeiro, N. M. D. S.; Gomes, J. A. N. F. *J. Comput. Chem.* 1993, *14*, 629.
(58) Subramanian, V.; Shankaranarayanan, C.; Nair, B. U.; Kanthimathi, M.; Manickkavachagam, R.; Ramasami, T. *Chem. Phys. Lett.* 1997, *274*, 275.
(59) Gresh, N.; Policar, C.; Giessner-Prettre, C. *J. Phys. Chem.* 2002, *106*, 5660.
(60) Ledecq, M.; Lebon, F.; Durant, F.; Giessner-Prettre, C.; Marquez, A.; Gresh, N. *J. Phys. Chem. B* 2003, *107*, 10640.
(61) Schwerdtfeger, P.; Krawczyk, R. P.; Hammerl, A.; Brown, R. *Inorg. Chem.* 2004, *43*, 6707.
(62) Neese, F. *Magn. Reson. Chem.* 2004, *42*, S187.
(63) Konopka, M.; Rousseau, R.; Stich, I.; Marx, D. *J. Am. Chem. Soc.* 2004, *126*, 12103.
(64) Bauschlicher, C. W.; Langhoff, S. R.; Partridge, H. *J. Chem. Phys.* 1991, *94*, 2068.
(65) Burda, J. V.; Pavelka, M.; Simanek, M. *J. Mol. Struct.* 2004, *683*, 183.
(66) Pavelka, M.; Burda, J. V. *Chem. Phys.* 2005, *312*, 193.
(67) Hurley, M. M.; Pacios, L. F.; Christiansen, P. A.; Ross, R. B.; Ermler, W. C. *J. Chem. Phys.* 1986, *84*, 6840.
(68) The usage of the originally suggested pseudoorbitals leads to a wrong description of the basic physical properties, such as the IP or EA, of the copper atom. Here, at least qualitative agreement can be obtained when original orbitals are augmented with diffuse and polarization functions.
(69) Poater, J.; Sola, M.; Rimola, A.; Rodriguez-Santiago, L.; Sodupe, M. *J. Phys. Chem. A* 2004, *108*, 6072.
(70) Boys, S. F.; Bernardi, F. *Mol. Phys.* 1970, *19*, 553.
(71) Tiraboschi, G.; Roques, B.-P.; Gresh, N. *J. Comput. Chem.* 1999, *20*, 1379.
(72) Tiraboschi, G.; Gresh, N.; Giessner-Prettre, C.; Pedersen, L. G.; Deerfield, D. W. *J. Comput. Chem.* 2000, *21*, 1011.
(73) Šponer, J.; Burda, J. V.; Sabat, M.; Leszczynski, J.; Hobza, P. *J. Phys. Chem. A* 1998, *102*, 5951.
(74) Ostlund, N. S.; Sabo, A. *Modern Quantum Chemistry*; McGraw-Hill: New York, 1989.
(75) Zakrzewski, V. G.; Ortiz, J. V. *Int. J. Quantum Chem.* 1995, *53*, 583.
(76) Reed, A. E.; Weinstock, R. B.; Weinhold, F. *J. Chem. Phys.* 1985, *83*, 735.
(77) Frisch, M. J.; Trucks, G. W.; Schlegel, H. B.; Scuseria, G. E.; Robb, M. A.; Cheeseman, J. R.; Zakrzewski, V. G.; Montgomery, J. A., Jr.; Stratmann, R. E.; Burant, J. C.; Dapprich, S.; Millam, J. M.; Daniels, A. D.; Kudin, K. N.; Strain, M. C.; Farkas, O.; Tomasi, J.; Barone, V.; Cossi, M.; Cammi, R.; Mennucci, B.; Pomelli, C.; Adamo, C.; Clifford, S.; Ochterski, J.; Petersson, G. A.; Ayala, P. Y.; Cui, Q.; Morokuma, K.; Malick, D. K.; Rabuck, A. D.; Raghavachari, K.; Foresman, J. B.; Cioslowski, J.; Ortiz, J. V.; Stefanov, B. B.; Liu, G.; Liashenko, A.; Piskorz, P.; Komaromi, I.; Gomperts, R.; Martin, R. L.; Fox, D. J.; Keith, T.; Al-Laham, M. A.; Peng, C. Y.; Nanayakkara, A.; Gonzalez, C.; Challacombe, M.; Gill, P. M. W.; Johnson, B. G.; Chen, W.; Wong, M. W.; Andres, J. L.; Head-Gordon, M.; Replogle, E. S.; Pople, J. A. *Gaussian 98*, revision A.1x; Gaussian, Inc.: Pittsburgh, PA, 2001.
(78) Weinhold, F. *NBO 5.0*; University of Wisconsin: Madison, WI, 2001.
(79) Schaftenaar, G. *Molden*, version 3.9 (http://www.cmbi.kun.nl/~schaft/molden/molden.html).
(80) Flükiger, P. F. http://www.cscs.ch/molekel/.
(81) Portmann, S.; Lüthi, H. P. *Chimia* 2000, *54*, 766.
(82) Parr, R. G.; Pearson, R. G. *J. Am. Chem. Soc.* 1983, *105*, 7512.
(83) Kothekar, V.; Pullman, A.; Demoulin, D. *Int. J. Quantum Chem.* 1979, *14*, 779.
(84) Gresh, N. *J. Comput. Chem.* 1995, *16*, 856.
(85) Gresh, N.; Stevens, W. J.; Krauss, M. *J. Comput. Chem.* 1995, *16*, 843.
(86) Piquemal, J. P.; Gresh, N.; Giessner-Prettre, C. *J. Phys. Chem. A* 2003, *107*, 10353.
(87) Taylor, M.; Muntean, F.; Lineberger, W.; McCoy, A. *J. Chem. Phys.* 2004, *121*, 5688.
(88) Lee, S. U.; Han, Y. K. *J. Mol. Struct.* 2004, *672*, 231.
(89) Satta, M.; Di Palma, T. M.; Paladini, A.; Giardini Guidoni, A. *Appl. Surf. Sci.* 2002, *168*, 215.
(90) Webelements. http://www.webelements.com/webelements/elements/text/Cu/thdyn.html.
(91) Parr, R. G.; Yang, W. *Density Functional Theory of Atoms and Molecules*; Oxford University Press: Oxford, U.K., 1989.
(92) Zimmermann, T.; Zeizinger, M.; Burda, J. V. *J. Inorg. Biochem.* 2005, *99*, 2184.

Theoretical Study of Redox Active Centers of Blue Copper Proteins: A Computational DFT Study.

Matěj Pavelka[1] and Jaroslav V. Burda[1]

[1]*Department of Chemical Physics and Optics, Faculty of Mathematics and Physics, Charles University, Ke Karlovu 3, 121 16 Prague 2, Czech Republic*

Abstract

Active sites of blue copper proteins in both reduced and oxidized states were studied at the DFT level. Two families of these redox sites were examined: the Type A centers with Methionine ligand as 4th residue and the Type B with Glutamine residue. Constrained and full optimizations were performed on PDB structures in vacuo and in solvent (COSMO) simulating peptide and water environment. They revealed that redox sites do not possess their optimal geometries regardless the oxidation state. Axial Cu-ligand bond elongates/shortens in fully optimized Cu(I)/Cu(II) complexes. The reduced centers have a tendency to lower-coordination, while four "equivalent" bonds are preferred in oxidized centers. It corresponds to our earlier results for small inorganic complexes. The Type A centers exhibit smaller relaxation energies with full optimization. The least pronounced relaxation was obtained in protein-like environment. In constrained structures, larger ionization potential was predicted for Type A centers regardless the influence of environment. For fully optimized complexes, the influence of surrounding on redox properties is clearly visible (while *IP*(type B) > *IP*(type A) was obtained in vacuo and in water). The calculated relative difference of redox potentials between Type A and Type B proteins is in agreement with experiment. Distributions of charge and spin density (obtained by NPA) were analyzed as well as calculated EPR spectra.

1. Introduction

Nearly half of entries in protein data bank (PDB) contain metal cofactor. Such statistics demonstrate, how important metal ions are for catalytic processes in a living cell. Hence, investigation of metal sites such as copper redox centers is essential for determination of molecular mechanisms in biochemistry. Cu ions often exhibit interesting spectral properties, which originate from the unusual geometric and electronic structures that are imposed through their interactions with peptide environment. Such proteins provide many functions: electron transfer, oxidation-reduction processes, oxygen transport and insertion, and so forth. They can be organized according to the type of their active centers (*see **Figure 1***):

a) Type 1 Cu proteins also called blue copper proteins. These simple Cu proteins have a an intense absorption band near 600 nm in the oxidized Cu(II) state. This transition is assigned with the S(cysteine)-Cu charge transfer (LMCT). Structures of the active sites usually contain a four-coordinated Cu ion, though a coordination number of five was found in azurins. Structural motif consists of the arrangement Cu(I)/Cu(II):$(His)_2CysX$, where X is Met or Gln. Examples of this motif can be found in pseudoazurin, rusticyanin, plastocyanin, mavicyanin, auracyanin, stellacyanin, umecyanin,

and amicyanin. Interestingly, reduction of the Cu(II) ion to Cu(I) in type 1 proteins causes minimal structural changes. It results in low activation barrier for Cu(I)→Cu(II) redox process and thus rapid electron-transfer rate.

b) Type 2 Cu proteins. They have an less-intense absorption band at 350-420 nm. In this group of proteins, the copper ion is usually found in a square planar or tetragonal coordination. After binding of substrate, catalytic oxidation is facilitated by vacant coordination sites around the central metal ion. Type 2 Cu proteins include superoxide dismutase (which catalyzes dismutation of superoxide radical to O_2^- and H_2O_2), galactose oxidase (reduces O_2 to $H2O_2$, thus oxidizing galactose to aldehyde), and amine oxidase (which oxidatively deaminates primary amines to aldehydes).

c) Type 3 Cu proteins. This family is characterized by an antiferromagnetically coupled pair of Cu ions and a strong absorption band near 330 nm. Examples can be found in the hemocyanin, which is involved in oxygen transport, and tyrosinase, which is a monooxygenase that hydroxylates monophenols and oxidizes diphenols to quinones.

d) Proteins with Cu_A site. This coupled dinuclear copper site can be found in Cytochrome C oxidase, and N_2O reductase.

e) Proteins with Cu_B site. In these peptides, there is bridging ligand between Cu_B and Fe of Heam. For example, Cytochrome C oxidase, and ubiquinone oxidase can be mentioned.

f) Multi-copper oxidases. They combine several types of Cu sites, which can be found in Ascorbate oxidase, Ceruloplasmin, and Laccase.

There is a large number of works investigating biological activity of the copper proteins using both experimental and theoretical approaches. By means of UV-VIS and EPR spectroscopy, Cu-center of Azurin was studied.[1] Spectroscopic tools in combination with DFT calculations were used to investigate the role of amino acid in axial position to the copper complex and its influence on a reduction potential.[2] Published experimental works include fluorescence spectroscopy,[3] electron paramagnetic resonance (EPR) and electron-nucluear double resonance (ENDOR) techniques,[4] X-ray absorption near-edge structure (XANES) spectra,[5] and EPR and UV-VIS spectra.[6] The basic

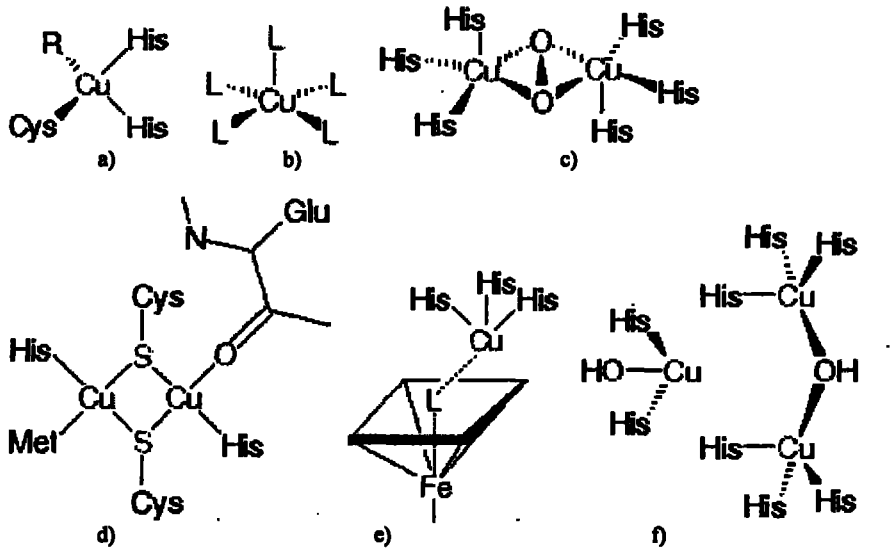

Figure 1: Comparison of a) type 1, b) type 2, c) type 3, d) Cu_A, e) Cu_B, and f) multi-copper sites in copper proteins. {ProMiS, 1998 #3044}

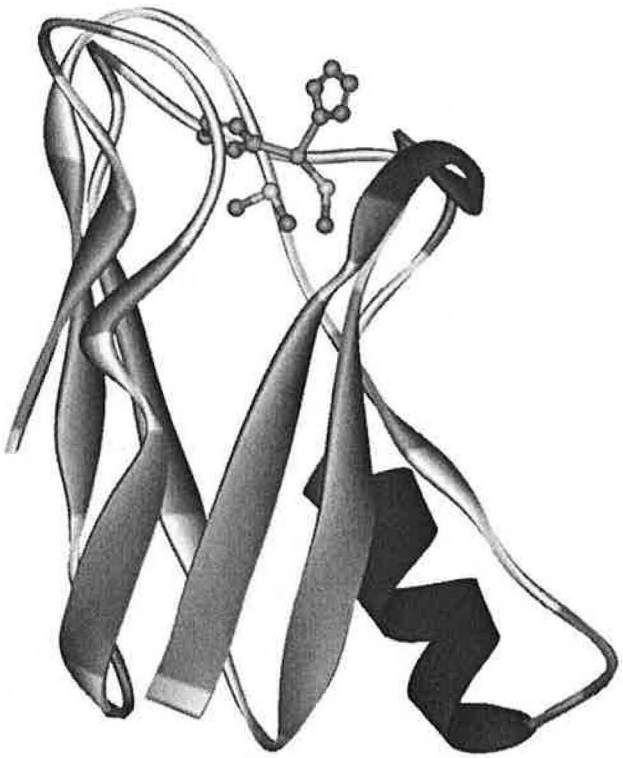

Figure 2: PDB structure of plastocyanin (1KDI).

aspects of a copper coordination in peptide environment are summarized in reviews.[7-10] The first theoretical spectra of plastocyanin were computed by Solomon group.[11,12] However, recent studies of plastocyanin exist too.[13-19] Charge transfer (CT) dynamics were carried out by pump-probe[20] and resonance Raman spectroscopy.[21] Other experimental studies should be also mentioned.[22-24] The redox processes were studied on Tyrosinase.[25] A lot of computational effort was devoted to the examination of copper proteins.[26-34] Theoretical studies of the copper interactions with amino acids have been reported too.[35-46]

DNA/RNA helix rollout often proceed in presence of metals or their hydrates. Hence, some effort was also spent on examination of copper interaction with nucleo bases. Experimental studies include crystal structures,[47] IR spectroscopy,[48] thermodynamical measurements, and so forth.[49-51] Some effort have been put into theoretical studies as well.[52-58] Suggested order in copper-N(base) bonding strength is: guanine > adenine > uracil. Such bonds have influence on Watson-Crick base pairing. Interaction of hydrated Cu(I)/Cu(II) with guanine was studied in our works.[58,59]

A great attention was paid to examination of "small inorganic complexes" in order to determine coordination geometries and electronic properties of various copper compounds. Considering such models can give deeper insight and easier interpretation of Cu(I)/Cu(II) behavior. The interactions of the both Cu cations with molecules like water, ammonia, or hydrogen-sulphide were intensively studied using various computational approaches. [60-83]

This study is focused on models of active mononuclear centers, which are present in blue copper proteins (***Figure 2***). Although this work utilizes experiences obtained from our previous studies, where small models were exlored,[61,65,83] it is based on extensive quantum chemical investigation of these unusual redox centers. Insight into interactions of these Cu(I)/Cu(II) complexes is more detailed than in other papers and reviews.

2. Computational Details

Active sites of blue copper proteins (***Scheme 1***) were studied at the DFT level of theory. In the family of Type A of the blue proteins (with Met residue), the following protein structures from PDB database[84] were considered: amicyanin (1AAC), auracyanin (1QHQ), plastocyanin (1KDI and 1KDJ), and rustycyanin (1A3Z and 1RCY). In the case of Type B centers (with Gln residue), the following peptides were analyzed: mavicyanin (1WS8), stellacyanin (1JER), and umecyanin

(1X9R and 1X9U). These X-ray crystal structures were obtained with resolution in range from 1.33 to 1.90 Å. Azurins were omitted, since they contain the second axial ligand resulting in 5-coordinated copper center. This study concerns only on 4-coordinated redox centers, where the Cu(I)/Cu(II) cation (***Scheme 1***) is coordinated with: cysteine, two histidines, and methionine (A) or glutamine (B).

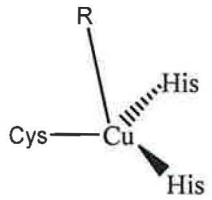

Scheme 1: The 4-coordinated Cu(I)/Cu(II) redox center of blue copper proteins. Residue R can be methionine or glutamine.

In present work, histidine residues were substituted by imidazol, cysteine by methyl-thiolate $[S(CH_3)]^{1-}$, thioether group of methionine by dimethyl-sulphide $S(CH_3)_2$, and carbonyl group of glutamine by acetyl-amine $OC(CH_3)(NH_2)$. These models are illustrated in ***Figure 3***.

Structure optimizations were performed at several levels. In the first step (label as "Opt. phase I"), PDB structures are used as starting geometries. The Cu-ligand distances as well as orientation of ligands were kept frozen according to ***Scheme 2a***. This way, orientations of amino acids stay undisturbed.

During the second optimization step (label as "Opt. phase II"), copper cations could move freely (***Scheme 2b***) in the fixed framework of frozen ligands (from Opt. phase I). In the last step, the full optimization of the whole complex was allowed.

Quantum chemical calculations were performed at the Density Functional Theory (DFT) level using the B3PW91 functional. For the H, C, O, N atoms, the *6-31+G(d)* basis set was applied. The copper and sulphur core electrons were described by Christiansen averaged relativistic effective pseudopotentials (AREP)[85] and Stuttgart effective-core pseudopotentials (ECP), respectively. A consistent basis set was adopted for the valence electrons. Double-ζ pseudoorbitals of Cu were augmented by diffuse and polarization functions (α_s = 0.025, α_p = 0.35, α_d = 0.07, and α_f = 3.75). Similarly, pseudoorbitals of the sulphur atom were extended by analogous functions with exponents: α_s = 0.077, α_p = 0.015, and α_d = 0.50.

Reduced centers with the Cu^+ cation were represented by a closed shell singlet electronic ground state, while oxidized Cu(II) complexes ($3d^9$ electron configuration) possess doublet ground states. Hence, some attention was devoted to correct initial guess for the SCF procedure and an appropriate testing of wave function.

a) *b)*

Scheme 2: Illustration of optimization ***a)*** phase I and ***b)*** phase II.

All optimizations were preformed in vacuo as well as with inclusion of solvation effects. The Conductor-like screening model (COSMO) was used to simulate two environments: water (with permittivity equal to 78) and protein-like environment (ε = 4).

After obtaining optimized structures from all three

optimization phases, further analyses were performed at the higher computational level. More accurate description was used for the H, C, N, and O atoms: extended by *6-311++G(2df,2pd)* basis set. Here the same Stuttgart ECP pseudopotentials were used for both Cu and S atoms. The basis sets on the copper/sulphur atoms were consistently enlarged by *spd/sp* diffuse functions and *2fg/2df* polarization functions (α_f= 1.00, 0.26, α_g= 0.66/ α_d= 0.92, 0.29, α_f = 0.57). Moreover, slower but probably more accurate B3LYP functional were used.

Energy analysis consists of evaluation of stabilization ΔE^{Stab} and bond ΔE^{BE} energies. In these calculations, Basis Set Superposition Error (BSSE) corrections and corrections on the deformation energies[86] were considered according to the equation

(1) $$\Delta E^{Stab} = -(E_{complex} - \sum E_{monomer} - \sum E^{deform})$$

where $E_{complex}$ represents the total energy of the whole complex and $E_{monomer}$ represents the energy of a given subsystem computed with basis functions on the ghost atoms from the complementary part of the system. In case of BSSE calculations within COSMO model, it is not clear how to estimate the $E_{monomer}$ energies. In the present work, it is proposed that solvation cavity is only around monomer (***Scheme 3***) despite the basis functions on ghost atoms are located outside the cavity. Although in this way, it is necessary to correct dispersion and repulsion interaction with continuum in $E_{monomer}$ estimation, it is possible to include deformation correction.

In addition, total coordination energies (ΔE^{TCE}) were also computed, when all interacting ligand molecules are treated as one subsystem and the central Cu ion as another one. They can be understood as the binding energies of the cation with a pre-formed ligand shell. In our previous work,[61,65,83] these ΔE^{TCE} energies were labeled as ΔE^{Stex}. The difference between ΔE^{Stab} and ΔE^{TCE} estimates the energy, which must be invested for formation of the ligand shell arrangement in the absence of the ion. However, the real interligand repulsion is larger in the presence of the cation due to the polarization effects.[87]

The ΔE^{BE} energies of the examined Cu-L ligand

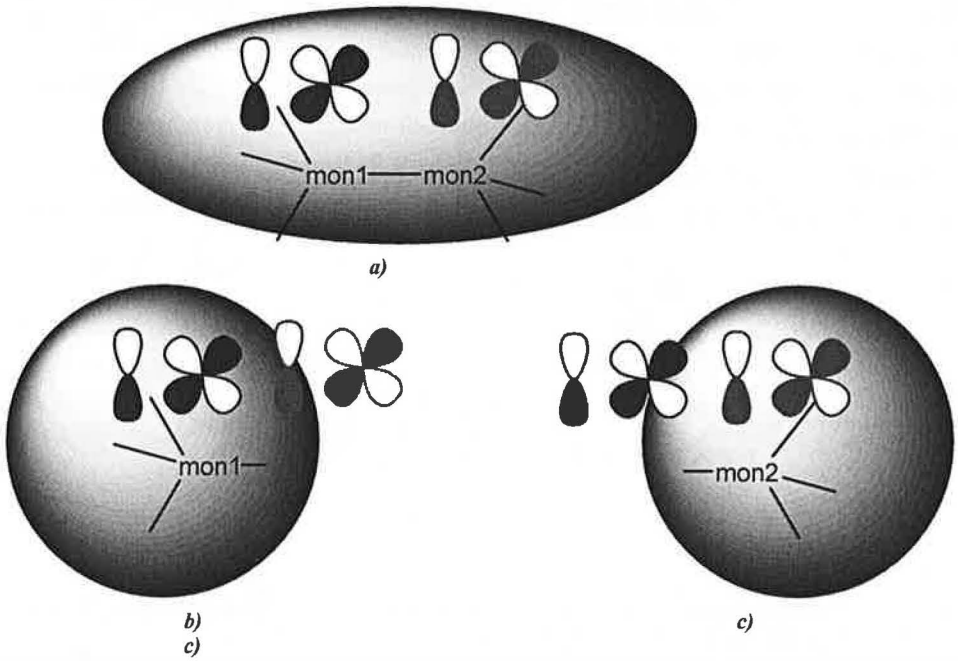

Scheme 4: Construction of boundary between the continuum and the solute within BSSE scheme. In equation **(1)**, ***a)*** represents $E_{complex}$ while ***b)*** and ***c)*** illustrate estimations of $E_{monomer}$ energies.

bonds were obtained using the same (BSSE) scheme but without the deformation corrections. However, these values are still contaminated by same portion of electrostatic (dipole-dipole) interactions between ligand L and remaining Cu ligands.

In order to describe redox activity of studied complexes, vertical and adiabatic ionization potentials (IP) were calculated for the reduced Cu(I) centers according to formula:

$$IP = E_{Cu(II)} - E_{Cu(I)}. \quad (2)$$

In the case of vertical IP the $E_{Cu(II)}$ term represents the energy of a (2+) charged system calculated in the Cu(I) optimized structure. For adiabatic IP the $E_{Cu(II)}$ energy was computed based on the Cu(II) optimized structure.

Charge and spin distributions were analyzed in terms of partial atomic charges and spin densities obtained by Natural Population Analyses (NPA).[88] Spin isodensities (ρ_s = 0.01) were plotted together with selected Molecular Orbitals (MO).

Main axes of diagonalized g-tensor were estimated in order to investigate EPR spectrum and consequently the behavior of unpaired electron for all studied Cu(II) complexes.

All quantum chemical calculations were performed using program package *Gaussian 03*.[91] Program NBO v. 5.0 from Wisconsin University[92] was used for evaluation of the Natural Bond Orbital (NBO) characteristics. For visualization of geometries, spin densities, and molecular orbitals, graphical programs Molden 4.4[93] and Molekel 4.3[94,95] were used.

3. Results and Discussion

3.1 Structures

Structures of both oxidized and reduced centers of the A and B Types (see ***Figure 3***) of blue copper proteins were optimized in three sequential steps with selected redundant coordinates frozen in order to enlighten the role of protein constraints.

3.1.1 Protein structures

The averaged coordination distances for oxidized Cu(II) centers are compiled in ***Table 1*** for the centers of Types A and B. Bond lengths obtained from Opt. phase I corresponds to PDB distances from X-ray structures.

In average, Cu(II)-S(cysteine) bonds are about 2.2 Å long. For a comparison, Cu-X (S, O, N) distances (in Å) for $[Cu(H_2S)_m(H_2O)_n(NH_3)_k]^{2+/+}$ cations from our previous study[83] are presented in ***Table 3*** together with values obtained from CSD database by Katz et al.[38] Significantly larger Cu^{2+}-S distances (about 2.4 Å) were found in the 4-coordinated complexes with H_2S ligands. In the models of blue copper proteins, shorter Cu-S(Cys) bond is explained by stronger enhancement of the dative bond by electrostatic interaction between

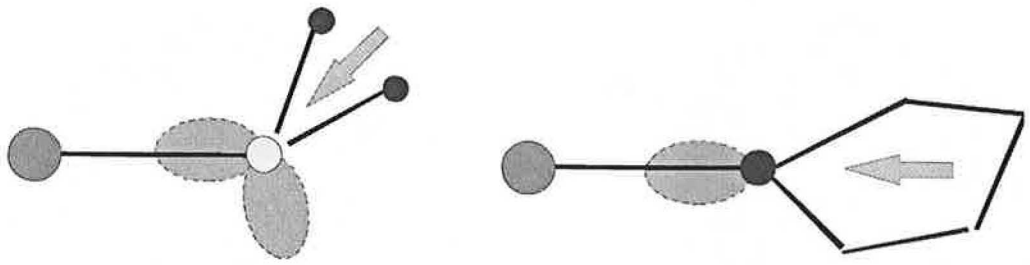

a) *b)*

Scheme 4: Metal-ligand arrangements for ***a)*** methionine and ***b)*** histidine molecules. Dashed ellipses represent lone pairs of ligands, while arrows stand for dipole orientations.

Table 1: Coordination distances for oxidized Cu(II) Type A and B centers of blue copper proteins (in Å). Bond lengths for structures after optimization phase I, phase II, and full optimization are presented. The optimizations were performed in vacuo, protein-like, and water environment. **Bold** indicates PDB distances, which are equivalent to those of optimization phase I.

		Oxidized Type A center			Oxidized Type B center		
		in vacuo	protein-like	water	in vacuo	protein-like	water
Cu-S(Cys)	Opt. phase I.	**2.197**			**2.210**		
	Opt. phase II.	2.160	2.172	2.179	2.176	2.192	2.204
	Full opt.	2.169	2.169	2.177	2.252	2.262	2.270
Cu-N(His)	Opt. phase I.	**1.966**			**1.971**		
	Opt. phase II.	2.015	2.007	2.005	2.018	2.009	1.995
	Full opt.	2.036	2.008	2.006	2.042	2.039	2.022
Cu-N(His)	Opt. phase I.	**2.042**			**2.041**		
	Opt. phase II.	2.044	2.021	2.015	2.026	2.015	2.017
	Full opt.	2.037	2.014	2.008	2.059	2.027	2.032
Cu-S(Met)/ Cu-O(Gln)	Opt. phase I.	**2.858**			**2.153**		
	Opt. phase II.	2.850	2.880	2.871	2.179	2.173	2.156
	Full opt.	2.734	2.843	2.798	2.043	2.039	2.034

Cu^{2+} cation and present Cys model (thiolate $[S(CH_3)]^{1-}$). Its dipole moment is about 10.6 D, while for Met model (thioether group $S(CH_3)_2$), substantially weak dipole (μ = 1.6 D) was obtained. This fact correlates with long Cu-S(Met) bond (2.86 Å). The glutamine exhibits shorter coordination distances 2.15 Å. It is affected by less diffuse oxygen atom (in comparison with sulphur) and by larger dipole moment (μ = 4.0 D) of acetyl-amine group. Corresponding bond lengths of Cu(II) aqua complexes from our previous study[83] were estimated to be about 2.01 Å long. The difference is probably caused by forced geometry of protein centers, which disfavored axial position.

Orientation of the ligand is a result of the dative interaction between metal and lone pairs of ligand molecules. According to ***Scheme 4***, histidine (as well as imidazol) has advantageous dipole orientation. Two Cu-N(His) distances are about 1.97 and 2.04 Å long, respectively. It is in agreement with our previous finding for ammine complexes (***Table 3***).

The PDB coordination distances display an influence by protein backbone structure and the orientation of these bonds are affected as well. X-ray crystal structures of blue copper proteins usually have S(Cys) and two N(His) atoms arranged in slightly distorted trigonal plane with

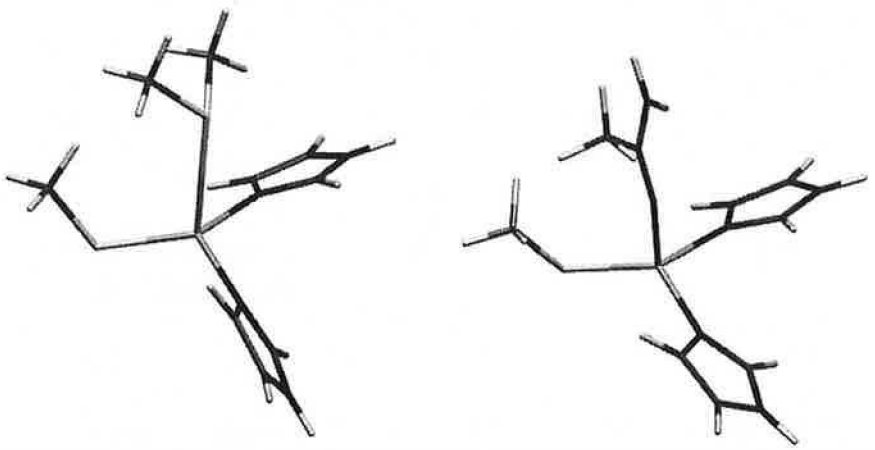

Figure 3: models of ***a)*** Type A and ***b)*** Type B centers of blue copper proteins. Family of Type A centers includes following peptides: amicyanin, auracyanin, plastocyanin, and rustycyanin. In case of Type B centers, following proteins were considered: mavicyanin, stellacyanin, and umecyanin.

Table 2: Coordination distances for reduced Cu(I) Type A and B centers of blue copper proteins (in Å). Bond lengths for structures after optimization phase I, phase II, and full optimization are presented. The optimizations were performed in vacuo, protein-like, and water environment. **Bold** indicates PDB distances, which are equivalent to those of optimization phase I.

		Reduced Type A center			Reduced Type B center		
		in vacuo	protein-like	water	in vacuo	protein-like	water
Cu-S(Cys)	Opt. phase I	**2.190**			**2.198**		
	Opt. phase II	2.193	2.217	2.228	2.176	2.184	2.205
	Full opt.	2.190	2.211	2.218	2.199	2.155	2.226
Cu-N(His)	Opt. phase I	**1.974**			**2.018**		
	Opt. phase II	2.030	2.033	2.022	2.025	2.008	2.012
	Full opt.	1.995	2.063	2.027	2.031	1.987	2.030
Cu-N(His)	Opt. phase I	**2.123**			**2.085**		
	Opt. phase II	2.134	2.070	2.071	2.093	2.044	2.056
	Full opt.	2.225	2.066	2.106	2.131	1.986	2.082
Cu-S(Met)/ Cu-O(Gln)	Opt. phase I	**3.168**			**2.645**		
	Opt. phase II	3.067	3.133	3.193	2.651	2.640	2.689
	Full opt.	4.430	4.662	4.974	3.728	3.675	3.845

central metal atom placed about 0.5 Å above this plane. The 4th residue is located in axial position, which can be modified by oxidation state of redox center.

In order to describe structure effects of reduction on studied copper centers, copper(I)-ligand bond lengths are presented in ***Table 2***. The Cu^{+}-S(Cys) distances go only over slight changes in comparison with oxidized centers. Nevertheless, pronounced elongation of coordination bond with remaining 4th residue occurs for both methione (3.17 Å) and glutamine (2.65 Å). An asymmetrical arrangement of the two Cu-N(His) distances is noticeable too.

The redox centers of blue copper proteins exhibit small changes in copper-ligand distances, when oxidation state is altered, and qualitatively the same geometry is conserved. This can be considered as a consequence of protein "matrix". For previously studied[83] 4-coordinated inorganic copper complexes, transition between Cu(II) and Cu(I) states is connected with pronounced structural changes from square-planar to tetrahedral ligand arrangements. When such systems are allowed to be even more relaxed, they transform to 2-coordinated structures illustrated in ***Figure 4***. This fact is important especially for electron transferring peptides. Small structural changes of active centers within the reduction process minimize the reorganization energy λ, and thus enable rapid electron transfer.

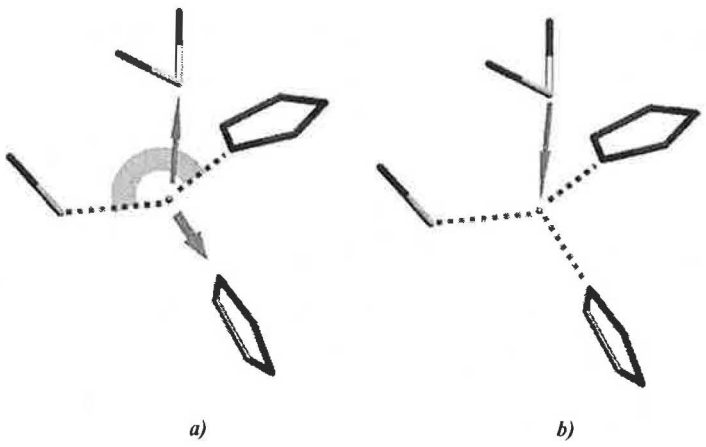

Scheme 5: illustration of the results of full optimizations of Type A centers in vacuo for ***a)*** reduced Cu(I) and ***b)*** oxidized Cu(II) centers.

3.1.2 Fully optimized structures in vacuo

When the models of reduced centers are fully optimized in

vacuo, interesting changes happen (see ***Figures 5a*** and ***5b***). The Cu atom, which lies above S, N, N-plane in non-optimized Cu(I) structures, moved so that it is situated within this plane. In Type B center, two additional H-bonds are created between carbonyl group and histidines (d(O..H(His)) = 2.16 and 2.41 Å). Weak hydrogen bond d(S(Met)..H(His)) = 2.96 Å is created in Type A center too.

would have a tendency to form 2-coordinated structures (cf. similar trend in bond energies bellow). This finding is in accord with our previous work, where Cu(I)/Cu(II) cations in hydrogen sulphide-aqua-ammine ligand fields were investigated. I was shown that small Cu(I) complexes with O- and N-ligands favor 2-coordinated structures,[65] while complexes with S-ligands prefer 4-coordination.[83]

Table 3: Average Cu-X (S, O, N) bond lengths (in Å) for small $[Cu(H_2S)_m(H_2O)_n(NH_3)_k]^{2+/+}$ models{Pavelka, 2006 #3037} and corresponding values obtained from CSD database by Katz et al.{Katz, 2003 #1361}

Cu(I)	Small models			CSD		
	2-coord.	3-coord.	4-coord.	2-coord.	3-coord.	4-coord.
Cu-N	1.91	2.02	2.12	1.90	1.98	2.04
Cu-O	1.88	2.04	2.21	1.84	2.14	2.05
Cu-S	2.19	2.29	2.35	2.17	2.26	2.33
Cu(II)	Small models			CSD		
	4-coord.	5-coord.	6-coord.	4-coord.	5-coord.	6-coord.
Cu-N	2.03	2.09	2.28	1.98	2.03	2.34
Cu-O	2.01	2.06	2.13	1.93	2.07	2.36
Cu-S	2.40	2.49	2.41	2.28	2.43	2.72

The fully optimized models of oxidized Cu(II) centers in vacuo revealed opposite trend. The difference between two Cu^{2+}-N(His) distances diminishes, especially for Type A centers. Both thioether Cu-S and carbonyl Cu-O bonds shorten by approximately 0.1 Å (see ***Scheme 5***). Therefore, formation of oxidized centers with 4-coordination geometry is favored

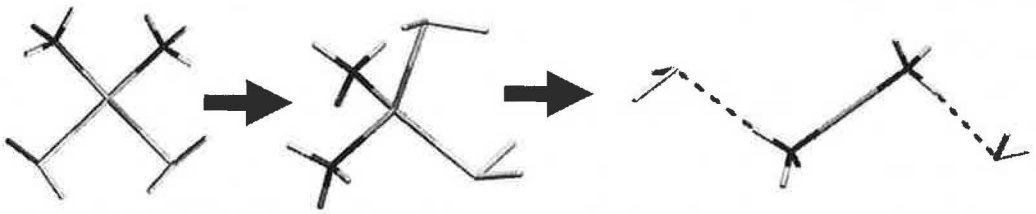

Figure 4: Example of 4-coordinated $[Cu(H_2S)_2(NH_3)_2]^{2+}$ complex, where transition from Cu(II) to Cu(I) state goes along with pronounced structural change from square-planar to tetrahedral ligand arrangement. When the system is even more relaxed, it evolves to 2-coordinated structure.

Coordination distances of fully optimized Cu(I) complexes are presented in ***Table 2***. While thiolate Cu-S(Cys) bond remains practically untouched, thioether Cu-S(Met) and carbonyl Cu-O(Gln) bonds elongate to 4.4 and 3.7 Å, respectively. The difference between Cu-N(His1) and Cu-N(His2) distances becomes more pronounced. Moreover in the case of Type A center, an angle between Cu-S(Cys) and the shorter Cu-N(His) bonds opens from 131° (in average) to 151°. These features (illustrated in ***Scheme 5a***) lead to an assumption that reduced centers without protein constraints

(same finding adopted for bond energies below). The 4-coordination is also preferred for the inorganic $[Cu(H_2S)_m(H_2O)_n(NH_3)_k]^{2+}$ complexes.[83] The full optimization had no effect on Cu-S(Cys) distances in case of Type A centers. However in Type B, the Cu-S(Cys) bonds partially elongate. Such a behavior can be the result of the competition of the ligand donation between carbonyl group and thiolate ligand. The donation effects were found negligible in case of the longer Cu-S(Met) bonds.

In Type B center, the full optimization interestingly leads to different coordination arrangement (***Figure***

5d). The relaxed complex possesses geometry halfway between square planar and tetrahedral, which has some impact on electronic structure as demonstrated later.

Many other works were devoted to investigation of protein constraints on active centers in blue copper proteins. Earlier paper[96] suggested that there are no constraints. However, such proposals had to be revised.[15,28,29] The role of axial ligand has also been widely studied.[2,16-19,28,97] The section above provides answers to some of the questions about constraints imposed by peptide backbone structure:

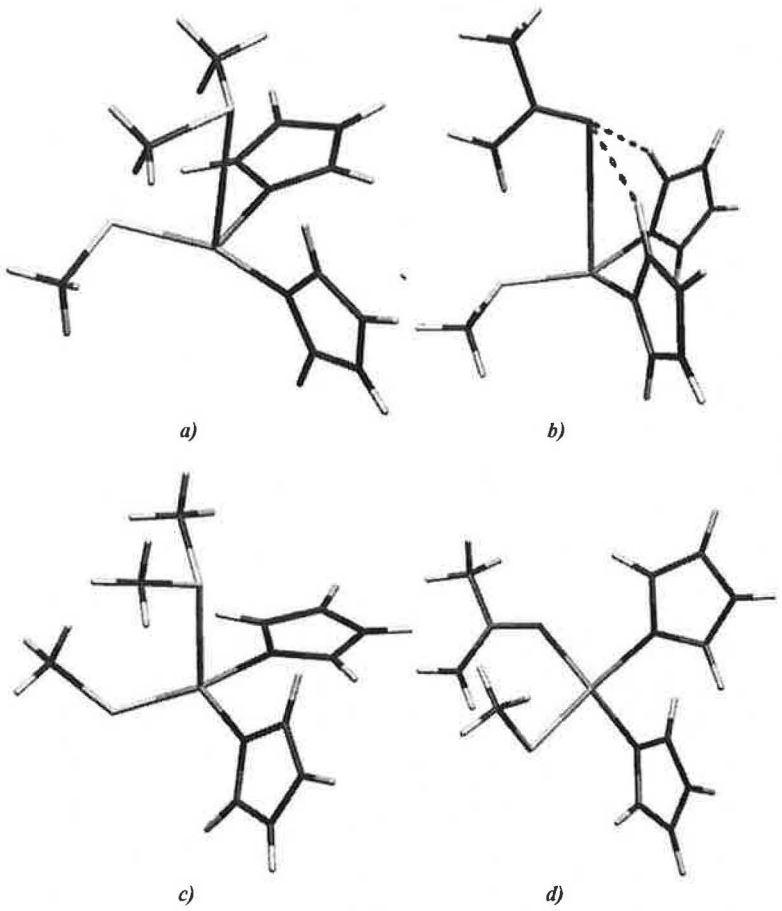

Figure 5: structures of reduced ***a)*** Type A and ***b)*** Type B centers after full optimization in vacuo. Optimized structure of oxidized centers of ***c)*** Type A and ***d)*** Type B are presented too.

a) Neither oxidized nor reduced centers have optimal geometries. The extent of these forces can be estimated from stabilization energies (cf. in section 3.3.1).

b) When no constraints are applied, axial copper-ligand bond elongates/shortens in dependence of reduced/oxidized state of metal, regardless the type of 4th residue (Gln or Met).

c) Changes in coordination in reduced centers correspond to the fact that the Cu(I) complexes prefer geometry with lower-coordination. Analogously, models of fully relaxed oxidized Cu(II) centers tend to four "equivalent" bonds as can be seen from unification of Cu-N(His) bonds.

3.1.3 Relaxed models in solvents

The studied redox centers are influenced by polarizability of its surrounding. Such effects were examined at the QM/MM level.[13,27,98] Polarized continuum models were also used for this kind of complexes in ref.[13] Unlike QM/MM, inclusion of solvation effects at COSMO level can not reproduce differences between individual proteins of Type A or B family. However it still introduces effects such as screening of electrostatic interaction, which can be important for description of the energetics of strong Cu^{2+}-Cys bonds.

In case of oxidized Cu(II) centers, solvation effects has only marginal influence on fully optimized geometries. Partially screened electrostatic interaction of thiolate Cu-S(Cys) bond results in the mild elongation. Since donation effect is very distance-sensitive, cysteine donation weakens correspondingly. Thus, shortening of Cu^{2+}-N(His) bonds occurs. Interestingly the distance of Cu-O(Gln) shortens slightly, while Cu-S(Met) bond in Type A elongates. Such a behavior is caused by more effective dative competition between Gln and Cys ligands. Hence, weaker Cu-S(Cys) bond causes slightly stronger and shorter Cu-O(Gln) bond.

For solvated reduced centers, Cu^{+}-S(Cys) distances elongated as well. When Cu(I) complexes are optimized within the COSMO model with dielectric constant simulating peptide environment ($\varepsilon = 4$), Cu-N(His) distances become nearly equal. Bond length between copper and the 4th residue increases. The S(Cys)-Cu-N(His) angles remain practically unchanged comparing the crystal structures. Hence, the 3-coordination is preferred for fully optimized structures in protein-like environment in contrast to vacuo structures, where the 2-coordination was favored. The Cu(I) complexes optimized in water return to the 2-coordination preference at least partially.

3.2 Electron structure

Electron structures of redox centers of blue copper proteins were investigated in terms of charge and spin density distributions, EPR and UV-VIS spectra, and molecular orbital (MO) analyses. These calculations were performed at the B3LYP/*6-311++G(2df,2pd)* level.

3.2.1 EPR spectrum of oxidized centers

More effort was spent on examination of the oxidized (than reduced) state of blue copper proteins. Spectra of electron paramagnetic resonance (EPR) represent important tool in Cu(II) complexes, since the method is based on the magnetic properties of the unpaired electron. The key tensor property called g-factor describes how a local magnetic field is induced by the external magnetic field. It approaches the value of 2.0023 for single free electron. Similar values should be obtained for systems with delocalized unpaired electron. Otherwise, it can markedly rise. Main axes of the diagonalized g-tensor were computed for all studied Cu(II) complexes (***Table 4***). Experimental values are listed as well. In case of protein imposed structures, $g_{\parallel}$ and $g_{\perp}$ values in vacuo were estimated to be about 2.12 and 2.05 a.u., respectively. This anisotropic splitting of g-factor is typical for blue copper proteins and can be compared with experimental values: 2.23 and 2.05 for Type A centers. Involving of environment effects in COSMO models slightly improves calculated $g_{\parallel}$ values. However, in order to obtain better agreement with experiment, hybrid functional needs to be modified by fitting the ratio of DFT exchange-correlation and Hartree-Fock exchange terms as discussed e.g. in rewiev.[9] On the other hand, B3LYP successfully produced larger $g_{\parallel}$ values for Type B centers, even in vacuo. Fully optimized Type A complex exhibits similar behavior as protein structures from database. In case of the Type B center, full optimization reveales different trend, where $g_{\parallel}$ is very similar to

Table 4: EPR g-factors for all studied Cu(II) centers (in a.u.). Experimental values are presented too.

		Exp.	in vacuo		protein-like		water	
			Opt. I	Full opt.	Opt. I	Full opt.	Opt. I	Full opt.
Type A	$g_{\parallel}$	2.226	2.115	2.131	2.131	2.137	2.138	2.143
	$g_{\perp}$	2.045	2.052	2.056	2.058	2.061	2.061	2.065
Type B	$g_{\parallel}$	2.297	2.123	2.085	2.140	2.090	2.147	2.120
	$g_{\perp}$	2.051	2.058	2.079	2.066	2.082	2.070	2.073

Table 6: Partial atomic charges (in electron units) on selected atoms S(Cys), N(His), S(Met), and O(Gln) for isolated models of amino acids. Presented values were obtained by Natural Population Analysis (NPA).

	isolated models		
	in vacuo	protein-like	water
S(Cys)	-0.738	-0.805	-0.830
N(His)	-0.504	-0.562	-0.585
S(Met)	0.227	0.189	0.174
O(Gln)	-0.641	-0.720	-0.751

$g_{\perp}$ = 2.08. Such a behavior can be explained by distinct geometry of fully optimized Type B center with more competitive Gln ligand, which affects distribution of unpaired electron. It is illustrated by plots of spin densities in ***Figure 6***. For solvated complexes, the distinction in $g_{\parallel}$ and $g_{\perp}$ increases, when dielectric constant is rising as a reaction on increased Cu-O(Gln) distance (cf. ***Table 2***).

3.2.2 Charge and spin density distribution

The electron spindensity in terms of partial atomic spin densities (ρ_i obtained by NPA method) are summarized in ***Table 5***. Since there is a strong dative interaction between Cu^{2+} and cysteine model $[S(CH_3)]^{1-}$, most of the spin density (80 - 90 %) is located on Cu-S(Cys) bond. Type B centers exhibit larger portion of spin density ρ_i on Cu and smaller ρ_i on the sulphur atom of cysteine model in comparison with Type A centers. Such behavior reflects the stronger ability of Gln (than Met) residue to donate electron density, which results in higher competition with other dative bonds. It is in coherence with longer/weaker Cu^{2+}-S(Cys) distances in oxidized Type B centers. Partial atomic charges δ obtained by NPA are compiled in ***Tables 7*** and ***8*** for copper and coordinated atoms. For both Cu(I) and Cu(II) complexes, atomic charges reflect coordination distances, since donation effect is strongly distance sensitive. To investigate nature of individual bonds, it is necessary to compare these values (from complexes) with charges obtained from isolated ligands (see ***Table 6***). The N(His) atom exhibit δ = -0.51 e in isolated imidazol optimized in vacuo, while in studied complexes δ(N) ranges from -0.63 (-0.58) to -0.66 (-0.65) e for oxidized (reduced) centers. Similar situation occurs in case of Gln ligand, where the oxygen partial charge is also lower in comparison with isolated Glutamine. Moreover in fully optimized Cu(I) complex, δ(O) is also affected by hydrogen bonds from both Histidine ligands. In case of Cysteine (δ(S) = -0.74 e for isolated $[S(CH_3)]^{1-}$ in vacuo), the donation extent influences the sulphur atomic charge. Inversely, the extent of dative interaction can be estimated from changes of atomic charge. Partial charge is reduced up to -0.57 e in protein structure of Cu(I) centers. In case of Cu(II) complexes, the effect is even more pronounced resulting in -0.13 e only. It can be recognized as transfer of almost the whole electron from Cys to Cu(II). For thioether residue (Met), positive δ(S) values were found on S atom. In case of reduced centers, sulphur partial charges do not change comparing the isolated

Table 5: Spin density (in electron units) on copper, cysteine model, and the rest of complex obtained by NPA method for oxidized Cu(II) Type A and B centers.

			Spin density		
			Cu	S(Cys)	N,N,S/O
Type A center	in vacuo	Opt. phase I.	0.34	0.56	0.09
		Full opt.	0.36	0.55	0.09
	protein-like	Opt. phase I.	0.40	0.48	0.12
		Full opt.	0.41	0.54	0.05
	water	Opt. phase I.	0.43	0.44	0.13
		Full opt.	0.44	0.44	0.12
Type B center	in vacuo	Opt. phase I.	0.39	0.51	0.10
		Full opt.	0.53	0.30	0.17
	protein-like	Opt. phase I.	0.47	0.41	0.13
		Full opt.	0.56	0.25	0.19
	water	Opt. phase I.	0.50	0.36	0.14
		Full opt.	0.57	0.23	0.19

molecule, since Cu-S(Met) distances are very long. The only exception is fully optimized complex in vacuo, where lower value of δ(S) is caused by hydrogen bonding with H(His). In Cu(II) complexes, partial charges in vacuo are lowered by about 0.04 e in comparison with isolated $S(CH_3)_2$ molecule. Results for thioether ligand can be also compared with our previous study,[83] where $[Cu(H_2S)_n]^{2+/+}$ complexes (n = 1 – 4) with neutral hydrogen sulphide displayed δ(S) = -0.1 and -0.2 e for Cu(II) and Cu(I) systems, respectively. These more negative values (in contrary to Met) are product of shorter coordination distances in these inorganic complexes.

Partial charge on Cu atom was estimated to be about 0.96 and 0.69 e for oxidized and reduced Type A centers in vacuo, respectively. For Cu(II) / Cu(I) Type B centers, slightly higher values δ = 1.04 e / 0.74 e were obtained. The difference can be explained by weaker Cu-Cys donation in Type B complexes, which represents main contribution to the partial charge reduction of the copper cations. When solvation effects are considered, Cu partial charge raises with decreasing dative interaction with ligands. It is a result of screened electrostatic interactions leading to longer coordination distances that affect donation ability of the ligands.

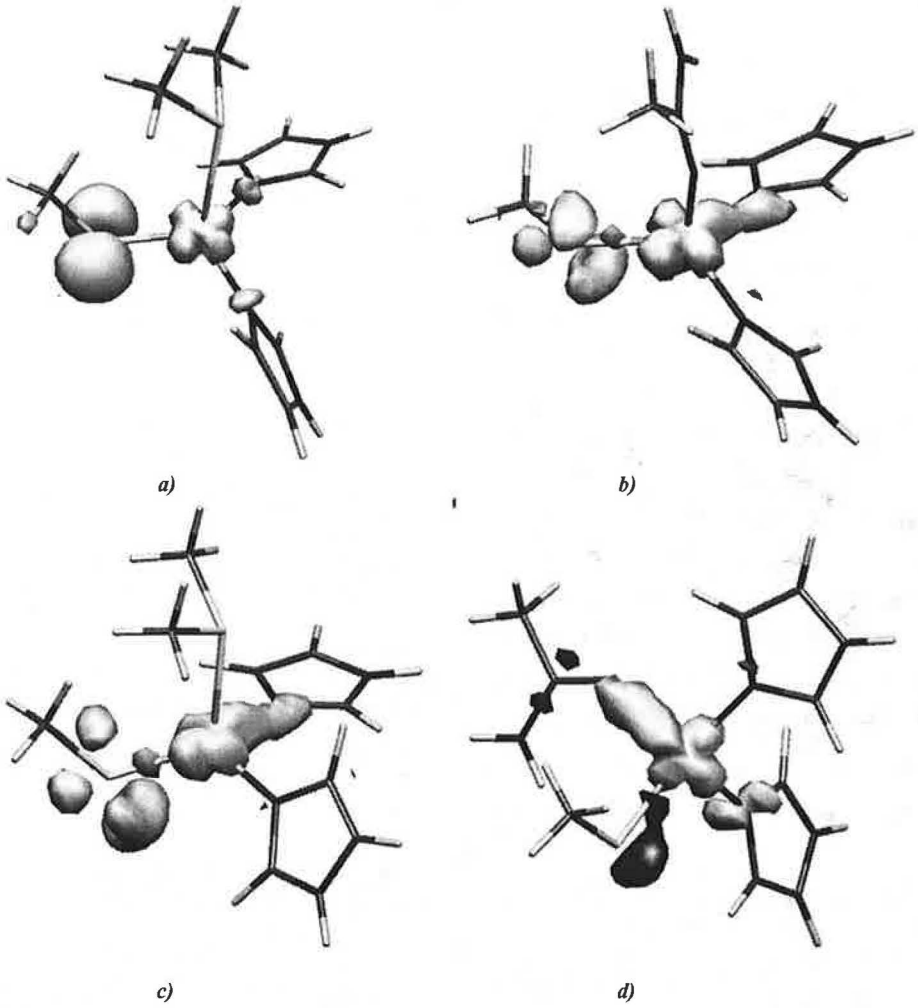

Figure 6: Plots of spin isodensities (ρ_s = 0.01) for selected Cu(II) complexes. Oxidized ***a)*** Type A (plastocyanin) and ***b)*** Type B (umecyanin) centers with imposed geometry (opt. phase I) and ***c)*** Type A and ***d)*** Type B centers after full optimization are considered.

Table 7: Partial atomic charges (in electron units) on copper and coordinated atoms S(Cys), N(His), S(Met), and O(Gln) obtained by NPA method. They are presented for oxidized Cu(II) Type A and B centers of blue copper proteins.

		Oxidized Type A center			Oxidized Type B center		
		in vacuo	protein-like	water	in vacuo	protein-like	water
Cu	Opt. phase I.	0.961	1.016	1.043	1.042	1.110	1.140
	Opt. phase II.	0.957	1.012	1.038	1.032	1.102	1.136
	Full opt.	0.964	1.015	1.038	1.166	1.197	1.208
S(Cys)	Opt. phase I.	-0.130	-0.225	-0.272	-0.174	-0.292	-0.346
	Opt. phase II.	-0.129	-0.221	-0.267	-0.167	-0.283	-0.340
	Full opt.	-0.149	-0.169	-0.272	-0.350	-0.424	-0.457
N(His)	Opt. phase I.	-0.634	-0.650	-0.655	-0.625	-0.651	-0.656
	Opt. phase II.	-0.629	-0.652	-0.657	-0.626	-0.643	-0.648
	Full opt.	-0.636	-0.646	-0.655	-0.645	-0.639	-0.658
N(His)	Opt. phase I.	-0.652	-0.657	-0.661	-0.644	-0.643	-0.649
	Opt. phase II.	-0.647	-0.651	-0.656	-0.637	-0.645	-0.651
	Full opt.	-0.636	-0.651	-0.651	-0.628	-0.655	-0.643
S(Met)/	Opt. phase I.	0.190	0.184	0.183	-0.738	-0.755	-0.770
O(Gln)	Opt. phase II.	0.191	0.184	0.182	-0.736	-0.753	-0.768
	Full opt.	0.193	0.218	0.184	-0.762	-0.770	-0.775

3.2.2 Molecular orbitals analysis

Interesting observations can be done in ***Figures 8***, where three types of single occupied molecular orbitals (SOMO) present in studied Cu(II) complexes are illustrated. The first type (***8a***) represents typical SOMO for Type A center, which has been presented in many works. The $3p_x$ orbital of S(Cys) is coplanar with $3d(x^2-y^2)$ of copper. The second type (***8b***) contains S(Cys) $3p_z$ orbital with perpendicular orientation to Cu $3d(x^2-y^2)$ plane. Fully optimized Type A centers and protein structures of Type B centers possess this type of SOMO. In the third type (***8c***), SOMO is dominantly composed of deformed copper $3d(x^2-y^2)$ orbital aimed to all four Cu-ligand bonds.

Table 8: Partial atomic charges (in electron units) on copper and coordinated atoms S(Cys), N(His), S(Met), and O(Gln) obtained by NPA method. They are presented for reduced Cu(I) Type A and B centers of blue copper proteins.

		Reduced Type A center			Reduced Type B center		
		in vacuo	protein-like	water	in vacuo	protein-like	water
Cu	Opt. phase I.	0.697	0.712	0.715	0.737	0.750	0.752
	Opt. phase II.	0.690	0.714	0.715	0.725	0.745	0.752
	Full opt.	0.648	0.687	0.686	0.675	0.697	0.698
S(Cys)	Opt. phase I.	-0.573	-0.647	-0.678	-0.570	-0.652	-0.684
	Opt. phase II.	-0.572	-0.651	-0.682	-0.565	-0.649	-0.682
	Full opt.	-0.561	-0.633	-0.659	-0.546	-0.636	-0.654
N(His)	Opt. phase I.	-0.594	-0.613	-0.626	-0.590	-0.623	-0.635
	Opt. phase II.	-0.584	-0.618	-0.632	-0.584	-0.621	-0.634
	Full opt.	-0.598	-0.622	-0.628	-0.586	-0.621	-0.635
N(His)	Opt. phase I.	-0.604	-0.630	-0.643	-0.603	-0.616	-0.631
	Opt. phase II.	-0.603	-0.621	-0.635	-0.604	-0.616	-0.631
	Full opt.	-0.582	-0.622	-0.637	-0.603	-0.623	-0.651
S(Met)/	Opt. phase I.	0.223	0.205	0.197	-0.676	-0.708	-0.735
O(Gln)	Opt. phase II.	0.222	0.204	0.195	-0.675	-0.709	-0.735
	Full opt.	0.194	0.185	0.184	-0.718	-0.727	-0.742

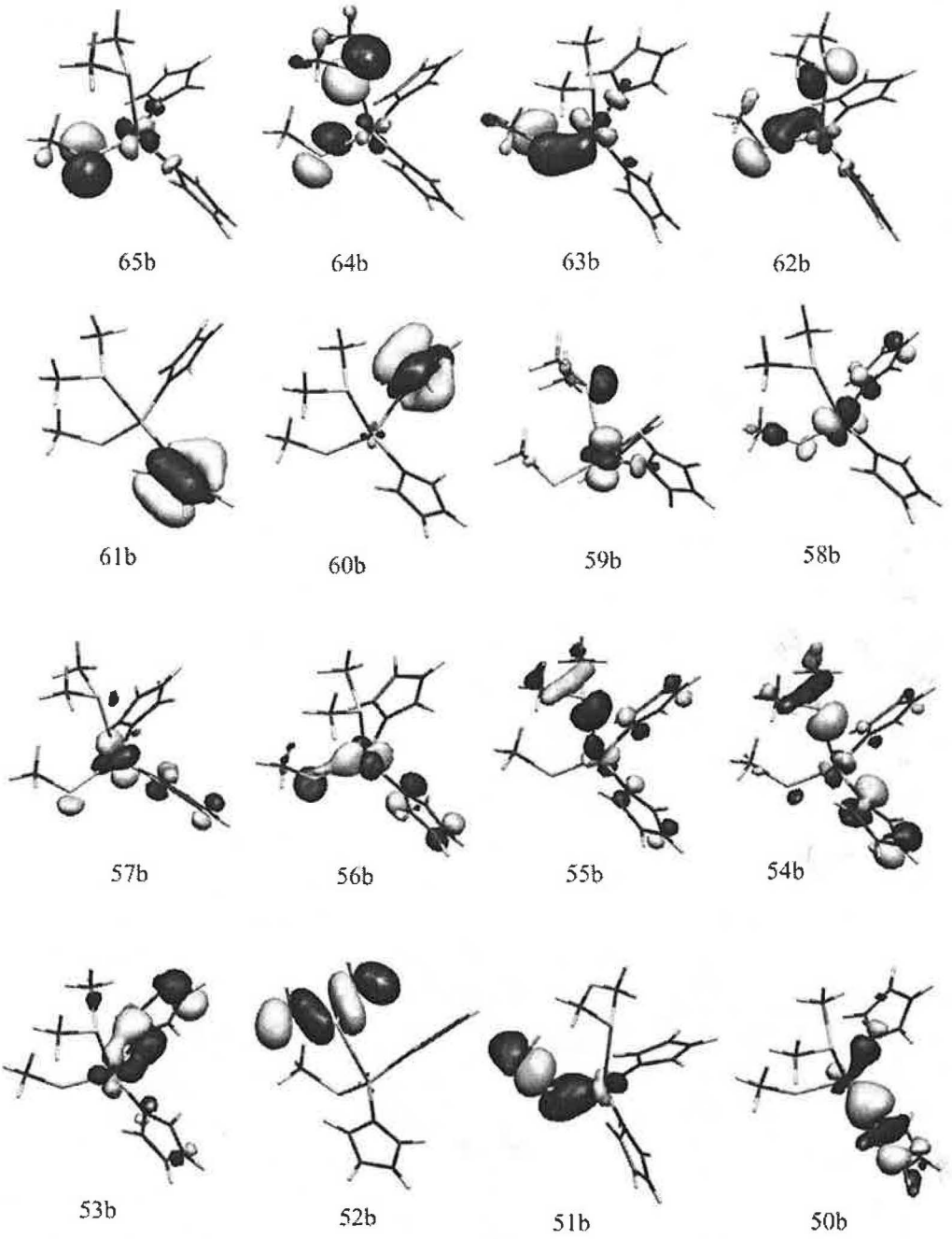

Figure 7: Pictures of selected molecular orbitals (MO) for oxidized plastocyanin center (Type A) optimized through opt. phase I. The 65th MO represents LUMO within beta orbitals. Corresponding MO from alpha set (not necessary 65th) is single occupied molecular orbital (SOMO).

3.3 Thermodynamics

Energy analyses were performed at the B3LYP/*6-311++G(2df,2pd)* level. In such analyses, the Cu(I)/Cu(II) optimized structures were considered with and without polarized continuum model (PCM).

3.3.1 Stabilization energies

Stabilization ΔE^{Stab} and total coordination ΔE^{TCE} energies are presented in ***Table 9*** and ***10*** for oxidized and reduced centers, respectively. In case of gas-phase calculations on oxidized Cu(II) complexes, the stabilization energies of Type B

Table 9: ΔE^{stab} stabilization and ΔE^{stex} sterically corrected stabilization energies (in kcal/mol) for oxidized Cu(II) Type A and B centers of blue copper proteins. Energies are presented for structures obtained by all optimization schemes with and without environment effects.

		Oxidized Type A center			Oxidized Type B center		
		in vacuo	protein-like	water	in vacuo	protein-like	water
ΔE^{stab}	Opt. phase I.	593.1	332.5	258.6	598.7	334.1	259.6
	Opt. phase II.	594.1	333.5	259.4	599.7	334.7	259.6
	Full opt.	597.4	335.7	295.1	609.0	342.8	307.5
ΔE^{stex}	Opt. phase I.	618.5			632.8		
	Opt. phase II.	619.6			633.9		
	Full opt.	620.6			638.7		

centers are about 5.5 kcal/mol higher than ΔE^{Stab} energies of Type A centers. For reduced Cu(I) centers, Type B centers are still preferred but only by about 0.8 kcal/mol. When comparing fully optimized structures, this difference raises to about 12 kcal/mol for both Types.

The difference between optimization phase I and II concerns the copper-ligand distances, which can be considered as the effect of protein matrices in the frozen ligand arrangement. The energy difference

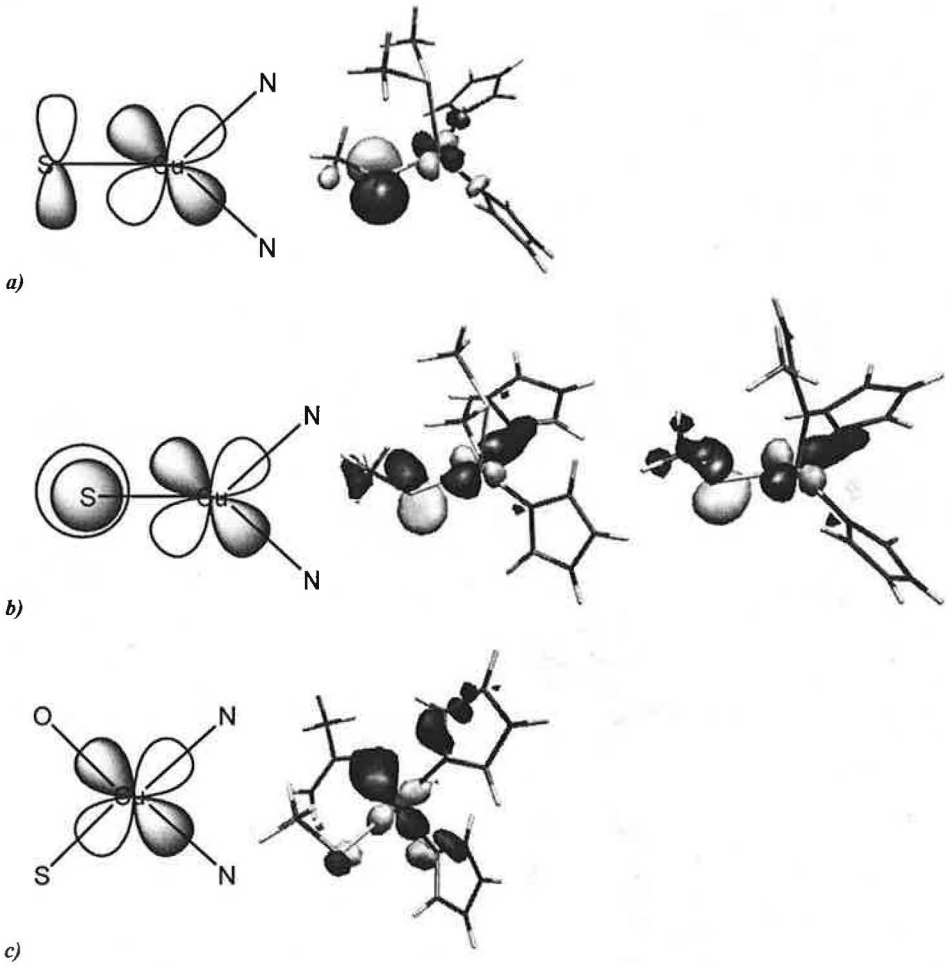

Figure 8: Three different schemes of SOMO with examples. The ***a)*** scheme occurs in Type A centers (opt. phase I), ***b)*** scheme is in Type A (full opt.) and Type B (opt. phase I) complexes, and ***c)*** can be found in fully optimized Type B center.

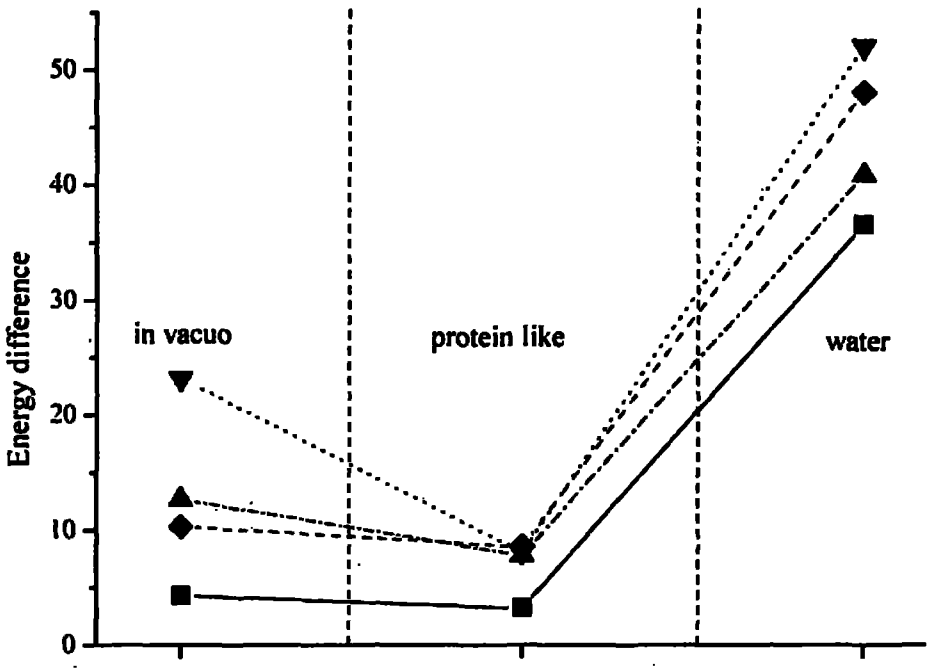

Figure 9: The relaxation energies (in kcal/mol), which were estimated as relative differences of ΔE^{Stab} energies of constrained (opt. phase I) and fully optimized structures for:

—■— oxidized Type A centers,
--♦-- oxidized Type B centers,
-.-▲-.- reduced Type A centers, and
...▼... reduced Type B centers.

[ΔE^{Stab}(Opt. phase II) - ΔE^{Stab}(Opt. phase I)] represents a constraint in coordination distances and was estimated in range from 0.4 to 1.0 kcal/mol. ΔE^{Stab}(Opt. phase II) should mimic the energy relations in optimized metal complexes under the sterical influence of neighboring protein environment. The difference [ΔE^{Stab}(Full opt.) - ΔE^{Stab}(Opt. phase II)] includes complete relaxation of ligands, when no constraints are applied. This relaxation is up to 22.8 kcal/mol in case of Cu(I) Type B center. In case of ΔE^{TCE} energies, differences between various optimization steps revealed minor changes for Type A centers. It means that even after full optimization, where orientations of coordination bonds are altered, only slight changes in coordination energy occurs. In contrary, full optimization of Type B center is connected with considerable change of ΔE^{TCE} energies.

Inclusion of environment effects affects

Table 10: ΔE^{stab} stabilization and ΔE^{ster} sterically corrected stabilization energies (in kcal/mol) for reduced Cu(I) Type A and B centers of blue copper proteins. Energies are presented for structures obtained by all optimization schemes with and without environment effects.

		Reduced Type A center			Reduced Type B center		
		in vacuo	protein-like	water	in vacuo	protein-like	water
ΔE^{stab}	Opt. phase I.	230.6	125.6	97.4	231.4	123.9	95.4
	Opt. phase II.	231.3	126.2	97.9	231.8	124.1	95.4
	Full opt.	243.4	133.4	138.2	254.6	132.1	147.4
ΔE^{ster}	Opt. phase I.	255.2			259.3		
	Opt. phase II.	255.5			259.5		
	Full opt.	255.6			273.6		

Table 12: ΔE^{BE} bond energies (in kcal/mol) for reduced Cu(I) Type A and B centers in vacuo.

		Type A	Type B
Cu-S(Cys)	Opt. phase I.	109.2	106.8
	Opt. phase II.	109.3	108.3
	Full opt.	130.6	131.7
Cu-N(His)	Opt. phase I.	8.2	5.7
	Opt. phase II.	8.8	7.0
	Full opt.	22.5	20.6
Cu-N(His)	Opt. phase I.	3.7	3.2
	Opt. phase II.	3.1	2.4
	Full opt.	5.9	10.0
Cu-S(Met)/	Opt. phase I.	-2.2	-1.5
Cu-O(Gln)	Opt. phase II.	-1.1	-1.7
	Full opt.	3.7	15.8

stabilization energy due to screening of electrostatic interaction between Cu(I)/Cu(II) cation and ligands. Especially remarkable influence can be seen in the negatively charged model of cysteine. Therefore, obtained ΔE^{Stab} values are pronouncedly lower in comparison with in vacuo calculations. The higher the dielectric constant is, the lower the stabilization energies are. The interesting behavior was found for total 'protein' constraints, which can be estimated by differences of ΔE^{Stab} energies of phase I and fully optimized structures. These values are drawn in ***Figure 9***. From this Figure, several trends can be observed: a) In both Types of centers, reduced Cu(I) complexes are less stable under protein constraints than the oxidized centers. b) Type B centers exhibit larger energy relaxation after full optimization. c) The relaxation energies are most pronounced in water environment, where ΔE^{Stab} energies are increased (about 40 and 50 kcal/mol for Type A and Type B centers, respectively). The least effects can be seen in peptide-like environment (with $\varepsilon = 4$).

3.3.2 Gas-phase Ligand bonding energies

Bonding energies ΔE^{BE} of all the ligands in studied redox centers are compiled in ***Tables 11*** and ***12***. Partitioning of the system on ligand and remaining part of complex provides useful insight into the strength of individual dative bonds. The Cu-Cys coordination clearly dominates in all investigated complexes with ΔE^{BE} energies in vacuo around 240 and 120 kcal/mol for oxidized and reduced centers, respectively. Such high bonding energies are products of dative coordination strengthened by electrostatic interaction between $Cu^{2+/+}$ and cystein model $[S(CH_3)]^{1-}$. For Cu(II) complexes, ΔE^{BE} of copper-imidazol(His) bonds are by an order of magnitude lower ranging from 28 kcal/mol (in opt. phase I) to 42 kcal/mol (in full opt.). The weakest bonding energies are visible for thioether Cu-Met bonds, less than 10 kcal/mol. Coordination of the acetyl group in Cu-O(Gln) model was estimated to be about 11 kcal/mol, when structure is constrained by protein, and about 20 kcal/mol for fully optimized complex. This coordination energy for 4th residue reflects the shortening of these bonds described in the discussion of the geometry parameters above. It

Table 13: Vertical and adiabatic ionization potentials (in eV) representing the transition from reduced to oxidized state. Values are presented for both Type A and B complexes obtained in vacuo as well as in protein-like and water environment.

		Vertical ionization			Adiabatic ionization		
		in vacuo	protein-like	water	in vacuo	protein-like	water
Opt. phase I	Type A	5.03	4.29	4.15	4.97	4.23	4.08
	Type B	4.85	4.13	4.00	4.73	4.04	3.93
Opt. phase II	Type A	5.08	4.33	4.19	4.96	4.22	4.08
	Type B	4.87	4.13	4.00	4.70	4.03	3.92
Full opt.	Type A	5.92	5.08	4.92	5.30	4.41	4.24
	Type B	6.03	4.23	5.06	5.36	3.83	4.13

Table 14: Redox potentials (in mV) for selected blue copper proteins. {Solomon, 1992 #3039}

	protein	redox potential
Type A	amicyanin	261
	auracyanin	240
	plastocyanin	370
	rustycyanin	680
	averaged	388
Type B	mavicyanin	285
	stellacyanin	184
	umecyanin	283
	averaged	251

also partially confirms the tendency for 4-coordination when no protein constraints are applied.

In case of reduced centers, coordination bonds in protein imposed structures are noticeably weaker than in Cu(II) case mainly due to the reduction of electrostatic contributions. The ΔE^{BE} energies of Cu-Met/Gln bonds exhibit, in our model, even negative values. This can be explained by the fact that ΔE^{BE} energies also contain an inter-ligand repulsion, which for these ligands is larger than a weak copper(I)-ligand interaction. For fully optimized complexes without peptide constraints, no negative bonding energies were obtained. It is caused by minimization of the repulsive ligand-

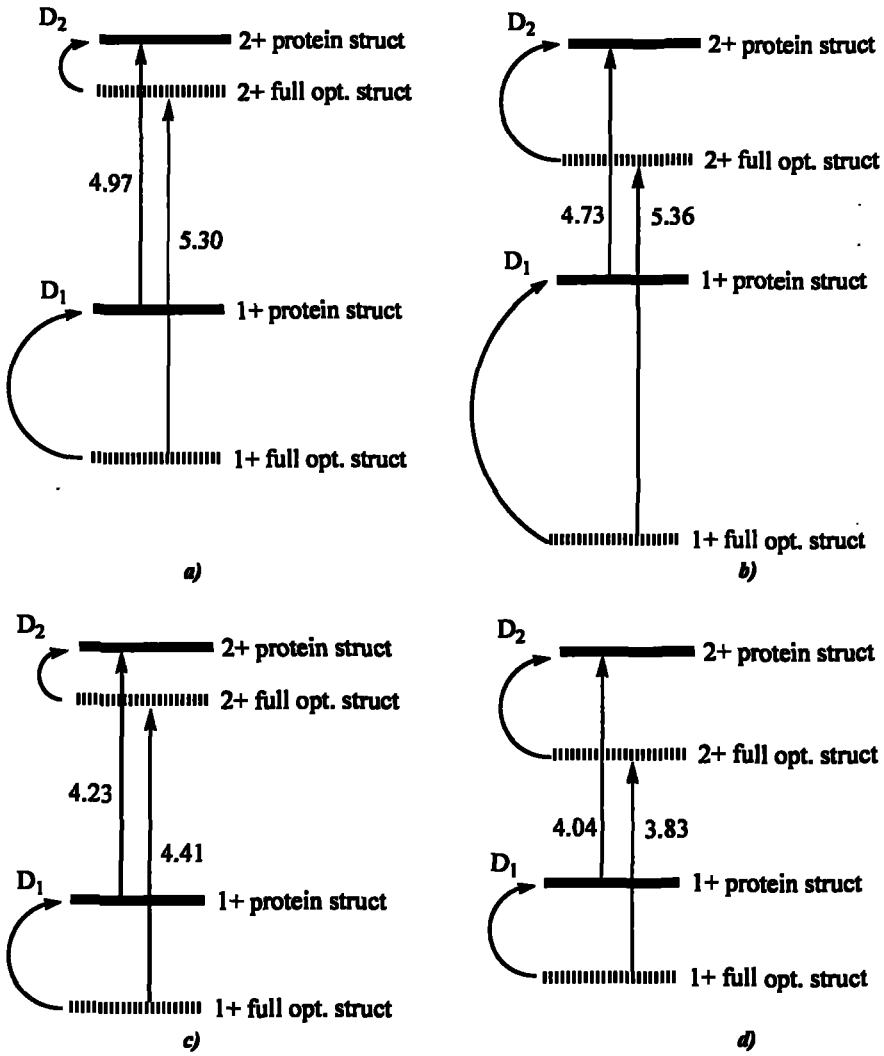

Figure 10: The studied redox processes for *a)* Type A and *b)* Type B centers in vacuo. Scheme is also illustrated for centers *c)* and *d)* optimized in protein like environment. Solid and dashed lines stand for energies of protein structures (opt. phase I) and fully optimized structures, respectively. Red and blue arrows represent adiabatic ionization potentials.

ligand interactions. In geometry discussion, it was proposed that reduced Type A centers tend to form 2-coordinated structures. A partial support can be seen in differencing of the ΔE^{BE} values for Cu-His1 and Cu-His2 bonds. Such an argument is not convincing for Type B Cu(I) centers in accord with larger stability of the 3-coordinated $[Cu(H_2S)(H_2O)_2(NH_3)_2]$ complexes.

3.3.3 Ionization potentials

In order to describe transition between Cu(II) and Cu(I) oxidation states, vertical IP^{vert} and adiabatic IP^{adiab} ionization potentials were calculated according to equation (2). The obtained values are listed in ***Table 13***. In vacuo, Type B centers optimized through phases I and II exhibit lower ***IP*** than Type A centers. When environment is considered, the difference ***IP(type A) - IP(type B)*** decreases by ca 0.16 eV with increasing dielectric constant from 0 (vacuum) to 78 (water) for vertical transition. IP^{adiab} energies are naturally lower than IP^{vert}, since oxidized structures are relaxed but the behavior is similar for both.

In fully optimized structures, several interesting trends can be noticed: vertical ***IPs*** obtained in vacuo and in water are greater for Type B than for Type A centers. This altered order in comparison with complexes having protein imposed structure means that surrounding of studied centers plays important role in their redox properties too. Interestingly, the ***IP(type A) > IP(type B)*** relation is conserved for fully optimized centers in models of peptide-like environment. The studied redox processes are illustrated in ***Figures 10***, where red and blue arrows represent Cu(I)→Cu(II) transition for protein structures (opt. phase I) and fully optimized structures, respectively. Figures also contain D_1 and D_2 parameters, which correspond to relative differences of stabilization energies: [ΔE^{Stab}(Full opt.) - ΔE^{Stab}(Opt. phase I)] (the extend of protein constraints) for reduced and oxidized centers, respectively. This scheme is presented for Type A and B centers optimized in vacuo and in protein-like environment. It reflects natural ability of studied proteins to modify redox center properties by protein constraints and solvation effects.

Experimentally obtained redox potentials E_θ for studied proteins are presented in ***Table 14***. Although our calculations are not able to reveal E_θ values for individual proteins, it is possible to compare relative differences between Type A and Type B proteins. The difference 0.14 eV obtained from experiment is in good agreement with the difference IP^{adiab}*(type A)* - IP^{adiab}*(type B)* from present work, 0.20 eV.

4 Conclusions

Models of mononuclear centers of blue copper proteins were investigated in the present study. Two families of such proteins were examined: the Type A centers with Met side chain as the fourth residue and the Type B centers with Gln residue.

Selected structures were optimized at B3PW91/*6-31+G(d)* level. Starting geometries of these complexes were taken from PDB database (active centers from seven proteins: amicyanin, auracyanin, plastocyanin, rustycyanin, mavicyanin, stellacyanin, and umecyanin). Both reduced and oxidized states were investigated in vacuo as well as in solvent (modeled by COSMO) simulating water and protein-like environment. Partial optimizations reflecting protein structures were followed by full optimizations. Final changes revealed that neither oxidized nor reduced protein structures of the copper center belong to optimal geometries. In comparison with PDB structures, axial copper-ligand bond elongates/shortens in dependence of reduced/oxidized state of metal, regardless the protein Type (A or B). In reduced centers, relaxation of coordination bonds correspond to fact that Cu(I) complexes prefer geometry with lower-coordination. Analogously, models of fully relaxed oxidized Cu(II) centers tend to four "equivalent" bonds.

Detailed insight into interactions of these Cu(I)/Cu(II) complexes is provided by energy analyses performed at the more accurate B3LYP/*6-31++G(2df,2pd)* level. Estimated stabilization and bonding energies showed several trends. Under protein constraints, reduced Cu(I) complexes are less stable than oxidized complexes comparing with the energy of optimal structures for the both Types of centers. Larger relaxation energy is released within the full optimization for Type B centers.

For Cu(II) complexes, the calculated EPR spectra were also examined. Charge and spin distributions were obtained by NPA method. They revealed that most of the spin density (80-90%) is located on Cu-S(Cys) bond, which corresponds to strong dative interaction between copper cation and Cysteine. Type B centers exhibit larger portion of spin density on Cu and larger copper partial charge in comparison with Type A centers. Such behavior reflects stronger ability of Gln ligand to donate electron density in comparison with Met ligand. Interesting behavior was found for fully optimized Type B center, for which distinct EPR spectrum and character of SOMO orbital were found. This feature can be explained by the different near-tetrahedral geometry of this complex.

Ionization potentials were computed in order to describe transition between Cu(II) and Cu(I) oxidation states. For constrained structures, IP(type A) > IP(type B) trend was obtained in all three types of environment. Interestingly, the order is altered for fully optimized complexes in vacuo and in water. It reflects the ability of the neighborhood to influence the redox properties of studied proteins. Comparing relative difference between Type A and Type B proteins, the redox potential difference ΔE_θ = 0.20 eV was obtained, which is in very good accord with experimentally known data of about 0.14 eV.

References

(1) Wang, X.; Berry, S. M.; Xia, Y.; Lu, Y. *J. Am. Chem. Soc.* **1999**, *121*, 7449.
(2) Palmer, A. E.; Randall, D. W.; Xu, F.; Solomon, E. I. *J Am. Chem. Soc.* **1999**, *121*, 7138.
(3) Santra, S.; Zhang, P.; Tan, W. *J. Phys. Chem. A* **2000**, *104*, 12021.
(4) Manikandan, P.; Epel, B.; Goldfarb, D. *Inorg. Chem.* **2001**, *40*, 781.
(5) Shimizu, K.; Maeshima, H.; Yoshida, H.; Hattori, T. *Phys. Chem. Chem. Phys.* **2001**, *3*, 862.
(6) Sigman, J. A.; Kwok, B. C.; Gengenbach, A.; Lu, Y. *J Am. Chem. Soc.* **1999**, *121*, 8949.
(7) Gray, H. B.; Malmstroem, B. G.; Williams, R. J. P. *J. Biol. Inorg. Chem.* **2000**, *5*, 551.
(8) Solomon, E. I.; Baldwin, M. J.; Lowery, M. D. *Chem. Rev.* **1992**, *92*, 521.
(9) Solomon, E. I.; Szilagyi, R. K.; George, S. D.; Basumallick, L. *Chem. Rev.* **2004**, *104*, 419.
(10) Mirica, L. M.; Ottenwaelder, X.; Stack, T. D. P. *Chem. Rev.* **2004**, *104*, 1013.
(11) Penfield, K. W.; Gewirth, A. A.; Solomon, E. I. *J. Am. Chem. Soc.* **1985**, *107*, 4519.
(12) Gewirth, A. A.; Solomon, E. I. *J. Am. Chem. Soc.* **1988**, *110*, 3811.
(13) Sinnecker, S.; Neese, F. *Journal of Computational Chemistry* **2006**, *27*, 1463.
(14) LaCroix, L. B.; Shadle, S. E.; Wang, Y. N.; al, e. *J. Am. Chem. Soc.* **1996**, *118*, 7755.
(15) Pierloot, K.; De Kerpel, J. O. A.; Ryde, U.; Roos, B. O. *J. Am. Chem. Soc.* **1997**, *119*, 218.
(16) Randall, D. W.; Gamelin, D. R.; LaCroix, L. B.; Solomon, E. I. *J. Biol. Inorg. Chem.* **2000**, *5*, 15.
(17) LaCroix, L. B.; Randall, D. W.; Nersissian, A. M.; al, e. *J. Am. Chem. Soc.* **1998**, *120*.
(18) Randall, D. W.; George, S. D.; Holland, P. L.; Hedman, B.; Hodgson, K. O.; Tolman, W. B.; Solomon, E. I. *J. Am. Chem. Soc.* **2000**, *122*, 11632.
(19) Guckert, J. A.; Lowery, M. D.; Solomon, E. I. *J. Am. Chem. Soc.* **1995**, *117*, 2817.
(20) Book, L. D.; Arnett, D. C.; Hu, H.; Scherer, N. F. *J. Phys. Chem. A* **1998**, *102*, 4350.
(21) Fraga, E.; Webb, M. A.; Loppnow, G. R. *J. Phys. Chem.* **1996**, *100*, 3278.
(22) Holland, A. W.; Bergman, R. G. *J. Am. Chem. Soc.* **2002**, *124*, 9010.
(23) Holland, P. L.; Tolman, W. B. *J Am Chem. Soc.* **1999**, *121*, 7270.
(24) Taylor, M. K.; Stevenson, D. E.; Berlouis, L. E. A.; Kennedy, A. R.; Reglinski, J. *J. Innorg. Biochem.* **2005**, *100*, 250.
(25) Siegbahn. Electronic Structure Calculations for Molecules Containing Transition Metals. In *Advances in Chemical Physics, Volume XCIII*; Prigogine, I., Rice, S. A., Eds.; John Wilet & Sons, Ltd., 1996; Vol. XCIII; pp 333.
(26) Shuku, T.; Sugimori, K.; Sugiyama, A.; Nagao, H.; Sakurai, T.; Nishikawa, K. *Polyhedron* **2005**, *24*, 2665.
(27) Olsson, M. H. M.; Hong, G. Y.; Warshel, A. *J. of Amer. Chem. Soc.* **2003**, *125*, 5025.
(28) Olsson, M. H. M.; Ryde, U. *J. Biol. Inorg. Chem.* **1999**, *4*, 654.
(29) Olsson, M. H. M.; Ryde, U.; Roos, B. O.; Pierloot, K. *J. Biol. Inorg. Chem.* **1998**, *3*, 109.
(30) Corni, S.; De Rienzo, F.; Di Felice, R.; Molinari, E. *Int. J. Quantum Chem.* **2005**, *102*, 328.
(31) Warshel, A. *Computer Modeling of Chemical Reactions in Enzymes and Solutions*; John Wiley & Sons, Ltd.: New York, 1991.
(32) Prabhakar, R.; Siegbahn, P. E. M. *Journal of Physical Chemistry B* **2003**, *107*, 3944.
(33) Yoshizawa, K.; Shiota, Y. *Journal of the American Chemical Society* **2006**, *128*, 9873.

(34) van den Bosch, M.; Swart, M.; Snijders, J. G.; Berendsen, H. J. C.; Mark, A. E.; Oostenbrink, C.; van Gunsteren, W. F.; Canters, G. W. *Chembiochem* **2005**, *6*, 738.
(35) Raffa, D. F.; Gomez-Balderas, R.; Brunelle, P.; Rickard, G. A.; Rauk, A. *Journal of Biological Inorganic Chemistry* **2005**, *10*, 887.
(36) Sabolovic, J.; Liedl, K. R. *Inorg. Chem.* **1999**, *38*, 2764.
(37) Sabolovic, J.; Tautermann, C. S.; Loerting, T.; Liedl, K. R. *Inorganic Chemistry* **2003**, *42*, 2268.
(38) Katz, A.; Shimoni-Livny, L.; Navon, O.; Navon, N.; Bock, C.; Glusker, J. *Helv. Chim. Acta* **2003**.
(39) Rulíšek, L.; Havlas, Z. *J. Phys. Chem. A* **2002**, *106*, 3855.
(40) Rulíšek, L.; Havlas, Z. *J. Am. Chem. Soc.* **2000**, *122*, 10428.
(41) Rulíšek, L. *Chemicke Listy* **2002**, *96*, 132.
(42) Rulíšek, L.; Havlas, Z. *J. Phys. Chem. B* **2003**, *107*, 2376.
(43) Bertran, J.; Rodrigues-Santiago, L.; Sodupe, M. *J. Phys. Chem. B* **1999**, *103*, 2310.
(44) Shoeib, T.; Rodriquez, C. F.; Siu, K. W. M.; Hopkinson, A. C. *Phys. Chem. Chem. Phys.* **2001**, *3*, 853.
(45) Caraiman, D.; Shoeib, T.; Siu, K.; Hopkinson, A.; Bohme, D. *Int. J. Mass Spectrom.* **2003**, *228*, 629.
(46) Breza, M.; Kozisek, J. *Polyhedron* **2006**, *25*, 2559.
(47) Hemmert, C.; Pitie, M.; Renz, M.; Gornitzka, H.; Soulet, S.; Meunier, B. *J. Biol. Inorg. Chem.* **2001**, *6*, 14.
(48) Hackl, E. V.; Kornilova, S. V.; Kapinos, L. E.; Andruschenko, V. V.; Galkin, V. L.; Grigoriev, D. N.; Blagoi, Y. P. *J. Molec. Struct.* **1997**, *408/409*, 229.
(49) Atwell, S.; Meggers, E.; Spraggon, G.; Schultz, P. G. *J. Am. Chem. Soc.* **2001**, *123*, 12364.
(50) Meggers, E.; Holland, P. L.; Tolman, W. B.; Romesberg, F. E.; Schultz, P. G. *J. Am. Chem. Soc.* **2000**, *122*, 10714.
(51) Schoentjes, B.; Lehn, J.-M. *Helvetica Chimica Acta* **1995**, *78*, 1.
(52) Lamsabhi, A.; Alcami, M.; Mo, O.; Yanez, M.; Tortajada, J. *ChemPhysChem* **2004**, *5*, 1871.
(53) Gasowska, A.; Lomozik, L. *Monatshefte fur Chemie* **1995**, *126*, 13.
(54) Burda, J. V.; Šponer, J.; Hobza, P. *J. Phys. Chem.* **1996**, *100*, 7250.
(55) Burda, J. V.; Šponer, J.; Leszczynski, J.; Hobza, P. *J. Phys. Chem. B* **1997**, *101*, 9670.
(56) Šponer, J.; Sabat, M.; Burda, J.; Leszczynski, J.; Hobza, P.; Lippert, B. *J. Biol. Inorg. Chem.* **1999**, *4*, 537.
(57) Rulíšek, L.; Šponer, J. *Journal of Physical Chemistry B* **2003**, *106*, 1913.
(58) Burda, J. V.; Shukla, M. K.; Leszczynski, J. *J. Mol. Model.* **2005**, *11*, 362.
(59) Pavelka, M.; Shukla, M. K.; Leszczynski, J.; Burda, J. V. *J. Phys. Chem A* **2006**, *in preparation*.
(60) Frank, P.; Benfatto, M.; Szilagyi, R. K.; D'Angelo, P.; Della Longa, S.; Hodgson, K. O. *Inorganic Chemistry* **2005**, *44*, 1922.
(61) Burda, J. V.; Pavelka, M.; Šimánek, M. *J. Molec. Struct.* **2004**, *683*, 183.
(62) Konopka, M.; Rousseau, R.; Stich, I.; Marx, D. *J. Am. Chem. Soc.* **2004**, *126*, 12103.
(63) Tachikawa, H. *Chem. Phys.Lett.* **1996**, *260*, 582.
(64) Hamilton, I. P. *Chem. Phys. Lett.* **2004**, *390*, 517.
(65) Pavelka, M.; Burda, J. V. *Chem. Phys.* **2005**, *312*, 193.
(66) Marini, G. W.; Liedl, K. R.; Rode, B. M. *J. Phys. Chem. A* **1999**, *103*, 11387.
(67) Schwenk, C.; Rode, B. *ChemPhysChem* **2004**, *5 (3)*.
(68) Schwenk, C. F.; Rode, B. M. *Physical Chemistry Chemical Physics* **2003**, *5*, 3418.
(69) Pranowo, H. *Chem. Phys.* **2003**, *291 (2)*.
(70) Pranowo, H. D.; Rode, B. M. *J. Phys. Chem. A* **1999**, *103*, 4298.
(71) Pranowo, H. D.; Setiajin, A. H. B.; Rode, B. M. *J. Phys. Chem. A* **1999**, *103*, 11115.
(72) Feller, D.; Glendening, E. D.; de Jong, W. A. *J. Chem. Phys.* **1999**, *110*, 1475.
(73) Schroeder, D.; Schwartz, H.; Wu, J.; Wesdemiotis, C. *Chem. Phys. Lett.* **2001**, *343*, 258.
(74) Pranowo, H. D.; Rode, B. M. *Chem. Phys* **2001**, *263*, 1.
(75) Haeffner, F.; Brinck, T.; Haeberlein, M.; Moberg, C. *Chem. Phys. Letters* **1997**, *397*, 39.
(76) Cordeiro, N. M. D. S.; Gomes, J. A. N. F. *J. Comput. Chem.* **1993**, *14*, 629.
(77) Subramanian, V.; Shankaranarayanan, C.; Nair, B. U.; Kanthimathi, M.; Manickkavachagam, R.; Ramasami, T. *Chem. Phys. Lett.* **1997**, *274*, 275.
(78) Gresh, N.; Policar, C.; Giessner-Prettre, C. *J. Phys. Chem.* **2002**, *106*, 5660.
(79) Ledecq, M.; Lebon, F.; Durant, F.; Giessner-Prettre, C.; Marquez, A.; Gresh, N. *J. Phys. Chem. B* **2003**, *107 (38)*.
(80) Schwerdtfeger, P.; Krawczyk, R. P.; Hammerl, A.; Brown, R. *Inorg. Chem.* **2004**, *43*, 6707.
(81) Berces, A.; Nukada, T.; Margl, P.; Ziegler, T. *J. Phys. Chem. A* **1999**, *103*, 9693.
(82) Neese, F. *Magn. Res. Chem.* **2004**, *42*, S187.
(83) Pavelka, M.; Šimánek, M.; Šponer, J.; Burda, J. V. *J. Phys. Chem. A* **2006**, *110*, 4795.
(84) Berman, H. M.; Westbrook, J.; Feng, Z.; Gilliland, G.; Bhat, T. N.; Weissig, H.; Shindyalov, I. N.; Bourne, P. E. *Nucleic Acids Research* **2000**, *28*, 235.
(85) Hurley, M. M.; Pacios, L. F.; Christiansen, P. A.; Ross, R. B.; Ermler, W. C. *J. Chem. Phys.* **1986**, *84*, 6840.
(86) Boys, S. F.; Bernardi, F. *Mol. Phys.* **1970**, *19*, 553.
(87) Šponer, J.; Burda, J. V.; Sabat, M.; Leszczynski, J.; Hobza, P. *J. Phys. Chem. A* **1998**, *102*, 5951.
(88) Reed, A. E.; Weinstock, R. B.; Weinhold, F. *J. Chem. Phys.* **1985**, *83*, 735.
(89) Casida, M. E.; Jamorski, C.; Casida, K. C.; Salahub, D. R. *J. Chem. Phys.* **1998**, *108*, 4439.
(90) Hirata, S.; Head-Gordon, M. *Chem. Phys. Lett.* **1999**, *314*, 291–299.
(91) Frisch, M. J.; Trucks, G. W.; Schlegel, H. B.; Scuseria, G. E.; Robb, M. A.; Cheeseman, J. R.; Montgomery, J. A.; Vreven, J., T.; Kudin, K. N.; Burant, J. C.; Millam, J. M.; Iyengar, S. S.; Tomasi, J.; Barone, V.; Mennucci, B.; Cossi, M.; Scalmani, G.; Rega, N.; Petersson, G. A.; Nakatsuji, H.; Hada, M.; Ehara, M.; Toyota, K.; Fukuda, R.; Hasegawa, J.; Ishida, M.; Nakajima, T.; Honda, Y.; Kitao, O.; Nakai, H.; Klene, M.; Knox, X. L., J. E.; Hratchian, H. P.; Cross, J. B.; Adamo, C.; Jaramillo, J.; Gomperts, R.; Stratmann, R. E.; Yazyev, O.; Austin, A. J.; Cammi, R.; Pomelli, C.; Ochterski, J. W.; Ayala, P. Y.; Morokuma, K.; Voth, G. A.; Salvador, P.; Dannenberg, J. J.; Zakrzewski, V. G.; Dapprich, S.; Daniels, A. D.; Strain, M. C.; Farkas, O.; Malick, D. K.; Rabuck, A. D.; Raghavachari, K.; Foresman, J. B.; Ortiz, J. V.; Cui, Q.; Baboul, A. G.; Clifford, S.; Cioslowski, J.; Stefanov, B. B.; Liu, H.; Liashenko, A.; Piskorz, P.; Komaromi, I.; Martin, R. L.; Fox, D. J.; Keith, T.; Al-Laham, M. A.; Peng, C. Y.; Nanayakkara, A.; Challacombe, M.; Gill, P. M. W.; Johnson, B.; Chen, W.; Wong, M. W.; Gonzalez, C.; Pople, J. A. Gaussian 03, Revision A.1; Gaussian, Inc.: Pittsburgh PA, 2003.
(92) Weinhold, F. NBO 5.0 Program 5.0 ed.; University of Wisconsin, Madison, Wisconsin 53706: Wisconsin, 2001.
(93) Schaftenaar, G.; Noordik, J. H. *J. Comput.-Aided Mol. Design* **2000**, *14*, 123.
(94) Flükiger, P. F. *http://www.cscs.ch/molekel/*.
(95) Portmann, S.; Lüthi, H. P. *Chimia* **2000**, *54*, 766.
(96) Ryde, U.; Olsson, M. H. M.; Pierloot, K.; Roos, B. O. *J. Mol. Biol.* **1996**, *261*, 586.
(97) Solomon, E. I.; Penfield, K. W.; Gewirth, A. A.; al, e. *Innorg. Chim. Acta* **1996**, *243*, 67.
(98) Datta, S. N.; Sudhamsu, J.; Pandey, A. *J. Phys. Chem. B* **2004**, *108*, 8007.

Theoretical Study of Hydrated Copper(II) Interaction with Guanine: A Computational DFT Study

Matěj Pavelka[1], Manoj K. Shukla[2], Jerzy Leszczynski[2], and Jaroslav V. Burda[1]*

[1]*Department of Chemical Physics and Optics, Faculty of Mathematics and Physics, Charles University, Ke Karlovu 3, 121 16 Prague 2, Czech Republic*

[2]*Department of Chemistry, Jackson State University, 1325 J. R. Lynch Street, Jackson, Mississippi 39217-0510, USA*

Abstract

Detailed optimization of the hydrated Cu(II)(N7-Guanine) structures revealed number of minima on potential energy surface. For selected structures, energy decompositions together with determination of electronic properties (partial charges, electron spin densities, electrostatic potentials, MO analysis) were performed. For system without water molecules or with one water, charge transfer from guanine to Cu(II) occurs, which results in reduced Cu(I) cation. A complex with two aqua ligands is a borderline system with charge +0.7e on guanine with similar amount of spin density (0.6) localized there. Only when four-coordination on copper was achieved, the prevailing electron spin density is localized on copper. In case of lower numbers of coordinated aqua ligands, energetic ΔE^{max} preference of three-aqua Cu-(N7-guanine) structure over diaqua Cu-(N7,O6-guanine) chelate was found. Similar conclusion can also be drawn from tetraaqua complexes where the largest stability was obtained for three coordinated aqua ligands with one water molecule in second solvation shell of Cu(II) cation. Similarly neither pentacoordinated triaqua chelate is more stable. As a consequence of more bulky guanine ligand, it was found that pentacoordination in these complexes is less convenient than in case of small inorganic complexes above.

1. Introduction

Copper, despite its toxicity in pure form, is essential for many processes in bioorganisms. Hence, study of its activity has always been an aim of many theoretical as well as experimental laboratories. Thanks to development of high performance computers and effective quantum-chemical methods in last two decades, substantially larger systems can be addressed at present.

The roles of copper in active centers of many peptides was studied recently. Processes dealing with oxygen transportation and insertion, electron transfer, oxidation-reduction occur in such reaction centers. Copper proteins often exhibit unusual geometrical and electronic structures in these active centers. For instance, the redox centers became subjects of many experimental studies employing UV-VIS and EPR spectroscopy,[1-5] EPR and ENDOR techniques,[6] X-ray absorption near-edge structure (XANES) method,[7] pump-probe[8] and resonance Raman spectroscopy,[9] and some others.[10-14] Number of theoretical studies devoted to investigation of copper redox processes in various models for consideration of active side chain is growing very fast, see e.g. ref. 15-30.

The interaction of various metal cations with DNA/RNA bases represents usually initial stage for many biochemical processes. The opening of α-helix abolishing hydrogen bonds between WC base pairs often proceeds in presence of metals usually in hydrated form. Therefore a great deal of work was devoted to the investigation of copper complexes with various models nucleobases. IR spectra were measured and interpreted

for interactions of DNA with several divalent cations in a solution.31 Structural assignment of planar complexes based on an empirical equation was published,[32] which allows an estimation of the ligand field strength of involved donor groups. Such a relationship can be helpful assessing a criterion for the establishment of axial co-ordination mode of copper(II) ion. Crystal structures of several metal complexes with cleaving activity on DNA oligomers were characterized in ref.[33] X-ray structure of CuCl2:Guanine compounds was examined in another work.[34] Cu(II) adduct has been considered to be a predominant reason for DNA damage by carcinogenic heterocyclic aminesin a study of Murata et al[35] who examined the oxidation of 5 '-site guanine at GG and GGG sequences in the presence of Cu(II) and NADH by an electrochemical detector coupled to a high-performance liquid chromatograph. Absorption, fluorescence, CD spectra and viscosity experiments were performed on the interaction of the two macrocyclic copper(II) complexes with DNA.[36] Meggers et al.14 measured melting curves of copper(II) complexes with DNA duplex and later they also examined some structural aspects of a copper(II) coordination to WC base pairs[37]. The interactions of the polynuclear copper(I) complexes with double-strand DNA oligomers were explored by Lehn's group.[38] Very specific oxidation of guanine at a junction between single- and double-stranded DNA by a dinuclear copper(II) complex with H2O moieties was reported in ref.[39]. Thermodynamical measurements[40] on nucleosides coordinated with Ca and Cu divalent cations suggest the following order in bonding strength: Cu2+ > Ca2+ and GMP > IMP > AMP > CMP = UMP for the nucleotides. Formation of macrochelates was found to be energetically favorable but entropically unfavorable. Interactions of electronically excited Copper(II)-porphyrin complex with DNA were explored using Raman spectroscopy by Mojzes et al.[41]

A theoretical study of Cu^{2+} association with uracil and its thio derivatives has been published.[42] Another theoretical work of Martinez[43] investigates neutral, anionic, and cationic copper-guanine and -uracyl complexes but without considering hydration. Coordination and stability of Cu(II) and Zn(II) complexes with adenosine and cytidine were investigated by Gasowska.[44] Theoretical study on the copper(II) catalyzed Michael reaction was published in van Wullen's group[45] where enamine was deprotonated upon coordination to Cu2+, occupying three coordination sites of Cu(II) in a square planar geometry. Binding of Cu^{+} cations to guanine and adenine[46] and in a non-complementary DNA C-A base pair[47] were explored in our previous studies. The outer-shell and inner-shell coordination of phosphate group to hydrated metal ions (Mg2+, Cu2+, Zn2+, Cd2+) was explored in the work of Rulíšek.[48] A reduction of nitric oxide in bacterial nitric oxide reductase was recently published by Blomberg and Siegbahn [49]

In our previous papers,[50-52] small model complexes of Cu(I)/Cu(II) cations were intensively studied. The works were devoted to the investigation of coordination geometries and electronic properties of Cu cations interacting with molecules like water, ammonia, and hydrogen-sulphide. The present work can be regarded as a continuation of previous study[53] devoted to hydrated copper(I) interaction with guanine. Our work provides a detailed investigation of copper(II) interactions with guanine base in the presence of several water molecules. Structural, thermodynamic, and electronic properties were determined and used to characterize copper-guanine interactions. Obtained structures are also compared with results from other theoretical and experimental works.

2. Computational Details

The $[Cu(H_2O)_n]^{2+}$ complexes with guanine were studied, where number of water molecules varies from 0 to 5. Multiple gradient optimizations were performed utilizing different starting geometries. Such systems have great many distinct local minima. However, only several lowest conformers of each coordination were considered in the further analyses.

Quantum chemical calculations were performed at the Density Functional Theory (DFT) level using the B3PW91 functional for structure optimization. For the H,

C, O, N atoms, the 6-31+G(d) basis set was applied. The copper core electrons were described by Stuttgart effective-core pseudopotentials (ECP). A consistent basis set was adopted for copper valence electrons, i.e. the double-ζ pseudoorbitals were augmented by diffuse (α_s = 0.005, α_p = 0.01, and α_d = 0.05) and polarization (α_f = 0.758) functions. The frequency analysis was performed at the same computational level, confirming that the obtained structure has character of local minima. This analysis also served for obtaining thermochemical potentials (in NVE microcanonical model).

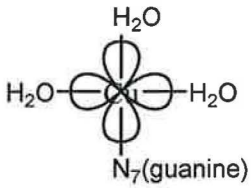

Scheme 1: Correct single occupied molecular orbital for the square-planar complexes.

Cu(II) complexes contain metal cation in the $3d^9$ electron configuration resulting in doublet ground states. Some attention has to be devoted to the construction of an appropriate initial guess of wave function in the SCF procedure. First, the correct wave function (with single occupied molecular orbital according to ***Scheme 1***) was constructed at ROHF/STO-3G level passing subsequently to the final unrestricted B3PW91/6-31+G(d) level.

Single-point calculations for energy and charge distribution analyses were performed with the same B3LYP functional but more extended *6-311++G(2df,2pd)* basis set for H, C, N, and O atoms. Consistently, the basis sets on the copper atoms were enlarged by *spd* diffuse functions mentioned above and *2fg* polarization functions with exponents α_f= 1.00, 0.26, α_g= 0.66.

Several different energy characteristics of interactions were evaluated for every complex. First, the conventional stabilization energies with the Basis Set Superposition Error (BSSE) corrections and corrections on the deformation energies were determined according to the equation

$$(1)\quad \Delta E^{Stab} = -(E_{complex} - \sum E_{monomer} - \sum E^{deform})$$

Here $E_{complex}$ represents the total energy of whole complex and $E_{monomer}$ represents the energy of a individual subsystem computed with basis functions on the ghost atoms from the complementary part(s) of the system. Besides the ΔE^{Stab} energies, additional stabilization energies corrected on ligands repulsion (ΔE^{Stex}) were computed. In the ΔE^{Stex} energy all the interacting ligands (guanine and waters) are treated in eq. (1) as single subsystem while the the other subsystem is represented by the central Cu ion. Then, this energy equals to the binding energy of the cation with the fixed (pre-formed) ligand shell. The difference between ΔE^{Stab} and ΔE^{Stex} represents the energy, which is required for formation of the ligand shell arrangement without the cation (in fact it is lower since ligand polarization under the influence of Cu cation is missing). Also, estimations of bonding energies (ΔE^{BE}) were evaluated using modified form of Eq. (1) without the monomer deformation corrections. Determining this energy, partition of the complex into two parts according to the cleaved Cu-L bond gives the bonding energy of the desired ligand. Note that ΔE^{BE} value for remote water molecule represents its association energy. For copper-guanine interaction, energy of water...O6 hydrogen bonds is included in this way and therefore some estimation of this energy had to be subtracted in order to obtain the correct ΔE^{BE} of Cu-N coordination.

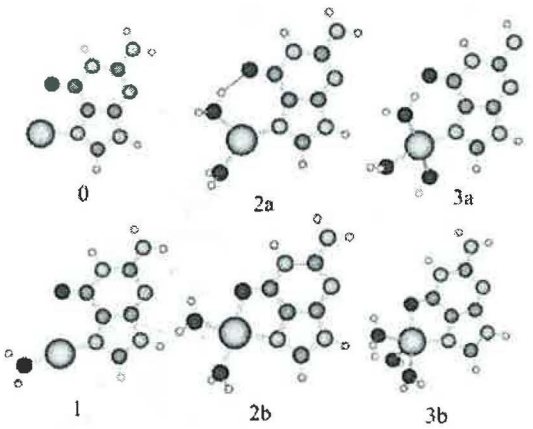

Figure 1: The aqua-copper $[Cu(H_2O)_n]^{2+}$ complexes with guanine, where *n = 0 - 3*.

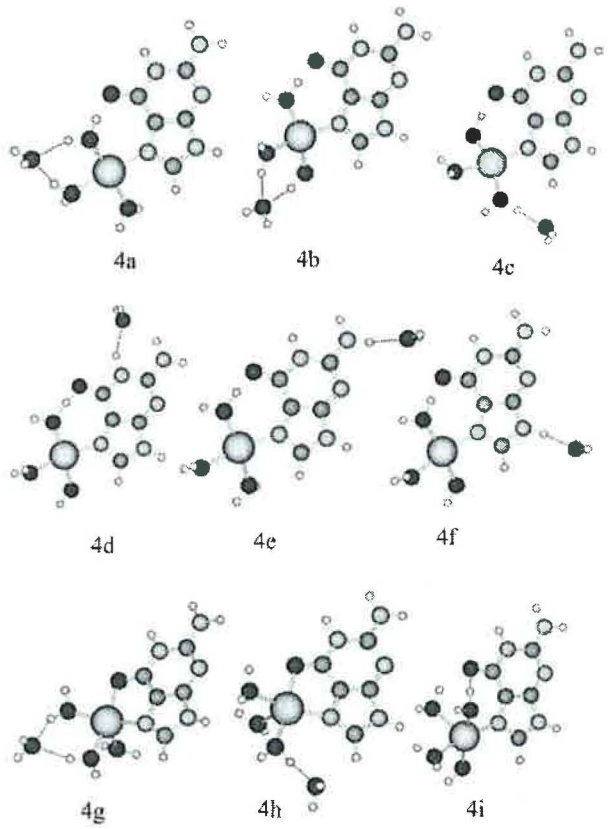

Figure 2: The tetraaqua Cu(II) complexes with guanine.

For comparison of various conformers, relative differences of total energies ΔE^1 and ΔE^2 were evaluated at *B3PW91/6-31+G(d)* and *B3LYP/6-311++G(2df,2pd)* level, respectively. The energy characteristics are extended by relative differences of Gibbs energies ΔG (at 298 K), enlightening the role of entropy contributions. Partial charges of the examined systems were explored using Natural Population Analyses (NPA)[54] together with spin-density analyses. Maps of electrostatic potential on isodensity surface (ρ = 0.001 e/Å^3) were plotted for easier insight. Package of programs *Gaussian 98*[55] was used for the determination of the electronic structure of studied complexes. Program NBO v. 5.0 from Wisconsin University[56] was employed for evaluation of the Natural Bond Orbital (NBO) characteristics. Geometries, molecular orbitals, spin densities, and vibrational modes were visualized using Molden 4.3[57] and Molekel 4.3[58] programs.

3. Results and Discussion

3.1 Structures

Optimized structures of hydrated copper $[Cu(H_2O)_n]^{2+}$ with guanine are shown in ***Figures 1***, where *n* varies from 0 to 3. Additional water molecules in tetraaqua- and pentaaqua-Cu(II)-guanine complexes (in ***Figures 2*** and ***3***, respectively) can be also localized around the NA moiety. In all the studied structures, guanine is coordinated to copper through N7 position, in the case of chelate structures O6 and N7 guanine sites are involved. Standard labeling of guanine atoms was used as presented e.g. in ref 59 and displayed in ***Scheme 2***. All the geometries reported in this paper are available in Supplementary material.

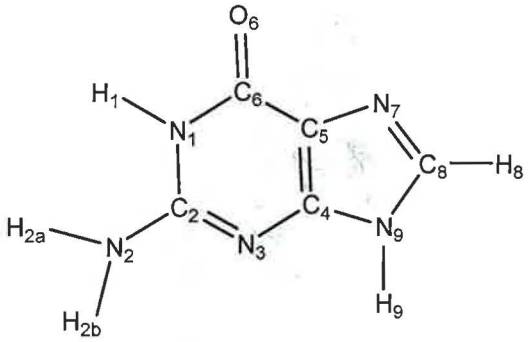

Scheme 2: Atom numbering in guanine.

The lengths of the Cu coordination bonds are listed in ***Table 1*** for all hydrated Cu(II)-guanine complexes. In the non-hydrated Cu(II)-guanine complex (***structure 0*** in ***Figure 1***), the Cu-N7 bond is 1.952 Å, which is markedly shorter than the Cu-O6 distance (about 2.7 Å). This bonding characteristics are completely different in comparison with similar structures with bare alkaline earth metals or zinc group metals studied in one of our earlier works.[46] Explanation can be seen in partial reduction of copper cation by electron transfer from guanine as discussed lower. When a water molecule is added into Cu(II)-guanine system, the Cu-N7 bond is slightly shortened to 1.894 Å. Moreover, the two-coordinated complex (***structure 1***) also exhibits one of

Table 1: Selected bond lengths of $[Cu(H_2O)_n]^{2+}$ complexes with guanine: Cu-N(guanine), Cu-O(water), and Cu-O6(guanine) distances (in Å). Abbreviation *c.n.* is used for coordination type and *struct.* corresponds to the identification number used in all Figures.

System	c.n.	*struct.*	Cu-N	Cu-O(water)				Cu-O6
$[CuG]^{2+}$	1	*0*	1.952					
$[CuG(H_2O)_1]^{2+}$	2	*1*	1.892	1.894				
$[CuG(H_2O)_2]^{2+}$	3	*2a*	1.940	1.992	1.992			
	4^{chel}	*2b*	2.004	1.966	2.005			1.996
$[CuG(H_2O)_3]^{2+}$	4	*3a*	1.971	2.012	2.047	1.893		
	5^{chel}	*3b*	2.032	2.026	2.000	2.258		2.024
$[CuG(H_2O)_4]^{2+}$	4	*4a*	1.969	2.040	1.985	1.911		
	4	*4b*	1.971	2.007	1.990	1.916		
	4	*4c*	1.965	1.969	2.026	1.936		
	4	*4d*	1.987	2.028	2.060	1.850		
	4	*4e*	1.969	2.017	2.052	1.886		
	4	*4f*	1.961	2.014	2.052	1.893		
	5^{chel}	*4g*	2.035	2.001	2.277	1.985		2.039
	5^{chel}	*4h*	2.037	1.969	2.276	2.022		2.031
	5	*4i*	1.979	2.021	2.055	2.229	1.974	
$[CuG(H_2O)_5]^{2+}$	4	*5a*	1.975	2.006	1.962	1.921		
	4	*5b*	1.960	2.004	1.977	1.933		
	4	*5c*	1.961	2.002	1.975	1.938		
	4	*5d*	1.972	1.966	1.983	1.944		
	4	*5e*	1.955	1.972	2.031	1.935		
	4	*5f*	1.955	2.003	1.976	1.941		
	5^{chel}	*5g*	2.031	2.004	1.988	2.285		2.031
	5^{chel}	*5h*	2.027	2.005	1.989	2.291		2.026
	5^{chel}	*5i*	1.970	2.002	1.978	1.999		2.608
	5^{chel}	*5j*	1.966	1.988	1.957	2.012		2.666
	5^{chel}	*5k*	1.968	2.002	1.950	1.986		2.719
	5^{chel}	*5l*	2.018	2.007	1.987	2.288		2.042
	5	*5m*	1.971	2.037	2.295	2.064	1.941	
	5	*5n*	1.993	2.019	2.022	1.938	2.404	
	5	*5o*	1.979	2.037	2.305	2.065	1.930	
	5	*5p*	1.978	2.038	2.296	2.062	1.936	
	5	*5q*	1.977	2.075	2.182	2.027	1.969	
	5	*5r*	1.996	2.036	2.376	2.044	1.933	
	5	*5s*	1.978	2.038	1.984	2.252	2.000	
	5	*5t*	1.990	2.050	2.312	2.035	1.933	

the shortest Cu-O(aqua) bonds (about 1.892 Å). Similar behavior was also already discussed in the previous study,[50] where $[Cu(H_2O)_2]^{2+}$ complex exhibited shorter Cu-O distances than $[Cu(H_2O)]^{2+}$ complex.

In the three-coordinated diaqua-Cu(II)G complex (***struct. 2a***), the both Cu-O and Cu-N bonds elongate in comparison to monoaqua-Cu(II)G system. One of the water is also H-bonded to O6 position of guanine d(O6..Hw) = 1.82 Å. (This H-bond energy can be roughly estimated about 7.5 kcal/mol from the difference of Cu-O bond energies – based on a comparison of ΔE^{BE}(Cu-O) for both aqua ligands in Table 2) However, this interaction influences the Cu-O distance only marginally, keeping both Cu-O bonds of practically the same length. The global minimum of diaqua system is formed by tetra-coordinated chelate, which total energy is about 7 kcal/mol lower. In this chelate, the Cu-O6 bond is shorter than Cu-N7, which one can rationalize by harder character of Cu^{2+} cation in comparison with e.g. Cu^{+} cation.

Similarly, the Cu(II)G complex with three water molecules exhibits two interesting minima (among other). The first one, 4-coordinated complex (***struct. 3a***), has one of the aqua ligands distinctively shorter Cu-O coordination, which is a consequence of H-bonding with neighboring O6 position. The second minimum (***struct. 3b***) corresponds to the five-coordinated chelate where again the Cu-O6 bond is shorter than Cu-N7 bond (2.024 versus 2.032 Å).

For quantification whether a structure is closer to trigonal bipyramid or octahedral arrangement, the τ coefficients are presented for the 5-coordinated complexes in ***Table 6***. These τ value is define by equation:

(2) $$\tau = \frac{\theta - \varphi}{60^o}$$

where θ is the largest ligand-metal-ligand angle and φ is the second one. For true octahedral structure τ=0 and for bipyramidal one τ =1. It was found that all 5-coordinated complexes (both chelated and non-chelated) have distorted octahedral geometry, since τ values range from 0.0 to 0.24.

Cu(II)G complexes hydrated by four water molecules exhibit many distinct local minima, nine lowest structures were chosen for further analyses (cf. ***Figure 2***). One subset contains six 4-coordinated structures (***4a-4f***) with three aqua ligands, while the remaining water molecule was used for exploration of potential energy surface (PES) of $[CuG(H_2O)_3]^{2+}$ system. In structures ***4a*** and ***4b,*** the remote water is localized in the second solvation shell of copper cation by bifurcated H-bonds. In structures ***4c-4f,*** the water molecule is associated to different guanine sites. Another subset is composed from three 5-coordinated chelate structures ***4g –4i.***

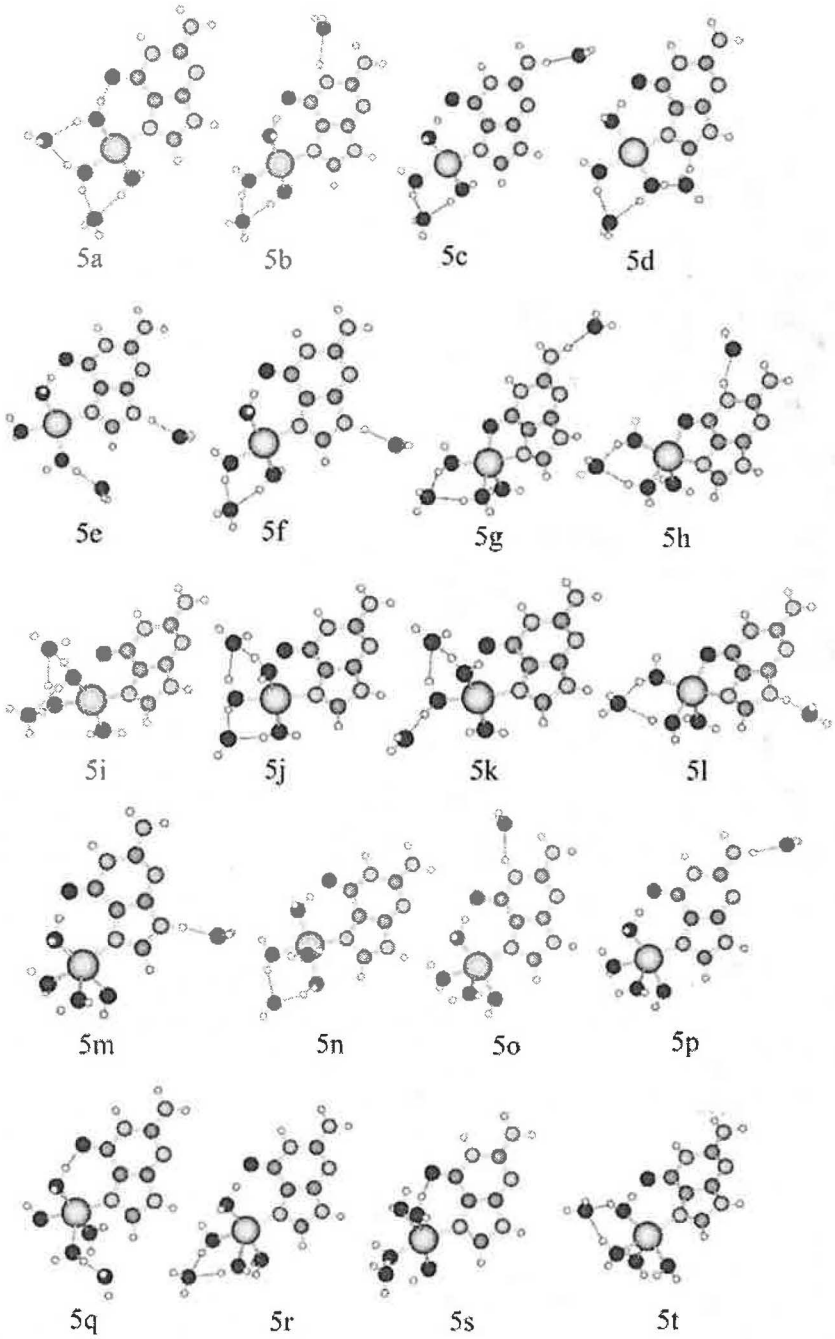

Figure 3: The pentaaqua Cu(II)G complexes.

In the case of pentaaqua Cu(II)G complexes, a very large number of local minima can be found on the given PES. From this set, only several most interesting conformers is presented in ***Figure 3*** and discussed further. First part is devoted to the exploration of the PES of triaqua Cu(II)G system with two remote water molecules either four-coordinated structures (***5c-5f***) or five-coordinated chelates (***5g-5l***). Second part deals with the PES of 5-coordinated systems with one remote water molecule (***5m-5t***). Interestingly, none 6-coordinated structure was found stable. Similar situation occurred in our

Table 2: ΔE^{stab} stabilization, ΔE^{ster} sterically corrected stabilization, and ΔE^{BE} bonding energies (in kcal/mol). Bold indicates the most stable conformer for given coordination number. Abbreviations *struct.* and *c.n.* correspond to identification and coordination type, respectively. Bond energies marked by * or " represent remote water molecules near the first coordination sphere or guanine sites, respectively.

System	c.n.	*struct.*	ΔE^{stab}	ΔE^{ster}	ΔE^{BE}					
					guanine	*water molecules*				
$[CuG]^{2+}$	1	*0*	292.7	302.6	302.6					
$[CuG(H_2O)_1]^{2+}$	2	*1*	337.5	348.8	229.5	45.5				
$[CuG(H_2O)_2]^{2+}$	3	*2a*	353.7	363.2	158.6	*32.3*	24.8			
$[CuG(H_2O)_2]^{2+}$	4^{chel}	*2b*	360.9	388.3	185.6	38.1	35.4			
$[CuG(H_2O)_3]^{2+}$	4	*3a*	377.0	403.6	126.1	32.9	33.1	44.2		
	5^{chel}	*3b*	379.0	409.2	159.0	30.1	32.4	20.8		
$[CuG(H_2O)_4]^{2+}$	4	*4a*	399.0	423.9	111.0	30.2	38.7	43.2	26.4*	
	4	*4b*	**401.2**	424.9	114.8	36.2	36.4	43.8	28.1*	
	4	*4c*	397.1	421.3	104.7	41.2	32.2	48.6	23.5*"	
	4	*4d*	393.8	433.4	105.2	31.6	31.1	47.5	18.3"	
	4	*4e*	389.2	415.6	107.9	31.5	31.5	44.7	12.9"	
	4	*4f*	392.9	417.5	104.5	31.4	31.7	43.7	16.8"	
	5^{chel}	*4g*	**399.6**	430.5	145.3	32.1	18.3	35.2	25.4*	
	5^{chel}	*4h*	397.8	429.1	146.2	41.2	18.8	29.6	20.5*"	
	5	*4i*	**393.9**	417.3	109.0	29.6	31.0	22.1	31.6	
$[CuG(H_2O)_5]^{2+}$	4	*5a*	**421.8**	446.2	102.2	35.0	41.4	44.6	25.8*	24.0*
	4	*5b*	417.7	436.9	100.7	35.1	35.9	43.0	27.1*	16.9"
	4	*5c*	413.4	434.7	96.1	35.0	36.2	41.7	27.3*	12.4"
	4	*5d*	419.8	444.4	95.6	48.0	35.7	43.9	25.1*	19.2*"
	4	*5e*	412.4	434.1	101.3	40.0	31.0	43.6	22.3*"	16.0"
	4	*5f*	417.0	437.8	98.8	34.8	36.4	41.8	27.0*	16.2"
	5^{chel}	*5g*	411.8	440.3	121.2	31.3	34.3	17.7	24.8*	12.8"
	5^{chel}	*5h*	**416.5**	442.3	127.4	31.0	33.9	17.4	24.7*	17.6"
	5^{chel}	*5i*	410.6	430.4	113.7	29.4	39.6	32.9	22.2*	24.0*
	5^{chel}	*5j*	415.9	437.3	109.5	33.4	40.7	31.9	25.6*	25.3*
	5^{chel}	*5k*	413.1	435.0	109.8	29.1	**51.1**	32.8	20.0*	24.8*
	5^{chel}	*5l*	414.7	443.0	123.8	30.7	34.4	17.4	24.7*	15.9"
	5	*5m*	410.4	434.7	96.1	27.6	19.7	26.4	42.3	16.0"
	5	*5n*	**416.1**	441.4	102.7	32.3	31.1	44.2	18.6	25.0*
	5	*5o*	411.2	434.4	99.1	28.1	19.8	26.2	47.1	16.9"
	5	*5p*	406.8	432.0	94.0	27.9	20.0	26.6	42.6	12.2"
	5	*5q*	411.0	437.3	90.8	24.1	29.7	28.4	39.1	18.0*"
	5	*5r*	413.8	439.6	105.2	26.9	21.7	30.7	43.3	24.0*
	5	*5s*	413.5	438.2	101.8	27.5	43.5	20.1	31.0	20.6*
	5	*5t*	413.7	438.4	100.9	27.9	17.9	32.0	43.0	23.2*

previous study of copper cations in mixed ammine-aqua ligand field.[51]

Cu-N bonds were found to be about 1.97 Å long in all non-chelated ***4x*** and ***5x*** structures. The chelated complexes (***structures 4g, 4h, 5g, 5h,*** and ***5l***) display a little bit longer Cu-N bonds (2.03 Å) and also the Cu-O distance of the water molecule in trans position is elongated similarly due to Jahn-Teller effect. (Notice that all these five-coordinated structures are close to octahedral arrangement – cf. Table 6). The remaining Cu-O(aqua) distances vary from 1.91 to 2.06 Å in dependence on the coordination number and the strength of possible H-bonds to remote waters or O6 guanine site. Generally Cu-O bonds in the 4-coordinated complexes are a little shorter.

In our earlier work,[51] the Cu-N bonds were about 2.05 Å while Cu-O bonds varied from 1.96 up to 2.11 Å in the Cu(II) complexes with ammonia and water molecules. It demonstrates higher donation affinity of guanine since the Cu-N7 bonds are by about 0.08 Å shorter than the Cu-N(NH_3) bonds. The Cu(II)-N7 bond can also be compared (with some care) with Cu(I)-N7 bond,[53] which

is usually by about 0.1 Å shorter. Considering Cu(I)G complexes, 2-coordinated structures are preferred, while Cu(II)G complexes prefer 4-coordinated arrangement. In another work,[34] the X-ray structures of $CuCl_2$:Guanine compounds were investigated by Blazic et al. They found the Cu-N7 distance are about 2.03 Å and Cu-O(aqua) about 1.98 Å long in good accord with our results.

3.2 Energy Analyses

Optimized structures were analyzed in terms of bond energies ΔE^{BE} and stabilization energies (with ΔE^{Stab} and without ΔE^{Stex} exclusion of mutual ligand interactions) computed according ***Equation 1*** at the B3LYP/6-311++G(2df,2pd) level. The obtained values are compiled in ***Table 2***. The total energies of all the conformers at both computational levels - ΔE^{1} (B3PW91/6-31+G(d,p)) and ΔE^{2} (B3LYP/6-311++G(2df,2pd)) together with Gibbs energies ΔG are compared in ***Table 3*** for more detailed insight in the stability of studied complexes.

Clearly, stabilization energy increases with the number of interacting water molecules in system. While in non-hydrated CuG complex the stabilization energy is about 293 kcal/mol due to strong electrostatic contribution to the dative Cu-N7 bond, the inclusion of first aqua ligand raises the stabilization by about 45 kcal/mol. Further including second up to the fifth water molecule, the stabilization energy increases as follows: 24, 18, 22, and 20 kcal/mol displaying a saturation limit of the H-bonding energy for water association to a (strongly) polarized system. The dependence of the stabilization energy on the number of water molecules is illustrated in ***Figure 4***. The drawn trend matches well our previous results for small copper complexes with aqua and ammine ligands.[51] An analogous dependence is visible in the ΔE^{Stex} energies.

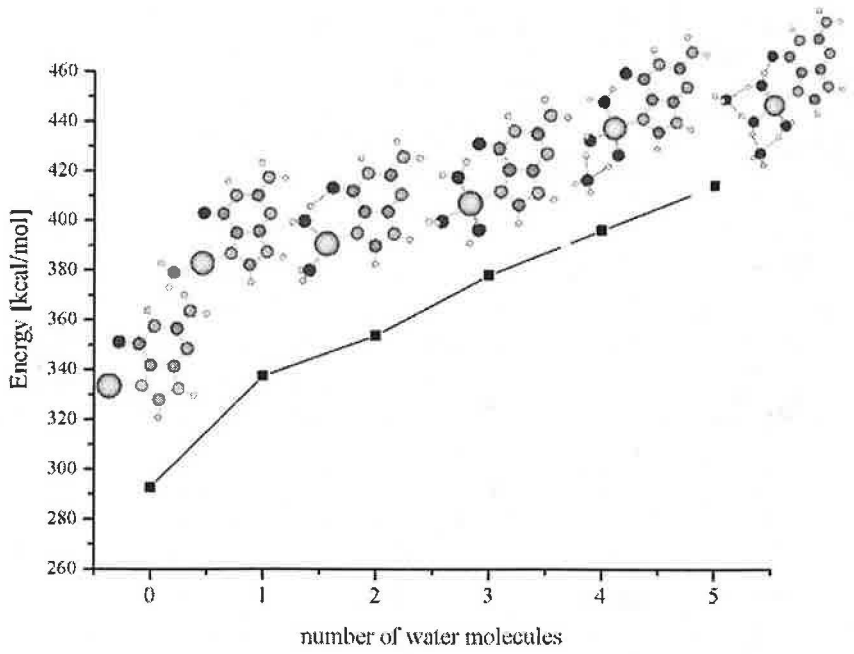

Figure 4: Stabilization energies for the $[Cu(H_2O)_n]^{2+}$ complexes with guanine, where $n = 0 - 5$.

Table 3: Relative differences ΔE^1 and ΔE^2 (in kcal/mol) of total energies obtained at the both computational levels 1 (B3PW91/6-31+G*) and 2 (B3LYP1/6-311++G**) with respect to global minima structure (marked by *), relative differences in stabilization energies $\Delta\Delta E^{stab}$ and relative Gibbs energies ΔG. Bold indicates the most stable conformer for given coordination. Abbreviation *c.n.* corresponds to the type of coordination and *struct.* is used for identification of the optimized structure.

System	c.n.	*struct.*	ΔE^1	ΔE^2	$\Delta\Delta E^{stab}$	ΔG^{total}
$[CuG(H_2O)_4]^{2+}$	4	*4a*	2.1	2.2	2.1	1.9
	4	***4b***	**0.0***	**0.0***	**0.0***	**0.0***
	4	*4c*	4.4	4.0	4.0	2.5
	4	*4d*	7.8	7.3	7.3	4.2
	4	*4e*	13.3	12.3	11.9	7.3
	4	*4f*	9.3	8.5	8.2	4.1
	5^{chel}	***4g***	**0.6**	**1.6**	**1.6**	**0.3**
	5^{chel}	*4h*	3.1	3.5	3.4	0.8
	5	***4i***	**6.5**	**7.1**	**7.2**	**6.5**
$[CuG(H_2O)_5]^{2+}$	4	*5a*	**0.0***	**0.0***	**0.0***	**0.0***
	4	*5b*	3.9	4.2	4.1	3.3
	4	*5c*	9.2	8.7	8.4	6.0
	4	*5d*	2.6	2.3	2.1	0.6
	4	*5e*	10.5	9.6	9.4	5.6
	4	*5f*	5.2	5.0	4.9	2.8
	5^{chel}	*5g*	10.0	10.3	10.0	6.2
	5^{chel}	*5h*	**4.5**	**5.5**	**5.4**	3.5
	5^{chel}	*5j*	**4.5**	5.7	5.9	6.4
	5^{chel}	*5k*	7.7	8.5	8.7	6.8
	5^{chel}	*5l*	6.7	7.1	7.1	**3.3**
	5	*5m*	11.5	11.5	11.4	7.1
	5	*5n*	**4.6**	**5.6**	**5.8**	**4.4**
	5	*5r*	7.0	7.9	8.1	6.7
	5	*5s*	7.8	8.3	8.4	6.0
	5	*5t*	7.2	8.0	8.1	7.0

Triaqua-Cu(II)-guanine system prefers (by 2 kcal/mol) 5-coordinated chelate structure (***struct. 3b***) over 4-coordinated complex (***struct. 3a***). The largest stabilization energy of tetraaqua-CuG complex is found for 4-coordinated conformer ***4b*** with one water in solvation shell. Similarly, in pentaaqua-complexes the global minimum is represented by the same structure with another water in Cu solvation shell. The relative energies of these conformers can be seen in ***Table 3*** for different computational schemes. From this ***Table***, it can be noticed that no change of the conformer order occurs passing between individual computational levels in $[CuG(H_2O)_4]^{2+}$ complexes. Differences of total energies ΔE^1 and ΔE^2 as well as relative changes in stabilization energies $\Delta\Delta E^{Stab}$ revealed that the most stable structure is the 4-coordinated complex with remaining water associated to the first coordination shell (***struct. 4b***). The ***4g*** conformer is the most stable chelate structure (by about 1.6 kcal/mol higher in stabilization energy). The 5-coordinated non-chelated complex ***4i*** is markedly less stable - about 7.2 kcal/mol when compared with global minimum (***4b***). When entropy corrections are taken into account, the structures with remote water in proximity of guanine become more favored. Especially, the relative Gibbs energy of the ***4g*** conformer is decreased to 0.3 kcal/mol above global minimum. It indicates that considering entropy corrections is significant in predicting correct thermodynamics of such systems.

Bonding (or better association) energy ΔE^{BE} (in ***Table 2***) between remote water and guanine also indicates that the most preferred guanine site is between N1 and N2 (***struct. 4d***) (ca 18 kcal/mol). In case of pentaaqua-

Table 4: Partial charges and spin densities (in electron units) summed for all guanine atoms. The same is done for water molecules, while copper partial charge is presented separately.

System	*charge*			*spin*		
	Cu	guanine	waters	Cu	guanine	waters
$[CuG]^{2+}$	0.927	1.073		0.006	0.994	
$[CuG(H_2O)_1]^{2+}$	0.822	1.081	0.097	0.023	0.975	0.001
$[CuG(H_2O)_2]^{2+}$ *2a*	1.128	0.734	0.138	0.332	0.620	0.048
$[CuG(H_2O)_2]^{2+}$ *2b*	1.432	0.357	0.211	0.696	0.204	0.132
$[CuG(H_2O)_3]^{2+}$	1.448	0.340	0.212	0.717	0.151	0.132
$[CuG(H_2O)_4]^{2+}$	1.441	0.326	0.234	0.711	0.125	0.164
$[CuG(H_2O)_5]^{2+}$	1.440	0.271	0.290	0.715	0.109	0.175

Cu(II)G complexes, the 4-coordinated structure (***5a***) with two remaining water molecules associated to the first coordination shell is the most preferred at all energy levels. Without entropy corrections, conformers ***5h*** and ***5n*** are the most stable chelate and 5-coordinated complexes. Both these structures have a remote water molecule attached by bifurcated hydrogen bonds to copper hydration shell. This position is preferred for tetraaqua-Cu(II)G complexes, too. When the remaining water hydrates the guanine, structure ***5h*** with H-bonded to N1/N2 sites is the most preferred. However if the Gibbs energy is considered, the ***5l*** conformer with H_2O linked to H9 site is more stable. The H9 position was also found to be favored by entropy in our previous work.[53]

Comparison of association energies ΔE^{BE} (***Table 2***) of remote water molecules revealed following trends:

i) The largest ΔE^{BE} occurs for water linked to the first coordination sphere of metal cation (20 to 27 kcal/mol.

ii) Smaller ΔE^{BE} energies (between 18-23 kcal/mol) connected with bifurcated H-bond between H8 and neighboring ligated water (in structures ***4c***, ***5d***, and ***5q***).

iii) A reduced ΔE^{BE} was found for water association to guanine sites (from 12 to 18 kcal/mol).

iv) Energy preference for H-bonded water to guanine sites is: N1/N2 (about 18 kcal/mol), N9 (17 kcal/mol), and N2 (13 kcal/mol).

Interaction of guanine with hydrated copper was investigated in terms of ΔE^{BE}*(Cu-N)* energies. For copper-guanine interaction, water...O6 association energies, which is usually present in the partition scheme for calculation of Cu-N bonding energy, must be subtracted in order to obtain appropriate estimation of Cu-N interaction. Energy of

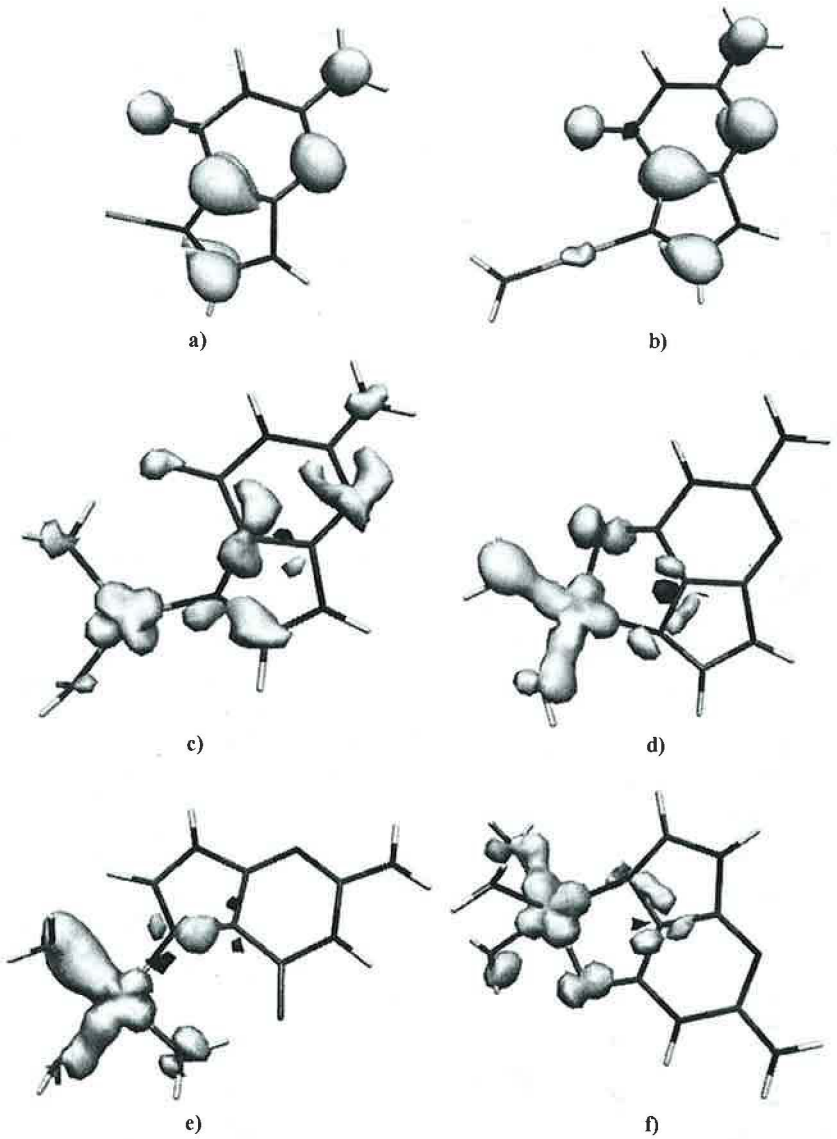

Figure 5: Plots of spin density ($\rho_s = 0.005$) of the selected aqua-Cu(II)G complexes:
a) and **b)** $[CuG]^{2+}$ and $[CuG(H_2O)]^{2+}$ structures,
c) and **d)** $[Cu(H_2O)_2]^{2+}$ structures ***2a*** and ***2b***,
e) and **f)** $[Cu(H_2O)_3]^{2+}$ structures ***3a*** and ***3b***.

Table 5: Partial atomic charges (in electron units) for copper and selected atoms on guanine (N7, N9, H9, H8, H1, H2a, H2b, and O6) obtained by NPA method. Averaged partial charge for O atoms of water molecules are presented too. **Bold** indicates the most stable conformer. Abbreviation *c.n.* corresponds to the coordination type and *struct.* is used for exact identification of the optimized structure.

System	c.n.	*struct.*	Partial atomic charges									
			Cu	N7	N9	H9	H8	H1	H2a	H2b	O6	Ow
$[CuG]^{2+}$	1	***0***	0.927	-0.627	-0.510	0.478	0.263	0.457	0.458	0.442	-0.504	
$[CuG(H_2O)_1]^{2+}$	2	***1***	0.822	-0.585	-0.511	0.474	0.257	0.453	0.454	0.439	-0.473	-0.979
$[CuG(H_2O)_2]^{2+}$	3	***2a***	1.128	-0.622	-0.509	0.468	0.247	0.446	0.448	0.431	-0.590	-0.993
	4^{chel}	***2b***	1.432	-0.624	-0.516	0.462	0.240	0.442	0.445	0.422	-0.725	-0.966
$[CuG(H_2O)_3]^{2+}$	4	***3a***	1.436	-0.625	-0.514	0.459	0.237	0.439	0.439	0.421	-0.648	-0.987
	5^{chel}	***3b***	1.461	-0.615	-0.520	0.459	0.236	0.439	0.443	0.420	-0.725	-0.973
$[CuG(H_2O)_4]^{2+}$	4	***4a***	1.426	-0.625	-0.516	0.456	0.234	0.436	0.437	0.419	-0.664	-0.984
	4	***4b***	1.442	-0.630	-0.515	0.457	0.235	0.438	0.438	0.420	-0.652	-0.992
	4	***4c***	1.440	-0.630	-0.515	0.456	0.241	0.438	0.438	0.420	-0.661	-0.987
	4	***4d***	1.424	-0.617	-0.519	0.457	0.236	0.470	0.433	0.441	-0.627	-1.000
	4	***4e***	1.430	-0.625	-0.517	0.457	0.235	0.437	0.468	0.409	-0.650	-0.982
	4	***4f***	1.430	-0.640	-0.531	0.482	0.232	0.437	0.436	0.419	-0.653	-0.979
	5^{chel}	***4g***	1.452	-0.607	-0.522	0.456	0.238	0.437	0.441	0.418	-0.727	-0.978
	5^{chel}	***4h***	1.455	-0.610	-0.522	0.455	0.240	0.437	0.441	0.419	-0.727	-0.974
	5	***4i***	1.466	-0.616	-0.518	0.457	0.236	0.436	0.439	0.419	-0.732	-0.980
$[CuG(H_2O)_5]^{2+}$	4	***5a***	1.435	-0.623	-0.518	0.454	0.233	0.434	0.436	0.417	-0.664	-0.991
	4	***5b***	1.422	-0.630	-0.518	0.455	0.234	0.465	0.430	0.439	-0.667	-0.984
	4	***5c***	1.423	-0.631	-0.519	0.455	0.234	0.434	0.467	0.408	-0.666	-0.981
	4	***5d***	1.425	-0.623	-0.518	0.454	0.236	0.436	0.436	0.418	-0.661	-0.987
	4	***5e***	1.434	-0.644	-0.532	0.480	0.236	0.436	0.435	0.418	-0.667	-0.980
	4	***5f***	1.422	-0.644	-0.532	0.481	0.232	0.435	0.435	0.417	-0.666	-0.979
	5^{chel}	***5g***	1.448	-0.609	-0.526	0.453	0.235	0.433	0.469	0.407	-0.735	-0.974
	5^{chel}	***5h***	1.446	-0.609	-0.525	0.453	0.235	0.465	0.433	0.436	-0.738	-0.976
	5^{chel}	***5i***	1.422	-0.616	-0.519	0.455	0.235	0.430	0.438	0.416	-0.745	-0.975
	5^{chel}	***5j***	1.443	-0.617	-0.519	0.455	0.236	0.428	0.438	0.416	-0.735	-0.981
	5^{chel}	***5k***	1.440	-0.632	-0.519	0.456	0.238	0.430	0.438	0.417	-0.724	-0.974
	5^{chel}	***5l***	1.446	-0.620	-0.540	0.481	0.234	0.434	0.438	0.416	-0.733	-0.973
	5	***5m***	1.449	-0.641	-0.534	0.480	0.230	0.435	0.435	0.417	-0.667	-0.977
	5	***5n***	1.442	-0.628	-0.518	0.454	0.238	0.436	0.436	0.418	-0.659	-0.987
	5	***5o***	1.448	-0.627	-0.519	0.454	0.232	0.465	0.430	0.439	-0.665	-0.982
	5	***5p***	1.450	-0.627	-0.520	0.454	0.232	0.434	0.467	0.408	-0.666	-0.979
	5	***5q***	1.462	-0.620	-0.519	0.454	0.229	0.436	0.437	0.419	-0.665	-0.984
	5	***5r***	1.440	-0.627	-0.518	0.454	0.237	0.436	0.437	0.418	-0.659	-0.986
	5	***5s***	1.451	-0.621	-0.520	0.456	0.236	0.435	0.438	0.419	-0.725	-0.977
	5	***5t***	1.445	-0.626	-0.518	0.454	0.235	0.434	0.436	0.418	-0.666	-0.985
isolated H_2O and guanine				-0.453	-0.557	0.416	0.192	0.409	0.401	0.383	-0.611	-0.928

water...O6 H-bond can be guessed to be about 13 kcal/mol based on comparison of ΔE^{BE}(Cu-O) for aqua ligands in structure 3a in Table 2, supposing that all three Cu-O bonds would be roughly equivalent if it were not of the H-bonding to O6 guanine (and omitting the influence of trans effect of N7 position). However, ΔE^{BE} energies still contain dipole-dipole interaction with ligands and copper interaction with O6 siteFor $[CuG(H_2O)_n]^{2+}$ complexes (where n = *3*, *4*, and *5*), Cu-N7 bonding energies range from 90 to 115 kcal/mol for non-chelate structures. When direct coordination between Cu and O6 is present, guanine ΔE^{BE} energies increase and vary from 110 to 130 kcal/mol. From these and some additional calculations performed one can guess that Cu-O6 bonding energy can be assessed between 20-40 kcal/mol according to number of surrounding water molecules.

In some cases, the ΔE^{BE} of Cu-O(aqua) increases from its average value of ca 30 kcal/mol up to 45 kcal/mol. This increase is caused by the fact that the electron

density of sigma O-H bond is decreased since the hydrogen atom is involved in additional H-bonding with oxygen from remote water molecules and therefore a part of the bonding electron density is released back to oxygen. Higher electron density on oxygen is available for better donation as well as larger partial charge can lead to an enhancement of electrostatic contribution to Cu-O coordination. In cases of even higher Cu-O bonding energy, two outer (non-coordinated) water molecules are present in vicinity of the given aqua ligand (cf. 5d, 5k). For chelate and 5-coordinated conformers, ΔE^{BE} energies drop to 18 kcal/mol.

In Cu^{2+} complexes with variable ammine-aqua ligand field,[52] ΔE^{BE} energies of Cu-O bonds were estimated in range 33 to 50 kcal/mol. It is in good agreement with Cu-water bond energies presented in this work. For Cu-NH_3 coordination, the bond energies vary from 50 to 63 kcal/mol. The ΔE^{BE} of Cu-N7(guanine) are approximately twice stronger. This is caused by larger dipole moment of guanine (μ(G) > 7 D) than in case of ammonia ($\mu(NH_3)$ = 1.5 D).

3.3 Partial Charge Analyses

Distribution of electron density was investigated in terms of partial atomic charges calculated with NPA method at the B3LYP/6-311++G(2df,2pd) level. Interesting insight in the examined complexes can be obtained from ***Table 4***, where partial charges of guanine and water atoms are summed together. Spin densities were utilized in the same way. These results demonstrate how the unpaired electron is distributed among considered subsystems. When no hydration is considered, one electron is used for copper cation reduction resulting in [Cu^{1+}guanine^{1+}] system. Increasing number of interacting water molecules from 1 to 5, spin density "moves back" to Cu atom (from 0.02 e to 0.72 e) as the electron transfers to guanine. For all the 4- and higher-coordinated Cu(II)G complexes, the unpaired electron is located on Cu atom resulting in partial charge δ = 1.44 e or spin density ρ_s = 0.7 e. Such a behavior can be explained, when ionization potential (IP) of guanine is compared with electron affinity (EA) of (hydrated) Cu^{2+} cation. IP of isolated guanine (8.8 eV) is more than twice lower than EA of bare Cu^{2+} (20.6 eV), both estimated at B3LYP/6-311++G(2df,2pd) level. It causes that electron moves from guanine to copper. In our previous study[52], EA of hydrated Cu^{2+} cation was predicted to be about 12 eV. This significant decrease of electron affinity leads to stabilization of Cu^{2+} state.

Theoretical study of Martinez[43] investigated neutral, anionic, and cationic copper-guanine and -uracyl complexes without considering hydration. As it was just shown, such simplification leads to incorrect electronic ground state. The work of Lamsabhi[42] suffers the same problem resulting in [Cu^{1+}uracyl^{1+}] system and we have noticed it in our previous works,[46,60] too.

Correct electronic ground states of studied complexes were inspected by plotting the spin densities (ρ_s = 0.005). Complete set of these spin density maps for systems collected in Table 4 is displayed in ***Figure 6***.

Partial charges on selected atoms are compiled in ***Table 5***. It contains a more detailed information necessary to investigate the polarization of guanine, when interacting with hydrated copper(II) cation. Strong dative coordination to copper cation results in polarization in

Table 6: The τ coefficients for the 5-coordinated complexes resolve whether a structure is trigonal bipyramid or octahedral. Abbreviation *c.n.* corresponds to the coordination type and *struct.* is used for exact identification of the optimized structure.

System	c.n.	*struct.*	τ
$[CuG(H_2O)_3]^{2+}$	5^{chel}	*3b*	0.01
$[CuG(H_2O)_4]^{2+}$	5^{chel}	*4g*	0.09
	5^{chel}	*4h*	0.12
	5	*4i*	0.02
$[CuG(H_2O)_5]^{2+}$	5^{chel}	*5g*	0.09
	5^{chel}	*5h*	0.08
	5^{chel}	*5i*	0.16
	5^{chel}	*5j*	0.12
	5^{chel}	*5k*	0.09
	5^{chel}	*5l*	0.07
	5	*5m*	0.19
	5	*5n*	0.16
	5	*5o*	0.20
	5	*5p*	0.20
	5	*5q*	0.16
	5	*5r*	0.24
	5	*5s*	0.00
	5	*5t*	0.19

N7-N9 direction. This clearly follows comparing partial charges of isolated and coordinated guanine. Different electron density distribution occurs in chelate structures. The O6 coordination to Cu cation results in decrease of the oxygen partial charge by about 0.1 e. It is also possible to observe additional polarization of guanine when water molecule associates (forms H-bonded adduct) to various guanine interacting sites (N1/N2, C8, or N9).

The subject of water polarization (when coordinated to Cu(II) cation) was already explored in our previous studies.[50-52]

4. Conclusion

In the present study the hydrated structures of Cu(II)(N7-Guanine) complex were explored. Al the investigated complexes were optimized at the B3PW91/6-31+G(d) level. For selected low-lying local minima on the potential energy surface, several types of energy decompositions were performed together with determination of electronic properties (partial charges, electron spin densities, electrostatic potentials, MO analysis). The B3LYP/6-311++G(2df,2pd) level was chosen for these single-point calculations.

It was found that for system without water molecules or with one water, charge transfer from guanine to Cu(II) occurs resulting in reduced Cu(I) cation and positively charged guanine moiety. Complexes with two aqua ligands represent a borderline systems with largely varying charge (and spin density) localized on guanine. Only when three-coordination on copper was achieved the prevailing electron spin density (more than (0.7) is already localized on copper cation.

Another result following from increasing number of aqua ligands concerns energetic ΔE^{stab} preference of three-aqua Cu-(N7-guanine) structure over diaqua Cu-(N7,O6-guanine) chelate by more than 15 kcal/mol (comparing structure 2b and 3a). A little bit more problematic is comparison of pentacoordinated copper complexes. Nevertheless, from ΔE^{stab} energies of 4i and 3b or 4g and 5d structures, disadvantage of chelate arrangement can be revealed. Similar conclusion can also be drawn from tetraaqua complexes where the largest stabilization energy (either ΔE^{stab} or ΔE^{stab}) was obtained for three coordinated aqua ligands with one water molecule in second solvation shell of Cu(II) cation (cf. structures 4b. Similarly neither pentacoordinated triaqua chelate is more stable. As a consequence of more bulky guanine ligand, it was found that pentacoordination is in these complexes visibly less convenient than in case of small inorganic ligands (either purely aqua ligands[prace a] or mixed aqua-ammine ligands).

Acknowledgement

This study was supported by grant MSM 0021620835 and MŠMT-NSF grant 1P05ME784. The computational resources from Meta-Centra Project as well as computational cluster of Faculty of Mathematics and Physics are acknowledged for access to their excellent computational facilities.

References:

(1) Sigman, J. A.; Kwok, B. C.; Gengenbach, A.; Lu, Y. *J Am. Chem. Soc.* **1999**, *121*, 8949.
(2) Palmer, A. E.; Randall, D. W.; Xu, F.; Solomon, E. I. *J Am. Chem. Soc.* **1999**, *121*, 7138.
(3) Randall, D. W.; Gamelin, D. R.; LaCroix, L. B.; Solomon, E. I. *J. Biol. Inorg. Chem.* **2000**, *5*, 15.
(4) Randall, D. W.; George, S. D.; Hedman, B.; Hodgson, K. O.; Fujisawa, K.; Solomon, E. I. *J. Am. Chem. Soc.* **2000**, *122*, 11620.
(5) Santra, S.; Zhang, P.; Tan, W. *J. Phys. Chem. A* **2000**, *104*, 12021.
(6) Manikandan, P.; Epel, B.; Goldfarb, D. *Inorg. Chem.* **2001**, *40*, 781.
(7) Shimizu, K.; Maeshima, H.; Yoshida, H.; Satsuma, A.; Hattori, T. *Phys. Chem. Chem. Phys.* **2001**, *3*, 862.
(8) Book, L. D.; Arnett, D. C.; Hu, H.; Scherer, N. F. *J. Phys. Chem. A* **1998**, *102*, 4350.
(9) Fraga, E.; Webb, M. A.; Loppnow, G. R. *J. Phys. Chem.* **1996**, *100*, 3278.
(10) Holland, A. W.; Bergman, R. G. *J. Am. Chem. Soc.* **2002**, *124*, 9010.
(11) Holland, P. L.; Tolman, W. B. *J Am Chem. Soc.* **1999**, *121*, 7270.
(12) Taylor, M. K.; Stevenson, D. E.; Berlouis, L. E. A.; Kennedy, A. R.; Reglinski, J. *J. Innorg. Biochem.* **2005**, *100*, 250.
(13) Wang, X.; Berry, S. M.; Xia, Y.; Lu, Y. *J. Am. Chem. Soc.* **1999**, *121*, 7449.
(14) Meggers, E.; Holland, P. L.; Tolman, W. B.; Romesberg, F. E.; Schultz, P. G. *J. Am. Chem. Soc.* **2000**, *122*, 10714.
(15) Sabolovic, J.; Liedl, K. R. *J. Am. Chem. Soc.* **1999**.

(16) Sabolovic, J.; Tautermann, C. S.; Loerting, T.; Liedl, K. R. *Inorg. Chem.* **2003**, *42*, 2268.
(17) Katz, A.; Shimoni-Livny, L.; Navon, O.; Navon, N.; Bock, C.; Glusker, J. *Helv. Chim. Acta* **2003**, *86*, 1320
(18) Rulíšek, L. *Chemicke Listy* **2002**, *96*, 132.
(19) Rulíšek, L.; Havlas, Z. *J. Am. Chem. Soc.* **2000**, *122*, 10428.
(20) Rulíšek, L.; Havlas, Z. *J. Phys. Chem. A* **2002**, *106*, 3855.
(21) Rulíšek, L.; Havlas, Z. *J. Phys. Chem. B* **2003**, *107*, 2376.
(22) Bertran, J.; Rodrigues-Santiago, L.; Sodupe, M. *J. Phys. Chem. B* **1999**, *103*, 2310.
(23) Shoeib, T.; Rodriquez, C. F.; Siu, K. W. M.; Hopkinson, A. C. *Phys. Chem. Chem. Phys.* **2001**, *3*, 853.
(24) Caraiman, D.; Shoeib, T.; Siu, K.; Hopkinson, A.; Bohme, D. *Int. J. Mass Spectrom.* **2003**, *228*, 629.
(25) Olsson, M. H. M.; Hong, G. Y.; Warshel, A. *J. Am. Chem. Soc.* **2003**, *125*, 5025.
(26) Olsson, M. H. M.; Ryde, U. *J. Biol. Inorg. Chem.* **1999**, *4*, 654.
(27) Olsson, M. H. M.; Ryde, U.; Roos, B. O.; Pierloot, K. *J. Biol. Inorg. Chem.* **1998**, *3*, 109.
(28) Warshel, A. *Computer Modeling of Chemical Reactions in Enzymes and Solutions*; John Wiley & Sons, Ltd.: New York, 1991.
(29) Prabhakar, R.; Siegbahn, P. E. M. *J. Phys. Chem. B* **2003**, *107*, 3944.
(30) Siegbahn. Electronic Structure Calculations for Molecules Containing Transition Metals. In *Advances in Chemical Physics, Volume XCIII*; Prigogine, I., Rice, S. A., Eds.; John Wilet & Sons, Ltd., 1996; Vol. XCIII; pp 333.
(31) Hackl, E. V.; Kornilova, S. V.; Kapinos, L. E.; Andruschenko, V. V.; Galkin, V. L.; Grigoriev, D. N.; Blagoi, Y. P. *J. Molec. Struct.* **1997**, *408*, 229.
(32) Prenesti, E.; Daniele, P. G.; Berto, S.; Toso, S. *Polyhedron* **2006**, *25*, 2815.
(33) Hemmert, C.; Pitie, M.; Renz, M.; Gornitzka, H.; Soulet, S.; Meunier, B. *J. Biol. Inorg. Chem.* **2001**, *6*, 14.
(34) Blazic, B.; et.al. *J. Innorg. Biochem.* **1993**, *51*, 737.
(35) Murata, M.; Kawanishi, S. *Carcinogenesis* **2002**, *23*, 855.
(36) Liu, J.; Lu, T. B.; Deng, H.; Ji, L. N.; Qu, L. H.; Zhou, H. *Transition Metal Chemistry* **2003**, *28*, 116.
(37) Atwell, S.; Meggers, E.; Spraggon, G.; Schultz, P. G. *J. Am. Chem. Soc.* **2001**, *123*, 12364.
(38) Schoentjes, B.; Lehn, J.-M. *Helv. Chim. Acta* **1995**, *78*, 1.
(39) Li, L.; Murthy, N. N.; Telser, J.; Zakharov, L. N.; Yap, G. P. A.; Rheingold, A. L.; Karlin, K. D.; Rokita, S. E. *Inorganic Chemistry* **2006**, *45*, 9145.
(40) Herrero, L. A.; Terron, A. *J. Biol. Inorg. Chem.* **2000**, *5*, 269.
(41) Mojzes, P.; Kruglik, S. G.; Baumruk, V.; Turpin, P. Y. *Journal of Physical Chemistry B* **2003**, *107*, 7532.
(42) Lamsabhi, A.; Alcami, M.; Mo, O.; Yanez, M.; Tortajada, J. *ChemPhysChem* **2004**, *5*, 1871.
(43) Martinez, A. *J. Chem. Phys.* **2005**, *123*, 024311.
(44) Gasowska, A.; Lomozik, L. *Monatshefte fur Chemie* **1995**, *126*, 13.
(45) Borowka, J.; van Wullen, C. *Journal of Organometallic Chemistry* **2006**, *691*, 4474.
(46) Burda, J. V.; Šponer, J.; Hobza, P. *J. Phys. Chem.* **1996**, *100*, 7250.
(47) Šponer, J.; Sabat, M.; Burda, J.; Leszczynski, J.; Hobza, P.; Lippert, B. *J. Biol. Inorg. Chem.* **1999**, *4*, 537.
(48) Rulíšek, L.; Šponer, J. *Journal of Physical Chemistry B* **2003**, *106*, 1913.
(49) Blomberg, L. M.; Blomberg, M. R. A.; Siegbahn, P. E. M. *Biochimica Et Biophysica Acta-Bioenergetics* **2006**, *1757*, 240.
(50) Burda, J. V.; Pavelka, M.; Šimánek, M. *J. Molec. Struct.* **2004**, *683*, 183.
(51) Pavelka, M.; Burda, J. V. *Chem. Phys.* **2005**, *312*, 193.
(52) Pavelka, M.; Šimánek, M.; Šponer, J.; Burda, J. V. *J. Phys. Chem. A* **2006**, *110*, 4795.
(53) Burda, J. V.; Shukla, M. K.; Leszczynski, J. *J. Mol. Model.* **2005**, xxxx, xxx.
(54) Reed, A. E.; Weinstock, R. B.; Weinhold, F. *J. Chem. Phys.* **1985**, *83*, 735.
(55) M. J. Frisch, G. W. T., H. B. Schlegel, G. E. Scuseria, M.; A. Robb, J. R. C., V. G. Zakrzewski, J. A. Montgomery, Jr., R. E. Stratmann, J. C.; Burant, S. D., J. M. Millam, A. D. Daniels, K. N. Kudin, M. C. Strain, O. Farkas, J.; Tomasi, V. B., M. Cossi, R. Cammi, B. Mennucci, C. Pomelli, C. Adamo, S. Clifford, J.; Ochterski, G. A. P., P. Y. Ayala, Q. Cui, K. Morokuma, P. Salvador, J. J. Dannenberg,; D. K. Malick, A. D. R., K. Raghavachari, J. B. Foresman, J. Cioslowski, J. V. Ortiz, A.; G. Baboul, B. B. S., G. Liu, A. Liashenko, P. Piskorz, I. Komaromi, R. Gomperts, R. L.; Martin, D. J. F., T. Keith, M. A. Al-Laham, C. Y. Peng, A. Nanayakkara, M. Challacombe, ; P. M. W. Gill, B. J., W. Chen, M. W. Wong, J. L. Andres, C. Gonzalez, M.; Head-Gordon, E. S. R., and J. A. Pople,. Program Gaussian 98; Revision A.1x ed.; Gaussian, Inc.: Pittsburgh PA, 2001.
(56) Weinhold, F. NBO 5.0 Program 5.0 ed.; University of Wisconsin, Madison, Wisconsin 53706: Wisconsin, 2001.
(57) Schaftenaar, G. Molden. In *http://www.cmbi.kun.nl/~schaft/molden/molden.html*; 3.9 ed.
(58) Portmann, S.; Lüthi, H. P. *Chimia* **2000**, *54*, 766.
(59) Saenger, W. *Springer advanced texts in chemistry* **1984**, *82*, 19445.
(60) Burda, J. V.; Šponer, J.; Leszczynski, J.; Hobza, P. *J. Phys. Chem. B* **1997**, *101*, 9670.

The DFT Calculations of Valence Tautomer Equilibrium of $[(L)Cu^{n+}(Q)^{n-}]$ (L=mtq or mmb, n=1 or 2, Q=Quinone) Complexes

Matěj Pavelka[a,b], Biprajit Sarkar[c], Wolfgang Kaim[c]* and Stanislav Záliš[a]*

[a] *J. Heyrovský Institute of Physical Chemistry, Academy of Sciences of the Czech Republic, Dolejškova 3, CZ-18223 Prague, Czech Republic*

[b] *Department of Chemical Physics and Optics, Faculty of Mathematics and Physics Charles University in Prague, Ke Karlovu 3, CZ-12116 Prague, Czech Republic*

[c] *Institut für Anorganische Chemie, Universität Stuttgart, Pfaffenwaldring 55, D-70550 Stuttgart, Germany*

Abstract

The geometry of complexes $[(L)Cu^{n+}(Q)^{n-}]$, L = (mtq - 8-methylthioquinoline or mmb - 1-methyl-2- (methylthiomethyl)-1 benzimidazole) and Q=2-methyl-o-quinone was fully optimized using DFT methodology in vacuo and in solvent modeled by conductor-like polarizable continuum model (CPCM). For both complexes two types of energy minima were found using CPCM model calculations: pseudo–planar structure corresponding to the spin density localized predominantly at Cu atom and pseudo–tetrahedral with spin density localized at quinone ligand. Pseudo–tetrahedral conformers were slightly lower in energy. As indicated by the transition energy search, potential energy surfaces were rather flat. The calculated free energy barriers with respect to the lower energy conformers were around 5 kcal/mol and 4 kcal/mol for mmb and mtq complexes, respectively. The calculated EPR anisotropic g-tensors reflect the differences in electron density redistribution in agreement with the experiment.

Introduction

Intramolecular metal-to–ligand electron transfer equilibria have been observed in complexes containing quinoide ligands and various central atoms.[1,2] Equilibrium according to eq. (1) was observed in a narrow temperature range for copper complexes.[3] The temperature-dependent intramolecular metal/ligand electron transfer equilibrium has been quantitatively analyzed by EPR as a function of the non-innocent o-quinonoid ligand Q and of the co-ligand L.[4] The following study[5] of temperature dependent EPR spectra found the variation of g-tensor. Anisotropic g-tensor corresponding to Cu^{II}/catecholate varied to isotropic g-factor close to free electron value, which indicates the electron density localization at semiquinone ligand in Cu^{I}/semiquinone form. The knowledge of the mechanism of valence – tautomer equilibria can help in understanding of some bio relevant processes (e.g. copper dependent amine oxidases).[6] This phenomena has also been discussed with respect to applications in molecular electronics [7-10] where the change of redox states should be potentially utilized for construction of molecular switches.

(1) $$[(L)Cu^{II}(Q^{2-})] \Longleftrightarrow [(L)Cu^{I}(Q^{-})]$$

The reorganization of the electron density in the molecule should be accompanied by the geometry change from closely planar to closely tetrahedral depending on the oxidation state of the central Cu atom and reflected by the corresponding properties e.g. EPR g anisotropic couplings.[6] Individual valence isomers were not isolated and the experimental structures are not known. Therefore

Figure 1: G03/B3LYP/CPCM (toluene) optimized structures of [(mmb)Cu(Q)] complex, *a)* pseudo-planar form, *b)* pseudo-tetrahedral form. The plane of mmb ligand is distorted and longer Cu-C distance of tetrahedral configuration corresponds to C atom facing up.

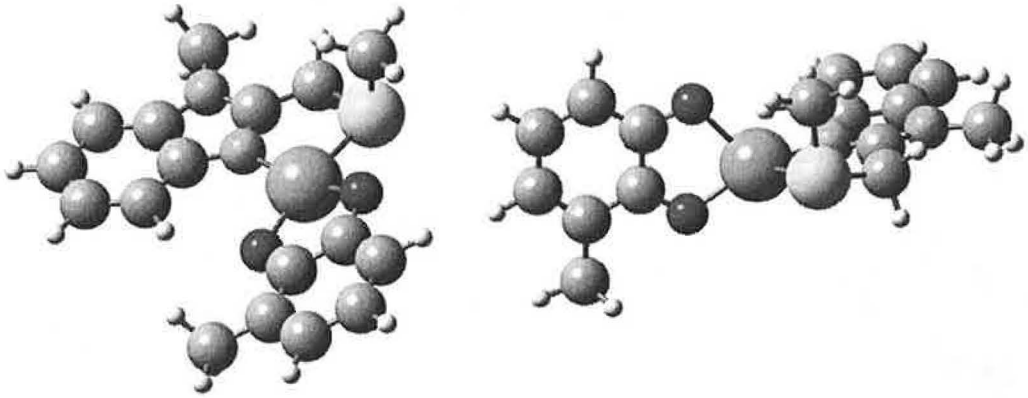

a) *b)*

the geometry optimization using quantum chemical calculations can point out the stable structures corresponding to the energy minima and the barriers between these minima.

Calculations

Due to the size of the system the model system in which the isobutyl substituents on Q ligands were replaced by methyl group without other substituents. Ground state electronic structure calculations on these model complexes have been performed at the density-functional theory (DFT) level using the Gaussian 03[11] and ADF2006.1 [12,13] program packages.

Within the Gaussian-03 program, 6-31+G* polarized double-ζ basis sets were used for H, C N and S atoms. The Cu atom was described by Christiansen's Averaged Relativistic Effective Pseudopotential (AREP),[14] and copper double-ζ basis was extended by a set of diffuse functions: α_s =0.025, α_p=0.35, and α_d=0.07 and polarization function α_f=3.75.[15,16] Becke's hybrid three parameter functional with the Lee, Yang and Parr correlation functional (B3LYP) [17] was used in G03 (G03/B3LYP). The solvent was described by the conductor-like polarizable continuum model (CPCM).[18]

Within the ADF program, Slater-type orbital (STO) basis sets of triple-ζ quality with additional polarization functions were employed. The inner shells were

Table 1: Selected G03/B3LYP calculated bond lengths [Å] and angles [°] for [(L)Cu(Q)] complexes in vacuo.

	L=mmb		L=mtq	
	planar[a]	tetrahedral[a]	planar	tetrahedral
Cu-O1	1.868	1.957	ss1.872	2.076
Cu-O2	1.881	2.471	1.896	2.023
Cu-S	2.592	3.037	2.449	2.412
Cu-N	2.053	2.058	2.020	2.013
O1-C1	1.337	1.279	1.352	1.285
O2-C2	1.335	1.241	1.354	1.287
O1-Cu-O2	89.5	75.2	89.0	82.1
S-Cu-N	79.7	73.2	84.1	86.3
O1-Cu-S	89.1	127.1	91.0	108.0
O1-Cu-N	162.4	156.9	165.9	126.9
O2-Cu-S	175.0	86.1	179.9	130.0
O2-Cu-N	100.8	121.2	95.9	127.2
C1-O1-Cu-S	-174.7	-130.1	177.0	130.3
tilt OCuO/SCuN	14.4	66.1	13.1	78.4

[a]UHF calculations

Table 2: Selected G03/B3LYP/CPCM (toluene) calculated bond lengths [Å] and angles [°] for [(L)Cu(Q)] in solvent CPCM model.

	L=mmb			L=mtq		
	planar	TS	tetrahedral	planar	TS	tetrahedral
Cu-O1	1.892	1.932	2.194	1.886	1.954	2.076
Cu-O2	1.914	1.961	1.979	1.906	1.972	2.041
Cu-S	2.457	2.475	2.750	2.408	2.395	2.381
Cu-N	2.000	1.995	1.948	2.023	2.019	2.025
O1-C1	1.350	1.330	1.280	1.354	1.323	1.288
O2-C2	1.349	1.327	1.289	1.353	1.321	1.288
O1-Cu-O2	88.1	86.3	80.4	88.5	85.5	81.6
S-Cu-N	83.6	83.7	80.9	84.5	85.9	86.7
O1-Cu-S	90.2	94.8	98.4	92.7	100.2	117.3
O1-Cu-N	163.8	155.7	123.8	169.6	151.6	124.1
O2-Cu-S	168.4	155.0	114.3	173.1	152.3	123.7
O2-Cu-N	100.8	105.2	150.7	95.5	101.9	127.9
C1-O1-Cu-S	-167.4	-153.5	-113.7	172.0	151.8	124.0
tilt OCuO/SCuN	19.6	35.7	84.1	12.4	41.7	88.9

represented by frozen core approximation (1s for C, N atoms, 1s-2p for S and 1s-2p for Cu were kept frozen). The density functional with local density approximation (LDA) and with VWN parametrization was used (ADF/BP), where Becke's gradient correction[19] to the local exchange expression is included in conjunction with Perdew's gradient correction[20] to the LDA correlation.

For the fully optimized structures, the EPR g-tensors were calculated. Moreover, the charge and spin density distribution was analyzed using NPA method[21]. Due to the convergence problems, the correct wave function was constructed in minimal basis set with Restricted Open Shell Hartree-Fock (ROHF) procedure first. Then the correct occupation was used in bigger basis *6-31+G(d)* and the UHF geometry optimization was performed. Finally, DFT re-optimization was done using B3LYP functional.

Results and Discussion

The geometry optimizations of valence tautomers defined by eq. (1) have been performed for both complexes in vacuo and in solution using the CPCM model. In vacuo calculated structural parameters are listed in ***Table 1***. The G03/B3LYP method in vacuo was employed in order to obtain Gibbs free energy profiles describing the valence-structure tautomerism (pseudo-planar ↔ pseudo-tetrahedral). Two minima corresponding to pseudo–planar and pseudo–tetrahedral forms were found only for the [(mtq)Cu(Q)] complex. In the case of [(mmb)Cu(Q)] compound, the DFT calculations in vacuo led to only one stable minima, the pseudo–tetrahedral structure. However, UHF method gives also the pseudo-planar minima. Unfortunately, optimizations in vacuo were not able to give transition state structures neither for mtq nor mmb complex. DFT calculations in vacuo indicate flat potential energy surfaces with either zero or very low rotation barrier. In order to compare energetics of both systems single point G03/B3LYP calculations were performed at UHF optimized geometries of [(mmb)Cu(Q)] complex. Relative energies of pseudo – planar and pseudo – tetrahedral forms are depicted in ***Figure 3*** for both examined systems (with mtq and mmb ligand).

The insertion of studied molecules into the solvent cavity stabilizes energy minima and enlarges rotational barriers. Two stable forms were found by B3LYP/CPCM calculations for both mmb and mtq complexes. Optimized structures of pseudo–planar and pseudo–tetrahedral forms

Figure 2: G03/B3LYP/CPCM (toluene) optimized structures of [(mtq)Cu(Q)] complex, ***a)*** pseudo-planar form, ***b)*** pseudo-tetrahedral form.

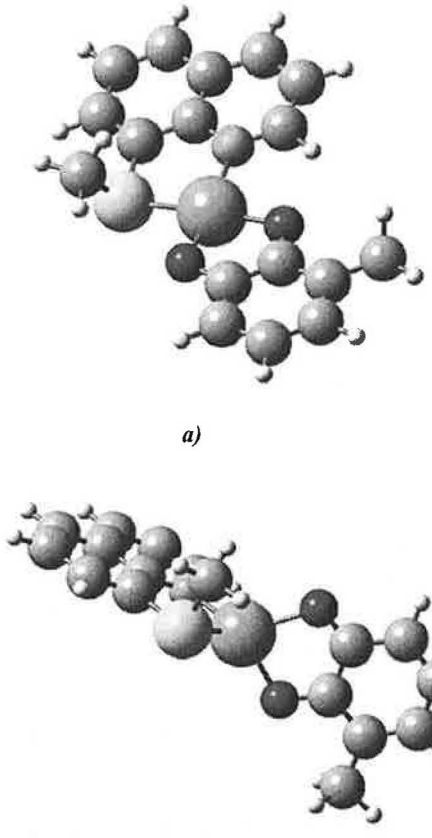

a)

b)

Figure 3: G03/B3LYP in vacuo calculated relative energy profiles for [(mmb)Cu(Q)] and [(mtq)Cu(Q)] complexes. Drawings schematically represent rotations of ligand L plane towards quinone plane (along dashed axis). Energies are in kcal/mol.

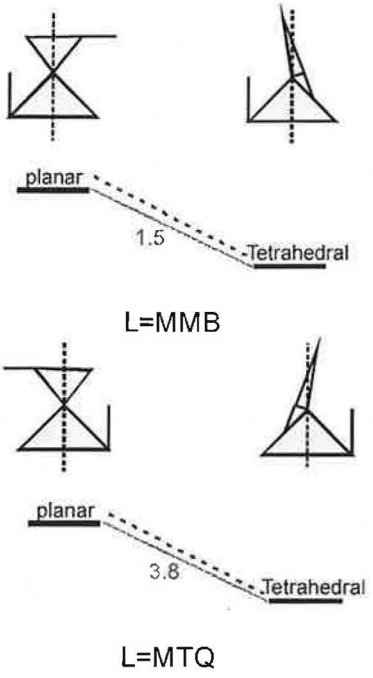

are depicted in ***Figures 1*** and ***2***. The calculated structural parameters are summarized in ***Table 2***. Gibbs energy profiles in solution presented in ***Figure 4*** indicate the existence of the energy barriers which separate minima, and thus confirm valence-structure tautomerism in both mmb and mtq complexes. Due to the asymmetry of studied ligands (mtq, mmb, and also quinone ligand), two minima for each type of conformer were considered and optimized. ***Table 2*** summarizes the structural changes connected with the valence tautomerism. The largest distance changes accompanied the pseudo–planar to pseudo–tetrahedral variation can be observed for Cu-O and Cu-S bonds. In the case of [(mmb)Cu(Q)] complex, a very distorted tetrahedron with different Cu – O (2.194 Å and 1.979 Å) distances are observed. The calculations for pseudo–tetrahedral form revealed the very long Cu-S bond, which indicates the change of Cu coordination in the course of the geometry transformation. Such change was not observed in the [(mtq)Cu(Q)] complex, where the Cu-S bond length does dot vary substantially (from 2.408 Å to 2.381 Å). The Cu-O distances are prolonged by 0.19 Å and 0.135 Å, when going from pseudo–planar to pseudo–tetrahedral form. In the both complexes, the structure of quinone is strongly influenced by the tautomeric change. The structure changes point to the catecholate – semiquinone transformation. Tilt OCuO/SCuN angles listed in Table 2 indicate for both complexes the deviation of real optimised structures from idealized planar or tetrahedral geometry.

The spin densities for the [(mmb)Cu(Q)] and [(mtq)Cu(Q)] complexes are shown in ***Figures 5*** and ***6***. In pseudo–

Figure 4: G03/B3LYP/CPCM (toluene) calculated Gibbs free energy profiles for the [(mmb)Cu(Q)] and [(mtq)Cu(Q)] complexes. Drawings schematically represent rotations of ligand L plane towards quinone plane (along dashed axis), while mutual orientation of methyl group on ligands is considered. Free energies are in kcal/mol.

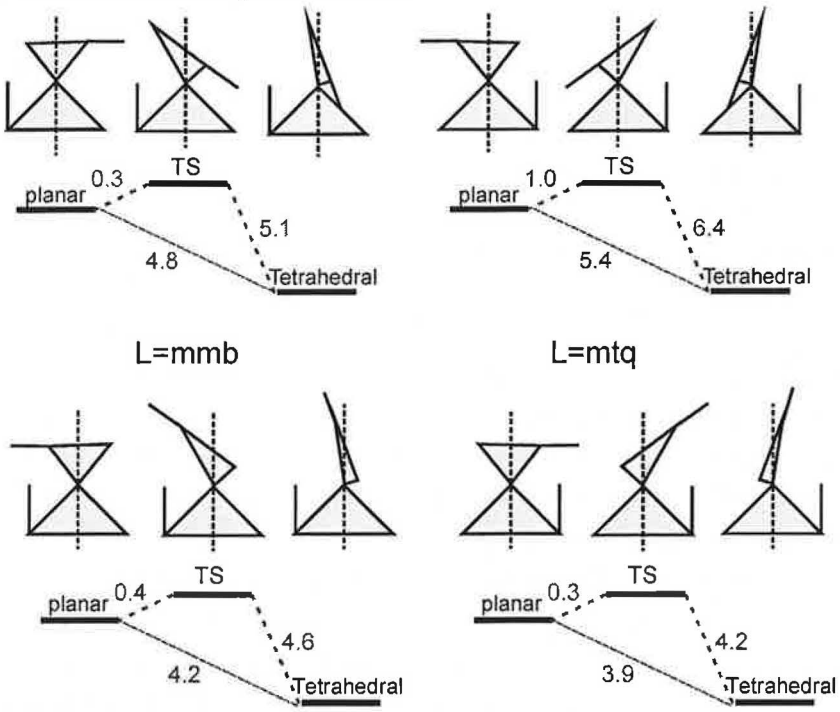

planar forms of both complexes, the spin density is located at central Cu atom and adjacent sigma coordination bonds. Calculated spin densities at Cu atoms are 0.552 and 0.559 for mmb and mtq complexes, respectively. The NPA partial atomic charges at Cu atoms are around 1.25 for the both complexes. The change in the geometry causes the reorganization of spin density, the intramolecular charge-transfer. ***Figures 5*** and ***6*** demonstrate that the spin density is located at π-system of semiquinone ligand (0.95 for mmb and 0.96 for mtq) and negligible spin density at Cu atom in the pseudo–tetrahedral form.

For both complexes, temperature dependent EPR spectra

Figure 5: G03/B3LYP/CPCM (toluene) spin densities for [(mtq)Cu(Q)] complex, ***a)*** pseudo-planar form, ***b)*** pseudo-tetrahedral form.

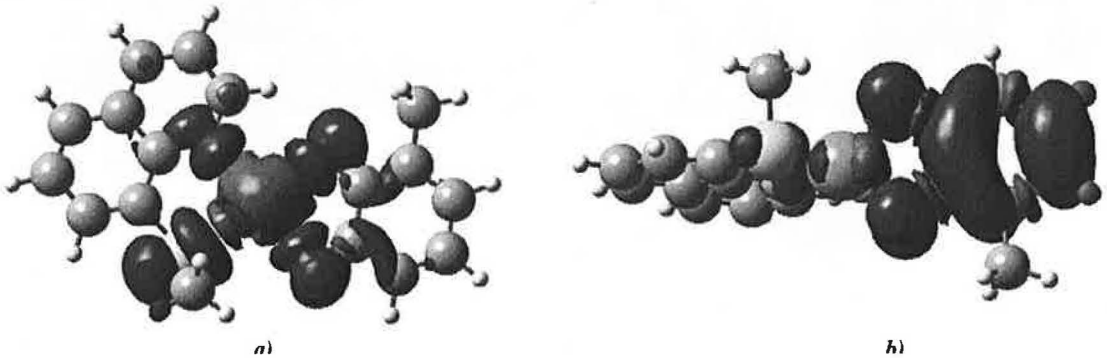

a) *b)*

were measured. At low temperature, the [(mmb)Cu(Q)] complex exhibits Cu^{II} features with anisotropic g-values g_1=2.248 and g_{23}=2.058. [4] The DFT calculated g-values for pseudo–planar [(mmb)Cu^{II}(Q)] (g_z=2.127, g_y=2.046 and g_x=2.034) correspond reasonably well to the experimental values. At temperatures above 250 K, the Cu^{II} EPR spectrum is replaced by an isotropic Cu^{I}/semiquinone signal at g_{iso}=2.005. The DFT calculated g-values for pseudo–tetrahedral reflect this change (g_z=2.022, g_y=2.000 and g_x=2.008). Analogical situation is observed in the case of the [(mtq)Cu(Q)] complex. Here the calculated g-values for pseudo–planar [(mtq)Cu^{II}(Q)] g_z=2.123, g_y=2.040 and g_x=2.035 describe the experimental EPR spectrum of Cu^{II}/catecholate form with g_1=2.160 and g_{23}=2.036.[5] The calculations also reproduce the change of Cu^{I}/semiquinone EPR spectrum, where g-values g_z=2.028, g_y=2.001 and g_x=2.011 correspond to the experimental isotropic g-factor g_{iso}=2.005.

Conclusions

The DFT calculations using CPCM model on [(L)Cu(Q)] (L=mmb, mtq) complexes located possible energy minima on potential energy surface corresponding to pseudo–planar to pseudo–tetrahedral forms. Transition state structures connecting individual minima were found too. Solvent effect diminishes the energy difference between conformers and enlarged energy barriers in comparison with in vacuo calculations. In vacuo two types of valence tautomers were found for the [(mtq)Cu(Q)] system only. The pseudo–tetrahedral conformers exhibit slightly larger stability than pseudo-planar forms. The variation of mtq vs. mmb ligands influenced the energy difference between individual forms. The calculated structural parameters indicate the Cu^{II}/catecholate to Cu^{I}/semiquinone transformation ongoing from pseudo–planar to pseudo–tetrahedral form. The electron density redistribution occurred due to described geometry variation in agreement with experimental findings. The change of character of calculated EPR g-tensors well reproduces the observations from EPR experiment.

Temperature dependent EPR measurements indicate slightly lower energy of pseudo-planar conformers. The disagreement can be coursed by the difference between model and real systems, calculations on larger systems with Q model ligands more close to experimental structure are in the progress.

Figure 6: G03/B3LYP/CPCM (toluene) spin densities for [(mtq)Cu(Q)] complex, ***a)*** pseudo-planar form, ***b)*** pseudo-tetrahedral form.

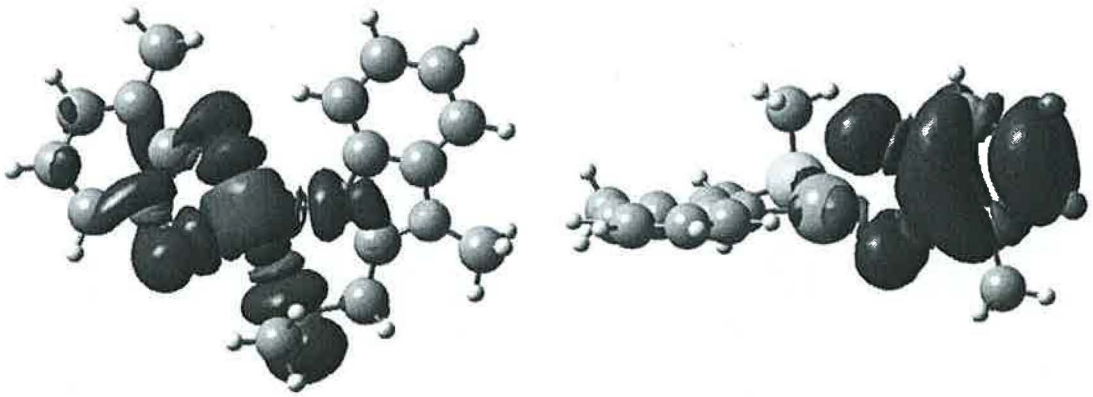

a) ***b)***

Acknowledgement

Support from the DFG, EU (COST action D35, also supported by the Ministry of Education of the Czech Republic - grant No. OC 139) and financial support by the HPC Europa and the Grant Agency of the Academy of Sciences of the Czech Republic (S.Z., grant 1ET400400413) is gratefully acknowledged.

References

1.a) C.G. Pierpont, C.W.Lange, Progr. Inorg. Chem. **1994**, *41*, 331.

b) C.G. Pierpont, Coord. Chem. Rev. **2001**, *216*, 99.

2. J. Rall, E. Waldhör, B. Schwederski, M. Schwach, S.Kohlmann, W. Kaim, in: Bioinorganic Chemistry: Transition Metals in Biology and their Coordination Chemistry, (Ed.: A.X. Trautwein), Wiley-VCH, Weinheim, **1997**, 476.

3. J. Rall, M. Wanner, M. Albrecht, F.M. Hornung, W. Kaim,, Chem. Eur. J. 5 **1999**, 2802.

4. W. Kaim, M. Wanner, A. Knodler and S. Zalis, Inorg. Chim. Acta 337 **2002**, 163.

5. S. Ye, B. Sarkar, M. Niemeyer, W. Kaim, Eur. J. Inorg. Chem. **2005**, 4735.

6. M. Mure, Acc. Chem. Res. **2004**, *37*, 131.

7. A. Dei, D. Gatteschi, C. Sangregorio, L. Sorace, *Acc. Chem. Res.* **2004**, *37*, 827;

8. H. Ohtsu, K. Tanaka, *Angew. Chem. Int. Ed.* **2004**, *43*, 6301.

9. O. Kahn, J. P. Launay, *Chemtronics* **1998**, *3*, 140.

10. G. Speier, Z. Tyeklár, P. Töth, E. Speier, S. Tisza, A. Rockenbauer, A. M. Whalen, N. Alkire, C. G. Pierpont, *Inorg. Chem.* **2001**, *40*, 5653;

11. M. J. Frisch, G. W. Trucks, H. B. Schlegel, G. E. Scuseria, M. A. Robb, J. R. Cheeseman, J. A. Montgomery, Jr., T. Vreven, K. N. Kudin, J. C. Burant, J. M. Millam, S. S. Iyengar, J. Tomasi, V. Barone, B. Mennucci, M. Cossi, G. Scalmani, N. Rega, G. A. Petersson, H. Nakatsuji, M. Hada, M. Ehara, K. Toyota, R. Fukuda, J. Hasegawa, M. Ishida, T. Nakajima, Y. Honda, O. Kitao, H. Nakai, M. Klene, X. Li, J. E. Knox, H. P. Hratchian, J. B. Cross, C. Adamo, J. Jaramillo, R. Gomperts, R. E. Stratmann, O. Yazyev, A. J. Austin, R. Cammi, C. Pomelli, J. W. Ochterski, P. Y. Ayala, K. Morokuma, G. A. Voth, P. Salvador, J. J. Dannenberg, V. G. Zakrzewski, S. Dapprich, A. D. Daniels, M. C. Strain, O. Farkas, D. K. Malick, A. D. Rabuck, K. Raghavachari, J. B. Foresman, J. V. Ortiz, Q. Cui, A. G. Baboul, S. Clifford, J. Cioslowski, B. B. Stefanov, G. Liu, A. Liashenko, P. Piskorz, I. Komaromi, R. L. Martin, D. J. Fox, T. Keith, M. A. Al-Laham, C. Y. Peng, A. Nanayakkara, M. Challacombe, P. M. W. Gill, B. Johnson, W. Chen, M. W. Wong, C. Gonzalez, and J. A. Pople, *Gaussian 03, Revision C.02*; Gaussian, Inc., Wallingford CT, **2004**.

12. te Velde, G.; Bickelhaupt, F. M.; van Gisbergen, S. J. A.; Fonseca Guerra, C.; Baerends, E. J.; Snijders, J. G.; Ziegler, T. *J. Comput. Chem.* **2001**, *22*, 931.

13. ADF2005.01, SCM, Theoretical Chemistry, Vrije Universiteit, Amsterdam, The Netherlands, http://www.scm.com

14 Hurley, M. M.; Pacios, L. F.; Christiansen, P. A.; Ross, R. B.; Ermler, W. C. *J. Chem. Phys.* **1986**, *84*, 6840.

15. Burda, J. V.; Pavelka, M.; Simanek, M. *J. Molec. Struct.* **2004**, *683*, 183.

16. Pavelka, M.; Burda, J. V. *Chem. Phys.* **2005**, *312*, 193.

17. Becke A. D. *J. Chem. Phys.* **1993**, 98, 5648

18. Cossi, M.; Rega, N.; Scalmani, G.; Barone, V., *J. Comput. Chem.* **2003**, *24*, 669.

19. Becke, A. D. *Phys. Rev. A* **1988**, *38*, 3098.

20. Perdew, J. P. *Phys. Rev. B* **1986**, *33*, 8822

21. Reed, A. E.; Weinstock, R. B.; Weinhold, F. *J. Chem. Phys.* **1985**, *83*, 735.

J Mol Model
DOI 10.1007/s00894-006-0151-x

ORIGINAL PAPER

Pt-bridges in various single-strand and double-helix DNA sequences. DFT and MP2 study of the cisplatin coordination with guanine, adenine, and cytosine

Matěj Pavelka · Jaroslav V. Burda

Received: 28 December 2005 / Accepted: 23 June 2006

Abstract In this study, various platinum cross-links in DNA bases were explored. Some of these structures occur in many *cis/trans*-platinated double-helixes or single-stranded adducts. However, in the models studied, no steric hindrance from sugar-phosphate backbone or other surroundings is considered. Such restrictions can change the bonding picture partially but hopefully the basic energy characteristics will not be changed substantially. The optimization of the structures explored was performed at the DFT level with the B3LYP functional and the 6-31G(d) basis set. Perturbation theory at the MP2/6-31++G(2df,2pd) level was used for the single-point energy and 6-31+G(d) basis set for the electron-property analyses. It was found that the most stable structures are the diguanine complexes followed by guanine-cytosine Pt-cross-links, ca 5 kcal mol^{-1} less stable. The adenine-containing complexes are about 15 kcal mol^{-1} below the stability of diguanine structures. This stability order was also confirmed by the BE of Pt–N bonds. For a detailed view on dative and electrostatic contributions to Pt–N bonds, Natural Population Analysis, determination of electrostatic potentials, and canonical Molecular Orbitals description of the examined systems were used.

Keywords *Cis*platin crosslinks · DFT calculations · MP2 calculations · DNA bases · Stabilization energy

Proceedings of "Modeling Interactions in Biomolecules II", Prague, September 5th–9th, 2005.

M. Pavelka · J. V. Burda (✉)
Faculty of Mathematics and Physics,
Department of Chemical Physics and Optics, Charles University,
Ke Karlovu 3,
121 16 Prague 2, Czech Republic
e-mail: Burda@karlov.mff.cuni.cz

Introduction

Platinum complexes represent one of the very promising classes for antitumor treatment since Rosenberg's [1] discovery. Many platinum compounds involving both Pt (II) and Pt(IV) have been examined since. Oncological in vivo research is supported by many in vitro experiments on oligo—and polynucleotides, see e.g. [2–10] Some more detailed insight into the physico-chemical description can also be achieved by computational techniques, which reveal structural and bonding relations in platinum complexes. Because of its high toxicity and resistance of tumor cells to *cis*platin when administered repeatedly, the applicability and properties of many derivatives of *cis*platin have been explored. In this way, second- and later third-generation drugs (like carboplatin, oxaliplatin, Pt(IV) complex JM216 or trinuclear BBR 3464) were discovered. At present, *cis*platin and carboplatin belong to the most often used drugs [11]. The final DNA adduct of both (and some other platinum drugs, too) includes the same *cis*-$[Pt(NH_3)_2$-1,2–d {GpG}$]^{2+}$ fragment. These adducts cause a roll of 25–50° between the guanine bases involved in the cross-link and a global bend of the helix axis towards the major groove of about 20–40° [12–16]. The molecular structure of this complex was solved by the Dickerson group at high resolution (2.6 Å) [17]. A similar structure, which also contains the *cis*platin G–Pt–G bridge [12], was measured with the same resolution. The distortion of DNA under the influence of *cis*platin was found by Lilley [18]. The structure of the interstrand *cis*platin bridge was published in Ref. [19] and the cross-linked adduct of oxaliplatin with 1,2–d(GpG) intrastrand bases of the DNA oligomer was studied by the Lippard's group [20]. Afterwards, some other platinum complexes were crystallized and described [21, 22]. The ternary complex of a DNA oligomer with

*cis*platin and HMG-protein was prepared and its crystal structure was solved and reported [23, 24].

Six-coordinated platinum(IV) complexes have also been explored extensively recently [25–29]. These complexes are relatively stable and can be passed through the digestive tract. After absorption into the bloodstream, they are metabolized and reduced to four-coordinated *cis*platin analogues [30]. Recent reviews of Wong [31] and Reedijk [32] summarize the current state of platinum-drug treatment. Another study of Reedijk deals with competition between S-donor ligands and DNA [33]. The interstrand cross-linked binding of DNA bases with *trans*platin complexes was studied in detail by Brabec [34]. Quaternary platinum complexes in solution were explored by Sigel and Lippert [35]. Various conformers of the *cis*platin adduct with d(GpG) were examined by the Marzilli group [36], where the phosphodiester backbone conformation was also discussed. In this study, they combined several experimental tools (NMR (^{1}H and ^{31}P), CD spectroscopy) with simulation based on molecular mechanics (MM) and molecular dynamics (MD).

*Cis*platin can also form interstrand cross-links as a minor adduct [37, 38] where complementary cytosines are extruded from the double helix. This link bends the helix axis towards the minor groove by 30–50° and unwinds the duplex by more than 80°. The formation of the interstrand platinum bridges can be as fast as the formation of intrastrand cross-links for short DNA oligomers [39–41]. The interstrand *cis*platin cross-links are unstable under physiological conditions [42], leading to monofunctional adducts. The difference between the interstrand and intrastrand Pt-bridges can be distinguished through the mutual orientation of the guanine bases. While intrastrand Pt-complexes contain a head-to-head orientation, in interstrand complexes *cis*platin usually forms a head-to-tail orientation of the bases.

In the *trans*platin case, the formation of the monofunctional adduct takes about 2–3 h, similarly to the *cis*platin complex [43]. The *trans*platin complexes evolve slowly (T_{12}=40 h) and interstrand cross-links between guanine and complementary cytosine residues are formed [44]. 2D-NMR confirms the *trans*-[Pt(NH_3)$_2$(N7-guanine)(N3-cytosine)]$^{2+}$ structure with guanine in the syn-conformation [45]. However, the formation of 1,3- and longer intrastrand platinum cross-links was described in another study [40]. Similar Pt-bridges were found in single-stranded DNA chains where sequences GXG also occur. However, such 1,3–d(GpXpG) bridges are not stable. When a cytosine base is in the adjacent position to the 5′-end guanine, a new cross-link 1,4-d(CpGpXpG) can be formed and equilibrium between these two structures is attained [46, 47]. The same instability was also observed in DNA duplexes where 1,3-intrastrand cross-link triggers isomerization reactions with rearrangement into interstrand cross-links [48, 49]. Interestingly, the cross-link is formed between the (less strongly bonded) 5′-end guanine base and complementary cytosine. An explanation for the preference of the 5′-end base consists of the steric conditions: this reaction represents a direct nucleophilic attack on the Pt–G(3′) bond by the cytosine residue opposite to G(5′) of the second DNA strand [50]. Considering the larger basicity of the N1 site over N7 site in the purine bases, the N7→N1 migration of Pt may be anticipated. In fact, this type of isomerization was observed in the Pt-complexes with inosine [51] or adenosine [52].

In the field of Pt-nucleobase interactions, there are also many computational studies. The complex of *cis*platin with 1,2-d(GpG) bases was examined by Carloni [53] who also considered some hydration aspects of *cis*platin using Car–Parrinello MD simulations. The effect of N7 platination on the strength of the N9–C1′ glycosyl bond of purine bases was revealed in the study of Baik [54]. In another work, the reaction mechanism of formation of the Pt(NH_3)$_2$ diguanine complexes was explored [55]. A similar study was performed by Eriksson [56] where both reaction steps that create monofunctional and bifunctional complexes were considered. The first step, the formation of a monofunctional adduct, was also explored by Chval [57]. The thermodynamics of Pt-bridges, bonding energy parameters, and the influence of a sugar-phosphate backbone were also studied in some of our other papers [58–60].

DFT techniques with the VTZP basis set were used recently by Deubel [61] to compare affinities of *cis*platin to S-sites and N-sites of amino acids and DNA bases. His results are in very good agreement with our previous calculations on the thermodynamics of platinum-complex hydration [62–65] as well as the interaction with sulphur-containing amino acids [66].

From all the examples of experimental works mentioned above, our motivation can be seen for a more extensive exploration of the close platinum vicinity. The bonding relations within the chosen Pt-bridges with two DNA bases need to be elucidated. The different base's orientations (HH or HT) correspond to different cross-link conditions in inter- and intrastrand Pt-bridges. Despite the fact that the geometric conditions play an important role in the cross-link formation, it can be expected that energetic and especially kinetic factors control the reaction course. This study clarifies the binding differences between individual Pt–N dative bonds in platinum coordination to various bases, which will be useful in future studies where some other factors (kinetic and steric effects from more extended models) of platinum cross-links will be examined.

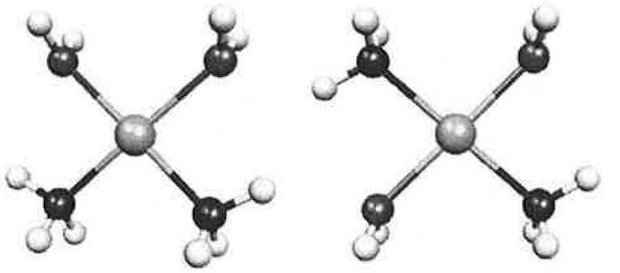

cis-$Pt(NH_3)_2(H_2O)_2$ trans$Pt(NH_3)_2(H_2O)_2$

Scheme 1 Hydrated forms of *cis/trans*platin

Computational details

This study investigates various *cis*- and *trans*platin complexes with two DNA bases in both head-to-head (HH) and head-to-tail (HT) arrangements (the 2+ charged hydrated structures of *cis*-/*trans*-diaquadiammineplatinum complexes are shown in Scheme 1). All platinum complexes were in the singlet ground state with the total charge of +2, deprotonation of DNA bases under formation of platinum adducts was not confirmed by any experimental tool. The following bridged base pairs were explored: *cis*-/*trans*-$Pt(NH_3)_2$(N7-guanine)(N7-adenine), $Pt(NH_3)_2$(N7-guanine)(N3-cytosine), $Pt(NH_3)_2$(N1-guanine)(N3-cytosine), and $Pt(NH_3)_2$(N7-guanine)$_2$. In the case of N1(G) coordination, a proton from N1 nitrogen was transferred to the N7 atom, preserving the same total charge of the complexes. All the structures were optimized at the DFT level with the B3LYP functional and the 6-31G(d) basis set. Stuttgart–Dresden energy averaged relativistic pseudopotentials were used for the description of the Pt atom [67]. The original basis set of pseudoorbitals was augmented by a set of diffuse functions with exponents α_s=0.0075, α_p=0.013, and α_d=0.025, and the exponent α_f=0.98 was used for additional polarization functions.

Second order perturbation theory (MP2) was used for the single-point energy evaluations of the systems examined. In this case, the larger basis set 6-31++G(2df,2pd) was used. For further discussion, stabilization energies (ΔE^{Stab}), stabilization energies corrected on the steric repulsion of ligands and the presence of H–bonds (ΔE^{Stex}), and binding energies (BE) were computed. The ΔE^{Stab} and ΔE^{Stex} energies were calculated with the inclusion of the Basis Set Superposition Error corrections (BSSE) together with the inclusion of deformation-energy corrections according to the formula:

$$\Delta E^{x} = -\left(E_{complex} - \sum E_{fragment}\right) - \Delta E^{deform}. \quad (1)$$

x means the given type of stabilization energy. The sum of fragment energies contains energies of the Pt cation and the corresponding isolated ligands in the case of ΔE^{Stab}. In the case of ΔE^{Stex} energies, only two terms enter the summation of $E_{fragment}$—the energy of the isolated Pt cation and the energy of all the ligands in the optimized position taken as one (neutral) system. The contributions of deformation energies are very important: $\Delta E^{deform} = E^{ligand}_{complex-geom.} - E^{ligand}_{most-stable-comformer}$ since the difference between the optimized N7- and N1-conformers of guanine is also covered in this term. In the case of ΔE^{BE} evaluation, the same Eq. (1) was employed without the deformation term. In the calculations of ΔE^{BE}, the $E_{fragment}$ energies were determined in the space partitioning according to the examined Pt–L_4 bond: $[Pt–L_1L_2L_3]^{2+}$ and $[L_4]$. In all cases the $E_{fragment}$ energies are evaluated in the complex-optimized geometry with the complete set of ghost AO functions on the complementary part(s) of the complex.

Starting from the diammine-diaqua-platinum complex (*cis*-$[Pt(NH_3)_2(H_2O)_2]^{2+}$), two steps were considered, where both aqua ligands were replaced subsequently by a chosen base. Gibbs reaction energies were determined for this process within a microcanonical ensemble using ideal gas and harmonic oscillator models.

Partial charges were computed within the Natural Population Analyses (NPA) [68–70] using MP2/6-31+G (d) correlated wave functions. The standard atom numbering of the nucleobases is used throughout (cf. Scheme 2).

Donation and back-donation effects were investigated using the canonical MOs. Charge transfer (CT) from a base to the central metal was computed as a sum of NPA partial charges of the base in the given complex since all the bases are electroneutral when they are isolated. For a better

Scheme 2 DNA bases considered in the study with atom numbering of the heterocycles

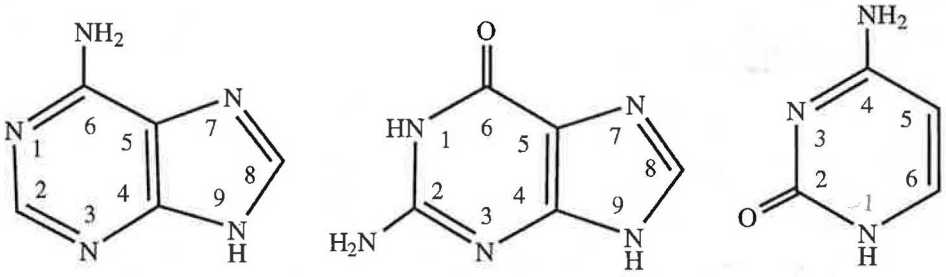

understanding of the systems studied, electrostatic potentials were mapped on the electron isodensity surfaces (ρ=0.001). All calculations were performed with the Gaussian 98 quantum chemical program package and the NBO v5.0 progam [71] was used for the NPA analyses. In this program, second order perturbative analysis of donor–acceptor interactions is available, labeled as E(2) energies. Using this tool, approximative values of Pt–N7(G), Pt–N7 (A) and Pt–N3(C) can be estimated.

Results

Structural parameters

The most important geometry parameters obtained from the complex optimizations are collected in Table 1. Besides distances of the Pt–N dative bonds, B–Pt–B valence angles and dihedral angles were chosen for discussion. From Table 1, we can see that Pt–N distances are shorter for the DNA base coordination than for the ammine ligands due to the possibility of back-donation in the case of nucleobases. The longest Pt–N bond (about 2.110 Å) was found for ammonia in the *trans*-$[Pt(NH_3)_2(N7\text{-guanine})_2)]^{2+}$ (HH) system. When the coordination distances for nucleobases are compared, the distinctly shortest Pt–N bonds can be found in the Pt–a_2GA systems. In the *cis*-$[Pt(NH_3)_2(N7\text{-guanine})(N7\text{-adenine})]^{2+}$ (HH) complex (Fig. 1-structure **1a**), the shortest Pt–N(adenine) bonds can be found (2.041 Å). The longest Pt–N distances (among the bases) occur in the cytosine complex of *cis*-$[Pt\text{–}a_2G(N7)C(N3)]^{2+}$.

Fig. 1 Diammine-platinum(II) cross-links with two DNA bases. ▶ Structures **a**, **b** represent *cis*platin head-to-head (HH), head-to-tail (HT) and structures **c**, **d** correspond to *trans*platin (HH), and (HT) conformers, respectively

In the complexes examined, the length of Pt–N dative bonds can be ordered: Pt–N7(A) (2.047 Å in average) <Pt–N7(G) (2.057) <Pt–N1(G) (2.069) <Pt–N3(C) (2.079) <Pt–N(a) (2.082 from the whole set of 32 bonds). The mutual repulsion between ammine ligand and protons of the NH_2 group of guanine, which is in the proximity of coordinated N1-site, is responsible for the fact that Pt–N1(G) bonds are longer than Pt–N7(G) in the Pt–a_2GC systems (especially in both *trans*platin complexes). The shortest Pt–N7(A) bond distance is supported by a better polarization of adenine (the largest change in the partial charge of N1 atom of adenine under platination among all partial charges from Table 2) and by larger E2 energies-cf. the discussion below.

From a detailed view on the Pt–N(ammine) bonds, one can recognize the changes caused by the influence of the H–bond of NH_3 ligands. The stronger the H–bond with an adjacent base, the shorter is the corresponding Pt–N(a) bond. The explanation lies in the reduction of N–H bond electron-density when its (ammine) hydrogen is involved in H–bonding. A higher effective electron density of N (ammine) can be used for donation to the Pt atom, resulting in a shorter Pt–N distance. The shortest Pt–N(a) bonds are about 2.075 Å (with H–bonds to the O6-guanine or O2-cytosine sites), while distances up to 2.11 Å can be seen for non-interacting ammine ligands. The strength of an H–bond also correlates indirectly with changes in the N–H stretching vibrations in comparison with isolated bases or ammonia

Table 1 Geometry parameters of investigated structures, Pt–$L_{1,2}$ and Pt–$B_{1,2}$ denote Pt–N bond lengths for ammonia ligands and nucleobases (in Å)

System	Pt–L_1	Pt–L_2		Pt–B_1		Pt–B_2		*D*1		*D*2	B_1–Pt–B_2
cis-Pt–a_2G(N7)A(N7) (HH)	2.089	2.095	G	2.041	A	2.044	G	−93.9	A	54.8	91.6
cis-Pt–a_2G(N7)A(N7) (HT)	2.087	2.076	G	2.058	A	2.053	G	−50.8	A	−50.1	91.1
trans-Pt–a_2G(N7)A(N7) (HT)	2.088	2.073	G	2.056	A	2.046	G	57.0	A	55.7	180.0
trans-Pt–a_2G(N7)A(N7) (HT)	2.088	2.072	G	2.057	A	2.046	G	−57.7	A	52.9	177.8
cis-Pt–a_2G(N7)C(N3) (HH)	2.082	2.077	G	2.058	C	2.083	G	−48.8	C	118.6	91.6
cis-Pt–a_2G(N7)C(N3) (HT)	2.075	2.085	G	2.062	C	2.084	G	−57.7	C	−111.5	92.7
trans-Pt–a_2G(N7)C(N3) (HH)	2.075	2.084	G	2.057	C	2.080	G	123.9	C	−56.4	178.0
trans-Pt–a_2G(N7)C(N3) (HT)	2.085	2.077	G	2.047	C	2.065	G	−66.3	C	−121.2	174.6
cis-Pt–a_2G(N7)G(N7) (HH)	2.074	2.074	G	2.065	G	2.065	G	60.9	G	−60.9	93.4
cis-Pt–a_2G(N7)G(N7) (HT)	2.073	2.073	G	2.061	G	2.061	G	−51.5	G	−51.4	90.1
trans-Pt–a_2G(N7)G(N7) (HH)	2.110	2.055	G	2.066	G	2.066	G	−51.1	G	51.1	175.0
trans-Pt–a_2G(N7)G(N7) (HT)	2.077	2.077	G	2.051	G	2.051	G	57.1	G	−57.1	180.0
cis-Pt–a_2G(N1)C(N3) (HH)	2.096	2.091	G	2.068	C	2.088	G	−88.5	C	123.2	93.1
cis-Pt–a_2G(N1)C(N3) (HT)	2.106	2.092	G	2.054	C	2.064	G	91.7	C	100.0	92.5
trans-Pt–a_2G(N1)C(N3) (HH)	2.081	2.080	G	2.083	C	2.086	G	−122.7	C	−132.4	175.3
trans-Pt–a_2G(N1)C(N3) (HT)	2.083	2.082	G	2.073	C	2.082	G	−126.1	C	121.1	178.8

*D*1 labels dihedral angles N(a)–Pt–N7–C5 (N(a)–Pt–N1–C6) of the base B_1 and *D*2 labels dihedral angles N(a)–Pt–N7–C5 (N(a)–Pt–N3–C4) of the base B_2, B_1–Pt–B_2 represents the angle between nucleobases.

1a: cis-Pt_a$_2$G(N7)A(N7) (HH)

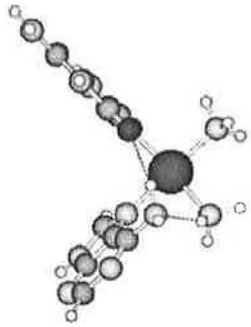

1b: cis-Pt_a$_2$G(N7)A(N7) (HT)

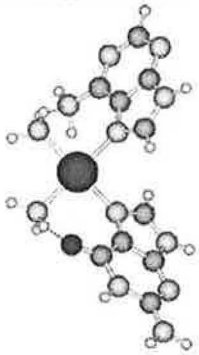

2a: cis-Pt_a$_2$G(N7)C(N3) (HH)

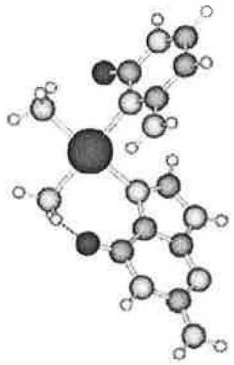

2b: cis-Pt_a$_2$G(N7)C(N3) (HT)

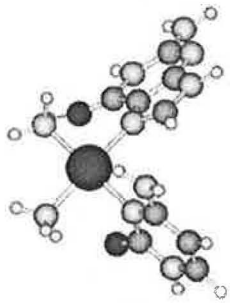

1c: trans-Pt_a$_2$G(N7)A(N7) (HH)

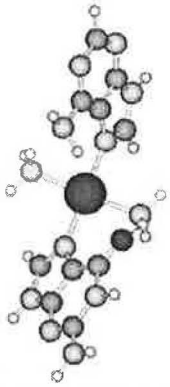

1d: trans-Pt_a$_2$G(N7)A(N7) (HT)

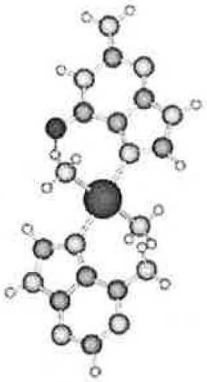

2c: trans-Pt_a$_2$G(N7)C(N3) (HH)

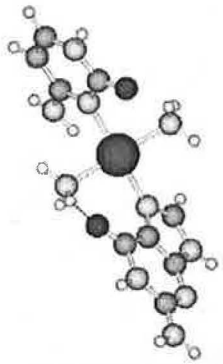

2d: trans-Pt_a$_2$G(N7)C(N3) (HT)

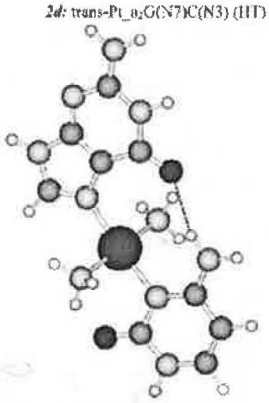

3a: cis-Pt_a$_2$G(N7)G(N7) (HH)

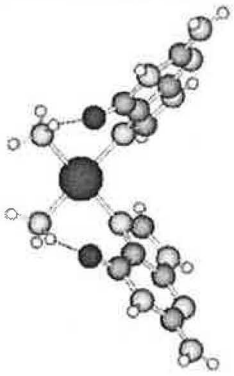

3b: cis-Pt_a$_2$G(N7)G(N7) (HT)

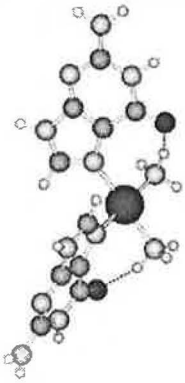

4a: cis-Pt_a$_2$G(N1)C(N3) (HH)

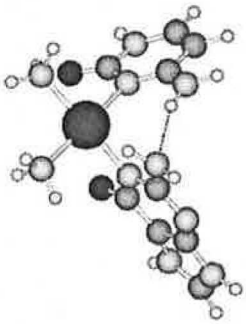

4b: cis-Pt_a$_2$G(N1)C(N3) (HT)

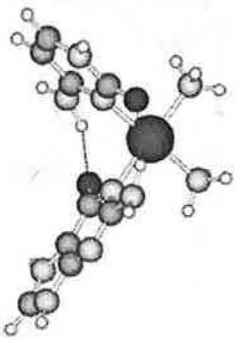

3c: trans-Pt_a$_2$G(N7)G(N7) (HH)

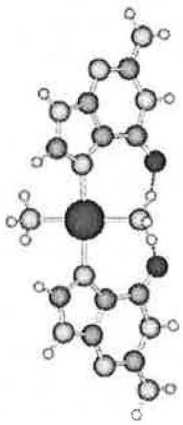

3d: trans-Pt_a$_2$G(N7)G(N7) (HT)

4c: trans-Pt_a$_2$G(N1)C(N3) (HH)

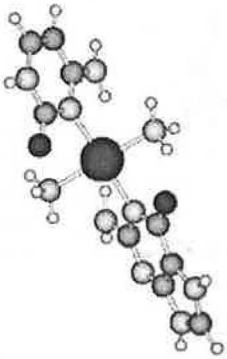

4d: trans-Pt_a$_2$G(N1)C(N3) (HT)

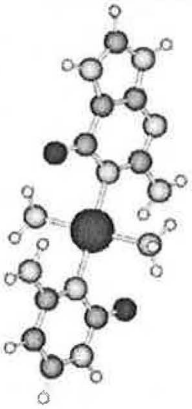

Table 2 Partial atomic charges on Pt, N(ammonia) and several important atoms of nucleobases: N7, N9, N2, N1, O6, H8, and H1 of guanine, N7, N9, N1, N6, and H8 of adenine, N3, N4, N1, O2, and H4 of cytosine (see Scheme 2), and charge transfer (CT) from base to Pt

System	Pt	N		N7/N3	N9/N4	N1	N7	X6/O2	H8	H1/H7	CT
cis-Pt-a_2G(N7)A(N7) (HH)	0.680	**−1.062**	G	**−0.485**	−0.530	−0.633	−0.813	−0.624	0.271	0.469	0.338
		−1.055	A	**−0.495**	−0.526	−0.459		−0.909	0.267		0.346
cis-Pt-a_2G(N7)A(N7) (HT)	0.673	**−1.056**	G	**−0.487**	−0.529	−0.628	−0.812	−0.616	0.269	0.472	0.358
		−1.056	A	**−0.512**	−0.525	−0.455		−0.898	0.264		0.337
trans-Pt-a_2G(N7)A(N7) (HT)	0.670	**−1.060**	G	**−0.487**	−0.528	0.635	−0.812	−0.625	0.271	0.471	0.348
		−1.051	A	**−0.505**	−0.523	−0.457		−0.897	0.272		0.346
trans-Pt-a_2G(N7)A(N7) (HT)	0.671	**−1.061**	G	**−0.485**	−0.528	−0.629	−0.812	−0.622	0.267	0.471	0.350
		−1.052	A	**−0.503**	−0.522	−0.457		−0.899	0.274		0.345
cis-Pt-a_2G(N7)C(N3) (HH)	0.673	**−1.054**	G	**−0.487**	−0.530	−0.629	−0.814	−0.622	0.272	0.471	0.346
		−1.049	C	**−0.627**	−0.785	−0.606		−0.610		0.448	0.331
cis-Pt-a_2G(N7)C(N3) (HT)	0.675	**−1.054**	G	**−0.482**	−0.530	−0.628	−0.815	−0.616	0.263	0.471	0.351
		−1.049	C	**−0.617**	−0.818	−0.601		−0.594		0.444	0.325
trans-Pt-a_2G(N7)C(N3) (HH)	0.667	**−1.057**	G	**−0.484**	−0.528	−0.630	−0.813	−0.613	0.268	0.471	0.355
		−1.056	C	**−0.618**	−0.802	−0.601		−0.604		0.444	0.342
trans-Pt-a_2G(N7)C(N3) (HT)	0.678	**−1.052**	G	**−0.485**	−0.530	−0.627	−0.813	−0.654	0.274	0.469	0.332
		−1.047	C	**−0.621**	−0.798	−0.604		−0.608		0.458	0.340
cis-Pt-a_2G(N7)G(N7) (HH)	0.688	**−1.052**	G	**−0.489**	−0.532	−0.630	−0.816	−0.613	0.271	0.470	0.338
		−1.052	G	**−0.489**	−0.532	−0.631	−0.816	−0.613	0.271	0.470	0.338
cis-Pt-a_2G(N7)G(N7) (HT)	0.689	**−1.050**	G	**−0.484**	−0.531	−0.632	−0.817	−0.611	0.258	0.469	0.334
		−1.050	G	**−0.484**	−0.531	−0.632	−0.817	−0.611	0.258	0.469	0.334
trans-Pt-a_2G(N7)G(N7) (HH)	0.687	**−1.074**	G	**−0.481**	−0.529	−0.634	−0.816	−0.596	0.261	0.469	0.342
		−1.033	G	**−0.481**	−0.529	−0.634	−0.816	−0.596	0.261	0.469	0.342
trans-Pt-a_2G(N7)G(N7) (HT)	0.688	**−1.057**	G	**−0.480**	−0.529	−0.631	−0.816	−0.619	0.271	0.469	0.345
		−1.057	G	**−0.480**	−0.529	−0.631	−0.816	−0.619	0.271	0.469	0.345
cis-Pt-a_2G(N1)C(N3) (HH)	0.666	**−1.061**	G	−0.471	−0.511	**−0.641**	−0.886	−0.569	0.292		0.374
		−1.053	C	**−0.612**	−0.786	−0.606		−0.614		0.447	0.328
cis-Pt-a_2G(N1)C(N3) (HT)	0.663	**−1.062**	G	−0.472	−0.515	**−0.624**	−0.836	−0.640	0.291		0.388
		−1.052	C	**−0.613**	−0.785	−0.607		−0.628		0.462	0.322
trans-Pt-a_2G(N1)C(N3) (HH)	0.648	**−1.047**	G	−0.470	−0.512	**−0.633**	−0.867	−0.619	0.293		0.381
		−1.055	C	**−0.620**	−0.802	−0.603		−0.602		0.440	0.322
trans-Pt-a_2G(N1)C(N3) (HT)	0.648	**−1.053**	G	−0.471	−0.512	**−0.628**	−0.870	−0.635	0.293		0.381
		−1.047	C	**−0.616**	−0.806	−0.602		−0.611		0.450	0.327
Isolated guanine(N7)			G	−0.448	−0.574	−0.661	−0.875	−0.573	0.236	0.448	
Isolated guanine(N1)			G	−0.477	−0.536	−0.615	−0.859	−0.641	0.2489	0.4781	
Isolated adenine			A	−0.493	−0.583	−0.534		−0.838	0.226		
Isolated cytosine			C	−0.591	−0.838	−0.634		−0.620		0.450	

In addition, partial charges of isolated bases are listed too. δ(N)=−1.136 e for ammonium molecule in vacuum. **Bold** font represents N atoms that coordinate to Pt (in e).

molecules. Some information can also be extracted from the changes in C=O and C–N6 vibration modes (cf. below).

An analysis of the bases' orientation and the H–bonding parameters represents a very interesting subject, which reflects several remarkable features. The distances of various H–bonds are shown in Table 3. In the *trans*platin complexes, the most frequent realization of H–bonding involves two H–bridges, both between an ammine-ligand and a DNA base: X...H–N(ammine) interaction (where X=guanine O6, adenine N6 or cytosine O2 site). In the *trans*-Pt-a_2G(N1)C(N3) complex, three for HH (Fig. 1 structure **4c**), and even four interactions of the X...H–N character for HT orientation (**4d**) can be noticed. Beside these two complexes, another interesting structure occurs in the *trans*-Pt-a_2G(N7)C(N3) (HT) complex (**2d**) where two X...H–N(ammine) interactions are accompanied by an additional (weaker) interbase H–bond (2.27 Å) O6...H–N4, which is the only *trans*platin complex with an interbase H–bond. This complex is also similar to the Hoogsteen base pairing, where a Pt cation mediates the N7(G)...N3(C) connection. The *trans*-Pt-a_2GG (HH) structure (**2c**) makes two H–bonds where the same ammine ligand is connected to both O6 atoms resulting in the shortest Pt–N(ammine) dative bond.

In the case of *cis*platin complexes, a larger variety of the base orientations can be observed. *Cis*platin complexes form interbase H–bonds more often. In the GA and G(N1)C complexes, relatively strong interbase H–bonds are present

Table 3 Hydrogen bonds X...H between ammine ligand and guanine O6, adenine N6 or cytosine O2 site

System		O6...H		O2/X6...H
cis-Pt-a_2G(N7)A(N7) (HH)	G	2.01(b)	A	2.09
cis-Pt-a_2G(N7)A(N7) (HT)	G	1.77	A	2.06
trans-Pt-a_2G(N7)A(N7) (HT)	G	1.87	A	2.14
trans-Pt-a_2G(N7)A(N7) (HT)	G	1.84	A	2.13
cis-Pt-a_2G(N7)C(N3) (HH)	G	1.82	C	2.05
cis-Pt-a_2G(N7)C(N3) (HT)	G	1.78	C	2.20
trans-Pt-a_2G(N7)C(N3) (HH)	G	1.80	C	2.00
trans-Pt-a_2G(N7)C(N3) (HT)	G	2.07/2.27(b)	C	2.04
cis-Pt-a_2G(N7)G(N7) (HH)	G	1.84	G	1.84
cis-Pt-a_2G(N7)G(N7) (HT)	G	1.80	G	1.80
trans-Pt-a_2G(N7)G(N7) (HH)	G	1.86	G	1.86
trans-Pt-a_2G(N7)G(N7) (HT)	G	1.85	G	1.85
cis-Pt-a_2G(N1)C(N3) (HH)	G	2.08(bN)[a]	C	1.95
cis-Pt-a_2G(N1)C(N3) (HT)	G	2.07(b)	C	1.89(b)
trans-Pt-a_2G(N1)C(N3) (HH)	G	1.88	C	2.15
trans-Pt-a_2G(N1)C(N3) (HT)	G	1.98	C	2.10

(b) labels the interbase interactions
[a] (bN) means interaction between N2(guanine)...H(N4-cytosine)

with O6...H(nucleobase) distance less than 2.10 Å. Structure **4b** partially resembles a bent Watson–Crick GC pair with two interbase H–bonds and the third base–base interaction is replaced by the Pt-cross-link. The *cis*-Pt-a_2G(N1)C(N3) is the only complex where other than the X6 atom of the DNA base is involved in the interbase H–bond. Here, an interaction between N2 atom of guanine and H(N4) of cytosine is established.

Energy analysis

Stabilization energies (ΔE^{Stab}, ΔE^{Stex}) and bonding energies (ΔE^{BE}) were evaluated for all complexes studied and are shown in Table 4.

Both *cis*- and *trans*platin complexes form fairly stable structures. Without the deformation corrections (ΔE^{deform}), the most stable compounds can be found in the group of Pt-a_2G(N1)C(N3) structures (the averaged ΔE^{Stab} is about 551 kcal mol^{-1}—not shown in Table 4). However, when the fact that the N1-conformer of guanine is about 18 kcal mol^{-1} less stable than the N7-conformer is

Table 4 ΔE^{Stab}, ΔE^{Stex} stabilization energies with and without inclusion of corrections on sterical repulsion, and bond energies ΔE^{BE}

System	ΔE^{Stab}	ΔE^{Stex}	ΔE^{BE}		ΔE^{BE}	
cis-Pt-a_2G(N7)A(N7) (HH)	535.8	547.9	G	112.5	A	95.0
cis-Pt-a_2G(N7)A(N7) (HT)	534.9	552.7	G	112.8	A	87.7
trans-Pt-a_2G(N7)A(N7) (HT)	536.7	552.6	G	113.9	A	90.9
trans-Pt-a_2G(N7)A(N7) (HT)	536.2	553.5	G	112.4	A	90.0
cis-Pt-a_2G(N7)C(N3) (HH)	545.2	560.3	G	112.1	C	100.2
cis-Pt-a_2G(N7)C(N3) (HT)	542.5	560.8	G	109.2	C	95.7
trans-Pt-a_2G(N7)C(N3) (HH)	545.4	562.5	G	110.3	C	100.9
trans-Pt-a_2G(N7)C(N3) (HT)	549.3	560.9	G	113.2	C	104.5
cis-Pt-a_2G(N7)G(N7) (HH)	551.1	573.9	G	103.2	G	103.2
cis-Pt-a_2G(N7)G(N7) (HT)	553.3	574.0	G	106.4	G	106.5
trans-Pt-a_2G(N7)G(N7) (HH)	547.8	571.4	G	104.3	G	104.3
trans-Pt-a_2G(N7)G(N7) (HT)	554.6	574.3	G	109.0	G	109.0
cis-Pt-a_2G(N1)C(N3) (HH)	552.8	568.7	G	120.0	C	99.6
cis-Pt-a_2G(N1)C(N3) (HT)	563.0	565.5	G	132.5	C	107.5
trans-Pt-a_2G(N1)C(N3) (HH)	558.0	575.3	G	124.1	C	93.8
trans-Pt-a_2G(N1)C(N3) (HT)	562.1	574.9	G	127.4	C	96.3

All values are in kcal mol^{-1}.

considered (which is included in the ΔE^{deform} term), the most stable complexes become the Pt–a_2GG systems. This holds for both the ΔE^{Stab} and ΔE^{Stex} values. An about 5 kcal mol^{-1} weaker stabilization was achieved in the case of Pt–a_2G(N7)C(N3) complexes. The structures with N1 coordination are on average about another 7 kcal mol^{-1} less stable than the corresponding G(N7) conformers. The least stable systems are the adenine-containing complexes (about 527 kcal mol^{-1}). This order is in good agreement with many previous studies on this subject.

Thanks to the formation of two strong interbase H–bonds: O6(G)...HN4(C) and O2(C)...HN2(G), the *cis*-Pt–a_2G(N1)C(N3) (HT) complex displays an exceptionally low steric repulsion; the difference between ΔE^{Stab} and ΔE^{Stex} energies, is only about 2.5 kcal mol^{-1}.

The strongest coordination to Pt is represented by the Pt–N1 bonds in Pt–a_2G(N1)C(N3) complexes, where the BE is about 126 kcal mol^{-1}. The highest BE energy is in the *cis*Pt–a_2G(N1)C(N3) (HT) complex. However, the Pt–N bonding is accompanied by two additional (relatively strong) interbase H–bonds. In the case of analogous Pt–a_2G(N7)C(N3) complexes, the ΔE^{BE} of Pt–N7(G) bonds are about 13 kcal mol^{-1} lower. The Pt–N3(C) exhibits very similar BE characteristics in both G(N1) and G(N7) conformers (about 100 kcal mol^{-1}). The explanation for the reduction of Pt–N7(G) BE can be seen in a lower electrostatic contribution. Considering the dipole moment of neutral conformers of guanine, a more advantageous interaction site for a positively charged Pt complex is N1 in the N1-conformer (with the N7 site protonated). The dipole moment is oriented in the N1→N9 direction and its value is about 9.5 D (B3LYP/6-31G+(d), cf. Fig. 2), while the regular N7 conformer has dipole μ=6.8 D with orientation C5→C4. The polarizability tensor has accordingly slightly larger Eigenvalues for the N1 conformer. The orientation of the main tensor axes is similar and the contribution in the C5–C4 direction is about 40% smaller than in the N1–C8 direction. On the contrary, in the case of N7-guanine, the HOMO (of π character) lies slightly closer to the vacant 5d-AO of the isolated Pt^{2+} cation, which enables a stronger dative interaction. In this way strength of both the Pt–N bonds is similar. It also correlates with the lower CT from cytosine to Pt atom in structures with G(N1) base (cf. below).

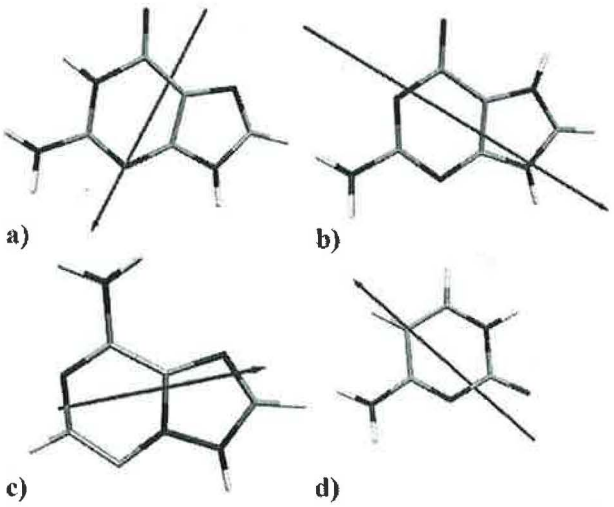

Fig. 2 Optimized conformers of DNA bases and their dipole moments: (**a**) N7-guanine, (**b**) N1-guanine, (**c**) adenine, (**d**) cytosine

The influence of the *trans* effect can be found in the case of *trans*platin coordination with N1(G), where a higher affinity of cytosine leads to the weakest Pt–N(G) bond. This effect is usually not as pronounced since some other energy terms (like H–bond or sterical repulsion) compensate it.

The strength of the Pt–N7(G) bond also reflects the donation ability of the DNA bases examined. As to stabilization energies, both ΔE^{Stab} and ΔE^{Stex} values increase in the order adenine<cytosine<guanine, which is in accord with the most abundant occurrence of 1,2-GpG cross-links (structure **3a**) in real (in vivo or in vitro) assays. The stabilization is, however, a too complex criterion for a more detailed insight and better correlation with the changes of Pt–N7(G) bonding is given by BE characteristics. It can be noticed that the weakest Pt–N7 coordination occurs in diguanine complexes due to the highest mutual bonding competition. In the cytosine–guanine complexes, the Pt–N7 bonds are by about 5 kcal mol^{-1} (on average) stronger. The weakest competition comes from adenine enabling strong Pt–N7(G) bonds (≈113 kcal mol^{-1}). The BE of Pt–N7(A) bonds is only about 91 kcal mol^{-1} and this fact is in good agreement with the very small dipole moment of isolated adenine.

The thermodynamics (Gibbs heat of reaction) of aqua-ligand replacement by the second DNA bases is evaluated in Table 5. We concentrated on the second step since the first one was already treated in previous work [58] where the reaction energy (ΔE) was estimated to be 51 for adenine and 72 kcal mol^{-1} for guanine (at a slightly worse level—MP2/6-31+G(d)) with diaqua-*cis*platin as a reactant. Also, the second reaction step is energetically comparable with previously calculated head-to-head systems: Pt-adenine+guanine (59 kcal mol^{-1}), Pt-guanine+adenine (39 kcal mol^{-1}), and Pt-guanine+guanine (52 kcal mol^{-1}). In our study, the Gibbs energies are systematically about 3–4 kcal mol^{-1} lower than these reaction energies.

From Table 5 it can be noticed that the smallest reaction Gibbs energies are for water replacement by adenine—about 41 kcal mol^{-1}. Smaller reaction energies were also obtained for cytosine replacement in both N7 and N1 *cis*platin+guanine adducts (below 54 and 50 kcal mol^{-1}, respectively). The largest amount of energy is for guanine

Table 5 Reaction energies ΔE and Gibbs energies ΔG for the reaction (in kcal mol^{-1}): Pt–a_2wB+B′→Pt–a_2BB′+water

Reactants		Products	ΔE	ΔG
cis-Pt–a_2wA(N7)	+G →	*cis*-Pt–a_2G(N7)A(N7) (HH)	−63.1	−60.7
	+G →	*cis*-Pt–a_2G(N7)A(N7) (HT)	−62.2	−59.7
trans-Pt–a_2wA(N7)	+G →	*trans*-Pt–a_2G(N7)A(N7) (HT)	−67.9	−65.4
	+G →	*trans*-Pt–a_2G(N7)A(N7) (HT)	−67.1	−64.4
cis-Pt–a_2wC(N3)	+G →	*cis*-Pt–a_2G(N7)C(N3) (HH)	−66.4	−65.4
	+G →	*cis*-Pt–a_2G(N7)C(N3) (HT)	−63.0	−61.9
trans-Pt–a_2wC(N3)	+G →	*trans*-Pt–a_2G(N7)C(N3) (HH)	−64.9	−62.3
	+G →	*trans*-Pt–a_2G(N7)C(N3) (HT)	−68.5	−65.4
cis-Pt–a_2wG(N7)	+G →	*cis*-Pt–a_2G(N7)G(N7) (HH)	−60.1	−58.3
	+G →	*cis*-Pt–a_2G(N7)G(N7) (HT)	−63.1	−61.4
trans-Pt–a_2wG(N7)	+G →	*trans*-Pt–a_2G(N7)G(N7) (HH)	−56.7	−55.8
	+G →	*trans*-Pt–a_2G(N7)G(N7) (HT)	−64.0	−61.6
cis-Pt–a_2wG(N7)	+A →	*cis*-Pt–a_2G(N7)A(N7) (HH)	−44.5	−41.9
	+A →	*cis*-Pt–a_2G(N7)A(N7) (HT)	−43.6	−40.9
trans-Pt–a_2wG(N7)	+A →	*trans*-Pt–a_2G(N7)A(N7) (HT)	−44.8	−41.7
	+A →	*trans*-Pt–a_2G(N7)A(N7) (HT)	−44.1	−40.8
cis-Pt–a_2wG(N7)	+C →	*cis*-Pt–a_2G(N7)C(N3) (HH)	−56.6	−54.1
	+C →	*cis*-Pt–a_2G(N7)C(N3) (HT)	−53.2	−50.6
trans-Pt–a_2wG(N7)	+C →	*trans*-Pt–a_2G(N7)C(N3) (HH)	−55.7	−52.6
	+C →	*trans*-Pt–a_2G(N7)C(N3) (HT)	−59.3	−55.7
cis-Pt–a_2wC(N3)	+G →	*cis*-Pt–a_2G(N1)C(N3) (HH)	−54.4	−53.2
	+G →	*cis*-Pt–a_2G(N1)C(N3) (HT)	−63.7	−62.9
trans-Pt–a_2wC(N3)	+G →	*trans*-Pt–a_2G(N1)C(N3) (HH)	−59.1	−56.1
	+G →	*trans*-Pt–a_2G(N1)C(N3) (HT)	−61.9	−58.7
cis-Pt–a_2wG(N1)	+C →	*cis*-Pt–a_2G(N1)C(N3) (HH)	−44.0	−42.7
	+C →	*cis*-Pt–a_2G(N1)C(N3) (HT)	−53.4	−52.3
trans-Pt–a_2wG(N1)	+C →	*trans*-Pt–a_2G(N1)C(N3) (HH)	−52.4	−50.1
	+C →	*trans*-Pt–a_2G(N1)C(N3) (HT)	−55.2	−52.7

In all cases the N7-conformer of guanine was considered.

replacement, which is in good accord with BE values. Practically all reactions where water was replaced by guanine have reaction energies above 58 kcal mol^{-1}. The most exothermic reactions are in the case where *cis*-Pt–a_2G(N7)C(N3) adducts are formed. Here energies of about 64 kcal mol^{-1} are released in the reaction course.

Charge distribution and electrostatic potentials

An investigation of charge distributions and MO analysis in systems give a deeper insight into system interactions. Therefore, NPA partial charges of key elements are shown in Table 2 and dipole moments, main axes of the polarizability tensor, and MO characteristics of isolated bases in Table 6. The orientation of the dipole moments can be seen in Fig. 3. As to the central Pt atom, the decrease in its charge reflects the extent of electron density donation from ammonia molecules and nucleobases. Simultaneously, changes in nitrogen charge of the ligands give an insight into the ratio of donation of individual Pt–N bonds in the complex. However, these criteria are not straightforward since back-donation occurs in the case of DNA bases, as discussed below.

The most positive Pt charge (about 0.69 e) was found in Pt_a_2GG systems. This points to a relatively smaller donation from the guanine bases in comparison with the other nucleobases explored, which can be ordered as follows: Pt_a_2GA (averaged Pt charge 0.673 e)≈Pt_a_2G(N^7)C(N^3) (0.673 e)>Pt_a_2G(N^1)C(N^3) with significantly lowest charges (0.656 e). The strength of Pt–N bonds can

Table 6 Electron properties of the used DNA bases: dipole moment μ (in D), main axes of polarizability tensor α (in Å^3), and eigenvalues (in a.u.); N7G means the regular guanine form, N1G labels the N1-tautomer (with protonated N7 site), C-cytosine, and A-adenine

	Pt(II)	N7G	N1G	C	A
μ		6.8	9.5	5.9	4.8
α (xx)		19.8	21.4	15.1	18.0
α (yy)		16.3	16.9	11.6	15.7
α (zz)		7.7	7.8	6.1	7.4
π^*(base)		0.09	0.10	0.08	0.09
π^*(LUMO)	−0.66	−0.03	0.03	0.05	0.06
π(HOMO)	−1.12	−0.30	−0.30	−0.32	−0.28
π(HOMO-1)		−0.41	−0.34	−0.39	−0.34
σ (HOMO-2)		−0.43	−0.38	−0.41	−0.41

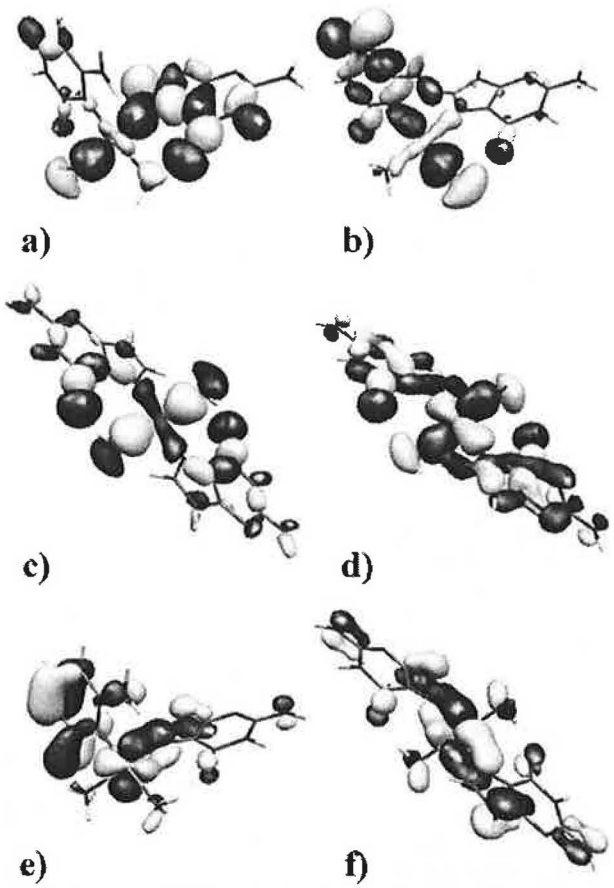

Fig. 3 Molecular orbitals with donation (**a**–**d**) and back-donation (**e**, **f**) characters for *cis*-Pt–a_2G(N7)C(N3) (HH) (**a**, **b**, **e**) and *trans*-Pt–a_2GG (HT) (**c**, **d**, **f**) conformations

be explained as the sum of a dative interaction and electrostatic forces, which are large in the guanine case (especially for the N1-conformer, notice its dipole moment in Table 6). From Table 2, polarization effects can be deduced from the changes in partial charges on the selected atoms. The largest decrease in partial charge occurs at the adenine N1 site, where the averaged difference against the isolated base is 0.08 e. The calculated tensor axes of base polarizability decrease as follows: N1-guanine>N7-guanine>adenine>cytosine as can be seen from Table 6 and Fig. 2, where dipole moments and main axes of the polarizability tensors are shown together with important MO Eigenvalues of isolated DNA bases.

The higher donation activity of the N7 atom of guanine in comparison with the N1 site of the N1-tautomer is related to the Eigenvalues of the highest occupied sigma (HOS) MO, where there is a strong localization of electron density on the interacting N-atom. This is in all cases examined the HOMO-2 orbital. The HOSMO of isolated N7-guanine has its Eigenvalue (of ε=−0.430 a.u.) closest to the vacant 5d-AO of Pt^{2+} (ε=−0.660 a.u.), clearly pointing to a higher donation than in the case of N1-guanine (with corresponding ε=−0.375 a.u.).

The strength of Pt–N coordination also correlates closely with the total charge transfer (CT) from a ligand to Pt atom. These values are included for DNA bases in the last column of Table 2. Here one can notice that CT from cytosine to Pt is larger (on average 0.334 e) for Pt–a_2G(N7)C(N3) complexes, while a smaller CT value of 0.325 e can be found for Pt–a_2G(N1)C(N3) complexes. Comparing CT from adenine and guanine in mixed Pt–GA systems, the CT from adenine is larger than CT from guanine only in the case of the *cis*-Pt–a_2GA (HH) complex. This is connected with the additional interbase donation from O6 of guanine to the NH_2 group of adenine, increasing its total charge. Nevertheless the larger preference for adenine donation over guanine one can be clearly seen from the E(2) perturbation energy approach in the NBO framework. While the interaction energy for donation from N7(A)→Pt is about 5.5, the corresponding value for N7(G)→Pt is only 3.8 kcal mol^{-1}. The energies for back donation from Pt→N7 are similar (70.1 (A) vs. 69.4 (G) kcal mol^{-1}).

When *cis* and *trans* conformers are compared, the donation (according to the decrease in Pt charge) is usually more pronounced in the *trans* structures. This explains the usually higher ΔE^{BE} energies of bases for *trans*platin complexes (the exceptions are caused by additional stabilization due to a higher number of H–bonds or sterical repulsion of the bases). Such a situation differs from "small" ligand (like NH_3 or H_2O) complexes where the *trans*-effect leads to a decrease in bonding energies. The reason for the difference is the fact that back-donation from the Pt AO with π-character to an antibonding π*-MO of bases is allowed (cf. Fig. 3e,f). Such π*-MOs are not available in ammonia or water.

Another insight into these effects can be obtained from charges of the bound nitrogen atoms, which vary according to the ligand type. While the negative charge of the N atom of the ammine ligand increases by about 0.06 e (less negative in coordination) in comparison with isolated ammonia, the N7/N3/N1 charge of the nucleobases is decreased upon coordination to Pt. This corresponds to the different characters of coordination of ammine-ligands and bases where back-donation makes the Pt–N(base) stronger. The decrease in partial charge due to polarization and back-donation is about 0.04 e on the N7 atom of guanine, 0.03 e on N3 of cytosine, and 0.01 e on N7 of adenine.

In *trans*-Pt–a_2GG (HH) structure (Fig. 1 structure **3c**), one of the N(ammine) charges is significantly lower (by about 0.1 e in comparison with isolated ammonia), since both bases are H–bonded to that ligand. This enables a higher donation of the ammine to the Pt atom with an exceptionally short Pt–N(ammine) distance −2.055 Å, even shorter than the Pt–N(base) one in this complex.

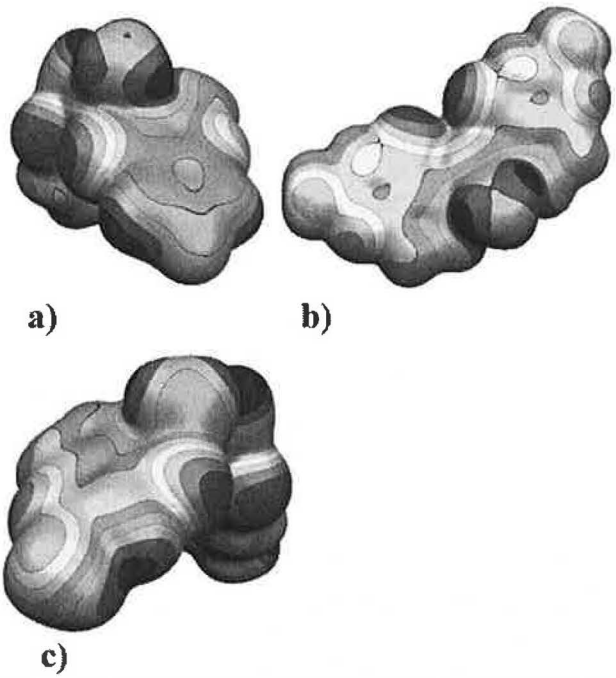

Fig. 4 Maps of electrostatic potentials on isodensity surface (ρ=0.001 electron/Bohr^3) for **a** *cis*-Pt–a_2G(N1)C(N3) (HH), **b** *trans*-Pt–a_2GG (HH), **c** *cis*-Pt–a_2GG (HH)

The remainder of the selected partial charges listed in Table 2 should demonstrate the extent of polarization of the DNA bases. In comparison with isolated bases, the shift of electron density towards the metal cation is clearly evident.

A manifestation of donation and back donation can be seen in the analysis of MOs of two Pt-complexes: *cis*-Pt–a_2G(N7)C(N3) (HH) and *trans*-Pt–a_2GG (HT). MOs with donation N→Pt (a–d) and back-donation N←Pt (e) and (f), which are involved in these effects are shown in Fig. 3. One can also notice that MOs with donation lie substantially lower (about −0.85 hartree)[1], while MOs with back-donation are about −0.70 hartree. For all the complexes explored electrostatic potentials were also determined. This potential was mapped onto the isodensity surface with ρ=0.001 e/Å^3. The plots obtained give illustrative insight into electrostatic repulsion of various (usually negatively charged) sites of bases involved in platinum complexes. In Fig. 4 three selected cases with the highest repulsions were chosen. The *cis*-Pt–a_2G(N1)C(N3) (HH) complex (Fig. 4a), which according to Table 4 exhibits a relatively modest electrostatic repulsion, has both oxygen atoms in close proximity. However, their actual repulsion is partially compensated by an interbase H–bond, as can be seen in Fig. 1 (structure **4a**). The *trans*-Pt–a_2GG (HH) complex belongs to systems where only weak H–bonds are present. Here the O6...O6 repulsion causes the largest steric repulsion between the two bases (Fig. 4b). A similar situation also occurs in the *cis*platin analog (*cis*-Pt–a_2GG (HH) Fig. 4c), where the second largest repulsion was achieved. The large electrostatic repulsion is usually (at least partially) removed in real assays since additional restrictions due to the sugar-phosphate backbone are present.

Canonical vibrational modes in the harmonic approximation were analyzed in order to obtain an estimate of the H–bond strength. From Table 7, it can be observed that the symmetrical stretching mode of isolated ammonia (estimated ca 3438 cm^{-1} at the DFT/6-31+G(d) level) was shifted below 3200 cm^{-1} in four systems: *cis*-Pt–a_2GA (HT) (3145 cm^{-1}), *cis*-Pt–a_2G(N7)C(N3) (HT) (3155 cm^{-1}), *trans*-Pt–a_2G(N7)C(N3) (HH) (3173), and *cis*-Pt–a_2GG (HT) (with 3179 and 3184 cm^{-1}). Therefore, strong additional stabilization must be expected in these complexes. Structures with (ammine)N–H...N6(adenine) and (ammine) N–H...O2(cytosine) interactions were not shifted so profoundly. An interesting situation occurs when comparing C=O6(guanine) and C=O2(cytosine) bond-stretching modes. While in isolated guanine the vibrational frequency is 1799 cm^{-1}, the N1-tautomer has the corresponding value $\tilde{\nu} = 1709\,cm^{-1}$ under the deprotonation of N1 site. This is due to the changes in π-conjugation of the six-membered ring (a partial double bonding character of the N1–C6 bond) shifting the character of the C=O double bond towards a single bond. Platination of the N1 site withdraws some electron density from N1, shifting the frequency back to the regular guanine form. The same effect can also be noticed in complexes containing cytosine, where the frequency shift from the H...O2 H–bond (towards lower values) competes with the shift from π-conjugation, and therefore both positive and negative deviations of the C=O frequency of isolated cytosine (ca 1777 cm^{-1}) can be noticed. Similarly, the C=O frequency of protonated cytosine is 1876 cm^{-1}. The only decreased frequency of the C=O bond occurs in *cis*-Pt–a_2G(N1)C(N3) (HT) structure, where two (strong) interbase H–bonds are present (see also the lowest C=O frequency of N1-guanine and extremal values of both Pt–N BEs in this case).

Conclusions

In this work, the DFT optimization at the B3LYP/6-31G(d) level was performed for various platinum cross-links with two DNA bases. These structures occur in many *cis*/*trans*-platinated double-helixes or single-stranded adducts. Nevertheless, no steric hindrance from the sugar-phosphate backbone or other surroundings is considered in the present models. These restrictions could modify the bonding

[1] 1 hartree = 27.211 eV = 627.51 kcal mol-1 = 2625.5 kJ mol-1

Table 7 Vibration frequencies of N–H, C–N6, and C=O bonds involved in H–bonding interactions (in cm^{-1})

Complex	ν_1		ν_2		ν_3		ν_4	
cis-Pt-a_2G(N7)A(N7) (HH)	3434	N6H...O6	3234	aH...N6	1626	C–N6	1763	C=O6
cis-Pt-a_2G(N7)A(N7) (HT)	3145	aH...O6	3238	aH...N6	1626	C–N6	1757	C=O6
trans-Pt-a_2G(N7)A(N7) (HT)	3232	aH...O6	3278	aH...N6	1628	C–N6	1752	C=O6
trans-Pt-a_2G(N7)A(N7) (HT)	3217	aH...O6	3285	aH...N6	1628	C–N6	1756	C=O6
cis-Pt-a_2G(N7)C(N3) (HH)	3198	aH...O6	3367	aH...O2	1754	C=O6	1776	C=O2
cis-Pt-a_2G(N7)C(N3) (HT)	3155	aH...O6	3388	aH...O2	1758	C=O6	1786	C=O2
trans-Pt-a_2G(N7)C(N3) (HH)	3173	aH...O6	3356	aH...O2	1759	C=O6	1781	C=O2
trans-Pt-a_2G(N7)C(N3) (HT)	3381	aH...O6	3368	aH...O2	1741	C=O6	1780	C=O2
cis-Pt-a_2G(N7)G(N7) (HH)	3212	aH...O6	3218	aH...O6	1757	C=O6	1764	C=O6
cis-Pt-a_2G(N7)G(N7) (HT)	3179	aH...O6	3184	aH...O6	1757	C=O6	1760	C=O6
trans-Pt-a_2G(N7)G(N7) (HH)	3284	aH...O6	3320	aH...O6	1764	C=O6	1782	C=O6
trans-Pt-a_2G(N7)G(N7) (HT)	3229	aH...O6	3233	aH...O6	1757	C=O6	1759	C=O6
cis-Pt-a_2G(N1)C(N3) (HH)	3352	aH...O6	3486	N4H...N2	1759	C=O6	1777	C=O2
cis-Pt-a_2G(N1)C(N3) (HT)	3323	N4H...O6	3483	N2H...O2	1724	C=O6	1758	C=O2
trans-Pt-a_2G(N1)C(N3) (HH)	3294	aH...O6	3409	aH...O2	1742	C=O6	1786	C=O2
trans-Pt-a_2G(N1)C(N3) (HT)	3351	aH...O6	3392	aH...O2	1733	C=O6	1776	C=O2

Frequencies determined for N–H, C–N6, and C=O bonds in isolated molecules:
$\tilde{\nu}(aH) = 3438\,cm^{-1}$, $\tilde{\nu}(N4H) = 3589\,cm^{-1}$, $\tilde{\nu}(N6H) = 3596\,cm^{-1}$, $\tilde{\nu}(N2H) = 3563\,cm^{-1}$,
$\tilde{\nu}(C-N6) = 1675\,cm^{-1}$, $\tilde{\nu}(C=O2) = 1777\,cm^{-1}$, *and* $\tilde{\nu}(C=O6) = 1799\,cm^{-1}$
aH means vibrational frequency of (ammine)N–H bond, N4H–(cytosine)N4–H bond, N2H–(guanine)N2–H bond, and N6H–(adenine)N6–H bond

picture, but the basic energy characteristics should not be changed substantially.

Using the MP2/6-31++G(2df,2pd) method, it was found that the most stable structures are the diguanine complexes followed by guanine-cytosine Pt-cross-links, roughly 5 kcal mol^{-1} less stable. The adenine-containing complexes are about 15 kcal mol^{-1} below the stability of diguanine structures.

A detailed insight in covalent bond relations is obtained using bonding energies. The coordination competition of different DNA bases can be elucidated from BE values. The strongest Pt–N bonds are formed with guanine molecules—from 105 to 135 kcal mol^{-1} in dependence on orientation and type of the adjacent base. Pt–N3 bonds of cytosine are on average about 100 and Pt–N7 of adenine about 90 kcal mol^{-1}. The order is in agreement with the stabilization energies. From these values, the energies of H–bonds must also be subtracted. Based on previous results and frequency shifts, the strength of H–bonds can be estimated to be up to 15 kcal mol^{-1} due to relatively high polarization effects caused by the metal cation. The energy characteristics are explained using NPA charges, electrostatic potentials, and MO analysis.

Ackowledgments This study was supported by Charles University grant 438/2004/B_CH/MFF, grant NSF-MŠMT ČR 1P05 ME-784, and grant MSM 0021620835. Computational resources from MetaCenters in Prague, Brno, and Pilsen are acknowledged for access to their excellent supercomputer facilities. Finally, special thanks must be given to the KFCHO department computer cluster administrated by Dr. M. Šimánek.

References

1. Rosenberg B, van Camp L, Trosko JL, Mansour VH (1969) Nature 222:385–391
2. Beljanski V, Villanueva JM, Doetsch PW, Natile G, Marzilli LG (2005) J Am Chem Soc 127:15833–15842
3. Najajreh Y, Kasparkova J, Marini V, Gibson D, Brabec V (2005) J Biol Inorg Chem 10:722–731
4. Marini V, Christofis P, Novakova O, Kasparkova J, Farrell N, Brabec V (2005) Nucleic Acids Res 33:5819–5828
5. Bhattacharyya D, Marzilli PA, Marzilli LG (2005) Inorg Chem 44:7644–7651
6. Brabec V, Kasparkova J (2005) Drug Resistance Updates 8:131–146
7. Malina J, Voitiskova M, Brabec V, Diakos CI, Hambley TW (2005) Biochem Biophys Res Commun 332:1034–1041
8. Bivian-Castro EY, Roitzsch M, Gupta D, Lippert B (2005) Inorganica Chimica Acta 358:2395–2402
9. Barnes KR, Lippard SJ (2004) Metal complexes in tumor diagnosis and as anticancer agents. In: Metal ions in biological systems, vol 42. pp 143–177
10. Carlone M, Marzilli LG, Natile G (2005) Europ J Inorg Chem 1264–1273
11. Kaim W, Schwederski B (1994) Bioinorganic chemistry: inorganic elements in the chemistry of life. Wiley, Chichester, England
12. Takahara PM, Rosenzweig AC, Frederick CA, Lippard SJ (1995) Nature 377:649–655
13. Takahara PM, Frederick CA, Lippard SJ (1996) J Am Chem Soc 118:12309–12321
14. Yang D, van Boom SSGE, Reedijk J, van Boom JH, Wang AH-J (1995) Biochemistry 34:12912–12921
15. Gelasco A, Lippard SJ (1998) Biochemistry 37:9230–9238
16. Dunham SU, Dunham SU, Turner CJ, Lippard SJ (1998) J Am Chem Soc 120:5395–5403
17. Wing RM, Pjura P, Drew HR, Dickerson RE (1984) EMBO J 3:1201–1212

18. Lilley DMJ (1996) J Biol Inorg Chem 1:189–191
19. Coste F, Malinge JM, Serre L, Shepard W, Roth M, Leng M, Zelwer C (1999) Nucleic Acids Res 27:1837–1845
20. Spingler B, Whittington DA, Lippard SJ (2001) Inorg Chem 40:5596–5602
21. Silverman AP, Bu W, Cohen SM, Lippard SJ (2002) J Biol Chem 277:49743–49754
22. Parkinson GN, Arvanitis GM, Lessinger L, Ginell SL, Jones R, Gaffney B, Berman HM (1995) Biochemistry 34:15487–15495
23. Ohndorf U-M, Rould MA, He Q, Pabo CO, Lippard SJ (1999) Nature 399:708–712
24. Jamieson ER, Lippard SJ (1999) Chem Rev 99:2467–2498
25. Kašparková J, Mackay FS, Brabec V, Sadler PJ (2003) J Biol Inorg Chem 8:741–745
26. Choi S, Delaney S, Orbai L, Padgett EJ, Hakemian AS (2001) Inorg Chem 40:5481–5482
27. Junicke H, Bruhn C, Kluge R, Serianni AS, Steinborn D (1999) J Am Chem Soc 121:6232–6241
28. Song R, Kim KM, Lee SS, Sohn YS (2000) Inorg Chem 39:3567–3571
29. Watanabe M, Kai M, Asanuma S, Yoshikane M, Horiuchi A, Ogasawara A, Watanabe T, Mikami T, Matsumoto T (2001) Inorg Chem 40:1496–1500
30. Kelland LR, Jones MM, Abel G, Harrap KR (1992) Cancer Chemother Pharmacol 30:43–50
31. Wong E, Giandomenico CM (1999) Chem Rev 99:2451–2466
32. Reedijk J (1996) Chem Commun 7:801–806
33. Reedijk J (1999) Chem Rev 99:2499–2510
34. Brabec V, Neplechova K, Kasparkova J, Farell N (2000) J Biol Inorg Chem 5:364–368
35. Sigel H, Song B, Oswald G, Lippert B (1998) Chem Eur J 4:1053–1060
36. Williams KM, Scarcia T, Natile G, Marzilli LG (2001) Inorg Chem 40:445–454
37. Paquet F, Perez C, Leng M, Lancelot G, Malinge JM (1996) J Biomol Struct Dyn 14:67–77
38. Huang HF, Zhu LM, Reid BR, Drobny GP, Hopkins PB (1995) Science 270:1842–1845
39. Payet D, Gaucheron F, Sip M, Leng M (1993) Nucleic Acids Res 21:5846–5859
40. Bancroft DP, Lepre CA, Lippard SJ (1990) J Am Chem Soc 112:6860–6867
41. Monjardet-Bas V, Chottard J-C, Kozelka J (2002) Chem Eur J 1144–1150
42. Perez C, Leng M, Malinge JM (1997) Nucleic Acids Res 25:896–903
43. Reedijk J (1992) Inorg Chim Acta 198:873–876
44. Brabec V, Leng M (1993) Proc Natl Acad Sci USA 90:5345–5346
45. Paquet F, Boudvillain M, Lancelot G, Leng M (1999) Nucleic Acids Res 27:4261–4268
46. Comess KM, Costello CE, Lippard SJ (1990) Biochemistry 29:2102–2114
47. Dalbies R, Boudvillain M, Leng M (1995) Nucleic Acids Res 23:949–957
48. Boudvillain M, Dalbies R, Aussourd C, Leng M (1995) Nucleic Acids Res 23:2381–2389
49. Boudvillain M, Guerin M, Dalbies R, Saison-Behmoaras T, Leng M (1997) Biochemistry 36:2925–2936
50. Lippert B (1999) *Cis*platin: chemistry and biochemistry of a leading anticancer drug. Wiley-VCH, Weinheim, Germany
51. Martin RB (1983) In: Lippard SJ (ed) Platinum, gold and other metal chemoterapeutic agents, vol 209. ACS Symposium Series, Washington District of Columbia, p 859
52. Arpalahti J, Klika KD, Sillanpaa R, Kivekas R (1998) J Chem Soc, Dalton Trans 1397–1402
53. Carloni P, Sprik M, Andreoni W (2000) J Phys Chem B 104: 823–835
54. Baik M-H, Friesner RA, Lippard SJ (2002) J Am Chem Soc 124:4495–4503
55. Baik MH, Friesner RA, Lippard SJ (2003) J Am Chem Soc 125:14082–14092
56. Eriksson LA, Raber J, Zhu C (2005) J Phys Chem 109:11006–11015
57. Chval Z, Šíp M (2003) Collect Czechoslov Chem Commun 68:1105–1118
58. Burda JV, Leszczynski J (2003) Inorg Chem 42:7162–7172
59. Burda JV, Šponer J, Hrabáková J, Zeizinger M, Leszczynski J (2003) J Phys Chem B 107:5349–5356
60. Zeizinger M, Burda JV, Leszczynski J (2004) Phys Chem Chem Phys 6:3585–3590
61. Deubel DV (2002) J Am Chem Soc 124:5834–5842
62. Burda JV, Zeizinger M, Šponer J, Leszczynski J (2000) J Chem Phys 113:2224–2232
63. Zeizinger M, Burda JV, Šponer J, Kapsa V, Leszczynski J (2001) J Phys Chem A 105:8086–8092
64. Burda JV, Zeizinger M, Leszczynski J (2004) J Chem Phys 120:1253–1262
65. Burda JV, Zeizinger M, Leszczynski J (2005) J Comput Chem 26:907–914
66. Zimmermann T, Zeizinger M, Burda JV (2005) J Inorg Biochem 99:2184–2196
67. Andrae D, Haussermann U, Dolg M, Stoll H, Preuss H (1990) Theor Chim Acta 77:123–141
68. Foster JP, Weinhold F (1980) J Am Chem Soc 102:7211–7218
69. Reed AE, Weinhold F (1983) J Chem Phys 78:4066–4073
70. Reed AE, Weinstock RB, Weinhold F (1985) J Chem Phys 83:735–746
71. Weinhold F (2001) University of Wisconsin, Madison, Wisconsin 53706, Wisconsin